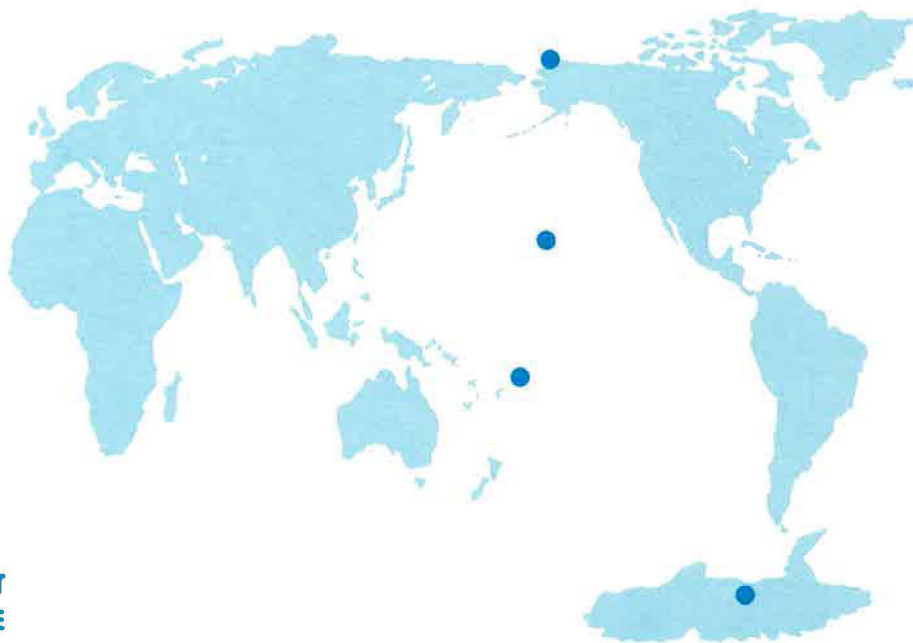*Geophysical Monitoring for Climatic Change*

No. 12

Summary Report 1983

U.S. DEPARTMENT
OF COMMERCE

NATIONAL
OCEANIC AND
ATMOSPHERIC
ADMINISTRATION

ENVIRONMENTAL
RESEARCH
LABORATORIES

Geophysical Monitoring for Climatic Change No. 12

Summary Report 1983

Joyce M. Harris and Everett C. Nickerson, Editors
Air Resources Laboratory
Geophysical Monitoring for Climatic Change

To the memory of Jerome Kizza Nimira, a scientist who worked with the Geophysical Monitoring for Climatic Change Division from 1978 to 1980.

Jerome was born in Uganda and studied at the University of Chicago before coming to Boulder. Following his employment with GMCC, he returned to Africa, where he was on the staff of the Meteorology Department of the University of Nairobi, Kenya, while studying for his doctorate. He died on April 13, 1984, after an automobile accident.

Jerome was a gentleman, compassionate husband and father, and scientist whose warmth, sincerity, and generosity touched everyone he worked with. He was an example to all of us in GMCC who were fortunate enough to know him and work with him. His death saddened us all; his memory will be with us.

American Meteorological Society

Special Award

is conferred upon

NOAA Mauna Loa Observatory

for service to the scientific community by providing measurements of the chemical and physical background state of the atmosphere. The continuous records of CO_2 and atmospheric transmission, in particular, are internationally unique and specially important as basic information applicable to understanding climate variability.

American Meteorological Society

January 1983

R.E. Hallgren
President

CONTENTS

FOREWORD

While I stand here on the seawall at the tip of Cape Florida, on Key
Biscayne, Florida, collecting a sample of tradewind air for the GMCC program,
a number of thoughts come to mind.

- It is because of the many thousands of weather and climate observers in
the past that data are now available to study how and why our climate changes.
The individuals in the GMCC program continue in that tradition of science in
an important and unique way.

- As this air, so recently over the waters of the Gulf Stream, is pumped
into these small glass flasks, I am painfully aware that the sampling time
(5 minutes, 2-3 days per week) is extremely short. Although the discrete
samples collected thus far have provided data for determination of the CO_2
annual cycle and long-term trend at this tradewind location, increased sampling
time would allow us to study the synoptic nature of CO_2 variations with
midlatitude circulations here. Clearly, the past and present economic neces-
sity for discrete sampling should not limit our scientific imagination and
quest to understand the details of the atmospheric circulation and transport
of this important constituent.

- The twice-daily changing water level on this seawall is witness to the
unseen presence of astronomically induced tidal forcing, which appears to play
some yet-to-be-determined role in altering our climate. It reminds us that,
even while we monitor, we must continue to evaluate what should be monitored.

- The global history of these few captured air molecules reminds us that
there are other individuals without resources to monitor atmospheric trace
constituents, but who share concern for the need to monitor them. How can the
international community contribute collectively in a more effective way to
provide answers to these truly global problems?

This Summary Report is the 12th in a series that is unique. The GMCC
program and its documentation are necessary for our times. The series shows
that since the program began collecting air samples at selected locations
around the world, it has changed in ways that are likely to help us understand
how atmospheric trace constituents may influence climate. I commend all the
individuals involved, from those who collect the samples in widely distributed
locations to those who define the program, and encourage them to continued
intelligent vigilance in carrying out the program and in planning and making
changes for the future.

                                        Kirby Hanson
                                        NOAA
                                        Miami, Florida

PREFACE

This document presents a summary of the research operations and accomplishments by the Geophysical Monitoring for Climatic Change (GMCC) program and by outside investigators working cooperatively with GMCC in 1983. It includes descriptions of management and operations at GMCC's four baseline sites, scientific data from the measurement projects, conclusions from analyses of data, and recent basic research achievements.

The GMCC program, established in 1971, is one of several research programs within the Air Resources Laboratory under the directorship of Lester Machta. Its four observatories are located at Barrow, Alaska (in service since 1973); Mauna Loa, Hawaii (in service since 1956); American Samoa (in service since 1973); and South Pole (in service since 1957). Background measurements of aerosols, gases, and solar radiation that are important to the climate of the Earth are made at the observatories. The primary groups within GMCC are Acquisition and Data Management, Monitoring Trace Gases, Aerosols and Radiation Monitoring, and Carbon Dioxide. Specific names of individuals in GMCC are not given in the main text of the report; however, the membership of each GMCC group is given in sec. 9. Publications and presentations by GMCC staff are given in sec. 7.

ACRONYMS AND ABBREVIATIONS

AC	alternating current
ACR	active cavity radiometer
AES	Atmospheric Environment Service, Canada
AGASP	Arctic Gas and Aerosol Sampling Program
AL	Aeoronomy Laboratory, Boulder, CO (ERL)
ALE	Atmospheric Lifetime Experiment
APC	Applied Physics Corporation
ARL	Air Resources Laboratory, Rockville, MD (ERL)
ASASP	active-scattering aerosol spectrometer probe
ASCS	Alaska Soil Conservation Service
ASRC	Atmospheric Sciences Research Center, SUNYA, Albany, NY
BAS	British Antarctic Survey
BDL	below detection level
BLM	Bureau of Land Management (USGS)
BOSS	Basic Operating System Software
BRW	Barrow Observatory, Barrow, Alaska (GMCC)
CAF	Clean Air Facility
CAMS	Control and Monitoring System
CDC	Control Data Corporation
CDIC	Carbon Dioxide Information Center, Oak Ridge, TN (DOE)
CIRES	Cooperative Institute for Research in Environmental Sciences, University of Colorado, Boulder
CMA	Chemical Manufacturers Association
CN	condensation nuclei
CNC	condensation nucleus counter
CPU	central processing unit
CSIRO	Commonwealth Scientific and Industrial Research Organization, Australia
DAS	data acquisition system
DC	direct current
DEC	Digital Equipment Corporation
DOE	Department of Energy
DOY	day of year, Julian
EC	elemental carbon
ECC	electrochemical concentration cell
EML	Environmental Measurements Laboratory (DOE)
ENSO	El Niño-Southern Oscillation
EPA	Environmental Protection Agency
EPROM	erasable programmable read-only memory
ERL	Environmental Research Laboratories, Boulder, CO (NOAA)
F.R.G.	Federal Republic of Germany
FSSP	forward-scattering spectrometer probe
GC	gas chromatograph
G.E.	General Electric
GMCC	Geophysical Monitoring for Climatic Change, Boulder, CO (ARL)
GMT	Greenwich mean time
GSFC	Goddard Space Flight Center (NASA)
HAO	High Altitude Observatory, Boulder, CO (NCAR)
HASL	Health and Safety Laboratory (EPA)
HBW	half bandwidth
HP	Hewlett-Packard
HPIB	Hewlett-Packard interface bus
IAEA	International Atomic Energy Agency, Vienna, Austria

IAMAP	International Association for Meteorology and Atmospheric Physics
ICDAS	Instrumentation Control and Data Acquisition System
IGY	International Geophysical Year
IICAMS	Interactive Instrumentation Control and Monitoring System
I/O	input/output
IOS	Institute for Ocean Sciences, British Columbia, Canada
IR	infrared
ISWS	Illinois State Water Survey
ITCZ	Intertropical Convergence Zone
IUGG	International Union of Geodesy and Geophysics
JSC	Johnson Space Center (NASA)
KUM	Cape Kumukahi, Hawaii
LBL	Lawrence Berkeley Laboratory (DOE)
LLL	Lawrence Livermore Laboratory (DOE)
LST	local standard time
MAP/ GLOBUS	Middle Atmospheric Project/Global Budget of Stratospheric Trace Constituents
MLO	Mauna Loa Observatory, Hawaii (GMCC)
MSL	mean sea level
NADP	National Atmospheric Deposition Program
NARL	Naval Arctic Research Laboratory, Barrow, AK
NASA	National Aeronautics and Space Administration
NBS	National Bureau of Standards
NCAR	National Center for Atmospheric Research, Boulder, CO
NCDC	National Climatic Data Center, Asheville, NC
NDIR	nondispersive infrared
NIAR	Norwegian Institute for Arctic Research
NIP	normal incidence pyrheliometer
NMC	National Meteorological Center, Suitland, MD
NOAA	National Oceanic and Atmospheric Administration
NRL	Naval Research Laboratory, Washington, DC
NSBF	National Scientific Balloon Facility
NSF	National Science Foundation, Washington, DC
NWS	National Weather Service
OGC	Oregon Graduate Center, Beaverton, OR
ONR	Office of Naval Research
OPC	optical particle counter
OPEC	Organization of Petroleum Exporting Countries
PE	phase-encoded
PISSA	particulate integrating sampling sector analyzer
PIXE	proton induced X-ray emission
PMS	Particle Measuring Systems
PMT	photomultiplier tube
PV	photovoltaic
P^3	portable pressurizing pack
RAM	random access memory
RH	relative humidity
RMS	root mean square
SAGA	Soviet-American Gases and Aerosols (Expedition)
SAGE	Stratospheric Aerosol and Gas Experiment
SEASPAN	SEAREX South Pacific Aerosol Network
SEAREX	Sea-Air Exchange Program
SEM	scanning electron microscope
SIO	Scripps Institution of Oceanography, La Jolla, CA
SMO	Samoa Observatory, American Samoa (GMCC)

SN	serial number
SOI	Southern Oscillation Index
SPO	South Pole Observatory, Antarctica (GMCC)
SRCF	Solar Radiation Calibration Facility (NOAA)
SRL	Smithsonian Radiation Laboratory
SST	sea surface temperature
STD BUS	standard bus
STP	standard temperature and pressure
SUNYA	State University of New York at Albany
TECOMAC	Technical Conference on Observation and Measurement of Atmospheric Contaminants
TRACS	Trace Atmospheric Constituent Study
TTO/TAS	Transient Tracers in the Ocean/Tropical Atlantic Study
URI	University of Rhode Island, Kingston, RI
USARP	United States Antarctic Research Program
USCG	United States Coast Guard
USGS	United States Geological Survey
UV	ultraviolet
WATOX	Western Atlantic Ocean Experiment
WDC-A	World Data Center-A, Asheville, NC
WMO	World Meteorological Organization, Geneva, Switzerland
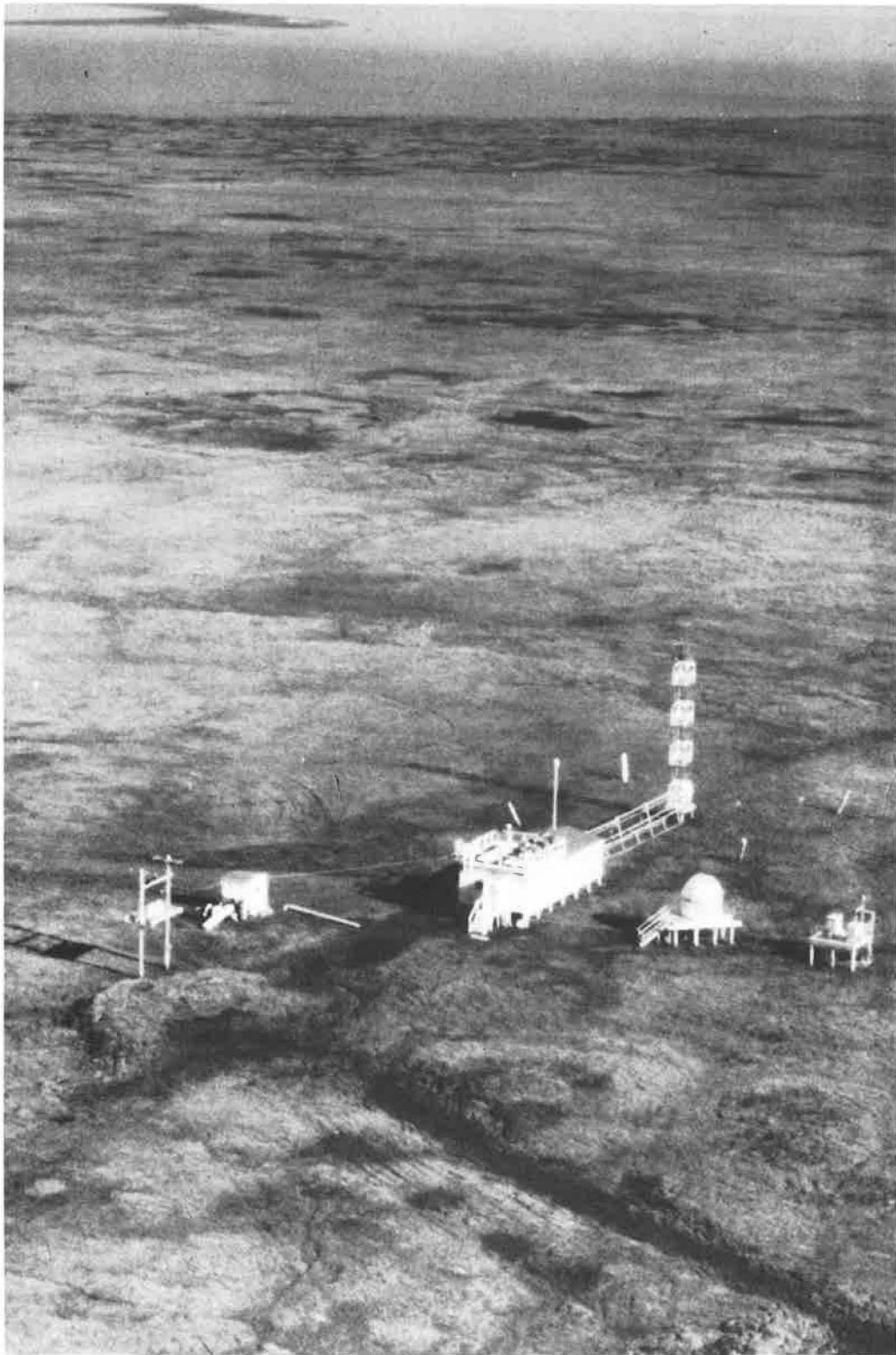
Barrow Observatory, Alaska, site of GMCC's surface-based measurements for AGASP, March-April 1983. The view is toward the Arctic Ocean.

GEOPHYSICAL MONITORING FOR CLIMATIC CHANGE

NO. 12

SUMMARY REPORT 1983

1. SUMMARY

At MLO, a special series of ozonesonde observations continued through 1983. The data acquisition system for the lidar was replaced to improve its reliability and streamline its operation. The 1983 lidar observations indicate that all measured stratospheric aerosol parameters decreased, and that no significant stratospheric aerosol injection was observed against the El Chichon background. Solar transmission as well as maximum polarization at sunrise generally increased; in addition, turbidity generally declined, reflecting the continuing cleansing of the atmosphere following the El Chichon eruption of 1982.

At BRW, the power capacity of the air sampling platform and the air sampling room was increased. In early spring, a tracking NIP was installed to provide continuous direct irradiance data. A new pressure transducer is giving excellent agreement with the mercurial barometer. In support of AGASP, the measurement program at BRW was expanded during the Arctic haze season, especially for surface aerosols and solar radiation.

At SMO, a photovoltaic power system was installed to provide a continuous source of power for data acquisition and CO_2 monitoring. After the sudden death of Chief Iuli Togi, with whom NOAA negotiated the original SMO land lease in 1974, a new lease was arranged. Assurances were received from the Iuli family and the Tula village that the continuity of GMCC operations in American Samoa would be maintained.

At SPO, temperature fluctuations, which had plagued CAF in the past, were reduced with the installation of larger capacity room heaters and a high-volume, thermostatically controlled blower. A long-term problem with back diffusion during periods of high winds was partially corrected by adding a second-stage blower to the stack exhaust. One of the most complete CN records was obtained this year by the G.E. counter. A solar infrared hygrometer, for making discrete observations of the total slant-path water vapor content, and a pyrgeometer, for measuring terres'rial IR radiation, were installed for the first time.

The measurement programs continued at the four observatories. These programs include CO_2, total columnar ozone, ozone vertical distribution, surface ozone, stratospheric water vapor, CFC-11 and -12, N_2O, stratospheric aerosols, volumetric aerosol scattering coefficient, CN concentration, solar radiation, meteorological variables, and precipitation chemistry. In addition, a wide variety of cooperative programs were conducted for university, other agency, and foreign investigators.

Continuous measurement of CO_2 with NDIR analyzers continued at the four observatories. Final processing of the data through 1983 was completed except for the selection of data for background conditions. Two gas chromatographs,

designed to measure CO_2 with precision comparable with the NDIR analyzer, were tested in the CO_2 laboratory in Boulder. The GC's require 3-4 times less reference gas than the analyzers and are capable of measuring CH_4 as well as CO_2.

Flask sampling for CO_2 continued at 22 globally distributed sites. Indications are that the new site near Christchurch, New Zealand, is not ideally suited for measurement of background CO_2, due to its proximity to Christchurch and vegetated areas. In 1983, 5600 flasks were analyzed, of which 3500 were from the flask network. The remainder were for special projects such as cruises and aircraft experiments or were test flasks to monitor analyzer performance.

A return to a higher CO_2 growth rate for 1982-1983 of 1.4 ppm yr^{-1} followed the lower rates for 1981-1982 of 1.0 ppm yr^{-1} (continuous data) and 0.6 ppm yr^{-1} (flask data). This temporarily reduced growth was probably indicative of a major perturbation of the natural global carbon cycle related to the 1982-1983 ENSO event.

Total ozone observations were continued at the 11 stations in the U.S. Dobson ozone spectrophotometer network. On 22 June 1983 an NWS station in Fresno, CA, was added to this network.

Automated Dobson instruments were installed at Poker Flat, AK, and Haute Provence, France. Standard lamp calibration checks on Dobson instruments in the global total ozone network continued during the year. The unusually low total ozone levels at MLO during late 1982 and early 1983 are thought to be associated with the stratospheric quasi-biennial oscillation phenomenon, although a small amount of apparent ozone depletion by stratospheric aerosols from the eruption of El Chichon cannot be ruled out. The decrease of total ozone at MLO since 1970 is about 3% per decade.

The program of weekly balloon soundings continued to obtain ozone profile data at Hilo, HI. The sonde data has aided in the interpretation and processing of Umkehr data, obtained since the eruption of El Chichon, which must be corrected for errors due to stratospheric aerosols. These errors in the 1983 Umkehr ozone profiles probably did not exceed ±10%. A number of tests, conducted to assess the performance of ECC ozonesondes in the troposphere and at altitudes between 30 and 40 km, produced generally positive results, although one experiment was hampered by balloon failure.

Surface ozone measurements continued at the four observatories. Concentrations at MLO reached their highest values since measurements began 11 years ago. The overall linear trend in the data for the period 1973-1983 is 1.6% yr^{-1}, which is greatly influenced by high values in 1983. Trends in the data at BRW and SMO are less marked.

The stratospheric water vapor measurement program was continued at Boulder. Balloon performance improved, although there were problems with measurements taken between 25 and 30 km.

Flask monitoring of halocarbons and nitrous oxide continued at BRW, NWR, MLO, SMO, and SPO. A gas chromatograph was installed at SPO late in 1983 to improve measurements of these trace gases. Trends in the data are consistent with previous years.

Lidar measurements acquired at MLO during 1974-1983 have all been processed for vertical profiles of aerosol backscattering ratio, ratio of total backscatter to Rayleigh backscatter, and cumulative optical depth. These data constitute one of the longest detailed records of lidar observations in existence.

Continuous measurement of CN concentration and aerosol scattering extinction coefficient provided another year of surface aerosol data at BRW, MLO, SMO, and SPO. The least-squares trend lines for the data show no significant long-term trends and are essentially unchanged from last year's trend analysis.

Solar radiation measurements continued at the four GMCC observatories. In support of Arctic haze studies, a continuous pyrheliometer was put online in March at BRW. In addition, spectral measurements of direct solar intensity zenith sky intensity, global diffuse flux, and global total flux were made during AGASP. A multilaboratory sunphotometer intercomparison was held in Boulder in October.

Routine and special precipitation chemistry measurements continued at GMCC sites of MLO and SMO, and at regional sites.

Development continued on the hardware and software for CAMS, the microprocessor-based data acquisition system that will eventually replace ICDAS.

The GMCC trajectory program was enhanced by adding the capability to the Northern Hemisphere isobaric model to compute forward trajectories. Backward trajectories for 1983 were added to the trajectory inventory for BRW, MLO, and SMO.

GMCC personnel conducted numerous research projects and data analyses, many of which are summarized in sec. 4. Several of these studies present analysis of data collected during AGASP in March-April 1983. An AGASP study of atmospheric trajectories to BRW indicated long-range pollution transport from Wesern Asia and Europe during an intense Arctic haze event. Events in surface aerosol data collected during AGASP corresponded to changes in origin indicated by back trajectories and meterology at BRW. Aerosol scattering extinction coefficient was well correlated with daily mean aerosol optical depth, indicating that surface measurements reflect Arctic haze above the ground. A wealth of data collected during AGASP has been analyzed and published in numerous papers. This experiment has greatly increased our understanding of the nature and origins of Arctic haze.

Another group of special projects dealt with CO_2 data. One study related CO_2 variability at SMO to the latitudinal gradient and changes in atmospheric circulation pattern. Another analyzed the record of SPO CO_2 data and found a change of the growth rate of CO_2 from 1.7 ppm yr^{-1} (1977-1980) to about 1.0 ppm yr^{-1} (1981-1982). Two reports presented CO_2 ocean cruise data that have helped to verify and fill gaps in the CO_2 flask data network, giving a more complete picture of CO_2 global distribution. A detailed report presents the results of the NOAA-SIO CO_2 intercomparison at MLO, which investigated systematic differences between the CO_2 values obtained by the two organizations. A preliminary average difference between NOAA and SIO concentration was -0.02 ppm with standard error of 0.039 ppm. Another report analyzed the possible relationships between the latest ENSO event and the global CO_2 record.

Other special studies include a climatology of 7 years of trajectories to Bermuda, which when compared with precipitation chemistry data revealed good agreement between high acidity and airflow from North America. An airborne survey studied the latitudinal variation in optical depth caused by the El Chichon volcanic cloud and found good agreement between MLO measurements and those taken during the flight series. Two reports summarize SO_2 measurements made with the Dobson spectrophotometer and a balloonborne ECC sonde.

In 1983, GMCC supported many cooperative research projects. Fifteen summary reports from these projects are presented in sec. 5. They cover such topics as air mass characteristics during AGASP at BRW; special solar radiation measurements made at BRW; elemental carbon measurements made at Whiteface Mountain; aircraft and surface observations of Arctic haze during AGASP; a new aerosol impactor-concentrator that allows aircraft sampling in polar regions; soil dust, particulate sulfur and chlorine, and trace gases in the Arctic during spring 1983; atmospheric particulates at MLO and SPO; meteorites at SPO; CO_2 and other air chemistry studies at Palmer Station; vertical profiles of carbon particles in the Arctic; SO_2, ozone, and aerosol over MLO since El Chichon; optical and chemical features of aerosol present in the Arctic snow-pack; and measurements of CH_4 and CO_2 by gas chromatography.

2. OBSERVATORY REPORTS

2.1 Mauna Loa

2.1.1 Facilities

During 1983, ICDAS operated for 98% of the time at MLO. This very good ICDAS performance was made possible because of extra efforts by the MLO staff, which included voluntary weekend computer watches that virtually eliminated any excessively long computer outages over the weekend.

A failure of the CPU in the NOVA 1220 computer was responsible for approximately 105 of the 184 hours of ICDAS downtime. Otherwise AC power failures and dropouts accounted for most of the remaining 79 hours.

Director Kinsell Coulson retired from government service on 30 November 1983, and a replacement was not named in 1983.

The MLO meteorological museum moved from the second to third floor to make room for the computer.

2.1.2 Programs

The principal programs carried out at MLO during 1983 are listed in table 1. Brief comments on the programs are given below.

Table 1.--Summary of sampling programs at MLO in 1983

Program	Instrument	Sampling frequency	Remarks
Gases			
CO_2	URAS-2 infrared analyzer	Continuous	
	3-L evacuated glass flasks	1 pair wk^{-1}	Mountain only
	0.5-L glass flasks, P^3	1 pair wk^{-1}	Mountain and seacoast
	0.5-L glass flasks, through analyzer	1 pair wk^{-1}	Mountain only
	5-L evacuated glass flasks	1 pair wk^{-1}	Mountain and seacoast
Surface ozone	Dasibi ozone meter	Continuous	
Total ozone	Dobson spectrophotometers nos. 63, 65	3 day^{-1}	No. 63, Jan-May; no. 65, Jun-Dec
Ozone profile	Dobson spectrophotometer no. 65	5 obs. wk^{-1}	Umkehr, Nov-Dec
	Balloonborne ECC	1 wk^{-1}	From Hilo Airport
CFC-11, CFC-12, and N_2O	300-mL stainless steel flasks	1 pair wk^{-1}	
Aerosols			
Condensation nuclei	Pollak CNC	Discrete	4 meas., weekdays; 0, weekends
	G.E. CNC	Continuous	
Optical properties	Four-wavelength nephelometer	Continuous	450, 550, 700, 850 nm
Stratospheric aerosols	Lidar	Discrete	694.3 nm; 2 J
Skylight polarization	Polarizing radiometer	Discrete	320, 365, 400, 500, 600, 700, 800, 900 nm; narrowband
Solar Radiation			
Global irradiance	Eppley pyranometers with Q, GG22, OG1, and RG8 filters	Continuous	
Direct irradiance	Eppley pyrheliometers (2) with Q filters	Continuous	
	Eppley pyrheliometer with Q, OG1, RG2, and RG8 filters	Discrete	
	Eppley pyrheliometer with 13 filters	Continuous	
	Eppley/Kendall active cavity radiometer	Discrete	
Diffuse irradiance	Eppley pyranometer with shading disk and Q filter	Continuous	

5

Table 1.--Summary of sampling programs at MLO in 1983--Continued

Program	Instrument	Sampling frequency	Remarks
Solar Radiation--Cont.			
Turbidity	J-series 1982 sunphotometers	Discrete	380, 500, 778, 862 nm; narrowband
	WPL seven-wavelength sunphotometer	Continuous	380, 422, 500, 596, 680, 778, 862 nm; narrowband
	PMOD three-wavelength sunphotometer	Continuous	380, 500, 778 nm; narrowband
Meteorology			
Air temperature	Thermistor	Continuous	
	Max.-min. thermometers	1 day^{-1}	
	Hygrothermograph	Continuous	MLO and Kulani Mauka
Soil temperature	Thermistor	Continuous	
Dewpoint temperature	Dewpoint hygrometer	Continuous	
Relative humidity	Hygrothermograph	Continuous	MLO and Kulani Mauka
	Sling psychrometer	Discrete	
Pressure	Capacitance transducer	Continuous	
	Microbarograph	Continuous	
	Mercurial barometer	Discrete	
Wind (speed and direction)	Bendix Aerovane	Continuous	
Precipitation	Rain gauge, 8-in	1 day^{-1}	
	Rain gauge, 8-in	1 wk^{-1}	Kulani Mauka
	Rain gauge, weighing gauge	Continuous	
Total precipitable water	Foskett infrared hygrometer	Continuous	
	HAO infrared hygrometer	Continuous	
Precipitation Chemistry			
pH	pH meter	Discrete	Rainwater collections, 6 sites
Conductivity	Conductivity bridge	Discrete	
Chemical components	Ion chromatograph	Discrete	
Cooperative Programs			
CO_2 (SIO)	Infrared analyzer (Applied Physics)	Continuous	
CO_2, ^{13}C, N_2O (SIO)	5-L evacuated glass flasks	1 pair wk^{-1}	Mountain and seacoast
Surface SO_2 (EPA)	Chemical bubbler system	Every 12 days	
Total surface particulates (DOE)	High-volume sampler	Continuous	Dependent on wind direction; 1 filter wk^{-1}
Atmospheric electricity (Univ. of Minnesota)	Field mill, air conductivity meter, surface antenna	Continuous	
Ultraviolet radiation (Temple Univ.)	Ultraviolet radiometer	Continuous	Radiation responsible for sunburning of skin
Precipitation collection (DOE)	HASL wet-dry collector	Continuous	
Precipitation collection (EPA)	Misco model 93	Continuous	
Precipitation collection (Univ. of Paris)	Likens funnel collector	Twice wk^{-1}	
Precipitation collection (IAEA)	Likens funnel collector	Twice wk^{-1}	
Wet-dry deposition (ISWS)	Exposed collection pails	Continuous	NADP
Aerosol chemistry (Univ. of Maryland)	Nuclepore filters	Continuous	Day-night discrimination
Aerosol chemistry (Univ. of Arizona)	Quartz filters	Continuous	Day-night discrimination
^{13}C (USGS, Denver)	10-L stainless steel flasks	2 wk^{-1}	
Radiocarbons (USGS, Menlo Park)	NaOH collector	Discrete	
Carbon Monoxide (Max Planck Inst.)	Chemical reaction with HgO	Continuous 1 pair wk^{-1}	Halocarbon flasks
Ozone and SO_2 (AES, Canada)	Brewer MK I spectrophotometer	Discrete	
Various trace gases (OGC)	Stainless steel flasks	1 set wk^{-1} (3 flasks set^{-1})	
Various trace gases (NCAR)	3-L stainless steel flasks	1 pair wk^{-1}	

Carbon Dioxide

The concentration of CO_2 in the atmosphere was monitored continuously by the URAS-2 infrared analyzer during 1983. The instrument performed satisfactorily without major problems. Preliminary results indicate that the rate of increase of CO_2 concentration was approximately 0.7-1.0 ppm yr^{-1} for 1983.

The weekly CO_2 flask sampling programs at MLO and Cape Kumukahi were continued during the year. Flasks were lost or broken during shipment on only four occasions.

Outgassing from the volcanic caldera at the summit of Mauna Loa caused disruptions of some of the CO_2 records in every month of the year. It occurred mainly between 0000 and 0800 LST during the downslope wind flow regime. The monthly occurrences are listed in table 2.

Table 2.--Monthly occurrences of outgassing from the volcanic caldera on Mauna Loa during 1983

	Jan	Feb	Mar	Apr	May	Jun	Jul	Aug	Sep	Oct	Nov	Dec
No. of days	7	7	6	5	10	6	7	12	16	7	2	4
Percent of days	23	25	19	17	32	20	23	39	53	23	7	13

Ozone

Total ozone in the atmospheric column was measured on 208 days during 1983. In addition, the Dobson spectrophotometer was used for measuring the ozone profile by the Umkehr technique on 5 days per week during the year, and 134 published Umkehr measurements were obtained. A special series of ozone-sonde observations was continued through the year; 34 flights were made.

Problems developed with the ozone generator, and it was returned to Boulder on 16 May 1983. A zero filter was used for the remainder of the year. A new chart recorder was installed and calibrated on 13 June 1983.

Surface Aerosols

The nephelometer operated well for most of 1983. During the last 2 months, however, it encountered an intermittent problem in channels 3 and 4. The problem was finally isolated and determined to be dirty contacts on the circuit boards and some bad operational amplifiers. The Boulder Laboratory nephelometer was installed, and it was operated in October alongside the MLO unit for comparison. No problems were encountered.

Stratospheric Aerosols--Lidar

Forty-three successful lidar stratospheric backscatter observations were performed during 1983.

The Data General NOVA 2 lidar computer system that was installed in 1974 was replaced with a Digital Equipment LSI-11/23. The new computer has improved the lidar system's reliability, simplified its operation, and significantly decreased the time required to perform an observation. The new system provides the base for many future lidar system upgrades.

The 1983 lidar observations indicated, as expected, a definite but erratic decrease in all measured stratospheric aerosol parameters. Total stratospheric non-Rayleigh backscatter decreased from a January average of approximately 1.2×10^{-3} sr^{-1} to a December average of approximately 0.6×10^{-3} sr^{-1}. Like-wise, the average monthly peak backscatter ratio decreased from approximately 8.2 to 3.3, and the center elevation of the main backscatter ratio peak value decreased from approximately 22 to 19 km from January to December.

During 1983 no significant stratospheric aerosol injection was observed against the El Chichon background at MLO.

Solar Radiation

A normal incidence pyrheliometer, four global pyranometers with Q, GG22, OG1, and RG8 cutoff filters, and a diffuse Q pyranometer with shading disk were operated the whole year to obtain continuous radiation measurements. A filter-wheel pyrheliometer with Q, OG1, RG2, and RG8 cutoff filters was oper-ated to obtain discrete broadband radiation measurements. Transmission gener-ally increased as the year progressed.

The active solar tracker operated the whole year with only minor problems. The 16-channel DAS was replaced by a 32-channel DAS in July, and both operated well after correction of an initial hardware problem with the 32-channel DAS that resulted in a 1-mo loss of observations. The dome and shutter controllers operated reasonably well. Instruments mounted on the spar included a normal incidence pyrheliometer, an infrared water vapor meter, a seven-wavelength sunphotometer, and a three-wavelength sunphotometer first installed in August. Overall operation was fairly good during the year.

Turbidity measurements were obtained with hand-held sunphotometers J202 (380 and 500 nm) and J314 (778 and 862 nm) during most of the year before being temporarily replaced in October by instrument J321 (380 and 500 nm) for the rest of the year. Atmospheric turbidity generally declined during 1983.

Skylight polarization was measured using an eight-wavelength polarizing radiometer. Maximum polarization at sunrise increased during the year, re-flecting the continuing cleansing of the atmosphere following the El Chichon eruption of 1982.

Meteorology

Meteorological measurements were continued without major problems through-out 1983.

Precipitation Chemistry

The precipitation chemistry program continued without difficulties at about the same level of activity as in prior years. Snow samples from SPO and rainwater samples from SMO were added to the existing program schedule for analyses at MLO. Weekly samples are being collected at both sites.

Cooperative Programs

The large number of cooperative programs continued normally through 1983. A brief summary of some cooperative efforts follows.

Aerosol particulates were collected on Nuclepore filters for the University of Maryland and on quartz filters for the University of Arizona on a weekly basis. The filter pumps were operated discriminately by a master controller on the basis of time of day, wind speed, wind direction, and CN concentration. An aerosol absorption study by the University of Washington required daily changes of special filters until the project was discontinued in June.

Erythema radiation was integrated on an hourly basis for Temple University throughout the year.

Total ozone and SO_2 in the atmosphere were measured during the whole year with a Brewer MK I spectrophotometer supplied by AES, Canada. Samples of CO_2, collected by relatively long-term exposure of vats of sodium hydroxide solution at MLO were analyzed by USGS, Menlo Park, CA, for radiocarbon content. A new instrument for CO from the Max Planck Institute in Mainz, Germany, was installed and online at the end of February. Many mechanical and logistical problems followed.

The SIO Applied Physics infrared analyzer continued to measure atmospheric CO_2 without major problems during 1983. Flask samples of air from MLO and Cape Kumukahi continued to be supplied to SIO on a weekly basis.

MLO continued to participate in NADP under the direction of ISWS, by sending wet and dry samples of atmospheric deposition collected at the observatory. Bulk collections of atmospheric deposition were supplied all year to DOE. Other precipitation chemistry projects added in 1983 included (1) a short-term project with J. Halbig of University of Hawaii in which samples were collected on an event basis starting mid-1983 and continuing until mid-1984 at Hilo and Kona sites; (2) W. Keene's (University of Virginia) organic acid analysis program on rainwater samples from MLO; and (3) negotiations for a berylium 10 project on MLO rainwater samples, to be coordinated by G. Stensland at ISWS.

Two sets of equipment were operated at MLO in 1983 for measuring various parameters related to atmospheric electricity. The equipment installed many years ago by W. Cobb (ARL) measures electrostatic potential, air-earth current, and positive/negative conductivity of the air. It operated well throughout the year. The second set of instruments from D. Olson of the University of Minnesota, which measured electrostatic potential and air-earth current, was shut down in May for the year due to lack of chart paper. Otherwise it operated normally.

2.2 Barrow

2.2.1 Facilities

During 1983, the safety and power capacity of the air sampling platform at BRW were upgraded. In addition, the amount of power available in the air sampling room was increased, as was the number of receptacles.

The lidar hut was moved from NARL to the observatory and placed adjacent to the garage.

A Honda ATC 200E three-wheel cycle was added to the observatory's fleet to allow tundra crossing during summertime. The Bombi all-terrain vehicle required some major engine maintenance, but is still running.

The BRW LST zone was increased by 1 hour and is now 9 hours behind GMT as of 30 October.

2.2.2 Programs

Programs carried out at BRW during 1983 are listed in table 3. Comments on selected programs follow.

Carbon Dioxide

The URAS-2T infrared analyzer performed quite well during the year. However, problems occurred with the aged strip chart recorder.

Flask sampling went well. Midway through 1983, P^3 samples were taken on the roof near the sampling stack to provide air sample conditions in closer agreement with the through-the-analyzer method.

Surface Ozone

The surface ozone detector, ozone generator, and strip chart recorder operated well all year.

Halocarbons and Nitrous Oxide

The weekly flask sampling occurred without problem in 1983.

Surface Aerosols

The G.E. CNC was problematic throughout the year. The main sources of downtime were flooding of the optical chamber during shipment and solenoid problems.

The Pollak counter and four-wavelength nephelometer performed well.

Solar Radiation

In early spring, a tracking NIP was installed to provide continuous direct irradiance data. An all-sky camera was set up during the Arctic haze study and continued to document sky conditions through summer.

Table 3.--Summary of sampling programs at BRW in 1983

Program	Instrument	Sampling frequency
Gases		
CO_2	URAS-2T infrared analyzer	Continuous
	0.5-L glass flasks, P^3	1 pair wk^{-1}
	0.5-L glass flasks, through analyzer	1 pair wk^{-1}
	5-L evacuated glass flasks	1 pair wk^{-1}
Surface ozone	Dasibi ozone meter	Continuous
CFC-11, CFC-12, and N_2O	300-mL stainless steel flasks	1 pair wk^{-1}
Aerosols		
Condensation nuclei	Pollak CNC	Discrete
	G.E. CNC	Continuous
Optical properties	Four-wavelength nephelometer	Continuous
Aerosol chemistry	Streaker, Cascade impactor	Discrete (Mar-May)
Aerosol chemistry	PMS aerosol spectrometer	Continuous (Mar-May)
Solar Radiation		
Global irradiance	Eppley pyranometers with Q and RG8 filters	Continuous
Direct irradiance	Tracking NIP	Continuous
Direct irradiance	Eppley pyrheliometer with Q, OG1, RG2, and RG8 filters	Discrete
Turbidity	Sunphotometers with 380-, 500-, 778-, and 862-nm narrowband filters	Discrete
Sky documentation	All-sky camera (Fisheye)	Continuous (Mar-Aug)
Meteorology		
Air temperature	Thermistor	Continuous
	Max.-min. thermometers	1 day^{-1}
	Hygrothermograph	Continuous
Dewpoint temperature	Dewpoint hygrometer	Continuous
Relative humidity	Hygrothermograph	Continuous
Pressure	Capacitance transducer	Continuous
	Microbarograph	Continuous
	Mercurial barometer	Discrete
Wind (speed and direction)	Bendix Aerovane	Continuous
Precipitation Chemistry		
pH	pH meter (samples analyzed at MLO)	Discrete
Conductivity	Conductivity bridge (samples analyzed at MLO)	2 mo^{-1}
Cooperative Programs		
Total surface particulates (DOE)	High-volume sampler	Continuous (1 filter wk^{-1})
Aerosol chemistry (URI)	High-volume sampler	Continuous (2 filters wk^{-1})
Global radiation (SRL)	6 Eppley pyranometers	Continuous
Ultraviolet radiation (Temple Univ.)	Ultraviolet radiometer	Continuous
CO_2, ^{13}C, N_2O (SIO)	5-L evacuated glass flasks	1 pair wk^{-1}
Precipitation gauge (ASCS)	Wyoming shielded precipitation gauge	2 mo^{-1}
Carbonaceous particles (LBL)	Dichotomous sampler (quartz and Millipore filters)	Continuous (1 set of filters wk^{-1})
	High-volume filter	Continuous (1 filter wk^{-1})
	Daily Millipore sampler	Continuous (1 filter day^{-1})
Various trace gases (OGC)	Stainless steel flasks	1 set wk^{-1} (3 flasks set^{-1})
Incident and reflected radiation (Univ. of Alaska)	Up-down pyranometers	Continuous (program ended in Dec 1983)
Magnetic fields (USGS)	Magnetometer	1 station check wk^{-1}
^{13}C (USGS)	10-L stainless steel flasks	1 pair mo^{-1}
Various trace gases (NCAR)	3-L stainless steel flasks	1 pair wk^{-1}
$^{13}C/^{12}C$ (CSIRO)	5-L glass flasks	1 pair mo^{-1}

Table 4.--Summary of sampling programs at SMO in 1983

Program	Instrument	Sampling frequency
Gases		
CO_2	URAS-2T infrared analyzer	Continuous
	0.5-L glass flasks, P^3	1 pair wk^{-1}
	0.5-L glass flasks, through analyzer	1 pair wk^{-1}
	5-L evacuated glass flasks	1 pair wk^{-1}
Surface ozone	Dasibi ozone meter	Continuous
Total ozone	Dobson spectrophotometer no. 42	3 day^{-1}
CFC-11, CFC-12, and N_2O	300-mL stainless steel flasks	1 pair wk^{-1}
Aerosols		
Condensation nuclei	Pollak CNC	Discrete
	G.E. CNC	Continuous
Optical properties	Four-wavelength nephelometer	Continuous
Solar Radiation		
Global irradiance	Eppley pyranometers with Q and RG8 filters	Continuous
	Eppley pyranometers (2) with Q filters on tilted mounts	Continuous
Direct irradiance	Eppley pyrheliometer with Q filter	Continuous
	Eppley pyrheliometer with Q, OG1, RG2, and RG8 filters	Discrete
Turbidity	Sunphotometers with 380-, 500-, 778-, and 862-nm narrowband filters	Discrete
Meteorology		
Air temperature	Thermistor	Continuous
	Max.-min. thermometers	1 day^{-1}
	Hygrothermograph	Continuous
Soil temperature	Thermistor	Continuous
Dewpoint temperature	Dewpoint hygrometer	Continuous
Relative humidity	Hygrothermograph	Continuous
	Sling psychrometer	Discrete
Pressure	Capacitance transducer	Continuous
	Microbarograph	Continuous
	Mercurial barometer	Discrete
Wind (speed and direction)	Bendix Aerovane	Continuous
Precipitation	Polyethylene funnel, bottle	1 day^{-1}
Precipitation Chemistry		
pH	Corning model 125 meter with semimicro combination electrode	1 day^{-1} (GMCC); 1 wk^{-1} (NADP)
Conductivity	Beckman model RC-16C meter	1 day^{-1} (GMCC); 1 wk^{-1} (NADP)
Cooperative Programs		
CO_2, ^{13}C, N_2O (SIO)	5-L evacuated glass flasks	1 pair wk^{-1}
ALE project: CFC-11, CFC-12, N_2O, CH_3CCl_3, CCl_4 (OGC)	HP5840A gas chromatograph	1 h^{-1}
ALE project: CH_4, CO, CO_2 (OGC)	Carle gas chromotograph	3 h^{-1}
Various trace gases (OGC)	Stainless steel flasks	1 set wk^{-1} (3 flasks set^{-1})
^{13}C (USGS)	10-L stainless steel flasks	2 pair mo^{-1}
Wet-dry deposition (NADP)	HASL wet-dry collector (new Chemetrics, Dec 81)	1 wk^{-1}, wet; 2 mo^{-1}, dry
Bulk deposition (EML)	Plastic bucket	1 mo^{-1}
Hi-Vol sampler (EML)	Hi-Vol pump and filter	1 wk^{-1}
Hi-Vol sampler (SEASPAN Project)	Hi-Vol pump and filter with clean sector controls	1 wk^{-1}

CO_2-in-air standards were in Boulder for a recalibration procedure, and a set of traveling standards was sent to SMO for use in the weekly calibrations. The original standards were returned to SMO and went back online in July.

No serious air line problems were experienced during the year; however, the section of aluminum line from the remote building at the Point to the top of the stairs, a distance of approximately 200 m, was replaced with Dekabon tubing. Also, because of erratic operation, the CryoCool freezeout trap located at the Point was taken offline in November, and the original condensation trap system was reinstalled. This reduced trap-tending chores at the Point to a once-per-week draining of the condensate collector bottles. These bottles retain approximately 75% of the ambient air moisture, or about 700 mL wk^{-1}. The remaining 25% is removed by a freezeout trap cooled by a Cincinnati Sub-Zero freezer located in the main observatory building next to the analyzer. To minimize servicing of this system's relatively low-volume trap, a modification was made in November. A large, ~2-L glass thimble trap was added to the Cincinnati freezer system to remove all remaining water from the ambient air arriving from the Point. This freed the low-volume trap from the task of removing the ambient air moisture, and hence lengthened its use before freeze-up from about 1 to 2 days to an essentially unlimited time. The thimble trap is changed once per week during the weekly calibration check, when ambient airflow through the analyzer is not required. This combination of condensation trap at the Point and large-volume thimble trap ahead of the low-volume trap permits uninterrupted ambient airflow through the analyzer between weekly calibrations, and results in a higher quality data set.

Ozone

Both the surface ozone instrument, a Dasibi ozone meter, and the Dobson ozone spectrophotometer operated routinely all year.

Surface Aerosols

The SMO complement of aerosol equipment remained unchanged during 1983, and operated routinely with only a few minor problems.

Solar Radiation

All sensors operated normally during 1983.

Meteorology

A new pressure transducer was received and put online during June. It is a replacement unit for the one destroyed by the lightning strike in March 1982.

The EG&G dewpoint hygrometer failed twice during the year and on both occasions had to be sent back to Boulder for repairs. The unit is extremely sensitive to power fluctuations and cannot tolerate the SMO powerline variations.

All other SMO meteorological sensors operated routinely.

Precipitation Chemistry

Three collection programs were maintained all year: NADP wet/dry collecting, DOE/EML monthly bulk precipitation sampling, and GMCC daily bulk sampling.

Flask Sampling Programs

During 1983 flask sampling methods were used to investigate three main types of trace gases: CO_2, chlorofluorocarbons, and light hydrocarbons. In addition to GMCC sampling for CO_2 and chlorofluorocarbons, cooperative program flasks were collected for the NCAR TRACS program, OGC, USGS, and SIO. A new cooperative flask program for CO_2 with G. Pearman, CSIRO, will be initiated early in 1984, and will involve filling a pair of flasks each month and sending them to Aspendale, Australia, for analysis of the $^{13}C/^{12}C$ ratio.

Cooperative Programs

One cooperative program was added during March 1983. A SEASPAN Hi-Vol sampler was installed on the GMCC tower at Matatula Point by the principal investigator, J. Prospero, University of Miami, and his assistant, T. Snowden. The SEASPAN network is a Southern Hemisphere complement to the Northern Hemisphere SEAREX Asian dust network.

2.3.3 A Special Tribute

Individuals within GMCC as well as cooperative scientists familiar with SMO operations were surprised and saddened in 1983 by the sudden death of Chief Iuli Togi, the Samoan Matai, with whom NOAA negotiated the original SMO land lease in 1974. Chief Iuli passed away suddenly on 15 September 1983 at his home in Tula village, just hours after returning to Samoa after a lengthy stay in San Francisco. The GMCC presence in Samoa is by definition an alien one, set in a different culture with different customs. The late Chief Iuli Togi was aware of this and took part in helping to bridge the gap between the daily life of Tula village and the high technology of the GMCC operation. The marriage of the village and the GMCC Observatory operation under his guidance was orderly, lasting, and trouble-free. We owe him a debt of gratitude for his understanding, commitment to purpose, and benevolent guidance. A large portion of the success of GMCC at Cape Matatula has been possible because of him.

GMCC is also grateful for the advice and assistance obtained from two Samoans in making the transition to the lease arrangement in effect now. One whose advice and assistance proved invaluable was the American Samoa delegate to the U.S. Congress, Fofo I. F. Sunia. Mr. Sunia was contacted in Washington by the NOAA Congressional Affairs Officer, Joan Barrows, and he provided advice concerning an appropriate NOAA response. Additionally, Mr. Sunia aided NOAA by contacting a second Samoan, High Chief Salanoa S. P. Aumoeualogo, the senior Matai (chief) of Tula village, and received Chief Salanoa's assistance in communicating with the surviving Iuli family members on behalf of GMCC concerning the death.

As a result of efforts by the above individuals, the NOAA response to Chief Iuli's death and funeral was appropriate, assurances were received from the Iuli family and Tula village concerning continuity of the GMCC lease operations in American Samoa, and interim arrangements agreed upon concerning disposition of lease funds during the transition period between Chief Iuli's death and selection of a new chief to hold the Matai title of Iuli.
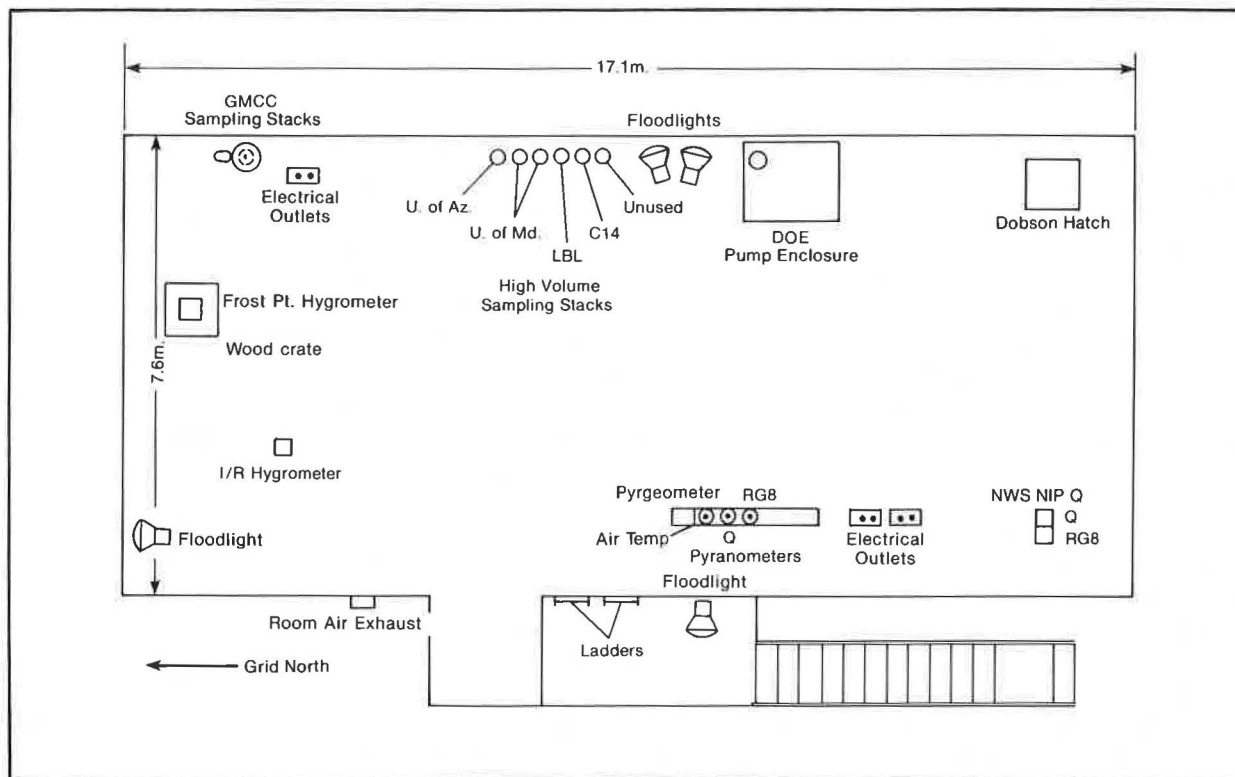
2.4 South Pole

2.4.1 Facilities

SPO continued excellent operation in 1983. Figures 3 and 4 show the current facility layout. The few changes made in the CAF from the previous year include the addition of the frost-point hygrometer and the NCAR gas chromatograph, and some minor modifications and relocations of equipment and storage areas. A high-volume thermostatically controlled blower was installed on the wall near the ICDAS rack, and several room heaters were replaced by larger capacity units. This greatly reduced the interior temperature fluctuations that had plagued the CAF in the past. The ceiling water leakage reported in 1982 was not present this season. Several outlets were added to the roof to facilitate flask sampling. In August, the vestibule was repainted, and new linoleum was laid to correct ice and frost damage.

The sampling stack required removal of internal frost buildup twice. In June, several leaks found on the stack manifold valve stems were repaired with steel-filled epoxy. A long-running problem with back diffusion during periods of high winds was partially corrected by adding a second-stage blower to the stack exhaust. Because the stack air is exhausted into the room, strong winds blowing over the sampling stack create a venturi effect that tends to set up a relative pressure difference between room and outside air, causing contaminated air to diffuse backward up through the stack exhaust. This could be corrected by venting the exhaust to the outside.

Increasingly heavy demand on the station powerplant resulted in 36 brownout-power interruptions. Although no instrument damage resulted, the fluctuations caused ICDAS to crash. Despite these problems, an ICDAS online efficiency of 99.3% was maintained.

Figure 3.--CAF floor plan at SPO, 1983.

Figure 4.--CAF roof plan at SPO, 1983.

2.4.2 Programs

Table 5 lists the 1983 programs, some of which are described below.

Carbon Dioxide

The URAS analyzer operated well all season. In December, a new version of BOSS was implemented to allow ICDAS control of the Q gas. Some data in May and June were affected by the sampling-stack leaks. Replacement of two regulators, the CryoCool unit, numerous dynapumps, and diaphragms was necessary. Flask samples were alternately taken through the analyzer and on the windward edge of the roof. The P^3 sampler was modified from parallel to series flow, and operated well after changing the operating procedure so that the entire unit was preheated indoors prior to going on the roof.

Ozone

Surface ozone and Dobson measurements continued with no major difficulties.

Halocarbons

Halocarbon sampling proceeded with no problems.

Table 5.--Summary of sampling programs at SPO in 1983

Program	Instrument	Sampling frequency	Length of Record
Gases			
CO_2	URAS-2T infrared analyzer	Continuous	Jan 74-present (excl. Nov 78-Nov 79)
	0.5-L glass flasks, P^3	1 pair $(2\ wk)^{-1}$	Jun 81-present
	0.5-L glass flasks, through analyzer	1 pair $(2\ wk)^{-1}$	Nov 79-present
Surface ozone	Dasibi ozone meter	Continuous	Jan 76-present
Total ozone	Dobson spectrophotometer no. 80	3 day^{-1}	Dec 63-present
CFC-11, CFC-12, and N_2O	300-mL stainless steel flasks	1 pair wk^{-1}	Jan 77-Dec 79
		1 pair wk^{-1}, summer; 1 pair mo^{-1}, winter	Jan 80-present
Aerosols			
Condensation nuclei	Pollak CNC	Discrete	Jan 74-present
	G.E. CNC	Continuous	Jan 74-present
Optical properties	Four-wavelength nephelometer	Continuous	Jan 79-Dec 79; Jan 81-present
Aerosol chemistry	Streaker, Cascade impactor	Discrete	Jan-Dec 82
Solar Radiation			
Global spectral irradiance	Eppley pyranometers with Q, OG1, and RG8 filters	Continuous	Feb 74-present; OG1 disc. Mar 83
Direct spectral irradiance	Eppley pyrheliometers with Q and RG8 filters	Continuous	Oct 75-present
	Eppley pyrheliometer with Q, OG1, RG2, and RG8 filters	Discrete	Jan 77-present
Turbidity	Sunphotometers with 380-, 500-, 778-, and 862-nm narrowband filters	Discrete	Jan 74-present
Albedo	Eppley pyranometers with Q, OG1, and RG8 filters	Continuous	Jan 82-present; OG1 disc. Mar 83
Terrestrial (IR) radiation	Eppley pyrgeometer	Continuous	Mar 83-present
Total water vapor	Infrared solar hygrometer	Discrete	Dec 81-Jan 82; Jan 83-Dec 83
Meteorology			
Air temperature	Platinum resistor	Continuous	Mar 77-present
Snow temperature at 1 m	Platinum resistor	Continuous	Mar 77-Apr 83
Snow temperature surface	Platinum resistor	Continuous	Apr 83-present
Room temperature	Platinum resistor	Continuous	Jul 78-present
Dewpoint temperature	General Eastern hygrometer	Continuous	Jan 83-present
Pressure	Capacitance transducer	Continuous	Dec 75-present
	Microbarograph	Continuous	Feb 80-present
	Mercurial barometer	Discrete	Jan 80-present
Wind (speed and direction)	Bendix Aerovane and recorder	Continuous	Dec 75-present
Cooperative Programs			
CO_2, ^{13}C, N_2O (SIO)	5-L evacuated glass flasks	2 mo^{-1} (3 flasks $sample^{-1}$)	1957-present
Total surface particulates (DOE)	High-volume sampler	Continuous (1 filter wk^{-1})	May 70-present
Total surface particulates (EPA)	High-volume sampler	Continuous (1 filter wk^{-1})	May 70-present
Aerosol chemistry (Univ. of Maryland)	High-volume samplers	Continuous	Jan 79-present
Aerosol chemistry (Univ. of Arizona)	High-volume samplers	Continuous	Jan 82-present
Aerosol physical properties (SUNYA)	Pollak CNC with diffusion battery	Discrete	Jan 74-present
	Nuclepore filters	Discrete	Nov 83-present
Carbon aerosol (LBL)	High-volume sampler	Continuous	Jan 82-present
Various trace gases (OGC)	Stainless steel flasks	Twice mo^{-1} (3 flasks set^{-1})	1980-present
$^{13}C/^{12}C$, CH_4 (USGS)	10-L stainless steel cylinder	1 mo^{-1} (2 cylinders $sample^{-1}$)	Jan 81-present
^{14}C (NOAA/ARL)	3,000 psi spheres	500 psi day^{-1}	1972-present
Snow acidity (NOAA/ARL)	125-mL Nalgene flasks	Weekly	1982-present
CH_4, CO (NCAR)	Baseline gas chromatograph	Daily	Apr 83-present
	Aluminum flasks	Weekly	Apr 83-present

19

Surface Aerosols

The Pollak CNC again operated with no major troubles. For the first time at SPO, two complete G.E. CNC's were at the station during the winter period, one online and another as backup. The G.E. CNC experienced all of its traditional problems during the year: air leaks, a flooded casting, valve seizure, sporadic drift in the daily set zero adjustment, PMT replacement, and two instances of circuit failure. Despite this, the instrument was kept running all year and yielded one of the most complete records to date.

The nephelometer operated with no major problems all season. Occasionally, a power brownout caused all four channels to drop to zero. A procedure was developed that allowed these to be reestablished at their previous levels, saving hours or days of lost data that formerly occurred when the instrument recovered on its own.

Solar Radiation

Two instruments were installed for the first time at SPO. In late summer, a solar infrared hygrometer was used to make discrete observations of the total slant-path water vapor content. Three months of data were returned before sunset. Beginning in March, a pyrgeometer and two temperature sensors were added to measure terrestrial IR radiation. The OG1 upward-facing and albedo pyranometers were discontinued at this time. A second Q pyrheliometer was installed to begin comparisons with the existing Q pyrheliometer. In December 1982, solar radiation intercalibrations were made by D. Nelson. Because of equipment failure, the discrete albedo program was discontinued. The old Voltz turbidity meter was replaced by the newer J-series dual-wavelength model.

Meteorology

A General Eastern dew-frost-point hygrometer was installed. During the winter months, it frequently became clogged with ice crystals and had to be brought indoors for cleaning. This problem was solved by enclosing the instrument in a wooden crate. All meteorological instruments operated normally with the exception of the wind direction component, in which a loose servo shaft coupling in the Aerovane was responsible for a 4-mo interval of questionable data before the problem was isolated and solved. Systematic differences between GMCC and station meteorology office parameters, which have been present for several years, were documented.

ICDAS

ICDAS operated exceptionally well all year, with an online efficiency of 99.3%. All failures were caused by station brownouts, and the NOVA computer was brought up quickly in most cases with no trouble.

Cooperative Programs

All programs operated without incident with the following exceptions:
The PISSA, which shuts off sampling pumps when the wind comes from outside the clean air sector or is calm, failed in February, and was operated in a manual mode until July. It was then repaired by a modification that allowed it to

work without the faulty relay for which there was no replacement. The ^{14}C sphere shipments arrived with damaged containers due to cold weather and rough handling. The 3000-psi-charged spheres were packed in vermiculite to avoid danger of an accidental breakage in shipment. Cascade and streaker filter programs were discontinued.

A major new program this season was the NCAR gas chromatograph, used to measure CH_4 and CO. Numerous problems were encountered in initiating the program. A valve damaged in shipment was overhauled. The hydrogen generator performed sporadically for the entire year, and problems maintaining instrument temperatures resulted in poor CO data. Nevertheless, usable CH_4 data were obtained, and the program is continuing for the 1983-1984 season.

3. CONTINUING GMCC PROGRAMS

3.1 Carbon Dioxide

3.1.1 Continuous CO_2 Measurements

In the GMCC program, 1983 was a milestone year for continuous measurement of atmospheric CO_2 by in situ NDIR analyzers. BRW has now produced a 10-yr continuous record and began a second decade of measurements in July 1983. The somewhat younger CO_2 programs at MLO, SMO, and SPO also continued in 1983, and within 3 years, each of these will attain 10 years of continuous CO_2 records. The methods of analysis, data acquisition, and preliminary processing have been described in preceding GMCC Summary Reports (Peterson, 1978, pp. 20-25; Mendonca, 1979, pp. 16-23). Provisional daily CO_2 concentrations from the four observatories through 1982 are archived with WMO.

The record from each observatory has now been processed to final values; however, the difficult procedure of selecting the data for background conditions has not been completed. When the selection is final, separate reports examining the continuous CO_2 record at each station will be made available. The monthly means in fig. 5 and table 6 reflect the current state of selection of the data and are therefore provisional.

This year a two-part, in-depth comparison was begun of the GMCC continuous CO_2 program at MLO with that of C.D. Keeling of SIO. The first part consisted of a comparison of monthly means, calculated using hourly data determined by SIO to be background, for the period May 1974-December 1983. This data comparison was followed by a field experiment in which the effects of analyzers, air lines, pumps, freezeout traps, etc., in each system were examined. A more detailed discussion of the methods and results of this comparison is given in sec. 4.12.
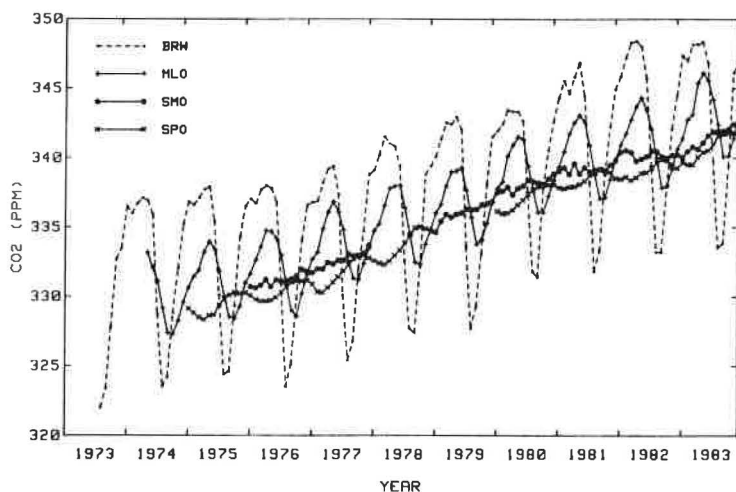

Figure 5.--Provisional selected monthly mean CO_2 concentrations from continuous measurements at BRW, MLO, SMO, and SPO. Values are in ppm with respect to dry air (X81 mole fraction scale).

Table 6.--Provisional selected monthly and annual mean CO_2
concentrations (ppm relative to dry air--X81 mole fraction scale)
for continuous measurements at BRW, MLO, SMO, and SPO

Year	Jan	Feb	Mar	Apr	May	Jun	Jul	Aug	Sep	Oct	Nov	Dec	Annual mean
BRW													
1973	--	--	--	--	--	--	--	322.0	323.4	327.8	332.7	333.5	--
1974	336.5	336.0	336.7	337.1	336.9	335.9	328.7	323.5	324.2	328.8	332.0	335.2	332.6
1975	336.8	336.6	337.1	337.7	337.9	335.4	330.1	324.4	324.6	329.3	334.3	336.5	333.4
1976	337.0	336.7	337.7	338.0	337.8	336.8	331.0	323.5	325.1	329.8	334.1	336.6	333.7
1977	336.8	336.9	338.2	339.2	339.4	337.4	330.1	325.4	326.8	332.0	334.7	338.8	334.6
1978	339.1	340.2	341.5	341.0	340.8	339.4	332.6	327.7	327.4	332.1	338.8	339.4	336.7
1979	340.1	341.3	342.5	342.4	342.9	342.0	333.6	327.7	329.3	333.1	338.1	341.5	337.9
1980	341.9	342.4	343.4	343.3	343.3	342.6	337.3	331.8	331.4	337.9	340.5	342.6	339.9
1981	344.3	345.5	344.6	345.8	346.8	344.4	338.2	331.8	333.3	338.8	342.2	344.9	341.7
1982	345.8	347.2	348.3	348.4	348.0	345.7	339.2	333.2	333.2	337.9	342.1	344.5	342.8
1983	347.4	347.0	348.2	348.2	348.3	346.8	339.8	333.6	333.8	339.4	346.1	346.9	343.8
MLO													
1974	--	--	--	--	333.1	332.1	331.1	329.1	327.4	327.3	328.2	329.6	--
1975	330.6	331.4	331.9	333.2	333.9	333.4	331.9	330.0	328.5	328.4	329.3	331.0	331.1
1976	331.6	332.6	333.6	334.7	334.7	334.2	333.0	330.8	329.0	328.6	330.2	331.6	332.0
1977	332.7	333.2	334.9	336.1	336.8	336.1	334.8	332.6	331.3	331.2	332.4	333.5	333.8
1978	334.7	335.2	336.5	337.8	338.0	338.0	336.4	334.5	332.5	332.3	333.8	334.8	335.4
1979	336.0	336.6	337.9	339.0	339.1	339.3	337.6	335.7	333.8	334.1	335.3	336.8	336.8
1980	337.8	338.3	340.1	340.9	341.5	341.3	339.4	337.7	336.1	336.1	337.2	338.4	338.7
1981	339.3	340.4	341.7	342.5	343.0	342.5	340.9	338.8	337.1	337.1	338.5	339.9	340.1
1982	340.9	341.7	342.7	343.7	344.3	343.4	342.0	340.0	337.8	338.0	339.2	340.6	341.2
1983	341.4	342.7	343.1	345.4	346.1	345.6	344.2	342.4	340.1	340.1	341.4	343.1	343.0
SMO													
1976	330.7*	330.6*	330.8	331.2	330.7	331.2	331.1	331.1	331.3	331.5	331.9	331.8	331.2
1977	331.7	332.0	332.0	332.4	332.3	332.6	332.6	333.1	332.9	332.9*	333.1*	333.7*	332.6
1978	--	--	--	--	--	--	--	--	--	--	--	--	--
1979	334.6*	335.4*	335.9*	335.7	335.9	336.0	336.3	336.3	336.3	336.6	336.7	336.8	336.1
1980	337.5	337.6	337.9	337.3	337.8	338.0	338.4	338.3	338.2	338.1	338.5	338.9	338.0
1981	339.0	339.3	338.8	339.6	338.8	339.3	339.0	339.1	339.2	339.0	339.5	339.8	339.2
1992	340.4	340.5	340.4	339.8	339.9	340.1	340.5	340.4	340.1	340.0	340.2	340.2	340.2
1983	340.0	340.5	340.8	340.6	341.1	341.6	341.9	341.9	341.9	342.1	342.4	342.6	341.4
SPO													
1975	329.1	328.8	328.5	328.3	328.6	328.6	329.4	329.8	330.1	330.3	330.2	330.3	329.3
1976	330.1	329.8	329.6	329.6	329.7	329.9	330.3	330.7	331.0	331.1	331.1	331.1	330.3
1977	330.9	330.3	330.3	330.6	331.0	331.4	331.8	332.2	332.7	333.0	333.0	332.7	331.7
1978	332.6	332.4	332.3	332.5	333.0	333.3	333.8	334.4	334.9	335.0	334.9	334.7*	333.7
1979	--	--	--	--	--	--	--	--	--	--	--	--	--
1980	336.1	336.0	336.0	336.2	336.6	336.9	337.4	337.7	337.9	338.1	338.0	338.0	337.1
1981	337.8	337.8	337.9	337.9	338.1	338.3	338.7	339.0	339.2	339.1	338.9	338.5	338.4
1982	338.5	338.6*	338.4	338.6	338.9	338.9	339.2	339.6	339.9	339.8	339.5	339.2	339.1
1983	339.7	339.5	339.5	340.0	340.4*	340.5	341.0	341.6	341.7	341.8	341.8	341.7	340.8

*Substituted flask data.

The in-house calibration of working gases for the observatories and the
flask sample analysis program continued in 1983. One hundred sixty-eight tank
calibrations were performed. All calibrations are traceable to GMCC secondary
standards calibrated manometrically by C.D. Keeling at SIO. These standards
were calibrated in 1982 and are due for calibration again in late 1984.

An experiment with new technology began in 1983 with the acquisition of
two gas chromatographs custom built by R. Weiss of SIO (Weiss, 1981). These
instruments are designed for measuring CO_2 with a precision comparable with

the NDIR analyzers (~0.1%). After initial testing in Boulder, a GC will be installed at MLO in 1984 to begin a program of CO_2 monitoring for comparison with the NDIR system. A primary advantage of the gas chromatographs is the decrease in the rate of reference gas usage; a single tank will last a year or more compared with 3-4 months with an NDIR. In addition, the gas chromatograph is capable of measuring CH_4, a trace gas with possible climatic significance.

3.1.2 Flask Sample CO_2 Measurements

The CO_2 flask sampling network (see fig. 6) consists of 22 globally distributed sites, at which whole air samples are collected in 500 cm^3 glass flasks once or twice per week for subsequent analysis in Boulder. The first year of sampling for three new stations (HBA, NZL, and KPA; see table 7) was completed in 1983. Although sampling at HBA began in December 1982, the flasks will not arrive in Boulder for analysis until the summer of 1984 because of the inaccessibility and complicated logistics associated with Antarctic research programs. Indications are that the NZL site, intended as a replacement for the Falkland Islands site, which has been inoperative since the war of February 1982, is not ideally suited for measurement of background CO_2. This is due to its location downwind of Christchurch and its proximity to vegetated and agricultural areas. Current plans are to begin flask sampling at Cape Grim, Tasmania, in 1984 to sample background air at midlatitudes of the Southern Hemisphere. This cooperative project with CSIRO will also provide a basis for intercomparisons between GMCC and another of the major CO_2 monitoring laboratories. The stations collecting samples in 1983 are listed in table 7. A WMO report giving detailed descriptions of the sampling sites is currently in preparation.

In 1983 some 5600 flasks were analyzed, of which ~3500 were from the flask network. The remainder were special project samples (e.g., cruises, aircraft experiments) and test flasks run to monitor analyzer performance. All flasks were analyzed on the semiautomatic flask analysis system in Boulder (Komhyr et al., 1983b). The only modification to the system was a new gas transfer pump that was installed in August 1983. This modification may reduce or eliminate a flask analyzer bias correction that has been applied to the
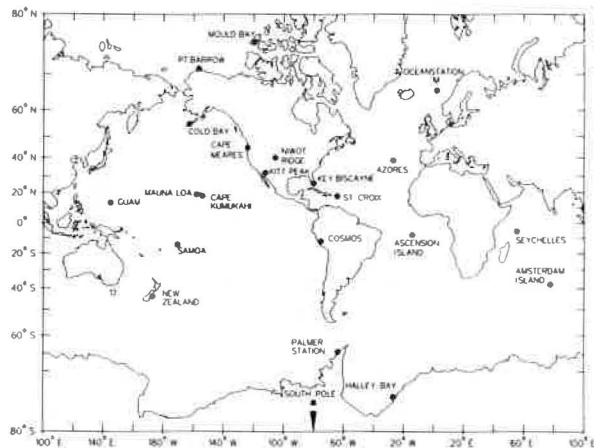

Figure 6.--Map showing the locations of the sampling sites in the GMCC CO_2 flask sampling network during 1983.

Table 7.--GMCC CO_2 flask network sampling sites during 1983

Code	Station	Latitude (deg)	Longitude (deg)	Elevation (m)
AMS	Amsterdam I.	37.95S	77.53E	150
ACS	Ascension I.	7.92S	14.42W	54
AVI	St. Croix, VI	17.75N	64.75W	3
AZR	Terceira I., Azores	38.75N	27.08W	30
BRW	Barrow, AK	71.32N	156.60W	11
CBA	Cold Bay, AK	55.20N	162.72W	25
CMO	Cape Meares, OR	45.00N	124.00W	30
COS	Cosmos, Peru	12.12S	75.33W	4600
GMI	Guam, Mariana Is.	13.43N	144.78E	2
HBA	Halley Bay, Ant.	75.00S	27.00W	0
KEY	Key Biscayne, FL	25.67N	80.17W	3
KPA	Kitt Peak, AZ	32.00N	112.00W	2095
KUM	Cape Kumukahi, HI	19.52N	154.82W	3
MBC	Mould Bay, Canada	76.23N	119.33W	15
MLO	Mauna Loa, HI	19.53N	155.58W	3397
NWR	Niwot Ridge, CO	40.05N	105.63W	3749
NZL	New Zealand	43.83S	172.63E	3
PSA	Palmer Station, Ant.	64.92S	64.00W	10
SEY	Mahé I., Seychelles	4.67S	55.17E	3
SMO	Cape Matatula, Am. Samoa	14.25S	170.57W	30
SPO	South Pole, Ant.	89.98S	24.80W	2810
STM	Station M	66.00N	2.00E	0

1980-1982 flask data. The bias was believed to be caused by a slight (~0.25 ppm) absorption of CO_2 in the original transfer pump (Komhyr et al., 1984a). Another change in methodology was an improved testing procedure whereby each flask was checked for leaks between analysis and return to the field. This procedure appears to be effective in reducing the number of samples contaminated by stopcock failure. Also in 1983 tests were begun on 3-L O-ring stopcock flasks as a possible replacement for the greased, ground-glass-type stopcock.

The flask analysis procedure was further modified in April 1983 with the inception of a GMCC-CSIRO-OGC cooperative program to measure by gas chromatography the CH_4 in flasks from the GMCC CO_2 network. Initial tests demonstrated the feasibility of using the overpressure in P^3-collected samples to inject two sample aliquots into the GC without contaminating the remaining sample prior to NDIR analysis. The standard procedure now is to analyze one member of each flask pair for CH_4, then recombine the pair for NDIR CO_2 analysis. A global atmospheric CH_4 distribution analogous to that now available for CO_2 should prove quite valuable in understanding the global carbon cycle. The CH_4 program is discussed in sec. 5.15.

The complete flask CO_2 data set for 1968-1982 has been processed into final concentrations this year, and the data have been archived with WMO,

WDC-A, and DOE/CDIC. Processing to final concentrations included (1) analyz-
ing for systematic errors and, when the errors could be quantified (e.g.,
pressure broadening effect, nonlinearity), making appropriate corrections;
(2) determining drift-corrected, X81 mole fraction scale CO_2 concentrations
for all tanks used for flask analysis and recalculating each sample concen-
tration using the final tank values; (3) deleting samples that were defective
because of sampling error or instrument malfunction during analysis. The
final data set was then examined and a subset of the data considered represent-
ative of background air was selected. Details of the data processing and
selection, and an analysis of the final 1968-1982 CO_2 flask data set are given
by Komhyr et al. (1984a).

In table 8 the annual mean CO_2 concentrations for the flask sites are
given, including preliminary values for 1983. A convenient way to display the
global distribution of atmospheric CO_2 concentration as determined by the GMCC
flask network is the zonally averaged CO_2-latitude-DOY surface shown in
fig. 7. The smoothness of the surface is obtained by first selecting a back-
ground subset that includes ~85% of the total data set. Cubic spline functions
are then fit to the data, and the spline functions become the input for gener-
ating the surface. Since the intent is to create a smooth surface, continental
and high-altitude sites (except SPO) and sites indicating strong longitudinal
gradients have not been included. Despite all the smoothing, the surface and
companion two-dimensional contour plot (fig. 8) are a powerful way to convey
the main features of the seasonality and latitude dependence of atmospheric
CO_2 on a global scale. Flask sampling programs carried out on ships in remote
regions have generally supported both the accuracy of the surface and the
representativeness of the flask network sites (Harris and Bodhaine, 1983,
pp. 99-102; this report, sec. 4.11).

One objective of the CO_2 monitoring program is to document the increase
in atmospheric CO_2 due primarily to the burning of fossil fuels. A detailed
discussion of the variation of the rate of increase over space and time based
on the 1968-1982 flask network data is given by Komhyr et al. (1984a). With

Table 8.--Annual mean atmospheric CO_2 concentrations (ppm relative to
dry air--X81 mole fraction scale) for the flask network sites

Station	1968	1969	1970	1971	1972	1973	1974	1975	1976	1977	1978	1979	1980	1981	1982	1983
AMS	0	0	0	0	0	0	0	0	0	0	0	(335.9)	337.8	339.3	339.4	[340.9]
ASC	0	0	0	0	0	0	0	0	0	0	0	[337.3]	338.8	339.7	340.7	342.6
AVI	0	0	0	0	0	0	0	0	0	0	0	337.1	339.6	340.4	340.9	342.0
AZR	0	0	0	0	0	0	0	0	0	0	0	0	338.4	339.6	341.2	343.0
BRW	0	0	0	327.4	330.2	332.0	333.4	333.0	333.9	335.0	336.6	337.7	340.2	341.5	342.7	344.0
CBA	0	0	0	0	0	0	0	0	0	0	0	337.8	339.8	341.3	341.9	343.4
CMO	0	0	0	0	0	0	0	0	0	0	0	0	0	0	341.2	342.9
FLK	0	0	0	0	0	0	0	0	0	0	0	0	0	339.7	0	0
GMI	0	0	0	0	0	0	0	0	0	0	0	337.7	340.0	341.2	341.0	342.7
KEY	0	0	0	0	0	330.7	[333.4]	0	332.7	335.2	336.7	338.8	(340.2)	342.0	341.6	343.4
KUM	0	0	0	0	0	0	0	0	332.3	334.4	335.7	337.4	339.3	340.4	341.2	342.5
MBC	0	0	0	0	0	0	0	0	0	0	0	0	340.3	341.9	342.5	343.7
MKO	0	0	0	0	0	0	0	0	0	0	0	337.3	0	0	0	0
MLO	0	[322.8]	325.2	0	0	0	0	0	332.1	333.6	335.2	336.7	338.9	340.4	341.0	342.5
NWR	323.1	324.1	325.6	325.2	326.3	330.2	[334.0]	0	332.1	334.8	335.7	337.0	338.1	339.9	340.9	342.4
PSA	0	0	0	0	0	0	0	0	0	0	333.9	335.2	(337.5)	340.0	339.8	341.0
SEY	0	0	0	0	0	0	0	0	0	0	0	0	339.3	340.1	340.5	340.8
SMO	0	0	0	0	0	[330.2]	330.8	330.7	331.5	332.8	334.3	336.0	338.1	339.3	340.4	341.4
SPO	0	0	0	0	0	0	0	329.4	330.2	331.5	333.7	335.5	336.7	338.5	339.3	340.8
STC	0	324.0	326.4	326.9	327.6	0	0	0	0	0	0	0	0	0	0	0
STM	0	0	0	0	0	0	0	0	0	0	0	0	0	341.9	341.7	342.7

Note: ( ) = number of interpolated points ≥ one-half of total number of points; [ ] = incomplete year.
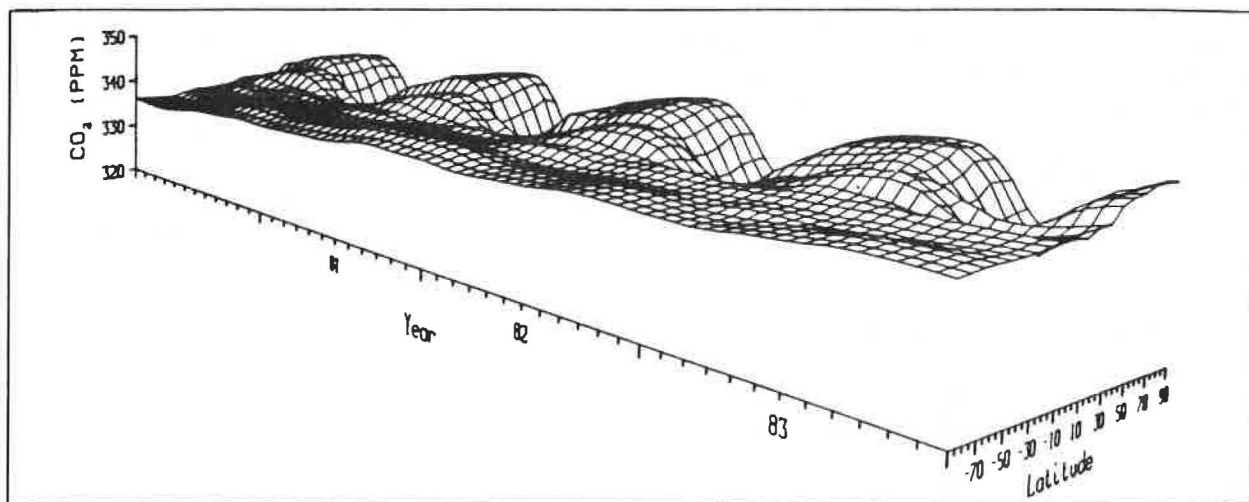
26

Figure 7.--A three-dimensional representation of the variation in space and time of atmospheric CO_2 at the surface, synthesized from the flask network measurements for 1980-1983. The resolution of the zonally averaged surface is 20 days and 10° latitude. The Northern Hemisphere is dominated by the seasonal biospheric cycle.

the addition of the 1983 flask and continuous analyzer data to the record, an interesting anomaly in the growth rate trend has emerged. From 1976 to 1981 both the flask and continuous analyzer records show a mean growth rate of 1.6 ppm yr^{-1}. From 1981 to 1982 the growth rate drops to 1.0 ppm yr^{-1} for the continuous analyzer data and 0.6 ppm yr^{-1} for the flask data. This drop is followed by a return to a higher value for 1982-1983 of 1.4 ppm yr^{-1} for both the flask and continuous data. Since this sharp decrease in the CO_2 growth rate is not paralleled by a similar decrease in fossil fuel production (Rotty and Marland, 1984), it is probably indicative of a major perturbation of the natural global carbon cycle. For a discussion of the possible connection of this growth rate anomaly with the intense ENSO event of 1982-1983, see sec. 4.13.

From tables 6 and 8 it is possible to compare the continuous analyzer and flask annual means at the four GMCC baseline observatories. For 1976-1983 the mean differences are 0.1 ± 0.2, -0.1 ± 0.2, 0.1 ± 0.2, and 0.0 ± 0.2 ppm for BRW, MLO, SMO, and SPO respectively. This agreement is quite good considering the differences in sampling methodology and analysis and the differences in selection procedures applied to each data set.
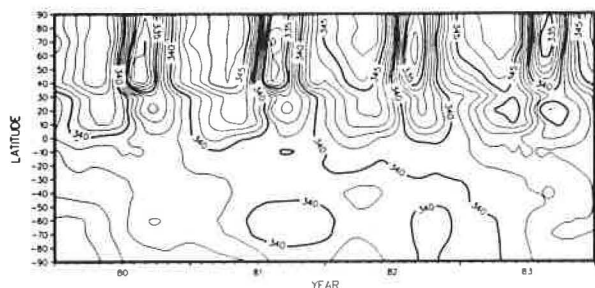
Figure 8.--The surface of fig. 7, shown as contours in the latitude-time plane. Note the slight increase from 1981 to 1982 compared with that from 1980 to 1981.

27

The quality of the CO_2 flask data is further monitored through an ongoing exchange of data for flasks collected quasi-similtaneously by GMCC and SIO at BRW, KUM, MLO, and SMO (Bodhaine and Harris, 1982, p. 27; Harris and Bodhaine, 1983, p. 31). Figure 9 presents the comparison data through the end of 1983. In general, the agreement is good; the mean difference for 506 samples is 0.0 ± 0.5 ppm. SMO shows the most scatter, which may be related to the high moisture content of the samples collected there. It can be concluded that if any systematic difference exists between the GMCC and SIO flask programs, it is not larger than 0.2-0.3 ppm.
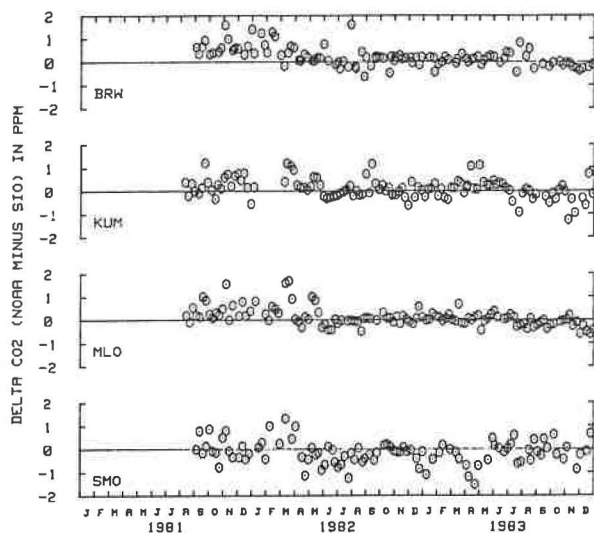
Figure 9.--Differences between the atmospheric CO_2 concentrations in quasi- simultaneously collected flask samples as measured by NOAA/GMCC (0.5-L flasks) and SIO (5.0-L flasks).

3.2   Total Ozone

3.2.1   Routine Observing Program

Routine total ozone observations were continued in 1983 at three GMCC stations, one foreign cooperative station, two domestic cooperative stations, three NWS stations, and GMCC headquarters, Boulder. On 22 June 1983 a fourth NWS station was put into operation at Fresno, CA.

Table 9 lists the 11 stations of the U.S. Dobson ozone spectrophotometer network, the periods of record when observations were made, the instrument numbers, and the agencies responsible for taking the observations.

In November 1983 an automated Dobson instrument was installed at Poker Flat, AK. Because of the low elevation angle of the Sun, no observations were made during the rest of the year. Plans are to begin the automatic Umkehr observations and total ozone observations at this station in early February 1984.

The standard lamp technique of checking Dobson spectrophotometers for gross calibration errors is based on experimental observations that instruments accurately calibrated on relative and absolute scales yield standard lamp readings:

$$N = \log (I/I') + K$$

28

Table 9.--U.S. Dobson ozone spectrophotometer station network, 1983

Station	Period of record	Inst. no.	Agency
Bismarck, ND	01 Jan 1963-present	33	NOAA
Caribou, ME	01 Jan 1963-present	34	NOAA
Wallops I., VA	01 Jul 1967-present	38	NOAA; NASA
SMO	19 Dec 1975-present	42	NOAA
Tallahassee, FL	02 Jun 1973-present	58	NOAA; Fla. State Univ.
Boulder, CO	01 Sep 1966-present	61	NOAA
MLO	02 Jan 1964-present	65	NOAA
Nashville, TN	01 Jan 1963-present	79	NOAA
SPO	17 Nov 1961-present	80	NOAA
Huancayo, Peru	14 Feb 1964-present	91	NOAA; Huancayo Obs.
Fresno, CA	22 Jun 1983-present	94	NOAA

at the A, B, C, and D Dobson instrument wavelength pairs that are essentially constant provided, also, that the internal light-scattering characteristics of the instruments are similar. (In the above equation, I/I' is the lamp light intensity ratio for, say, the A wavelength pair, and K is an associated instrumental constant.) Mean absolute calibration error for such instruments, calibrated with standard lamps, is estimated to be ±1.5% at the 95% confidence interval. This error is about twice as large as that which occurs when spectrophotometers are calibrated by direct comparison of instruments. Thus, use of standard lamps for calibrating spectrophotometers on an absolute scale is not generally recommended.

Accurate relative calibration of Dobson spectrophotometers implies accurate optical wedge and wavelength-setting calibrations for the instruments. An instrument with an improperly calibrated optical wedge will, for example, yield wrong N values in most instances for a standard lamp whose N values have been correctly determined. Because only a limited portion of the optical wedge is used when a standard lamp test is performed, the calibration error determined from correct and observed N-value differences is not, in general, representative of the instrument as a whole. Thus, it is important that spectrophotometer calibration errors determined from tests with standard lamps not be used for correcting ozone data obtained in the past with the improperly calibrated instruments. At most, the lamp tests indicate that an instrument calibration problem exists, and that remedial action is required.

3.2.2 Calibration Checks on Dobson Instruments in the Global Network

Calibrated standard lamps were sent to 87 Dobson spectrophotometer observatories during 1981-1983 to check on the calibration level of Dobson instruments in the global total ozone station network (Grass and Komhyr, 1984). Data received from 77 stations (table 10) indicated that 21 instruments required recalibration. As a result of this effort, arrangements are under way to conduct international comparisons of Dobson instruments in Melbourne, Australia, in 1984. Participating countries will be Australia, India, and Japan.

29

Table 10.--Results of calibration checks on Dobson spectrophotometers
using traveling standard lamps

Station	Inst. no.	Date of calib. check	Instr. calib. error (%)*
Region 1--North America			
Toronto, Canada	77	811015	-0.15
Resolute, Canada	59	811211	-0.74
Churchill, Canada	60	820101	+1.62
Goose Bay, Canada	62	810511	+0.00
Edmonton, Canada	102	811130	+0.08
Reykjavík, Iceland	50	820323	+0.44
SPO	80	820125	+1.32
Bismark, ND	33	820715	+0.88
Caribou, ME	34	820602	-1.25
Wallops I., VA	38	820617	-0.96
Tallahassee, FL	58	821001	+0.88
Nashville, TN	79	820927	+1.18
MLO	63	820602	-1.25
SMO	42	820828	+0.81
BRW	76	820429	+1.62
Boulder, CO	61	820602	-0.37
Boulder, CO	82	820709	+0.30
Region 2--South America			
Mexico City, Mexico	98	811030	+1.32
Huancayo, Peru	87	820418	-4.84
Cachoeira Paulista, Brazil	114	821021	-3.67
Natal, Brazil	93	820909	+0.73
Buenos Aires, Argentina	97	830120	-0.15
Buenos Aires, Argentina	99	830314	-0.07
Region 3--Western Europe (1)			
Bracknell, U.K.	41	820622	-0.15
Bracknell, U.K.	2	820622	+0.59
Halley Bay, U.K.	31	--	--
Argentine Is., U.K.	73	--	--
Seychelles, Seychelles	57	--	--
St. Helena I., U.K.	35	--	--
King Edward VII Point, U.K.	103	--	--
Lerwick, U.K.	32	820707	+2.13
Arosa, Switzerland	15	821108	-0.88
Arosa, Switzerland	101	821108	-0.08
Hohenpeissenberg, F.R.G.	104	821130	-6.10
Cologne, F.R.G.	44	--	--
Oslo, Norway	8	830408	-0.96
Oslo, Norway	56	830411	-0.29
Tromsø, Norway	14	830408	-1.17
Region 4--Western Europe (2)			
Aarhus, Denmark	92	810610	+0.74
Uccle, Belgium	40	811027	+1.25
Biscarrosse, France	11	82----	-2.42
Magny-Les-Hameaux, France	85	820502	+1.98
Lisbon, Portugal	13	820422	-0.07
El Arenosillo, Spain	120	82----	+0.66
Vigna Di Valle, Italy	47	821213	+0.44

Table 10.--Results of calibration checks on Dobson spectrophotometers
using traveling standard lamps--Continued

Station	Inst. no.	Date of calib. check	Instr. calib. error (%)*
Region 4--Western Europe (2)--Cont.			
Brindisi, Italy	46	821227	+3.30
Sestola, Italy	48	830110	-0.08
Cagliari/Elmas, Italy	113	821221	-1.25
Casablanca, Morocco	106	830602	--
Cairo, Egypt	69	840309	-1.47
Cairo, Egypt	96	840310	+0.52
Region 5--Eastern Europe, U.S.S.R.			
Leningrad, U.S.S.R	108	811022	+0.29
Belsk, Poland	84	820107	+1.32
Hradec Kralové, Czechoslovakia	74	820204	-3.30
Budapest-Lorinc, Hungary	110	820103	-3.52
Bucharest, Romania	121	820420	+3.30
Potsdam, G.D.R.	71	8205--	+0.59
Potsdam, G.D.R.	64	8205--	-0.44
Region 6--India			
New Delhi, India	36	82----	-0.44
New Delhi, India	112	82----	-1.47
Srinagar, India	10	82----	+1.76
Varanasi, India	55	82----	-1.62
Mt. Abu, India	54	82----	+2.27
Poona, India	39	82----	+0.44
Kodaikanal, India	45	82----	+2.57
Quetta, Pakistan	43	--	--
Quetta, Pakistan	100	830408	+1.91
Bangkok, Thailand	90	830610	+10.79
Singapore (U.K.)	7	--	--
Manila, Philippines	52	831101	-1.25
Region 7--Australia, Japan			
Sapporo, Japan	5702	820105	-0.44
Sapporo, Japan	5703	820106	-0.44
Kagoshima, Japan	5704	811210	+4.55
Tateno, Japan	116	811120	+3.08
Tateno, Japan	122	811120	+3.37
Tateno, Japan	5706	811124	+1.32
Naha/Kagamizu, Japan	5705	811221	-3.52
Shiangher, China	75	820330	+0.15
K´un-ming, China	3	820413	-2.05
Aspendale, Australia	105	820906	+0.59
Aspendale, Australia	115	820618	+0.15
Perth, Australia	111	820817	-8.95
Cairns, Australia	81	820713	+6.60
Brisbane, Australia	6	820715	-4.11
Hobart, Australia	12	820705	-8.80
McQuarie Island, Australia	78	821028	-0.29
Invercargill, New Zealand	17	830303	+0.15

*See text for significance of calibration errors. Positive error means
that instrument yields ozone values that are too large.

3.2.3 Modernization and Calibration of Dobson Spectrophotometers

During 1983, GMCC personnel continued to participate in the WMO Global
Ozone Research and Monitoring Project to upgrade the quality of Dobson ozone
spectrophotometers throughout the world. Table 11 lists the instruments that
were reconditioned and calibrated.

All instruments in table 11, except the one in Bangkok, Thailand, have
been automated for Umkehr observations and semiautomated for total ozone
observations. A Dobson instrument is now in operation at Haute Provence Ob-
servatory in France. Instrument 63 has been installed at Poker Flat, AK.
Instruments 76, 87, 81, and 72 will be installed in 1984 at MLO, HI; Huan-
cayo, Peru; Perth, Australia; and Pretoria, South Africa; respectively.

Table 11.--Dobson instruments modernized and calibrated during 1983

Station	Instrument number
Bangkok, Thailand	90
Haute Provence, France	85
MLO	63
Hauncayo, Peru	87
Boulder, CO	76
Boulder, CO	72

3.2.4 Data

Daily 1983 total ozone amounts (applicable to local apparent noon at each
station) for all stations in the U.S. network have been submitted for publica-
tion by the World Ozone Data Centre, Atmospheric Environment Service,
4905 Dufferin Street, Downsview, Ontario M3H5T4, Canada, in Ozone Data for the
World. Table 12 lists provisional monthly mean 1983 total ozone amounts for
the NOAA observatories and cooperative stations.

3.2.5 Data Analysis

Total ozone values at MLO during late 1982 and early 1983 were unusually
low compared with most previous years, and the possibility was considered that
partial destruction of ozone may have occurred by stratospheric aerosols from
the eruption of El Chichon volcano in late March-early April 1982 (Komhyr et
al., 1984c). Although a small amount of ozone depletion by the aerosols
cannot be ruled out, the major effect appears to be a temporary natural ozone
decrease associated with the stratospheric quasi-biennial oscillation
phenomenon. Figure 10 is a plot of the 12-mo running means of total ozone

Table 12.--Provisional 1983 monthly mean total ozone amounts (milli-atm-cm)

Station	Jan	Feb	Mar	Apr	May	Jun	Jul	Aug	Sep	Oct	Nov	Dec
Bismarck, ND	328	352	381	395	380	338	305	295	301	291	296	348
Caribou, ME	341	367	384	385	380	355	346	332	304	302	310	341
Wallops I., VA	325	327	353	370	349	340	326	314	303	300	284	292
SMO	264	256	257	263	260	265	264	265	266	272	274	261
Tallahassee, FL	284	291	306	318	323	328	--	--	303	294	279	282
Boulder, CO	305	317	356	372	357	321	314	291	292	277	282	338
MLO	225	236	249	276	277	283	271	268	266	261	255	257
Nashville, TN	316	334	349	384	361	352	338	337	315	305	292	320
Huancayo, Peru	256	258	254	253	251	251	259	261	265	265	260	260
Fresno, CA	--	--	--	--	--	326	316	311	299	282	276	296
SPO	309	312	--	--	--	--	--	--	--	--	311	--

data for MLO since 1958. The 12-mo filter removes the annual cycle from the data and reveals the prominent quasi-biennial oscillation as well as longer period variations in ozone shown in the figure. Note that a minimum occurred in the quasi-biennial ozone oscillation in early 1983. Ozonesonde observations at Hilo, HI (sec. 3.3) in December 1982 and December 1983 showed the atmospheric region of reduced ozone to be above the ozone maximum. The lower ozone amounts probably resulted from stratospheric circulation changes and associated changes in ozone transport, of which the quasi-biennial oscillation in ozone is a manifestation.

A longer period variation in ozone is clearly evident in fig. 10, and the decrease in ozone at MLO since 1970 is about 3% per decade. Whether this decrease in ozone is due to ozone depletion by chlorofluorocarbons, or the result of a long-term variation in the strength of the stratospheric circulation between equatorial and polar regions (associated, for example, with solar intensity variation) is unknown.
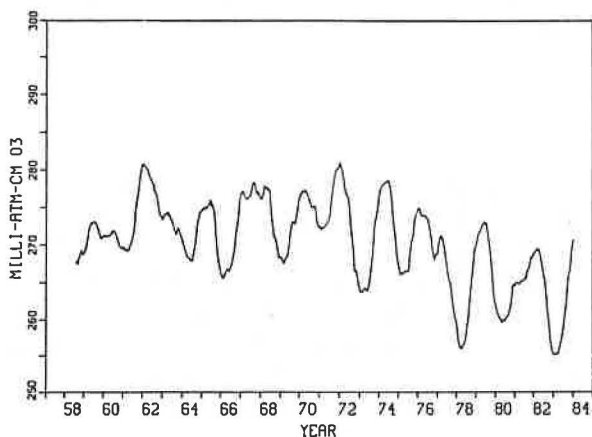
Figure 10.--The 12-mo running means of total ozone data for MLO.

3.3 Ozone Vertical Distribution

3.3.1 Umkehr and Ozonesonde Observations at MLO Following the Eruption of El Chichon Volcano

A classic set of Umkehr data obtained at MLO since 17 May 1982, following the eruption of El Chichon volcano in late March-early April 1982, has illustrated dramatically the adverse effects of stratospheric aerosols on Umkehr observations. To aid in interpretation and processing of the Umkehr data, and to obtain ozone profile data for comparison with satellite ozone measurements, a program of weekly balloon ozone soundings was begun in Hilo, HI, in September 1982 and continued throughout 1983.

The Umkehr observations were made with specially calibrated Dobson instrument 65. On the average, 10 observations were made per month during May-December 1982; 11 per month during 1983; and 7 per month during January-March 1984. Measured apparent changes in ozone per year, in standard and short Umkehr layers 1-9, are plotted month by month in fig. 11. The ozone changes are expressed in percent relative to the ozone amounts present during the months indicated on the plots. (For example, the May 1982 ozone value minus the May 1983 value, expressed in percent, is plotted for May 1983.) This method of data presentation not only eliminates annual cycle ozone variations, but it focuses on errors in the ozone measurements due to aerosols, assuming that the aerosol error effect became markedly diminished 1 year after the eruption of El Chichon. Evidence for substantial clearing of the stratosphere from May 1982 to early 1983 is available from optical photometry at MLO, indicating that the stratospheric aerosol optical depth decreased during this time period from about 0.27 to 0.05 (DeLuisi et al., 1984).

The plots of fig. 11 show that the stratospheric aerosols caused ozone amounts initially to be overestimated by the standard and short Umkehr methods in layers 1-3. Maximum overestimates in layer 2, for example, were 230% and 166% for the standard and short Umkehr methods, respectively. Both methods
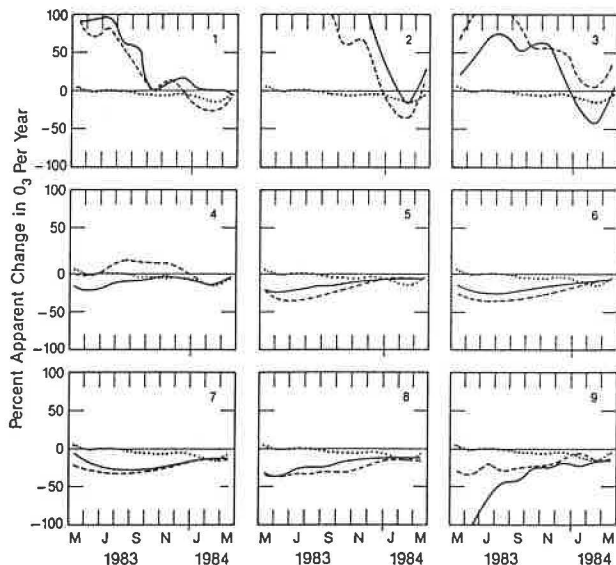
Figure 11--Ozone changes per year at MLO in standard (——) and short (---) Umkehr layers 1-9, plotted month by month, and expressed in percent relative to the ozone amount present during the month indicated. (For example, the May 1982 ozone value minus the May 1983 value, expressed in percent, is plotted in May 1983.) The dotted curves (...) are similar data for total ozone.

underestimate ozone amounts by up to 30%-40% in Umkehr layers 5-8. In layer 9, the standard method underestimates ozone amounts by 115% in May 1982, causing fictitious negative ozone values to be recorded. By December 1982, however, the ozone underestimates in layers 5-9 are reduced to between 5% and 15%, and remain essentially unchanged through March 1983, suggesting that the results are not wholly fictitious, but reflect real differences in ozone, with the early 1983 values being lower than the early 1984 values.

That a real change in ozone occurred at MLO is indicated by the total ozone difference plot of fig. 11. The plot shows that August 1982-March 1983 total ozone values at MLO were lower than values during August 1983-March 1984. The February 1983 value, in particular, was lower than the February 1984 value by 15%.

Balloon ozone observations were made at Hilo with ECC sondes (Komhyr, 1969). Monthly mean ozone partial pressures measured during September 1982-December 1983 are listed in table 13. Because the sondes yield ozone amounts too low above 10 mb (Komhyr et al., 1984b), the measured values were increased by 2.5% at 10 mb, 5.0% at 7 mb, and 8.0% at 5 mb, and are believed to be in error by not more than 10% at 5 mb.

Mean ECC sonde and Umkehr ozone profiles are plotted in fig. 12. The plots for September 1982, when the stratospheric aerosol optical thickness was still relatively high (0.15), clearly demonstrate the adverse effect of aerosols on the Umkehr measurements. Relative to the sonde data, Umkehr ozone amounts are particularly low in layers 5 and 6, but much too high in layers 2 and 3. The ozone maximum is erroneously indicated by the short Umkehr method to be in layer 4 instead of layer 5. By December 1982, however, when the

Table 13.--Monthly mean ozone partial pressures at select atmospheric pressure levels derived from ECC ozonesonde soundings at Hilo, HI

Mo-Year	No. flts.	1013 mb	700 mb	500 mb	300 mb	200 mb	150 mb	100 mb	70 mb	50 mb	30 mb	20 mb	10 mb	7 mb	5 mb
09-82	3	11	26	16	12	5	6	18	46	75	116	137	94	55	29
10-82	1	19	29	29	13	13	14	30	74	90	137	147	72	30	--
11-82	--	--	--	--	--	--	--	--	--	--	--	--	--	--	--
12-82	3	6	29	27	12	6	6	13	42	80	123	134	77	48	30
01-83	3	20	30	20	11	8	6	6	23	74	113	125	75	56	35
02-83	4	5	35	28	13	8	4	9	26	53	132	122	84	55	35
03-83	4	28	36	27	18	10	9	12	28	68	97	124	94	63	38
04-83	2	36	33	34	15	13	10	14	29	83	129	138	105	63	33
05-83	1	16	40	34	24	22	17	52	39	60	112	142	94	54	30
06-83	2	29	46	31	15	18	27	28	47	81	131	142	88	57	36
07-83	2	8	33	14	7	5	11	18	46	88	122	144	96	63	36
08-83	2	11	27	20	12	7	8	29	51	85	118	141	91	62	41
09-83	3	7	23	15	9	10	13	21	45	78	131	142	92	60	40
10-83	1	17	28	21	8	7	4	20	48	80	127	141	86	58	32
11-83	3	10	23	17	11	9	7	9	35	72	118	134	95	59	36
12-83	2	13	24	33	13	10	10	9	35	86	112	134	95	58	38
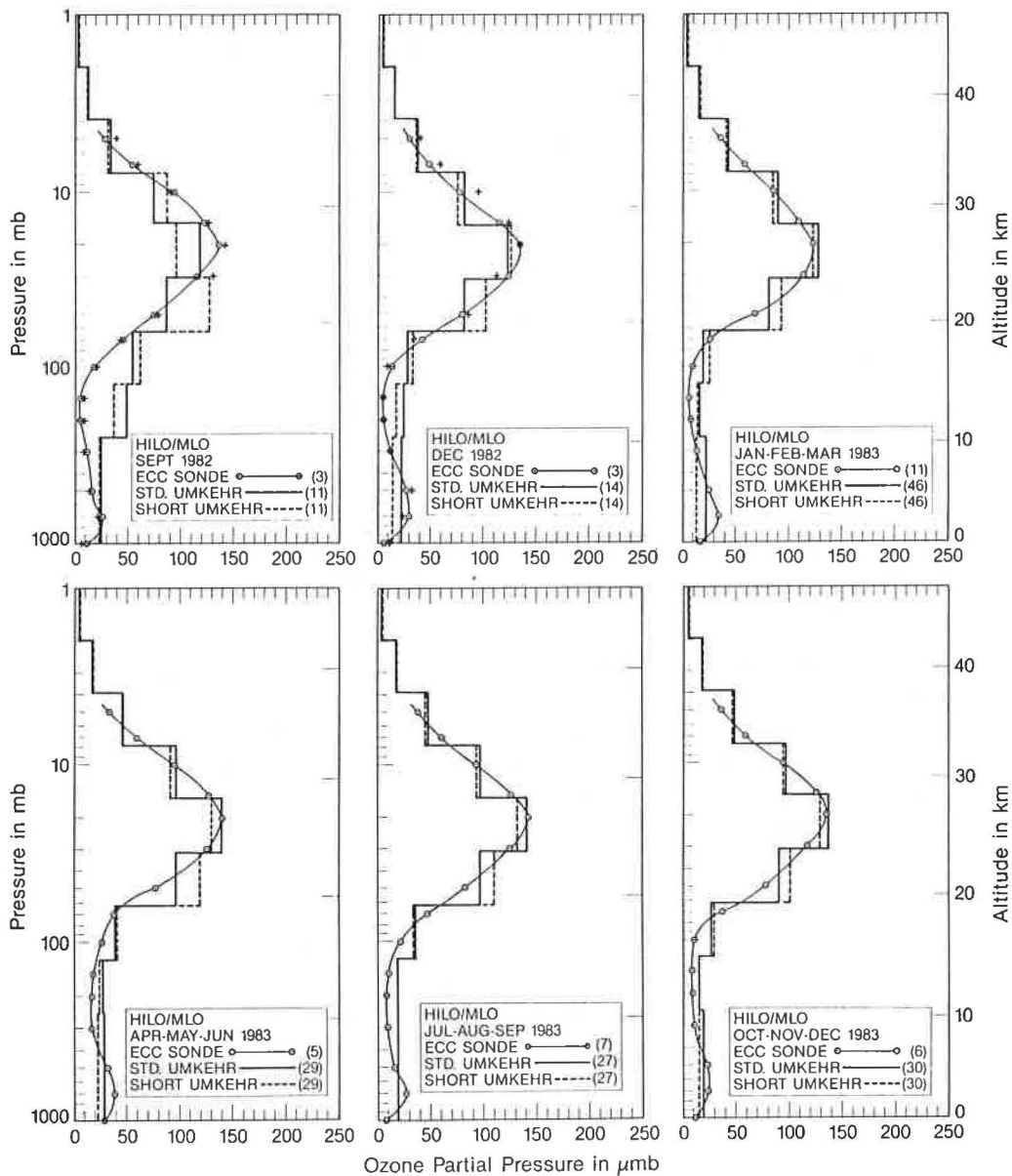
Figure 12.--Monthly mean ozone profiles for September and December 1982, and seasonal profiles for 1983, all derived from Umkehr and ozonesonde observations in Hawaii. Monthly mean values for September and December 1983 are shown by crosses (+). Numbers in parentheses denote the number of observations per month.

stratosphere had substantially cleared (aerosol optical thickness ~0.06), representation of the correct mean ozone profile by the Umkehr observations is considerably improved, the main discrepancy being ozone values still too high in Umkehr layers 2 and 3. In 1983, the mean seasonal Umkehr data agree well with corresponding ECC sonde data, except for short Umkehr ozone values in layer 4 that are too high. This and other differences among the 1983 Umkehr and sonde ozone profiles are not necessarily due to aerosols, but may stem from deficiencies in the algorithms used in processing the Umkehr data. From

comparison of the Umkehr and sonde data, it is estimated that the aerosol-effect errors in the 1983 Umkehr ozone profiles probably do not exceed ±10%.

3.3.2 Umkehr Observations with Automated Dobson Spectrophotometers

Considerable concern has been expressed in recent years about possible partial destruction of atmospheric ozone by anthropogenic pollutants. The region near 40-km altitude has been shown to be particularly vulnerable to ozone depletion by chlorofluorocarbons (NRC, 1984). A potentially favorable method of monitoring long-term changes in ozone near 40 km is by means of Dobson ozone spectrophotometer Umkehr observations (Reinsel et al., 1984).

Manual Umkehr observations are difficult and tedious to make. With automation of Dobson spectrophotometer no. 61 in 1981 at GMCC, Boulder, CO, new impetus was given to the possibility of using Umkehr observations for monitoring long-term changes in ozone. The automated observations are not subject to operator bias; an increased frequency of observations is likely; and a potential exists for obtaining high-quality data over extended time periods if all instruments in a network are subjected to uniform calibration procedures.

Funding was obtained in 1982 from EPA, CMA, WMO (Voluntary Cooperation Program), and NOAA for automating six additional Dobson instruments and establishing them in a global station network for long-term stratospheric ozone observations, and for providing comparison data for satellite ozone measurements. The seven automated Dobson instrument .Umkehr observatory sites are Boulder, CO (40°N, 105°W); Haute Provence Observatory, France (44°N, 6°E); Huancayo Observatory, Peru (12°S, 76°W); MLO (20°N, 156°E); Perth, Australia (32°S, 116°E); Poker Flat, AK (65°N, 148°W); and Pretoria, South Africa (26°S, 28°E). The sites were selected for wide latitudinal coverage, favorable observing conditions, logistics ease, and station proximity to an existing or future lidar aerosol observing facility. Stations implemented in 1983 were Haute Provence and Poker Flat. Observations at Haute Provence began in September. The installation at Poker Flat was made in October when the Sun was too low in the sky for observations to be made, but observations will begin in February 1984. Establishment of the remaining stations is expected to be completed in 1984.

In automating the Dobson instruments the principle and method of measurement are left unchanged, except that a computer rather than a human observer controls instrument functions. Modification of the Dobson instrument entails several alterations. To attain long-term optical wedge stability, the glue normally used to bind the wedge sections together is removed. Metal tracks of the optical wedge are replaced with tracks made of Rulon plastic bearing material to prevent possible binding of the wedges during operation. A stepper motor is added to the wedge mechanism for control. For smooth operation, Rulon bearings are also built into the instrument Q (wavelength-setting) lever mechanisms, to which stepper motors are also added. Temperature is monitored with transducers built into the instrument. The normally used photomultiplier high-voltage power supply is replaced with a programmable high-voltage supply. Finally, a signal-processing card is added to the output of the Dobson instrument for interfacing with the computer instrumentation.

A block diagram of the automated instrument system is shown in fig. 13. A Hewlett-Packard 9915A computer controls the Dobson instrument functions via

37
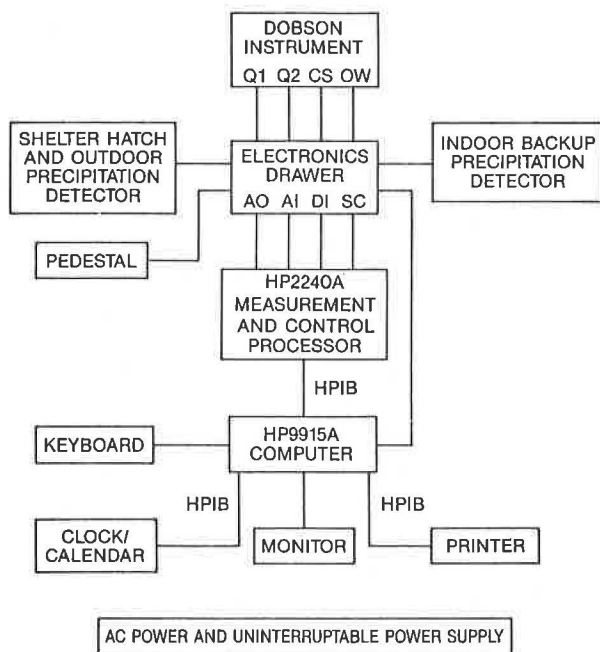
Figure 13.--Schematic diagram of the automated Dobson instrument system.

an HP2240A measurement and control processor and an electronics drawer. Each day at midnight, the computer calculates the times of Umkehr observations for that day and readies itself for the observations. At the appropriate time in the morning, the instrument shelter hatch opens, provided that precipitation is not occurring, and Umkehr observations commence. As observations progress, the instrument slowly rotates on its pedestal mount so that the axis of the instrument points at all times in the direction of the Sun to minimize variations in zenith skylight polarization effects. Observational data are recorded on cassette tape, plotted on a video monitor, and output by a printer. A calendar-clock times all operations. Commands and data are input into the computer with an external keyboard or a keyboard built into the 9915A computer.

At prescribed times during the day, the Umkehr observations may be interrupted for total ozone observations. Total ozone measurements are made semi-automatically. The observer inputs data to the computer, specifying what type of observation to make and, for observations on direct sunlight, places a Sun director with ground-quartz plate over the instrument's light inlet window. After aligning the instrument and Sun director correctly with respect to the Sun, the observer presses a button switch. The observation is then made automatically. Observational data and computed total ozone values (for direct Sun observations) are recorded on the cassette tape and output by the printer. During total ozone or Umkehr observations the instrument continually monitors its own temperature and makes appropriate adjustments to its wavelength selector lever positions so that observations are always made on correct wavelengths.

Up to 17 days of observations can be recorded on one cassette tape. Selected observational Umkehr data with applicable total ozone values are mailed to the World Ozone Data Center in Canada for reduction to Umkehr ozone profiles

by the standard (Mateer and Dütsch, 1964) and short (Mateer and DeLuisi, 1981) Umkehr data-processing techniques.

3.3.3 High-Altitude Ozonesonde Tests

Tests on ECC ozonesondes were continued during 1983 to assess their performance relative to other types of ozone-measuring instrumentation, in the troposphere and at altitudes between 30 and 40 km. In July 1983, NASA-sponsored balloon flights were conducted at NSBF in Palestine, TX, with the following instruments and missions: (1) Multiple-instrument gondola--This gondola carried six in situ UV photometers from Harvard University, NOAA/AL, NASA/JSC, and NASA/GSFC. There were 2 UV remote sensors from NASA/GSFC, and 12 ECC sondes from NOAA/GMCC, NASA/GSFC, the Canadian AES, and the F.R.G. Hohenpeissenberg Observatory. (2) The University of Minnesota Gondola--This gondola carried the University of Minnesota mass spectrometer, a second NASA/JSC in situ photometer, a second remote sensor from NASA/GSFC, and a NOAA/GMCC ozonesonde. (3) Triplets--This series of 16 balloons each carried 3 electrochemical sondes from F.R.G., Canada, NASA/GSFC, and NOAA/GMCC. During the balloon flights, total and Umkehr ozone profiles were taken by Dobson and Brewer spectrometers located at Palestine, TX.

The multiple-instrument gondola experiment was only partially successful because of balloon failure at an altitude of 23 km. (The experiment was repeated in October 1983, but balloon failure occurred again at about the same altitude.) Results from the University of Minnesota gondola experiment are shown in fig. 14. The triplet soundings with ECC ozonesondes were highly successful, and a report comparing the performance of the various instruments is in preparation at NASA/GSFC.

PRESS. (mb)	ECC-UV O$_3$ % DIFF.
283.6	43.9
205.9	19.6
95.1	−0.7
51.7	0.6
29.9	4.0
21.9	5.5
10.4	4.5
7.3	2.7
5.1	−2.5
3.0	−12.4
2.6	−5.9

JULY 18, 1983
PALESTINE, TEXAS
ROBBINS
UV PHOTOMETER ··········
KOMHYR
ECC SONDE ————
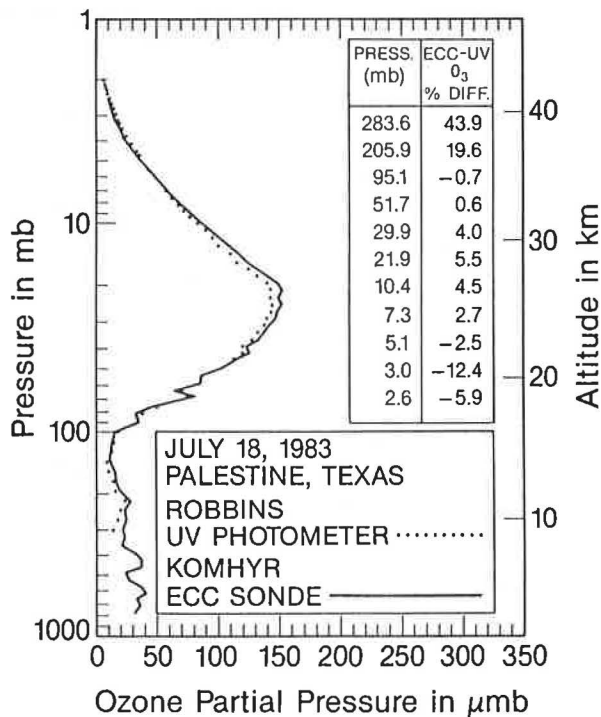
Figure 14.--Comparison of Komhyr's (GMCC) ECC ozonesonde and Robbins' (NASA/GSFC) UV photometer ozone vertical distribution data.

39

3.4 Surface Ozone

3.4.1 Operations

Measurement of ozone near the surface at the GMCC observatories continued
throughout 1983. The Dasibi ozone monitors used at MLO and BRW were recali-
brated early in 1984, and the data for these two stations reflect the applica-
tion of this calibration information. In addition, our network standard
Dasibi monitor was recalibrated against the NBS standard photometer in October
1983. This was the first time our standard had been compared with the new NBS
photometer; previous comparisons were made with a different NBS standard in-
strument. It appears that the two standards give very similar results, and no
major change was noted in the relationship between our standard and the two
NBS instruments. Results of the October 1983 comparison have been incorpo-
rated in the MLO and BRW data. Small adjustments for 1981 and 1982 also are
incorporated in the data presented here.

A comparison between the SMO instrument and our network standard was
delayed until 1984 to correspond to planned facilities improvements. Data for
1983 should, therefore, be considered preliminary. At SPO an apparent calibra-
tion shift at the end of 1982 has not been resolved, and further tests on the
instrument are required before the 1983 data are made available.

3.4.2 Data Analysis

Surface ozone concentrations at MLO reached their highest values in 11
years that measurements have been made there. This can be seen in fig. 15
where the monthly mean values corresponding 1100-1800 GMT (2100-0400 LST) are
plotted for 1973-1983. The hours 1100-1800 GMT correspond to the downslope
flow at the observatory, which is most representative of free tropospheric
air. It appears that the largest increases have taken place in the seasonal
maximum, which occurs in the spring. Two of the last 3 years have shown max-
ima about 20% higher than the typical value. Adding the data from 1983 to the
previous 10 years of data gives an overall linear trend of 1.6% yr^{-1} for 1973-
1983.
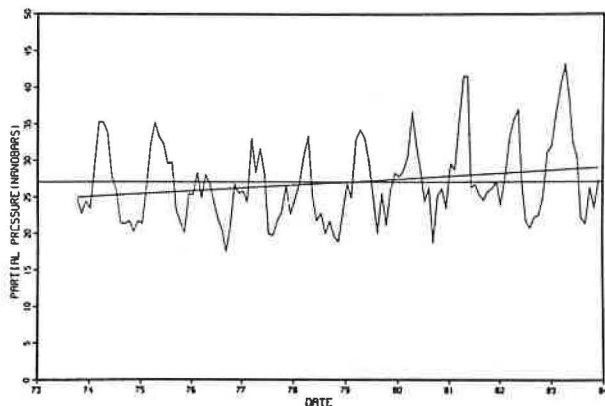
Figure 15.--Monthly mean surface
ozone amounts at MLO, with a linear
least-squares fit to the data.

The location of MLO above the tradewind inversion at an average pressure of 680 mb suggests that of all the GMCC observatories MLO should give surface ozone values that are the most representative of the free troposphere. During 1983, ozone profile measurements using the ECC ozonesonde were made on approximately a weekly schedule from Hilo, HI. These soundings provide an opportunity to compare the surface ozone measurements at MLO with the complete tropospheric profile from the ozonesondes. Figure 16 shows profiles on 4 days in February and 4 in March with the surface value at MLO plotted at 680 mb on the profile. These flights were all made at about 1800 GMT, which is still during the downslope regime at the observatory. The dashes indicate a line of constant mixing ratio. The surface ozone measurements appear to represent well the ozone amount at the 680-mb level as given by the ozonesonde profile. Even on 30 March 1983, where there appears to be a region of enhanced ozone at the observatory level compared with levels above and below, the surface ozone corresponds well to the profile.

Several interesting features of these ozonesonde profiles relate to the source of ozone that is observed at MLO. On 2 and 16 February there are broad layers higher in the troposphere where the mixing ratio is much less than that at the observatory, indicating that on these days ozone is being advected horizontally at the observatory level. On 23 and 30 March, on the other hand, there are relatively narrow layers of enhanced ozone at the observatory level. Below that level, the ozone decreases sometimes quite markedly, so that near sea level the values are considerably reduced. This is in keeping with destruction of ozone in the layer below the tradewind inversion near the ground, and is the reason generally lower values are observed at MLO during the upslope regime. For 36 days in 1982 and 1983 when ozonesonde soundings were available,
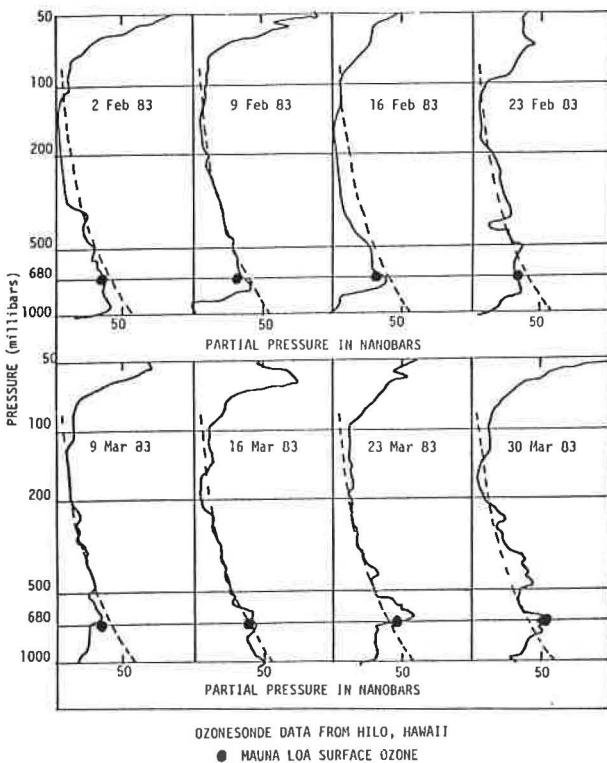
Figure 16.--Ozone profiles from Hilo, HI, during February and March 1983 compared with the surface ozone amount at the same time at MLO. A line of constant mixing ratio (dashed) is also shown.

the average concentration at the observatory level from the soundings was 31.3 nb, while the surface ozone concentration at the observatory was 29.8 nb with a standard deviation of the differences of 3.8 nb. Since the sounding location in Hilo is separated by approximately 55 km from the observatory, it is clear by looking at some of the smaller scale features of the profiles at the observatory that part of the variance is explained by the location differences. It can be concluded that indeed the surface measurements at the observatory are representative of free troposphere ozone values in this region. It also confirms that the ECC soundings give values in the troposphere that are on the same scale as the surface measurements that are traceable to UV photometry.

It is of some interest to determine the frequency of ozone soundings required to determine long-term ozone changes in the troposphere. The surface ozone data for hours 1100-1800 GMT at MLO can be used to compute the trends based on the full data set and for monthly means based on a decreasing number of days. Table 14 gives the linear trend and standard errors of the monthly

Table 14.--Linear least-squares trends of surface ozone monthly anomalies*

Station	Trend ($\% \, yr^{-1}$)	Std. error ($\% \, yr^{-1}$)
MLO (1973-1983)		
All days	1.62	1.11
15 days	1.54	1.09
10 days	1.59	1.15
7 days	1.55	1.17
6 days	1.15	1.29
5 days	1.74	1.23
4 days	2.16	1.22
3 days	1.46	1.24
BRW (1973-1983)	1.23	1.04
SMO (1976-1983)	-1.07	1.59

*At MLO the trends are computed using varying numbers of days to compute the monthly mean. Daily averages at MLO are based on hours 1100-1800 GMT.

anomalies (long-term monthly mean subtracted from each month) for decreasing numbers of daily values. On the basis of the magnitude of the trend and the variability in the trend estimate, it appears that with about 2 days a week of data the trends remain quite comparable with those when data is available every day. Thus an ozonesonde program with two soundings a week should be able to monitor long-term trends in tropospheric ozone behavior if variability at 680 mb is representative of variability in the rest of the troposphere.

Trends in the data at BRW and SMO are less marked than at MLO (figs. 17 and 18, and table 14). The significance of the trends at all of the stations is still questionable and at MLO the magnitude is greatly influenced by the high values in 1983.
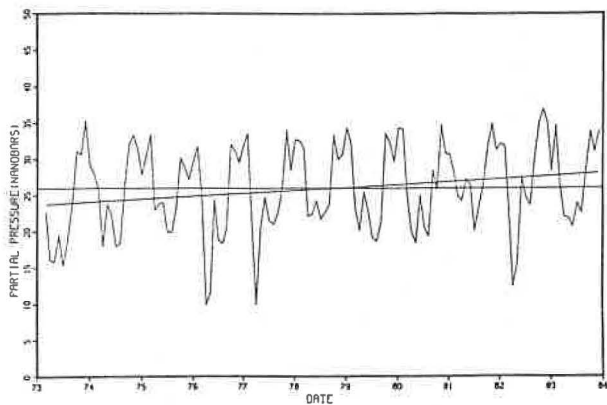
Figure 17.--Monthly mean surface ozone amounts at BRW, with a linear least-squares fit to the data.
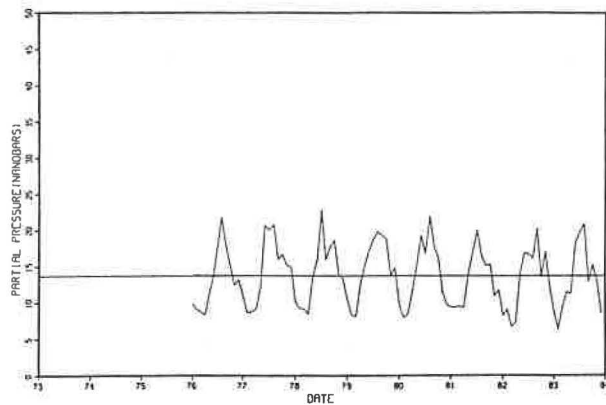
Figure 18.--Monthly mean surface ozone amounts at SMO, with a linear least-squares fit to the data.

3.5 Stratospheric Water Vapor

3.5.1 Operations

Routine stratospheric water vapor soundings were made in Boulder in 1983. In addition, four soundings were made at Palestine, TX, and two at Laramie, WY, as part of intercomparison programs designed to assess the reliability of stratospheric water vapor measurement systems.

The frost-point hygrometer used in the soundings has undergone only minor changes since inception of the program in 1980. Balloon performance, although greatly improved over 1982, is still not optimum. The use of the two balloon systems described last year (Harris and Bodhaine, 1983) led to greater relia-bility but limited the altitude from which good data could be obtained. Because initial descent rates at altitudes above 25 km are not fast enough to give good ventilation through the air intake of the system, the measurements at altitudes between 25 and 30 km often show evidence of contamination. It is hoped that modifications under way will extend the height of accurate measure-ments to about 30 km, as obtained in the past.

During 1983 it was discovered that an error was being made in correcting for hysteresis effects on the pressure sensor for descent pressure measure-ments. Since this involves a fixed offset in the mechanism of the baroswitch, the percentage errors in pressure determination are largest at low pressures (highest altitudes). These errors amount to about 9% in mixing ratio at 10 mb and decrease to less than 1% below 80 mb. Data prior to 1983 presented in previous Summary Reports are shown corrected in this report.

Prior to June 1982, the thermistors used to measure frost-point tempera-ture in the hygrometers were calibrated at NRL, Washington, DC, by J. Masten-brook. These calibrations were performed using platinum resistance probes with a Mueller bridge. The thermistors in Boulder are calibrated using two quartz thermometers manufactured by HP. With the termination of the program in Washington, DC, the platinum thermometers of NRL were transferred to NOAA/GMCC. Simultaneous calibrations of thermistors using both the platinum and

43

quartz probes show differences that lead to frost-point temperature discrepancies of less than 0.05°C at -90.0°C. This leads to water vapor mixing ratio differences of less than 0.5% at stratospheric levels near 15 mb.

3.5.2 Data Analysis

During 1983 nine stratospheric water vapor balloon soundings were made at Boulder from which valid data were obtained. In addition, two soundings were made from Laramie, WY, and four from Palestine, TX. Figures 19a and 19b are profiles of soundings made in 1981 and 1982. These profiles were presented in previous Summary Reports but are shown here corrected for the pressure error discussed earlier. The data from Boulder and Laramie are shown in fig. 19c. Because one of the Laramie flights yielded data from about 40 mb down and the other down to 55 mb, the two flights were combined into a single profile. Figure 19d shows the profiles obtained at Palestine.

The two flights at Palestine in October 1983 and the one in May 1981 were conducted as part of an international intercomparison of stratospheric water vapor measuring systems. Preliminary results of these comparisons, as well as a comparison carried out in Laramie (data shown in fig. 19c) with the NOAA/AL Lyman-alpha water vapor instrument, indicate that the NOAA/AL instrument gives results about 0.5 ppmm higher than the GMCC frost-point hygrometer. Comparisons with other types of equipment were not as conclusive. The NCAR cryogenic
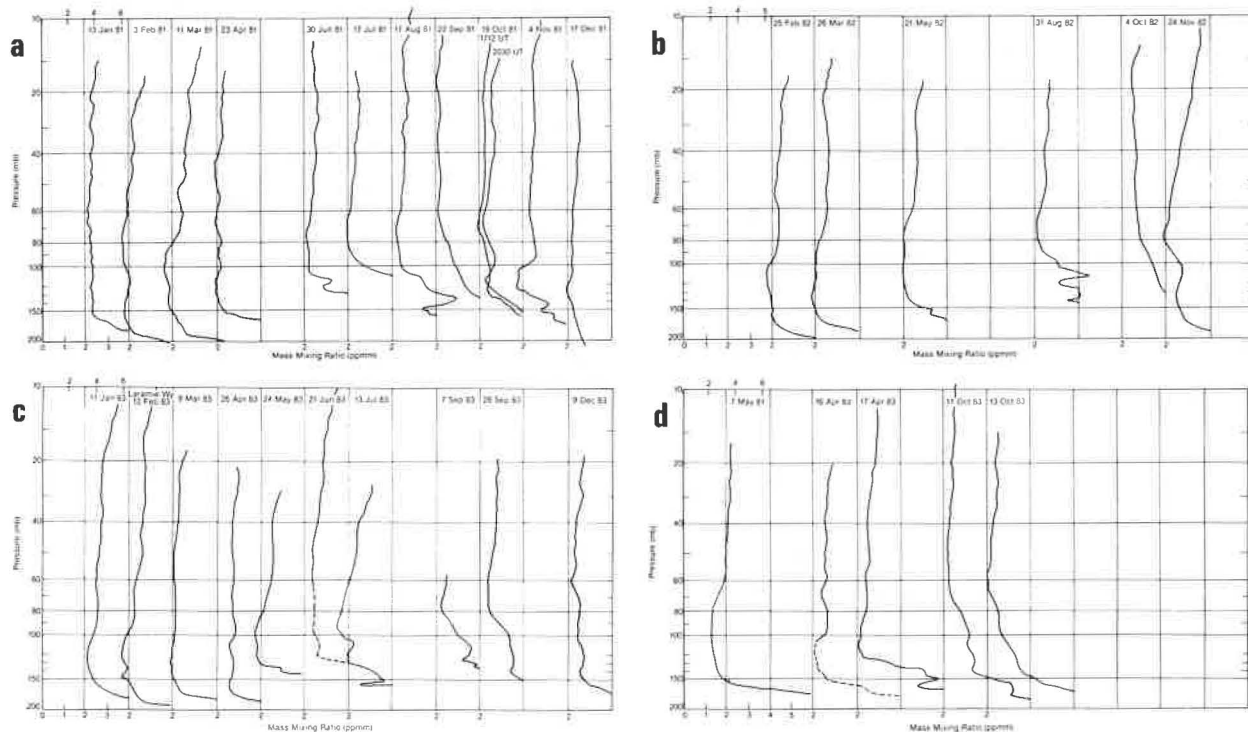
Figure 19.--Profiles of stratospheric water vapor mass mixing ratio in ppmm at Boulder, CO, for (a) 1981, (b) 1982, and (c) 1983, and at Palestine, TX, for (d) 1981 and 1983. A profile at Laramie, WY, for 12 February 1983 is also shown in (c). Numbers along the top for the first profile give volume mixing ratio in ppmv.

sampler appears to give values at about the same level as the frost-point hygrometer. Complete results of this intercomparison series will be available in 1984.

Sufficient soundings have been made in Boulder to obtain average seasonal patterns in the stratosphere between 200 and 20 mb. Figure 20 shows the seasonal values averaged for 1981-1983. For each season there are from 6 to 8
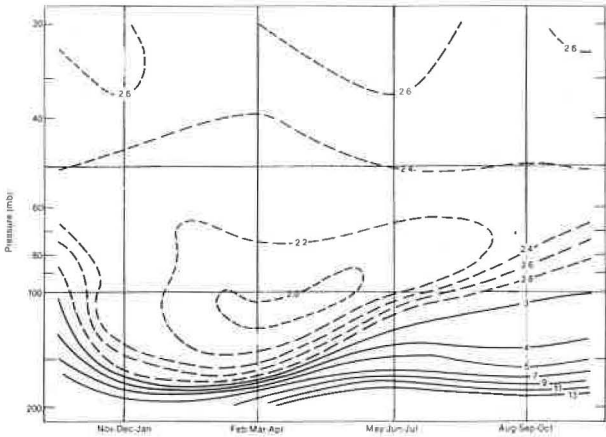
Figure 20.--Seasonal variation of stratospheric water vapor at Boulder, CO, based on data for 1981-1983. Isopleths are of mass mixing ratio in ppmm. Note that the spacing of the isopleths changes so that from 2 to 3 ppmm, it is 0.2 ppmm; from 3 to 5 ppmm, it is 1 ppmm; and from 5 to 13 ppmm, it is 2 ppmm.

soundings. The seasonal groupings were chosen to emphasize the minimum that appears in the spring. Below 60 mb the seasonal cycle dominates with the driest values appearing between 150 and 100 mb in the spring. This minimum moves upward and fills as the year progresses. If there is any annual cycle above 60 mb, it is very weak. Also above this level the mixing ratio increases gradually during all seasons so that the average increase between 19 and 26 km is about 0.042 ppmm km^{-1}. The increase is usually attributed to a source from the oxidation of methane in the middle and upper stratosphere. In this case, the increase is somewhat larger than that shown by Mastenbrook and Oltmans (1983), which was based on data from Washington, DC, and included many more soundings. The minimum near 70 mb is considerably drier at Boulder than at Washington, DC, and at all levels the mixing ratio at Boulder is less than the long-term average at Washington. The average annual profile over Boulder of the stratospheric mass mixing ratio is given in table 15. This can be compared with a similar table in Mastenbrook and Oltmans (1983).

Table 15.--Annual average mass mixing ratio at Boulder, CO, for selected pressure levels for 1981-1983

Pressure level (mb)	Mean mixing ratio (ppmm)	Pressure level (mb)	Mean mixing ratio (ppmm)
20	2.59	90	2.32
30	2.57	100	2.40
40	2.47	120	2.58
50	2.37	140	3.11
60	2.30	160	4.46
70	2.25	180	7.98
80	2.25	200	16.28

3.6 Halocarbons and Nitrous Oxide

3.6.1 Operations

Air samples in paired stainless steel flasks were collected weekly during 1983 at BRW, NWR, MLO, and SMO for CFC-11 (CCl_3F), CFC-12 (CCl_2F_2), and nitrous oxide (N_2O) analyses. At SPO, samples in paired flasks were collected weekly only during January and December; at other times, they were collected once per month.

The samples were analyzed on a gas chromatograph at GMCC, Boulder. A Hewlett-Packard 87XM computer was procured in September and interfaced with the laboratory integrating recorders so that chromatographic peak-height data could be processed and stored on disk at the end of each analysis.

In September, a Shimadzu mini-2E gas chromatograph was procured for use at SPO. The chromatograph was modified by removing the injection port and installing a gas sampling valve, and by removing carrier gas inlet controls and installing a metal diaphragm flow controller. Operating and servicing instructions for the chromatograph were prepared for use by SPO personnel. After testing, the chromatograph, an HP 3390A integrating recorder, calibration gas (tank 3081), and accessories were shipped to SPO in early November. The apparatus was installed and became operational at SPO in late December.

3.6.2 Calibration

In early September, three 48.7-L steel gas cylinders (tanks 3077, 3081, and 3093) were filled with clean mountain air to serve as CFC-11, CFC-12, and N_2O gas standards. The tanks were filled at Climax, CO, at an elevation of 3.8 km. Pumping equipment consisted of a 15-μm inlet air filter, a -70°C water vapor cold trap, a metal bellows forepump, and a RIX high-pressure three-stage air compressor. The pumps were powered by a gas-powered generator. Tanks 3077, 3081, and 3093 were pressurized to 1800, 2050, and 2050 psi, respectively.

The NOAA/GMCC halocarbons and N_2O calibration gas standard (tank 3072), as well as tanks 3081 and 3093, were transported for calibration to OGC (Beaverton, OR) in late September. Calibrations of the standard indicated that CFC-11 and N_2O concentrations have remained stable since 1977. The CFC-12 concentration has been increasing in the past, but appears to have stabilized during the last 2 years.

3.6.3 Data Analysis

CFC-11, CFC-12, and N_2O selected data are shown in figs. 21-23, respectively, for 1977-1983. The BRW halocarbon data exhibit an annual cycle with highest concentrations during November-December and lowest values during June-July. Similar periodicity in the data is not evident at the other stations. SPO data continue to exhibit the most variability due to sampling problems. The N_2O data have not been corrected for CO_2 interference during chromatographic gas analyses.
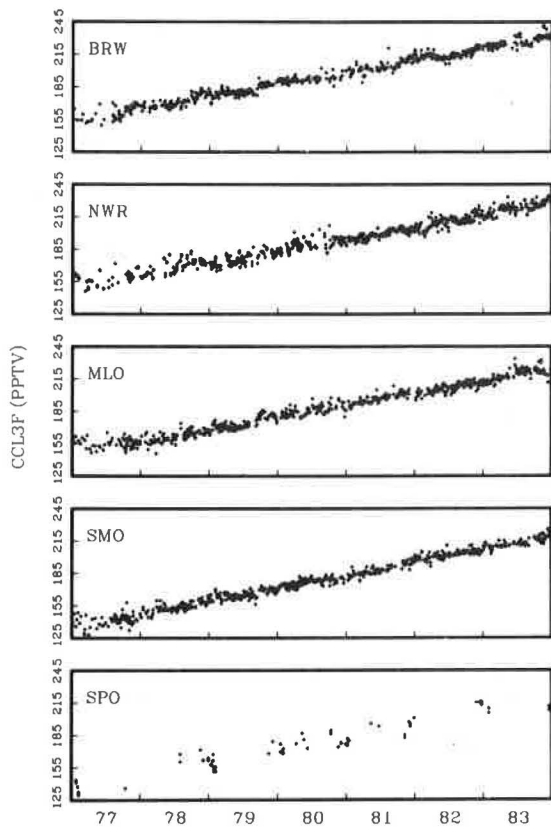
Figure 21.--CFC-11 data record.
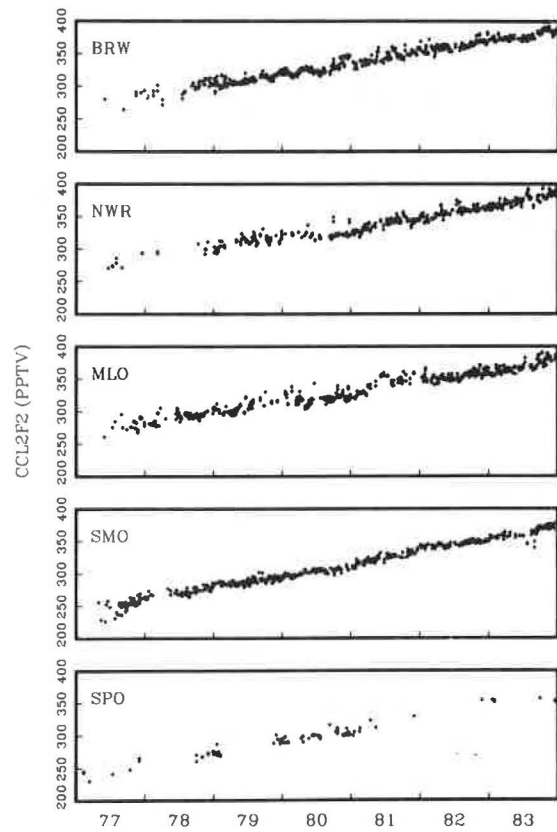
Figure 22.--CFC-12 data record.
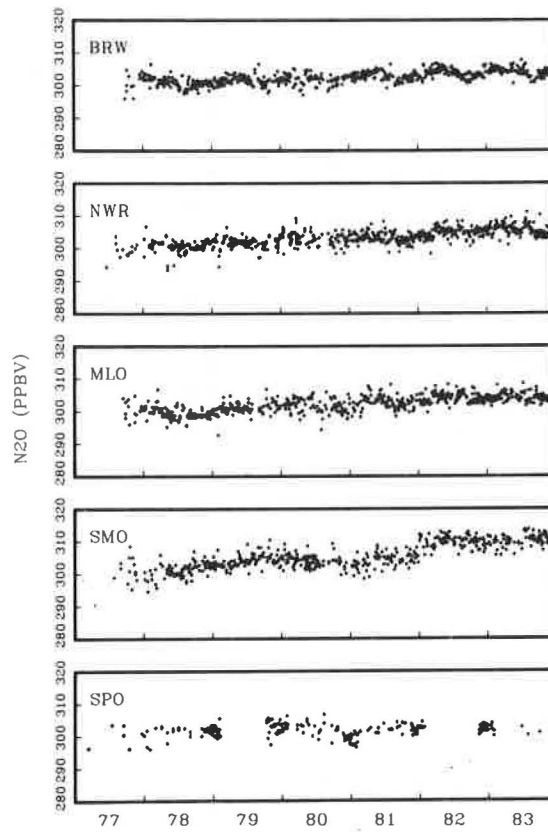
Figure 23.--N$_2$O data record.

47

Table 16.--Mean mixing ratios for 1983, and results of second-
order regression analyses of CFC-11, CFC-12, and N_2O data for 1977-1983[*]

Station	No. of obs.	Mean mixing ratio for 1983	Mixing ratio on 1 Jan 1977	Growth rate	Growth rate change
CFC-11		(pptv)	(pptv)	(pptv yr^{-1})	(pptv yr^{-2})
BRW	524	227.3	154.2 ± 0.58	11.09 ± 0.36	0.01 ± 0.05
NWR	555	223.2	154.0 ± 0.71	8.93 ± 0.42	0.26 ± 0.05
MLO	517	218.7	148.2 ± 0.62	10.02 ± 0.39	0.13 ± 0.05
SMO	541	213.7	135.4 ± 0.51	11.81 ± 0.32	0.03 ± 0.04
SPO	66	208.6	135.5 ± 1.97	12.10 ± 1.33	-0.03 ± 0.20
CFC-12		(pptv)	(pptv)	(pptv yr^{-1})	(pptv yr^{-2})
BRW	436	378.3	269.7 ± 1.77	16.11 ± 0.92	0.10 ± 0.11
NWR	347	374.6	279.6 ± 2.25	9.72 ± 1.10	0.77 ± 0.13
MLO	414	368.9	268.3 ± 1.66	15.00 ± 0.95	0.10 ± 0.12
SMO	473	362.9	241.0 ± 0.92	18.02 ± 0.55	0.10 ± 0.07
SPO	80	353.3	238.2 ± 2.38	17.02 ± 1.38	0.10 ± 0.19
N_2O		(ppbv)	(ppbv)	(ppbv yr^{-1})	(ppbv yr^{-2})
BRW	539	304.1	300.2 ± 0.34	0.48 ± 0.19	0.01 ± 0.02
NWR	544	305.6	299.1 ± 0.42	1.07 ± 0.23	-0.01 ± 0.03
MLO	538	304.1	298.4 ± 0.41	1.10 ± 0.23	-0.03 ± 0.03
SMO	470	310.1	300.2 ± 0.54	0.84 ± 0.31	0.11 ± 0.04
SPO	190	302.0	300.3 ± 0.61	0.69 ± 0.36	-0.07 ± 0.05

[*]Coefficients are followed by their standard deviations.

Mean concentrations for 1983 and results of second-order least-squares
regression analyses of the 7-yr halocarbon and N_2O data sets are summarized in
table 16. Indicated growth rates are all highly significant. Significance
(95% confidence interval) of the growth rate changes appears to be highly de-
pendent from year to year on the last year's data. For the full 7-yr record,
only the MLO and NWR CFC-11 and the NWR CFC-12 second-order terms are statis-
tically significant.

Table 17 contains CFC-11 monthly average data for each station during the
period 1977-1983. SPO data should be used cautiously since they are quite
scattered and sparse (see fig. 21). This SPO variability problem is caused,
we believe, by air samples having to be stored many months before analysis.

CFC-12 and N_2O data are not tabulated because calibration gas instability
and CO_2 interference corrections have not been ascertained completely.

3.7 Stratospheric Aerosols--Lidar

Lidar measurements acquired since 1974 by GMCC at MLO have been uniformly
processed for vertical profiles of aerosol backscattering ratio, ratio of total
backscatter to Rayleigh backscatter, and cumulative optical depth. For 1974-
1981, 173 profiles were analyzed. A NOAA Data Report, soon to be printed,
will provide details of the processing procedure and results. Lidar measure-
ments from 1982 to the present were also processed in the same fashion as the

Table 17.--Monthly average CFC-11 concentrations (pptv)
using pressurized flask pairs

Month	BRW	NWR	MLO	SMO	SPO	Month	BRW	NWR	MLO	SMO	SPO
1977						**1980 (cont.)**					
Jan	--	--	--	--	141.4	Jul	191.7	187.2	189.3	177.9	--
Feb	--	--	--	--	130.1	Aug	193.0	--	187.0	176.6	--
Mar	--	--	--	--	--	Sep	193.6	184.6	186.6	181.1	--
Apr	--	--	--	--	--	Oct	193.8	190.0	194.5	179.3	185.9
May	--	--	--	--	--	Nov	193.0	195.1	192.4	178.7	--
Jun	--	--	--	--	--	Dec	199.0	190.9	190.9	179.3	176.9
Jul	--	--	--	--	--	**1981**					
Aug	156.8	--	--	144.1	--	Jan	198.6	194.1	188.4	181.2	178.4
Sep	156.9	--	--	144.2	--	Feb	203.5	194.0	192.2	187.8	--
Oct	165.7	--	152.4	144.3	--	Mar	200.0	198.7	193.5	182.8	--
Nov	164.7	--	154.3	144.7	--	Apr	202.2	193.7	195.1	186.0	--
Dec	169.6	--	156.3	141.3	--	May	200.6	198.3	194.3	186.8	--
1978						Jun	202.5	199.0	197.8	186.3	--
Jan	168.1	--	160.2	148.5	--	Jul	202.2	199.0	198.6	188.1	--
Feb	164.9	--	154.3	146.7	--	Aug	203.7	201.2	197.8	189.4	--
Mar	166.3	--	158.4	153.2	--	Sep	203.4	202.3	200.2	191.1	--
Apr	168.9	--	158.8	152.8	--	Oct	208.1	203.9	202.3	192.1	--
May	167.6	--	160.1	151.8	--	Nov	210.4	201.7	200.7	194.1	183.7
Jun	168.4	--	160.5	152.0	--	Dec	213.0	202.8	203.1	194.7	194.1
Jul	169.6	--	159.6	152.0	162.4	**1982**					
Aug	169.7	--	164.1	154.7	--	Jan	211.1	204.3	200.8	198.5	--
Sep	179.3	--	166.5	154.4	--	Feb	214.3	202.4	205.5	200.7	--
Oct	175.5	--	164.0	156.6	--	Mar	214.9	208.4	202.8	197.5	--
Nov	180.8	--	166.6	159.8	171.9	Apr	213.4	208.6	203.6	201.3	--
Dec	179.6	--	166.1	158.7	160.8	May	211.5	208.9	206.1	199.9	--
1979						Jun	210.5	209.4	204.4	202.8	--
Jan	175.1	--	169.3	161.6	157.1	Jul	213.8	213.0	205.7	201.6	--
Feb	178.2	--	170.9	165.4	165.4	Aug	214.0	210.6	207.7	203.5	--
Mar	181.2	--	171.0	162.7	--	Sep	216.2	212.9	209.6	204.0	--
Apr	180.8	--	170.6	163.5	--	Oct	217.5	212.0	210.3	204.9	--
May	179.8	--	169.6	163.8	--	Nov	221.0	217.0	210.4	204.7	233.4
Jun	179.3	--	170.0	162.5	--	Dec	221.2	217.5	209.6	204.5	214.5
Jul	180.7	--	172.8	164.8	--	**1983**					
Aug	180.0	--	--	167.7	--	Jan	223.1	215.1	211.6	210.2	207.4
Sep	186.5	--	177.0	163.9	--	Feb	222.4	218.8	212.9	206.9	--
Oct	186.6	--	183.2	170.6	--	Mar	223.5	219.7	214.6	211.7	--
Nov	188.1	--	180.5	168.8	--	Apr	224.8	223.2	215.5	211.1	--
Dec	188.6	182.8	179.4	169.4	--	May	--	220.8	217.6	210.7	--
1980						Jun	226.3	222.2	222.9	212.0	--
Jan	191.4	183.3	181.7	172.6	169.5	Jul	229.1	223.3	222.2	213.8	--
Feb	190.1	183.3	181.3	173.0	168.8	Aug	225.0	223.5	221.4	211.7	--
Mar	192.5	--	184.3	174.8	--	Sep	226.6	224.6	219.7	213.6	--
Apr	190.9	187.6	183.9	174.3	--	Oct	230.1	226.3	223.4	217.4	--
May	191.0	--	181.3	177.4	187.1	Nov	233.9	227.6	223.3	215.8	--
Jun	192.2	--	185.6	178.5	--	Dec	231.9	231.0	217.8	221.2	209.8

1974-1981 measurements, and some results were published in Harris and Bodhaine (1983). A NOAA Data Report is also being prepared for presentation of lidar observations for 1982-1983, covering the El Chichon event.

Presented here is a brief summary of the 1974-1981 lidar observations. Figure 24 is a plot of number of lidar data sets per month vs. time spanning 1974-1981. A data set consists of an average of a few to about 20 lidar shots, and more than one data set is usually obtained during an evening or morning (darkness) measurement episode. The data acquisition system only permitted storage of averages of single shots, so measurement noise statistics could not be calculated by conventional mathematical procedures. Results of processed measurement sets were compared to gain some quantative understanding of measurement variability.

Figure 25 shows stratospheric aerosol optical depth data determined from the 1974-1981 lidar observations. Optical depth was determined by integrating a lidar profile starting at 15 km and ending at the highest altitude at which a signal is detectable. For periods of stratospheric quiescence, the highest altitude was about 25-28 km. During the El Chichon event, the highest altitude was about 10 km higher than the quiescent period.

A closer look at fig. 25 shows a rather high optical depth in the winter of 1974-1975. The higher values are attributed to the well-known eruption of DeFuego in the fall of 1974. From 1976-1977 stratospheric optical depth was very low and probably representative of stratospheric quiescence or background conditions. In 1978 there appears to be some activity that might be attributable to the eruptions of Westdahl in the fall of 1977, and Bezymianny in the spring of 1978. The number of observations made in 1979 are too few for clear
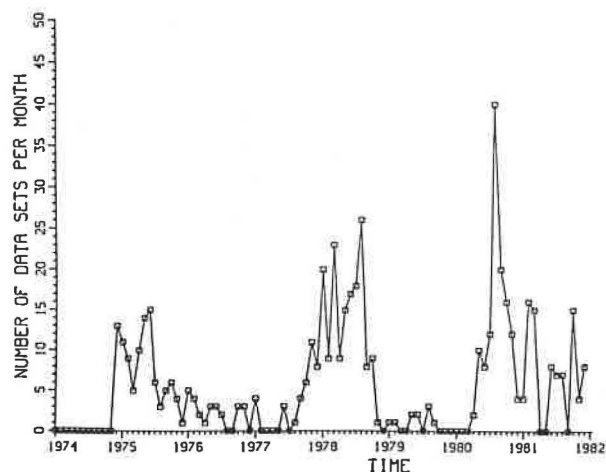
Figure 24.--Distribution of MLO sets of lidar data per month vs. time. A set consists of up to 20 shots, and usually 3 sets are taken per observation episode. Previous to 1980, many sets consisted of only a few observations.
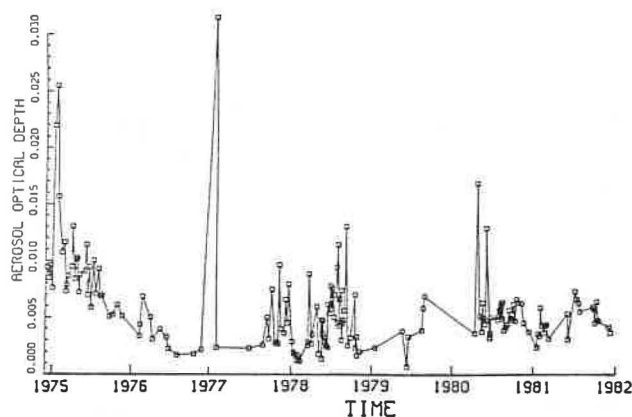
Figure 25.--Stratospheric aerosol optical depth over MLO, determined by lidar. The optical depth is representative of a layer of atmosphere with base at 15 km and top at the highest point of a lidar sounding. The time axis starts in November 1974 and ends in December 1981.

50

interpretation; however, Mount Soufrière erupted in April 1979 and was known to have increased the stratospheric aerosol concentration. In 1980 Mount St. Helens erupted, and a stratospheric aerosol cloud was observed over the Northern Hemisphere.

The data presented in fig. 25 constitute one of the longest detailed records of lidar observations in existence. It clearly complements the historical solar transmission measurement and will be a valuable additional source of data for studies of climatic effects of stratospheric aerosols and of Umkehr error effects of stratospheric aerosols.

3.8 Surface Aerosols

3.8.1 Introduction

The GMCC aerosol monitoring program during 1983 included the continuous measurement of CN concentration and aerosol scattering extinction coefficient (σ_{sp}) at BRW, MLO, SMO, and SPO. A Pollak CNC is located at each station to act as an onsite standard for CN measurements. A G.E. automatic CNC operates continuously at each station, and daily calibration points are provided by the Pollak counter.

A four-wavelength nephelometer at each station continuously measures σ_{sp} at 450-, 550-, 700-, and 850-nm wavelengths. Calibrations of the nephelometers are performed at 2-mo intervals by filling them with CO_2 gas and adjusting the instrument outputs to the known Rayleigh scattering coefficients of CO_2. The use of CO_2 as the calibration medium provides an additional check on the internal consistency of the instrument with respect to wavelength, because the Angstrom exponent of a Rayleigh scatterer is known to be nearly equal to 4. (The Angstrom exponent varies slightly with wavelength because of dispersion effects.)

All data were recorded as 1-min and 1-h means by ICDAS at all four sites. A Leeds and Northrup Speedomax 250 chart recorder running at a speed of 1 in h^{-1} provides a backup recording to fill in missing ICDAS data for each station. All data are available as 10-min or 1-h means in graphics, printout, or magnetic tape form.

3.8.2 Operations

All Pollak CNC's operated properly throughout 1983. Locations and serial numbers of GMCC instruments are given in table 18. Pollak observations for all stations have been keypunched and are available as data files on the

Table 18.--Serial numbers and locations of GMCC instruments during 1983

Instrument	BRW	MLO	SMO	SPO	Boulder
Pollak CNC	16	13	22	15	19, 20, 21
Nephelometer	105	103	106	107	104

51

Boulder computer. For the SPO Pollak counter data, coincident meteorological observations were also keypunched and are available in the same file.

The G.E. CNC's and nephelometers operated properly most of the year at all four stations. Approximate data recoveries for the GE CNC's and nephelometers respectively were 75% and 81% at BRW, 96% and 85% at MLO, 98% and 96% at SMO, and 93% and 97% at SPO. Data gaps were caused both by instrument downtime and ICDAS downtime. Data lost during ICDAS downtime will be recovered from backup chart recorder data.

3.8.3 Data

Daily means of σ_{sp} and CN concentration at the GMCC stations are presented in fig. 26, and monthly means for the entire data record at each station are
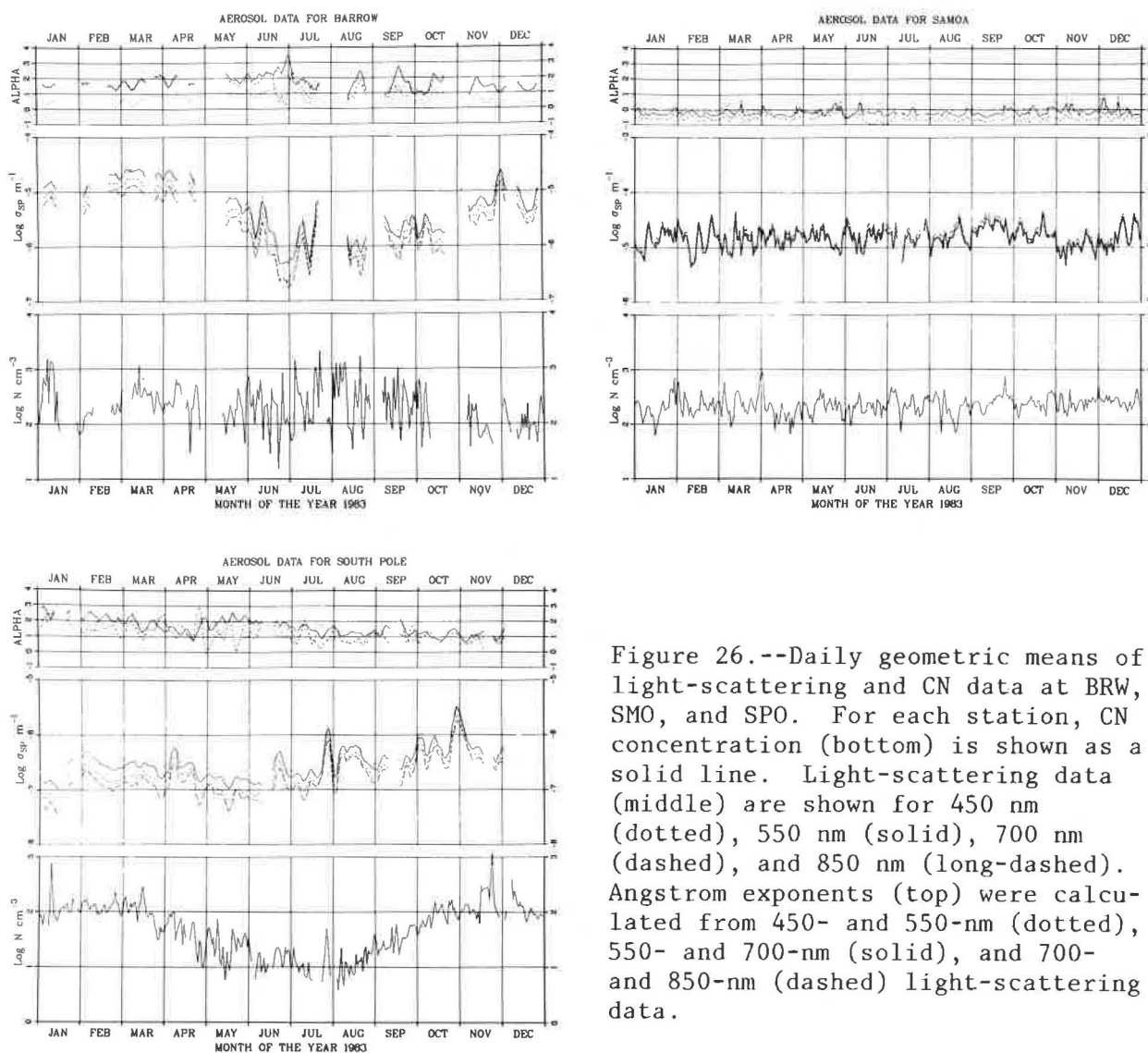
Figure 26.--Daily geometric means of light-scattering and CN data at BRW, SMO, and SPO. For each station, CN concentration (bottom) is shown as a solid line. Light-scattering data (middle) are shown for 450 nm (dotted), 550 nm (solid), 700 nm (dashed), and 850 nm (long-dashed). Angstrom exponents (top) were calculated from 450- and 550-nm (dotted), 550- and 700-nm (solid), and 700- and 850-nm (dashed) light-scattering data.

52

MONTHLY MEAN AEROSOL DATA FOR BARROW

MONTHLY MEAN AEROSOL DATA FOR SAMOA

MONTHLY MEAN AEROSOL DATA FOR SOUTH POLE
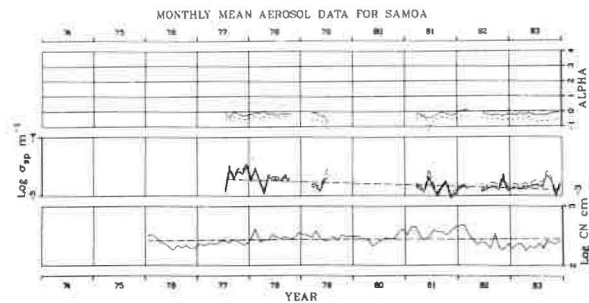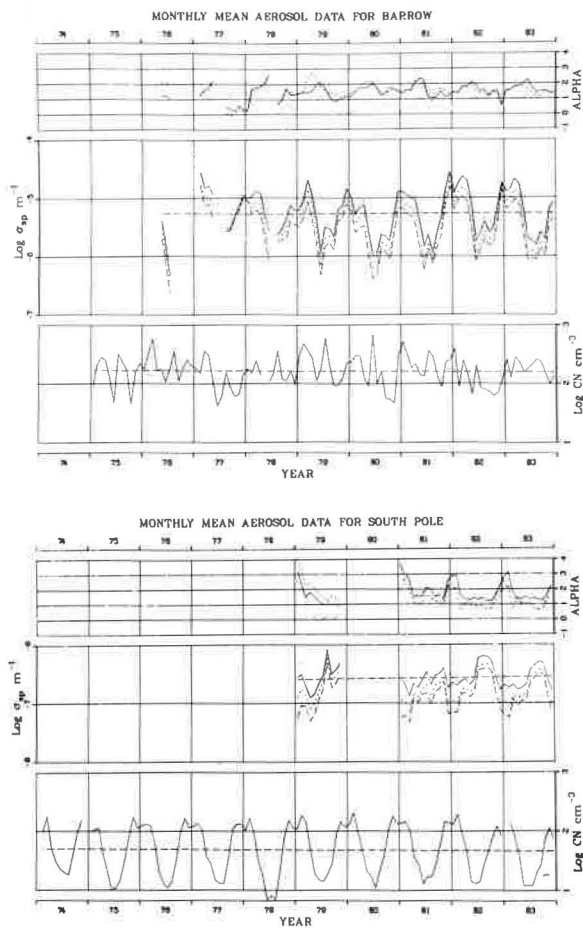
Figure 27.--Monthly geometric means of light-scattering and CN data for the entire data record, as in fig. 26. The straight dashed lines are least-squares linear trend lines.

presented in fig. 27. Monthly means for 1983 are given in table 19. The MLO data have been omitted from this year's report because of instrument problems that have delayed data editing.

The BRW data in fig. 26 clearly show the annual cycle in σ_{sp}, with a maximum in March and a minimum in June. The well-known Arctic haze, caused by the transport of anthropogenic and natural pollutants from the midlatitudes, is evident each spring in the σ_{sp} data shown in fig. 27. The CN data in figs. 26 and 27 show a more variable semiannual cycle, with maxima usually occurring in March and August, and minima occurring in June and November.

The SMO σ_{sp} and CN data continue as in previous years with no significant annual cycles or long-term trends. The Angstrom exponent data continue to show negative values, suggesting that the SMO seasalt aerosol size distribution has a strong peak near 1-μm diameter.

The 1983 SPO σ_{sp} data in figs. 26 and 27 show annual variations similar to those observed in 1979, 1981, and 1982: a minimum in May and large events dominating the record in late austral winter. These events, such as the one in late July in fig. 26, are caused by the transport of seasalt in the upper

53

Table 19.--Monthly geometric means of CN concentration (cm^{-3}) and σ_{sp} * (m^{-1}) at 450, 550, 700, and 850 nm for BRW, SMO, and SPO during 1983

	Jan	Feb	Mar	Apr	May	Jun	Jul	Aug	Sep	Oct	Nov	Dec
BRW												
CN	258	126	283	229	156	181	213	259	231	145	99	138
$\sigma_{sp}(450)$	1.40-5	1.57-5	2.39-5	1.94-5	7.35-6	2.58-6	2.27-6	1.76-6	2.89-6	2.31-6	6.93-6	9.20-6
$\sigma_{sp}(550)$	1.28-5	1.42-5	2.11-5	1.69-5	6.04-6	1.99-6	1.88-6	1.53-6	2.56-6	1.97-6	6.40-6	8.50-6
$\sigma_{sp}(700)$	8.79-6	9.72-6	1.36-5	1.09-5	3.72-6	1.15-6	1.22-6	1.09-6	1.78-6	1.36-6	4.55-6	6.19-6
$\sigma_{sp}(850)$	6.57-6	7.17-6	9.51-6	7.62-6	2.64-6	8.41-7	9.21-7	8.73-7	1.43-6	1.01-6	3.48-6	4.78-6
SMO												
CN	193	225	233	180	214	195	236	194	263	240	238	271
$\sigma_{sp}(450)$	1.34-5	1.36-5	1.29-5	1.42-5	1.39-5	1.53-5	1.51-5	1.42-5	2.28-5	1.84-5	1.05-5	1.60-5
$\sigma_{sp}(550)$	1.32-5	1.34-5	1.27-5	1.43-5	1.39-5	1.51-5	1.48-5	1.41-5	2.23-5	1.76-5	9.95-6	1.52-5
$\sigma_{sp}(700)$	1.39-5	1.42-5	1.32-5	1.51-5	1.42-5	1.60-5	1.57-5	1.50-5	2.36-5	1.82-5	1.01-5	1.55-5
$\sigma_{sp}(850)$	1.55-5	1.58-5	1.45-5	1.67-5	1.53-5	1.82-5	1.79-5	1.70-5	2.68-5	2.04-5	1.14-5	1.69-5
SPO												
CN	110	122	97	41	25	15	10	12	32	85	152	111
$\sigma_{sp}(450)$	3.00-7	4.75-7	3.60-7	3.46-7	2.27-7	2.70-7	3.36-7	4.65-7	4.35-7	9.28-7	7.25-7	--
$\sigma_{sp}(550)$	1.84-7	3.16-7	2.63-7	2.60-7	1.55-7	1.95-7	2.69-7	4.00-7	3.38-7	7.91-7	6.26-7	--
$\sigma_{sp}(700)$	2.40-7	1.85-7	1.69-7	1.82-7	9.47-8	1.24-7	1.89-7	2.97-7	2.36-7	5.99-7	4.99-7	--
$\sigma_{sp}(850)$	7.00-8	1.39-7	1.23-7	1.35-7	7.82-8	9.62-8	1.59-7	2.49-7	1.94-7	4.89-7	4.33-7	--

*A compact exponential format is used for σ_{sp} such that $1.40\text{-}5 = 1.40 \times 10^{-5}$.

troposphere from stormy regions near the coast to the interior of the Antarctic continent. The familiar annual cycle in CN concentration in figs. 26 and 27 show austral summer concentrations in excess of 100 cm^{-3} and winter concentration below 10 cm^{-3}.

The least-squares trend lines given in fig. 27 are essentially unchanged from last year's analysis (Harris and Bodhaine, 1983, p. 50). In no case is the trend from the beginning to the end of a data record significant compared with the standard error about the regression line.

3.9 Solar Radiation

3.9.1 Introduction

The basic solar radiation monitoring program at the four GMCC baseline observatories consists of two global pyranometers, two normal incidence pyrheliometers, and two dual-wavelength sunphotometers. The two pyranometers, quartz (Q, 0.30-2.80 μm) and RG8 (0.695-2.80 μm), and one quartz pyrheliometer operate continuously with the output voltages recorded on ICDAS. The second pyrheliometer has a filter wheel and, along with the two sunphotometers, is hand-operated several times a day when the Sun is unobstructed by clouds. The same pyranometers and pyrheliometers have been in operation since at least 1976 with only the following instrument changes. The RG8 at SMO has been changed three times because of filter deterioration. The quartz pyranometer at SMO was changed on 1 January 1983 because of detector deterioration. The continuous pyrheliometer at BRW was put online in March 1983. Several instruments, not considered part of the basic program, have been added or deleted from observatory programs between 1976 and 1984 (see previous GMCC Summary Reports).

3.9.2 Instrument Intercomparison

On an annual basis a traveling-standard pyranometer and pyrheliometer are sent to each station for a quality control intercomparison. The traveling standards are then routinely checked against absolute standards maintained by SRCF.

The present sunphotometer program was begun in early 1982, and calibration and quality control procedures are being instituted. The self-calibrating instruments are calibrated, when possible, at the observatories by the Langley technique, or are calibrated relative to standards maintained in Boulder. Principal responsibility for the sunphotometer calibration during 1983 has been with SRCF.

The following summarizes 1983 activities at the GMCC sites relative to the basic solar radiation monitoring program and to special activity.

3.9.3 Barrow

Prior to 1983, a continuous tracking pyrheliometer was not operated at BRW because of the large amount of cloud cover. As a result of recent interest in the clear-sky periods with respect to Arctic haze, and in an attempt to document the extent of clear periods better, a continuous pyrheliometer was put online in March 1983. The clock drive tracker has proved very accurate, and the solar declinator can be set from charts when conditions are too cloudy to align it directly. The clock drive mechanism was adapted for cold weather operation by removing the existing lubricants and replacing them with extreme cold-dry lubricants.

An all-sky, 190° field-of-view, time-lapse camera was operated at BRW for most of the sunlight portion of 1983. The speed was nominally one frame per 5 minutes. The 16-mm color movie film documented sky conditions at the station.

During March an intensive effort was made to measure spectral optical properties of Arctic haze using remote-sensing techniques at the observatory. This effort was in conjunction with the broader AGASP flight program. The remote-sensing techniques used involved relative measurements of various spectral components of short-wave solar radiation. Spectral measurements were made of direct solar intensity, zenith sky intensity, global diffuse flux, and global total flux. Aerosol optical depth was derived from the direct Sun-intensity measurements, and the results are reported by Dutton et al. (1984). The results from the diffuse and global measurements are being prepared for a NOAA Data Report.

The traveling-standard pyranometer and pyrheliometer were at BRW from 8 June to 6 July 1983. No significant change from previous years was detected in the station instruments' sensitivity relative to the traveling standard.

3.9.4 Mauna Loa

Mauna Loa is unique among the GMCC observatories because its location and climate offer reliably frequent opportunities for solar observation through a clean, dry atmosphere. As a result, more long-term and short-term GMCC solar

55

radiation programs have been carried out at MLO. Previous GMCC Summary Reports discuss several ongoing or terminated solar measurement projects at MLO. The following summary provides an update for 1983.

A computer-automated solar observatory now operates at MLO. The observatory consists of a moderate-sized, active solar-tracking spar housed in a 16-ft-diameter astronomical observatory dome. The dome aperture automatically opens, follows the Sun, and closes each day. Certain environmental conditions such as high wind, rain, or excessive clouds will automatically close the dome or prevent it from opening. A microcomputer-based data acquisition system records up to 32 channels of analog voltage data on magnetic tape. The active solar-tracking spar is accurate, in the absence of clouds, to about ±0.05°, and resets to the sunrise position at or near sundown. Instruments mounted on the spar include a pyrheliometer, a seven-wavelength sunphotometer, a three-wavelength sunphotometer, and a two-wavelength solar hygrometer.

An Eppley/Kendall ACR is occasionally operated at MLO as a reference calibration for the two basic-program pyrheliometers. Over a period of nearly 2.5 years, the sensitivity of this continuous tracking pyrheliometer has not changed by more than ±0.3% relative to the ACR.

Two pyranometers, GG22 (0.400-2.80 μm) and OG1 (0.530-2.80 μm), were put back online in late 1982 and operated throughout 1983. The instruments were put back online, after being removed in early 1981, to gather as much information as possible on the decay of the El Chichon debris cloud. The instruments operate continuously, but the data are no longer archived as was the case prior to 1981.

A shaded quartz pyranometer operates continuously at MLO measuring global diffuse solar flux. The shade mechanism is a small disk on a narrow rotating arm driven by a clock drive, which keeps the pyranometer detector from being exposed to the direct Sun. The instrument has operated on an experimental basis since 1979, but tracking problems until late 1981 reduced the amount of useful data.

A continuous-output three-wavelength sunphotometer (PMOD), designed after specifications provided by the WMO, began operating on the automated spar in September. Extraterrestrial calibration constants are derived several times per week and remained within ±1.0% throughout 1983. The GMCC PMOD sunphotometer was sent to Boulder for 3 weeks in October, where its calibration was compared with several other instruments.

A leveling error in the monitoring quartz pyranometer was detected in 1983 during detailed analysis of earlier MLO flux data. The leveling error (~1.0°) had no significant effect on daily averages or total energy integrals as archived at Asheville, but did affect instantaneous readings such as those used when evaluating the radiation field at specific times. The error was detected by examining ratios between different instruments and was verified in a continuous postcalibration of the pyranometer. The continuous calibration was accomplished by the shading-disk technique using the tracking pyrheliometer and diffuse pyranometer. The leveling error first occurred in February-March 1980 and was unknowingly corrected in August 1981. The actual error was a function of time of year and was less than 5% at a zenith angle of 60°.

Several calibrations of the hand-operated J series sunphotometers were carried out at MLO during 1983. Recalibration of two instruments, J202 and

J314, (380/500 and 778/862 nm) over a 2.5-yr period have shown them to be very stable; their calibration constants all remained within ±2%. These calibrations require extraordinary effort on the part of the station personnel, and were crucial to the evaluation of the El Chichon stratospheric cloud.

The traveling-standard pyranometer and pyrheliometer were at MLO from 19 July to 20 August. No changes in the sensitivity of the station instruments relative to the standards were detected.

3.9.5 Samoa

The location of SMO is of particular importance because of its sea level elevation in the Southern Hemispheric tropics. Here the solar flux is measured at the ocean-atmosphere boundary where the major global heating occurs. SMO is the only GMCC station where this measurement is made.

In the past, serious instrument degradation has occurred at SMO. This degradation is assumed to occur because of the warm, moist, and salty environment at the observatory. Deterioration of the RG8 pyranometer filter dome was prevented by fitting an additional clear glass dome over the RG8 dome. The area between the two domes is vented by pressurized dry air to prevent moisture, and to some extent, heat buildup. The modified instrument was tested and calibrated in Boulder prior to deployment in late 1983.

The traveling-standard pyranometer and pyrheliometer were at SMO from 26 September to 7 October. No change in the station instrument calibration was detected.

3.9.6 South Pole

Several changes to the program at SPO occurred during 1983. An upward-facing pyrgeometer was installed on the roof of CAF in April to measure downward terrestrial infrared flux. Ancillary air and snow surface temperature measurements were made to support the pyrgeometer measurements. Discrete albedo measurements with a portable instrument were discontinued. The discrete albedo instrument suffered from several shortcomings and rarely produced useful data. The continuous albedo measurements are still being made, however, and improvements are planned for the structure that supports the downward-facing detector. The current structure holds two shortwave pyranometers (Q and RG8) and will hold a pyrgeometer in early 1984. The structure is occasionally turned to an upward position for intercomparison with the normally upward-facing detectors.

A new Eppley pyrheliometer SN 21948 was sent to SPO to replace the quartz tracking NIP SN 2968 that had shown some alignment irregularities. Both instruments operated during most of 1983.

Observations with the OG1 pyranometers, global flux and continuous albedo, were discontinued in March 1983. The OG1 albedo measurements began in 1981, and the global flux in 1976. The instruments were removed to permit data acquisition space for the pyrgeometer and to conform with the basic solar program at the other GMCC sites.

A solar hygrometer for measuring precipitable H_2O was operated at various times at SPO, but experienced some mechanical and electrical problems. The instrument was returned to Boulder for maintenance and calibration.

The traveling-standard pyranometer and pyrheliometer were online at SPO in late December 1982 and in 1983.

3.9.7 Boulder

A semiautomated solar observatory, similar to the MLO facility, is now maintained in Boulder. The Boulder facility is used only as required for calibration and instrument testing. The dome uses analog logic for solar tracking and an HP85 for data acquisition.

A multilaboratory sunphotometer intercomparison was held in Boulder from 3 to 7 October 1983. Representatives from nine organizations made side-by-side measurements of atmospheric optical depth with 19 sunphotometers. Measurements at similar wavelengths were compared directly. The many varied wavelengths at which measurements were taken has complicated final complete analysis of the intercomparison. The most common wavelength used was 500 nm, and preliminary comparison showed good agreement (within ±0.01 optical depth units) between 7 of 11 instruments when the optical depths were tabulated using calibrations supplied by the instrument owners. Much larger discrepancies were occasionally seen at shorter wavelengths, particularly using owner-supplied calibration constants. The optical depths generally compared well at wavelengths longer than 500 nm and at all wavelengths when derived from Langley plot slopes. Of the 19 instruments, 4 gave consistently unacceptable results at one or more wavelengths. Good filters, careful maintenance, and recent calibration are all apparently necessary for maximum-quality results from modern sunphotometers.

Traveling-standard pyranometer SN 12617 and pyrheliometer SN 13909 have been frequently calibrated in the past few years. The most recent calibrations have been performed by SRCF. The results of these calibrations are given in table 20. Although the calibration values have changed somewhat, particularly

Table 20.--Calibration history of the GMCC traveling-standard radiometers (mV mW^{-1} cm^{-2} absolute)

Year	Pyranometer SN12617	Year	Pyrheliometer SN13909
1973	0.0790	1975	0.0758
1974	0.0788	1981	0.0759
1978	0.0763	1981 (Apr)	0.0756
1981/1982	0.0764	1983 (Oct)	0.0757
1983 (Jan)	0.0751	1984	0.0758
1983 (Oct)	0.0741		

for the pyranometer, the annual field station intercomparisons have been conducted using the original calibration value of both the station and standard instruments. Only at SMO has any station instrument shown a significant change relative to the traveling standards since 1976. At SMO the pyranometer drifted about 1.2% yr^{-1} for about 4 years. The SMO data were corrected to agree with the standard before being archived.

3.10 Station Climatology

3.10.1 Instrumentation and Data Reporting

The interpretation of local measurements of trace gases, aerosols, and atmospheric turbidity requires accurate measurements of station pressure, air temperature, and moisture content. Surface winds must also be known to evaluate the potential influence of local pollution sources. Standard off-the-shelf instrumentation was chosen for most of these measurements. Wherever possible, WMO-recommended standards for exposure were used.

A propeller-type anemometer is used (Aerovane, no. 141, Bendix, Inc., Environmental Science Division, Baltimore, MD) to measure the wind speed and direction. A synchro-to-DC converter is used to translate the phase representation of direction to a DC voltage. Orthogonal components are used to average the wind. Station pressure is measured with a capacitance-type transducer (no. 1201C, Rosemount, Inc., Minneapolis, MN). The voltage output of the transducer is recorded without further processing. At BRW, MLO, and SMO the air temperature is measured with linearized thermistors (no. 44212, Yellow Springs Instrument Co., Yellow Springs, OH). The thermistors are encapsulated in stainless steel shells that are exposed in aspirated Sun shields (no. 43404, R. M. Young Co., Traverse City, MI). A resistance-type thermometer, with a minimum acceptable temperature of -85°C (no. 954PL, Stow Labs., Hudson, ME) is mounted in a naturally ventilated radiation shield (no. 43103-A, R. M. Young Co., Traverse City, MI) at SPO. Dewpoint hygrometers are used at all four stations (no. 911, EG&G Inc., Newton, MA, at BRW and SMO; no. 1200ASP, General Eastern Instrument Co., Watertown, MA, at MLO and SPO).

Hourly average values, scaled in metric units, are processed and reported for each measurement listed above. The data are stored on microfiche and magnetic tape. The microfiche listings are organized by station, date, time, and variable. The files are usually available 6 months after the end of the year.

3.10.2 Barrow

A description of the BRW site, its surroundings, and climatology can be found in previous GMCC Summary Reports. Wind roses of the hourly average resultant wind speed, in three speed classes, as a function of direction for 1977-1983 and for 1983, are in general agreement (fig. 28). The predominant wind direction is northeasterly for 1983 as opposed to north-northeasterly for 1977-1983. At the same time, easterly winds (NE-SE) occurred 54% of the time in 1983 compared with 61% for the 7 years of observations. Southwesterlies were slightly more prevalent than in previous years. In December 1983 a maximum wind speed of 25.0 m s^{-1} was reported. This is the maximum for the 7-yr period as well. Wind speeds of 10 m s^{-1} and greater were observed 14% of the
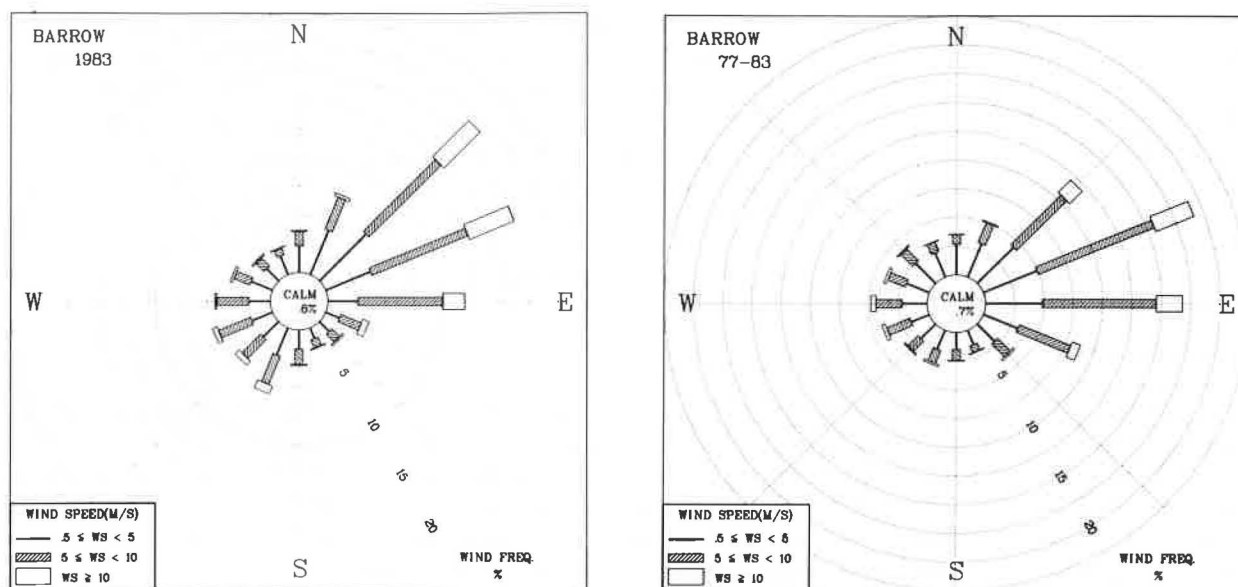
Figure 28.--Wind rose of surface winds for BRW for (left) 1983 and
(right) 1977-1983. The distributions of the resultant wind direction
and speed are in units of percent occurrence for the year and 7-yr
period, respectively. Wind speed is displayed as a function of
direction in three speed classes.

time in 1983 compared with a 7-yr average of slightly less than 10%. The
average pressure for 1983 was 1014.0 mb (see table 21). This value is 0.7 mb
greater than the 7-yr average. The average temperature is -14.7°C, which is
2°C colder than the 7-yr average. The -45°C minimum for the year was within
2°C of the minimum for the previous 6 years. The coldest temperature reported
by NWS in Barrow was -49°C in 1924.

3.10.3   Mauna Loa

A description of the MLO site and its climatology can be found in pre-
vious GMCC Summary Reports. The combined wind distribution for 1977-1983 in
fig. 29 shows a much higher occurrence of southerly winds than would be ex-
pected from synoptic-scale flow analysis. The effect of Mauna Loa Mountain is
to redirect stronger, predominantly easterly or westerly winds aloft down the
slope with a more southerly component. The distribution for 1983 is in excel-
lent agreement with the 7-yr average that is presented. The pronounced peak
in the southeast direction in 1983 is not as significant when combined with
the neighboring sectors. Thus 32% of the time the wind is southeasterly (ESE-
SSE) compared with 28% for the 7-yr average. Wind speeds equal to 10 m s^{-1}
and greater occurred 4.7% of the time in 1983 compared with 7.1% for the 7-yr
average. The significant change in the winds at MLO occurred in the first
half of the year, during which time a peak wind of only 13 m s^{-1} was observed
(see table 22). Typically peak winds associated with Pacific storms exceed
20 m s^{-1}. Associated with abnormally strong zonal flow across the subtropic
Pacific, almost no storms were encountered in Hawaii. April was most anoma-
lous, with 92% of the winds less than or equal to 5 m s^{-1}. For the 7-yr

60

Table 21.--BRW 1983 monthly climate summary*

	Jan	Feb	Mar	Apr	May	Jun	Jul	Aug	Sep	Oct	Nov	Dec	1983
Prevailing wind direction	ENE	ENE	ENE	ENE	ENE	E	ENE	E	SSW	ENE	NE	NE	NE
Average wind speed (m s⁻¹)	5.6	7.2	5.9	7.3	6.0	5.5	4.5	5.6	6.3	6.8	7.2	8.6	6.4
Maximum wind speed† (m s⁻¹)	14	15	12	17	13	12	8	15	19	18	21	25	25
Direction of max. wind† (deg.)	90	70	270	50	20	230	120	230	80	80	50	200	200
Average station pressure (mb)	1017.1	1011.6	1022.6	1019.5	1020.2	1010.1	1012.3	1005.1	1008.4	1010.9	1006.7	1024.0	1014.0
Maximum pressure† (mb)	1026	1028	1030	1038	1034	1024	1021	1019	1025	1029	1020	1045	1045
Minimum pressure† (mb)	1008	997	1007	1000	995	998	1001	987	983	984	991	1002	983
Average air temperature (°C)	-29.8	-27.2	-27.3	-19.0	-10.9	-1.3	0.4	-0.3	-6.2	-16.0	-19.7	-19.9	-14.7
Maximum temperature† (°C)	-18	-18	-18	-2	0	8	11	8	0	-1	-8	-3	11
Minimum temperature† (°C)	-45	-38	-37	-31	-17	-5	-3	-6	-17	-32	-31	-38	-45

*Instrument heights: wind, 16 m; pressure, 9.5 m (MSL); air and dewpoint temperature, 3 m. Wind and temperature instruments are on a tower located 25 m northeast of the main building.
†Maximum and minimum values are hourly averages.

average, 69% of the winds are in this range. No rain fell at the observatory in January through March. MLO received only 156 mm of precipitation in 1983 compared with 1242 mm in 1982. The average station pressure for the year was 681.8 mb compared with a 7-yr average of 681 mb. The average temperature was 7.9°C compared with a long-term average of 7.0°C. The winter and spring months were also warmer than usual.
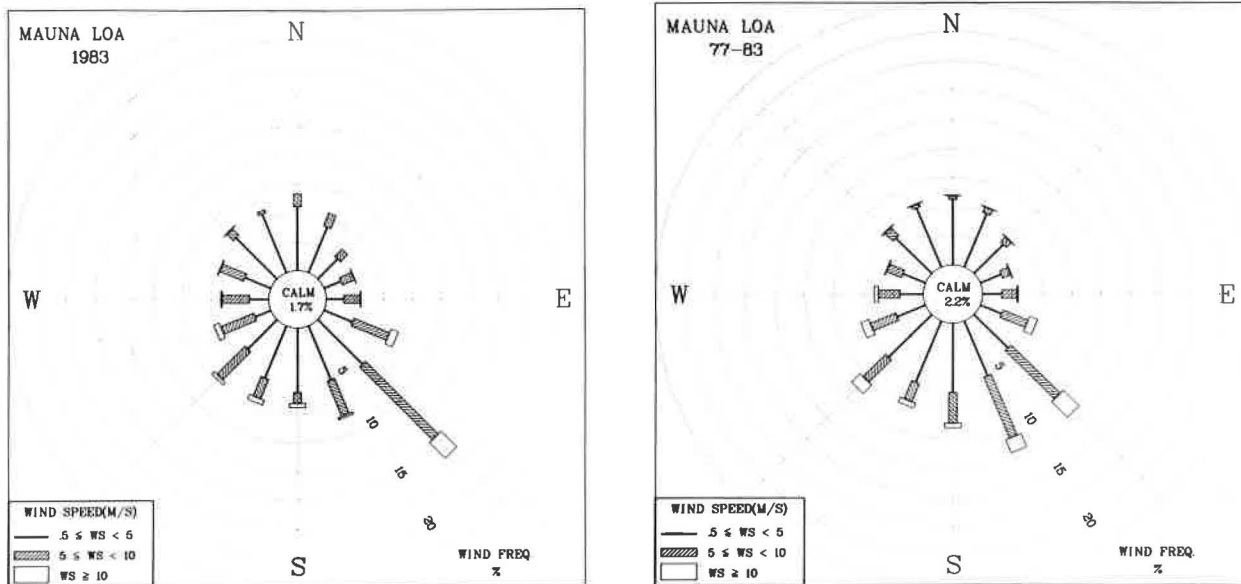
Figure 29.--Wind rose of surface winds for MLO for (left) 1983 and (right) 1977-1983. See legend for fig. 28.

Table 22.--MLO 1983 monthly climate summary*

	Jan	Feb	Mar	Apr	May	Jun	Jul	Aug	Sep	Oct	Nov	Dec	1983
Prevailing wind direction	WSW	SW	SW	SE	SE	SE	SE	SE	SE	SE	SE	SSW	SE
Average wind speed (m s^{-1})	6.2	4.5	4.2	3.1	4.1	4.7	5.1	4.9	4.6	4.4	5.5	6.2	4.8
Maximum wind speed† (m s^{-1})	13	11	11	11	9	13	14	13	12	13	14	15	15
Direction of max. wind† (deg.)	255	270	240	131	161	129	142	137	123	133	124	184	184
Average station pressure (mb)	681.3	681.3	682.3	680.8	681.7	682.5	682.4	682.9	681.6	681.5	682.9	680.4	681.8
Maximum pressure† (mb)	684	685	685	684	685	685	685	685	685	686	686	685	686
Minimum pressure† (mb)	677	678	680	678	679	679	679	681	679	678	679	674	674
Average air temperature (°C)	8.1	6.9	8.5	6.1	8.0	8.8	10.2	9.5	8.0	7.1	8.0	5.3	7.9
Maximum temperature† (°C)	18	16	16	14	16	18	19	18	17	16	18	15	19
Minimum temperature† (°C)	-2	-1	1	-2	0	0	2	1	1	0	0	-1	-2
Precipitation (mm)	0	0	0	8	3	64	1	20	21	3	3	34	156

*Instrument heights: wind, 10 m; pressure, 3399 m (MSL); air and dewpoint temperature, 2 m. Wind and temperature sensors are located approximately 15 m southwest of the main building on a tower. Pressure sensors are located in the observatory building.
†Maximum and minimum values are hourly averages.

3.10.4 Samoa

Southeasterly winds, including the directions east-southeast through south-southeast occurred 72% of the time in 1983 at SMO compared with an average of 63% for 1977-1983 (fig. 30). The shift in the occurrence frequency to more southerly direction is probably a result of the anomalous flow pattern caused by the ENSO event. A large high-pressure area over French Polynesia during January through March would explain more southerly winds and drier
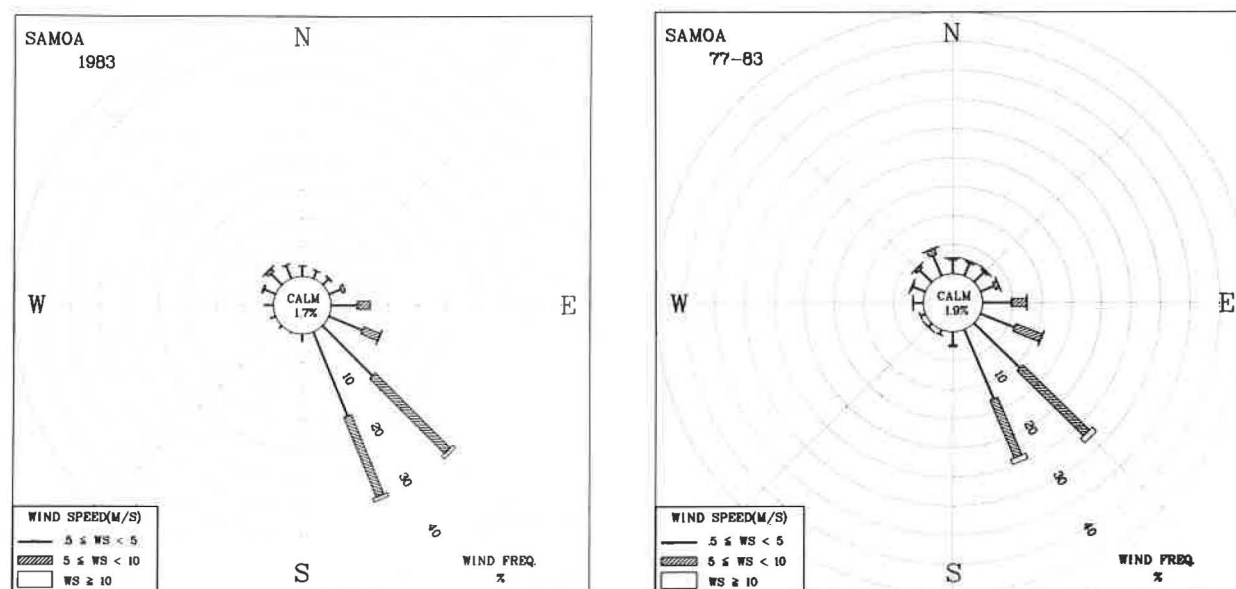
Figure 30.--Wind rose of surface winds for SMO for (left) 1983 and (right) 1977-1983. See legend for fig. 28.

62

Table 23.--SMO 1983 monthly climate summary*

	Jan	Feb	Mar	Apr	May	Jun	Jul	Aug	Sep	Oct	Nov	Dec	1983
Prevailing wind direction	SSE	SSE	SSE	SSE	SE	SSE	SE	SE	SE	SSE	SE	NW	SE
Average wind speed (m s^{-1})	4.1	3.8	3.1	4.6	4.5	5.0	5.4	6.5	6.0	5.3	3.7	3.5	4.7
Maximum wind speed† (m s^{-1})	10	9	8	9	10	10	14	11	11	11	8	11	14
Direction of max. wind† (deg.)	143	148	97	149	145	147	149	147	141	147	137	313	149
Average station pressure (mb)	--	--	--	--	--	--	1003.7	1004.6	1002.9	1001.9	1001.2	1000	1002.4
Maximum pressure† (mb)	--	--	--	--	--	--	1008	1010	1006	1005	1005	1003	1010
Minimum pressure† (mb)	--	--	--	--	--	--	999	1001	1000	999	999	996	996
Average air temperature (°C)	26.9	27.8	27.3	26.4	26.5	25.9	24.9	24.4	25.3	25.3	26.5	26.9	26.2
Maximum temperature† (°C)	31	31	30	30	30	29	29	27	29	31	31	31	31
Minimum temperature† (°C)	24	24	24	24	24	24	21	22	23	21	21	23	21
Precipitation (mm)	187	223	163	170	78	78	15	20	124	135	247	347	1787

*Instrument heights: wind, 14 m; pressure, 30 m (MSL); air and dewpoint temperature, 7 m. Wind and temperature sensors are located atop Lauagae Ridge, a distance 110 m northeast of the station. Pressure sensors are located in the station.
†Maximum and minimum values are hourly averages.

conditions at SMO. The wind shift was most noticeable in April when the wind was southeasterly 89% of the month. At no time during the first 5 months did the speed exceed 10 m s^{-1}. The precipitation amount of 1.79 m for the year was only slightly less than 1.81 m recorded the previous year. The months May-August had less precipitation than they did in 1982 (table 23). The average temperature for the year was 26.2°C; the maximum, 31°C.

The exposure of the instrumentation at SMO is considerably different from that at the other GMCC stations. Since February 1977, the anemometer has been located at a height of 14 m on a sampling tower atop Lauagae Ridge. In this location there are no major obstacles to the wind flow from the westerly direction, but the shape of the bluff displaces the wind from easterly directions. Temperature is measured at a height of 7 m on the same tower. Dewpoint temperature is measured from air samples drawn from the sampling stack. Station pressure is measured in the main building located about 100 m west of the sampling tower. On 28 March 1982 lightning hit the sampling tower causing damage to most instruments located on top of the ridge as well as to some in the station building. Some sensors could be repaired, but the wind and pessure sensors required replacement. A significant part of the pressure and humidity record is missing as a result of this lightning strike.

3.10.5 South Pole

The wind rose for 1983 is significantly different from the 7-yr average, (fig.31) in that 1983 is almost void of winds in excess of 10 m s^{-1}. Hourly average wind speeds of 10 m s^{-1} or greater usually occur about 3.5% of the time. In 1982 they were observed 7% of the time. In 1983 only 9 hours were reported. This is reflected in the peak wind statistics and in an annual average wind speed of only 3.9 m s^{-1} compared with the 7-yr average of 5.3 m s^{-1} (see table 24). The most prevalent wind direction is north-northeast, as in previous years. At SPO north is defined as being along the prime meridian.
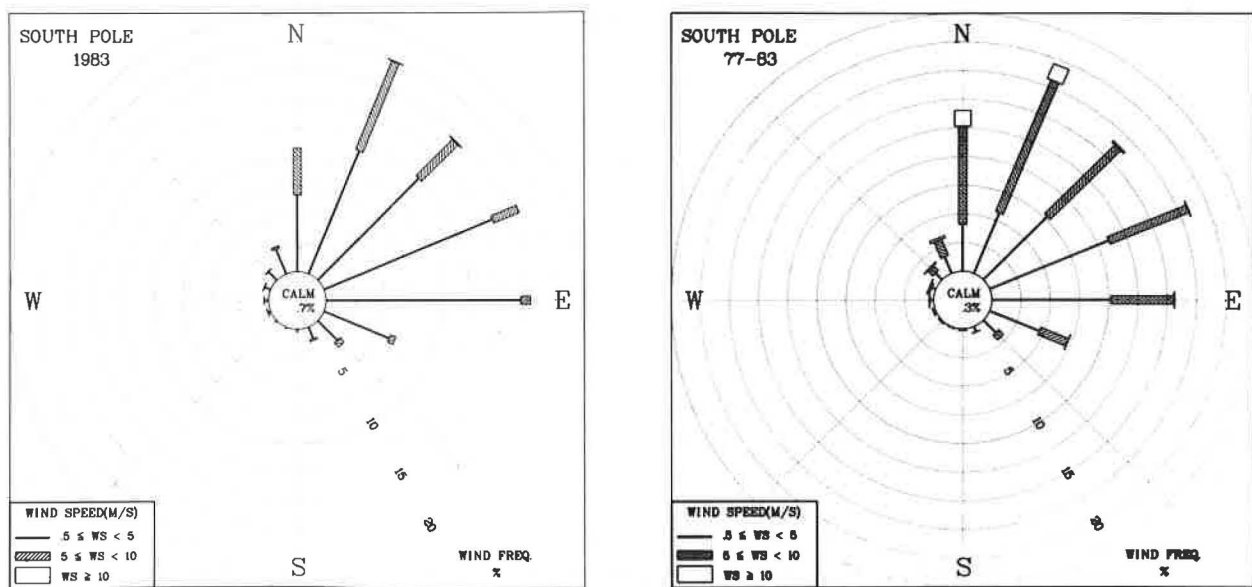
Figure 31.--Wind rose of surface winds for SPO for (left) 1983 and (right) 1977-1983. See legend for fig. 28.

The full extent of the austral winter on the Antarctic plateau is displayed by the fact that for 8 months the monthly average temperature is below the annual average. The average for 1983 is -53.2°C, 3.6°C below the 7-yr average. The hourly-average maximum temperature was -21.2°C; the minimum, -78.4°C.

Table 24.--SPO 1983 monthly climate summary*

	Jan	Feb	Mar	Apr	May	Jun	Jul	Aug	Sep	Oct	Nov	Dec	1983
Prevailing wind direction	N	E	ENE	E	E	E	ENE	NNE	NNE	NNE	ENE	NNE	NNE
Average wind speed (m s^{-1})	3.4	3.8	4.3	4.0	3.8	4.5	3.8	4.3	4.1	4.0	2.5	3.6	3.9
Maximum wind speed† (m s^{-1})	6	9	10	10	9	10	9	10	11	8	6	8	11
Direction of max. wind† (deg.)	28	20	12	40	31	26	22	15	39	3	307	25	39
Average station pressure (mb)	687.3	682.5	678.6	678.9	682.8	673.3	667.7	671.4	669.7	668.0	671.8	682.3	676.1
Maximum pressure† (mb)	694	695	694	688	706	699	681	689	690	693	680	695	706
Minimum pressure† (mb)	678	672	667	670	666	657	653	654	643	643	663	676	643
Average air temperature (°C)	-31.3	-44.7	-57.6	-58.7	-59.0	-64.7	-65.7	-61.4	-60.4	-57.3	-44.6	-32.1	-53.2
Maximum temperature† (°C)	-21	-33	-37	-42	-39	-44	-51	-47	-32	-48	-33	-23	-21
Minimum temperature† (°C)	-37	-55	-73	-71	-76	-75	-76	-74	-78	-70	-56	-41	-78

*Instrument heights: wind, 10 m; pressure, 2850 m (MSL); air temperature, 2 m. The anemometer and thermometer are located on a mast 30 m grid north of CAF. Pressure measurements are made inside CAF.
†Maximum and minimum values are hourly averages.

3.11 Precipitation Chemistry

Routine and special precipitation chemistry measurements continued at the GMCC sites of MLO and SMO, and at the regional sites. Special studies continued at MLO using the ion chromatograph for anion analyses for the six-site network. The Washington, DC, network continued to operate with two observers.

3.11.1 Baseline Measurements

The five-site special network on the island of Hawaii and a sixth site on Kauai operated on approximately a weekly schedule. Site locations were dis-
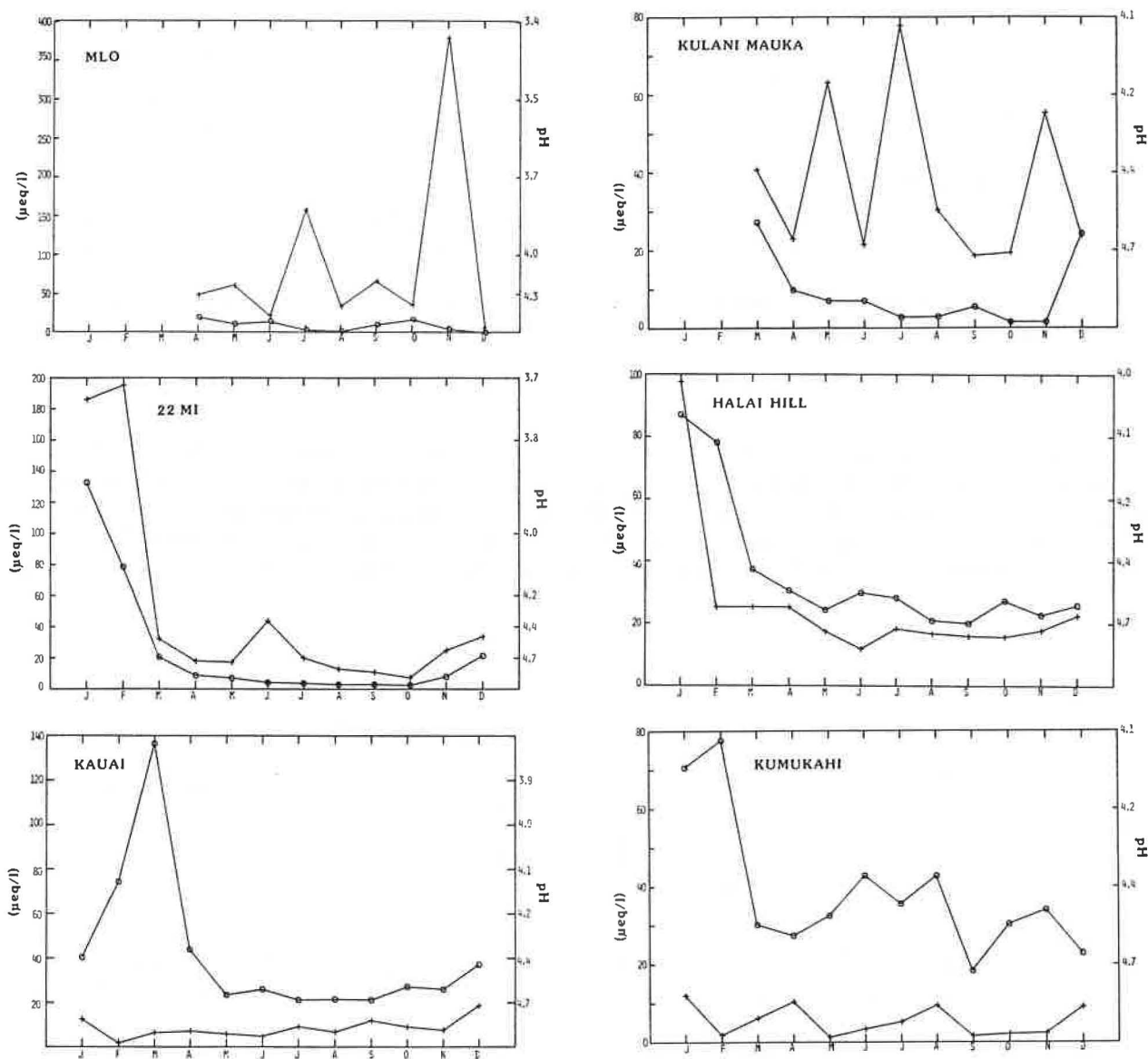
Figure 32.--Monthly precipitation weighted means for six sites on the islands of Hawaii and Kauai during 1983 (+ = H^+; O = $SO_4^=$). The sites in order of increasing elevation are Kumukahi, Kauai, Halai Hill, 22 Mile, Kulani Mauka, and MLO.

cussed in previous GMCC Summary Reports. As seen in fig. 32, the acidity at MLO and Kulani Mauka, the most elevated sites, remains at much higher levels than the acidity at the three sites at lower elevation on Hawaii. An opposite trend, a decrease in sulfate with increasing elevation, is also evident. However, the removal of the seawater component results in SO_4 values quite similar to those measured at MLO (fig. 33). Agreement of SO_4 at Halai Hill and Kauai, sites with similar elevation and orientation to the trade winds, was excellent (fig. 32) after the beginning of April.
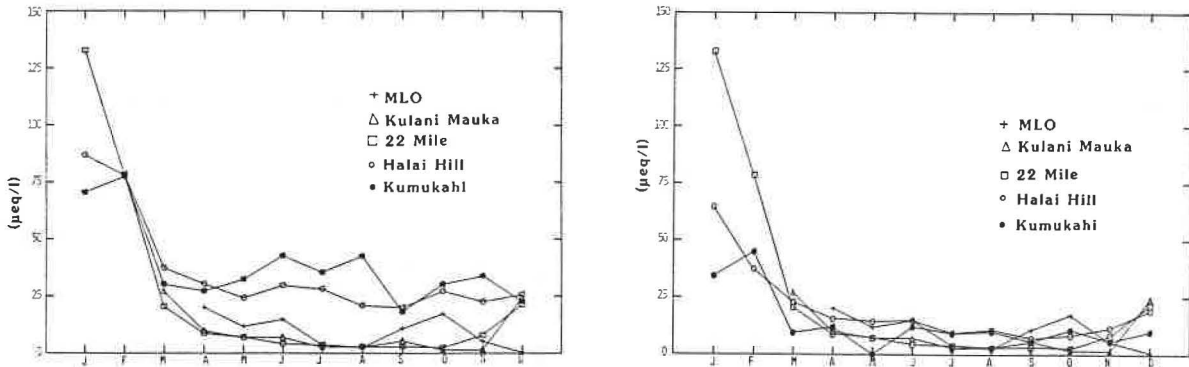
Figure 33.--Monthly precipitation weighted (left) sulfate means and (right) excess sulfate means for five sites on the island of Hawaii.

At MLO three independent pH measurements have been made for the past several years. The GMCC laboratory values (designated as event field pH in fig. 34) are measurements completed immediately after precipitation events at MLO. NADP field values were measured weekly at MLO, and NADP laboratory values were measured by ISWS at least 1 week after the field values from the same
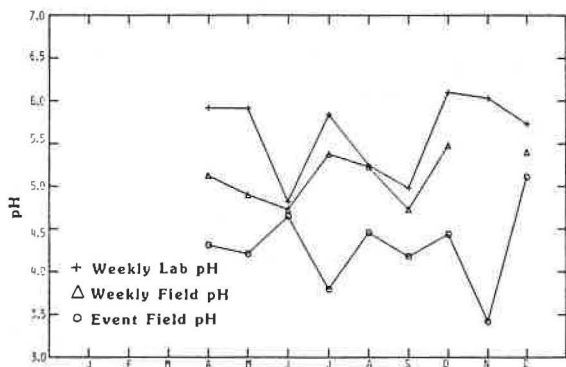
Figure 34.--Monthly precipitation weighted pH at MLO. Values vary as a function of time between sample collection and measurement. (No rain fell prior to 4 April.)
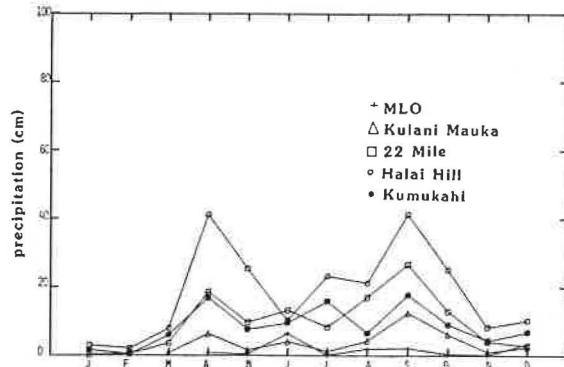
Figure 35.--Monthly precipitation at five Hawaiian sites for 1983.

Table 25.--Annual precipitation data for the six-site Hawaiian network

Site	Elevation (m)	Precipitation (cm)	
		1982	1983
MLO	3399	100.10	15.37
Kulani Mauka	2530	166.60	39.29
22 Mile	1829	251.63	116.62
Halai Hill	122	498.14	217.14
Cape Kumukahi	0	254.05	100.54
Kauai	152	382.98	161.30

precipitation sample bucket. It is evident that the pH of precipitation increases for several weeks following sample collection, probably due to the consumption of organic acids (Keene et al., 1983). Note that data from the first 3 months of 1983 in MLO are not missing. No rain fell prior to 4 April, and total annual rainfall was well below normal for the entire island of Hawaii See fig. 35 and table 25.

Snow sample data for BRW and SPO are shown in fig. 36. Monthly precipitation weighted H^+ and $SO_4^=$ means for SMO are shown in fig. 37.
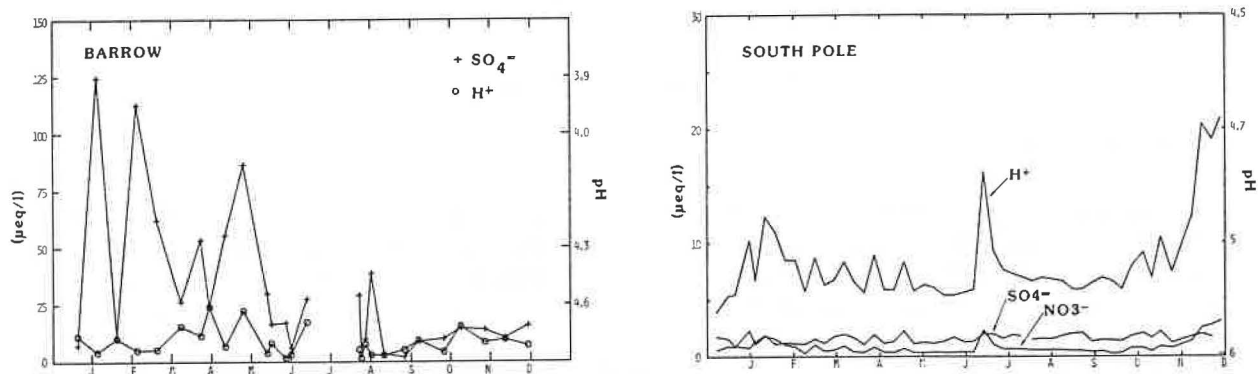
Figure 36.--Snow sample ion concentrations for BRW and SPO during 1983.

3.11.2 Regional Measurements

In a continuing effort to upgrade the NOAA regional precipitation sites, two stations have been closed and three new stations opened in 1983. The Research Triangle Park, NC, site was closed because of its proximity to several other NADP stations; the Huron, SD, site was closed because of a problem

67
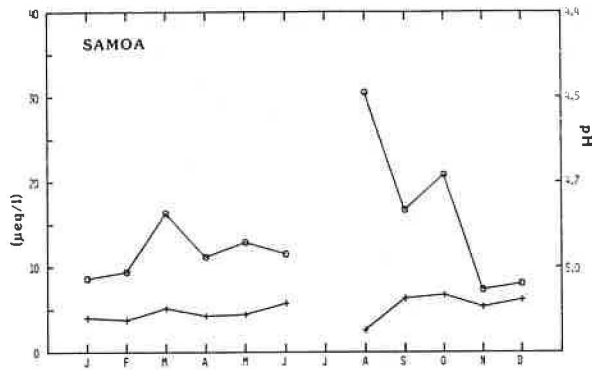
Figure 37.--Monthly precipitation weighted means for SMO during 1983 ($+ = H^+$; $O = SO_4^=$).
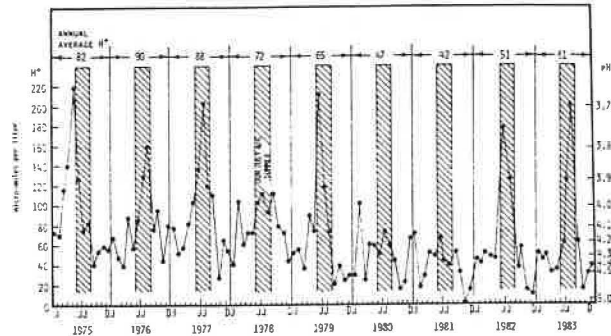
Figure 38.--Monthly precipitation weighted hydrogen ion concentration for the Washington, DC, area. The center bars highlight the summer data. Each annual mean is noted at the top of the corresponding column.

with local pollution sources. The three new sites are located in Cottonwood, SD, Lilley Cornett Woods, KY, and near Pennsylvania State University, State College, PA.

3.11.3 Washington, DC, Network

The data for the Washington, DC, network are shown in fig. 38.

3.12 Data Management

3.12.1 Acquisition

The passing of 1983 marks 10 years of operation for the minicomputer-controlled signal-recording system known as ICDAS. The first installation of ICDAS was in January 1974 at SPO. Similar systems were installed at BRW in May 1974 and at MLO in September 1974. The SMO installation was completed in January 1976. At MLO and SPO there were major interruptions to the data during the first 2 years of operation. At MLO, the main causes of the interruptions were inadequate control of the environmental temperature and the need to collect lidar data with the same minicomputer. At SPO, problems in 1975 were caused by incorrect changeover of the software.

ICDAS has performed well. The performance statistics by station and year beginning in 1978 are shown in fig. 39. The ICDAS unit at MLO has been operational 93.3% of the time since it was moved to a stable thermal environment in the main building in 1977. For the period 1978 to present, ICDAS has operated for 96.2% of the time at SMO, 98.8% at SPO, and 90.1% at BRW. During 1983, in particular, BRW had considerable problems with the magnetic tape drive, accounting for most of the failure time of 18%. Breakdowns at the other stations for 1983 were minimal: MLO, 2%; SMO, 1%; and SPO, 1%. All continuously measured variables are recorded on ICDAS including CO_2, ozone, solar irradiance, aerosols, winds, pressure, and temperature.

68
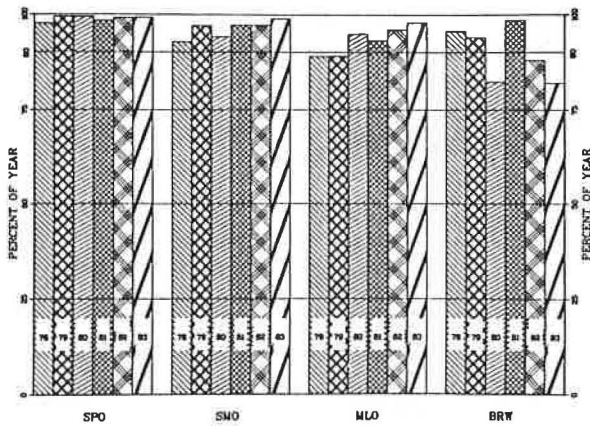
Figure 39.--ICDAS performance statistics by station and year for 1978-1983.

3.12.2 Data Processing

All data editing and processing is performed at the Boulder facility, employing a CDC 750 computer. A minicomputer system within GMCC, called the Reduction Facility, is intermediary to the CDC 750. In the Reduction Facility data are transferred from the station tapes to a tape format more acceptable to the larger facility. All the data are transferred in 1-mo segments to the CDC 750. No significant hardware or software changes were made in 1983. A DECtape II (TU-58) is used to read data from CAMS into the reduction system. In the future, all incoming CAMS tapes will be duplicated to 1600 bpi PE tapes for permanent storage before the data are transferred to a computer file. Work continued through the year on the software to transfer the data.

3.12.3 CAMS Development and Testing

The most significant advances in the development of a control and monitoring system to replace ICDAS were in the completion of hardware component testing and the preparation of software. For the most part, the electronic boards and peripherals were selected and tested early in the year. A deployment plan was prepared that suggested the implementation of four CAMS per station with a spare on the shelf. In the final analysis, the CAMS to support the aerosol measurement was combined with the unit for solar radiation, and the monitoring of ozone data was combined with meteorological sensor signals. A third CAMS operates the CO_2 analyzer. Once the configuration was determined, software specifications were revised for the specific units. By the end of the year the software for two of the units was written, but not completely tested. Twenty units were built: three active CAMS and one spare per station. About half were tested by the end of the year. Five additional CAMS are required in other applications and as spares to remain in Boulder.

CAMS uses the STD BUS as a means of interfacing with the Z80 microcomputer. The STD BUS uses a mother-board interconnecting system concept and is designed to handle any of a variety of STD-compatible modules. The compact modules for the STD BUS are 4.5 × 6.5 in, allowing for system partitioning by function (RAM, EPROM, I/O). With the completion of hardware testing, the following modules were found to be necessary. The first six modules are common to all units.

69

(1) Z80 Central Processor Module, MDX-CPU1 (Mostek MK77850).
(2) Universal Memory Expansion Board, MDX-UMC (Mostek MK77759).
(3) Battery Backup RAM Module, MDX-BRAM (Mostek MK77760).
(4) Battery Clock Module, MDX-BCLK (Mostek, MK77979).
(5) Serial I/O Module, MDX-S102 (Mostek, MK77670).
(6) Monitor board (developed and constructed in-house).
(7) Analog Input Board (Data Translation, DT2742).
(8) Analog Input Board (Data Translation, DT2744).
(9) Analog Input Power Converter Board (Data Translation, DT2715).
(10) Digital I/O Panel Controller, DIOP (Mostek, MK77672).
(11) Digital I/O Panel (Mostek, MK77673).
(12) Digital I/O Card (ProLog, 7601).
(13) Remote I/O Controller, RIOC (Mostek, MK78208).

The analog input boards are used in two modes: programmable gain mode DT2742 and fixed gain mode DT2744. Each analog input board requires a power converter board. The digital I/O panel and interface are used to control CO_2 calibration solenoids. The digital I/O card is used to acquire wind data in the meteorology CAMS. The remote I/O controller acquires asynchronous serial I/O from a companion unit (RS-422) at the Dasibi ozone monitor.

Using the serial I/O modules that provide an RS-232 port, CAMS interfaces with three devices. Data are recorded on preformatted cartridge tapes (DEC, TU-58). Each tape holds about 130,000 observations allowing, in most cases, 14 days or more operation between changes. Each CAMS contains two tape drives to facilitate automatic tape drive reassignment in case of a failure. A control panel is also supplied (Burr-Brown, TM-76; fig. 40). Designed as a durable, compact remote-entry terminal for computer access, this modular panel serves as a real-time data display as well as a means by which the operator controls processing and enters data. Hard copies are obtained on a dot-matrix printer (Epson MX-80). One printer is shared by the three CAMS in operation at the station. A switch is used to control access. Routine printouts give the results of instrument calibrations and summaries of daily observations. CAMS also maintains the time and date with a battery-powered clock. The random-access memory is also battery powered so that CAMS can recover to a normal state after a power outage. A thermometer on the monitor board measures the internal temperature. If the temperature exceeds the value specified for the electronics, a message is displayed to the observer. Figure 41
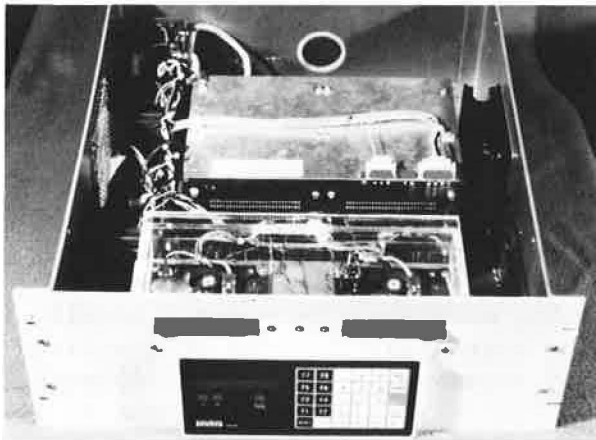
Figure 40--An exposed view of CAMS. In addition to the control panel, the tape drives, card cage, and power supplies are visible.
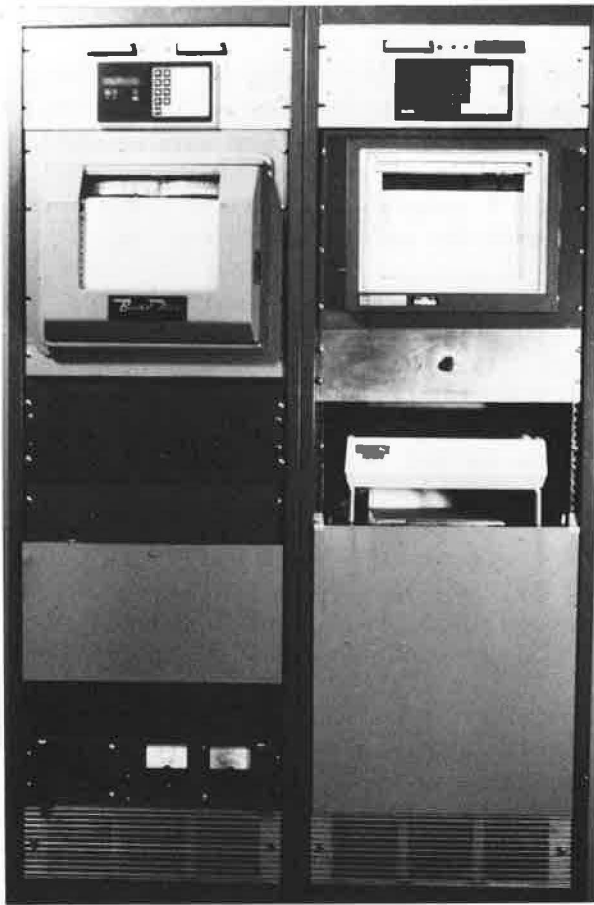
Figure 41--Station configuration of the aerosol-solar radiation and the meteorology-ozone CAMS.

shows the aerosol-solar radiation and the meteorology-ozone CAMS in station configuration.

Previously, all software for the microcomputer data logging and control requirements had been written in FORTRAN. These applications had limited I/O requirements that could be met by simply suspending acquisition tasks so that data could be output. The requirements for CAMS contained a significant increase in input and output such that a multitasking scheduler using interrupt priorities was necessary. Such a system was not feasible under FORTRAN. The problem was solved by changing to the language FORTH, which is more suitable to the microprocessor. A multitasking version of FORTH was purchased and device drivers were written. FORTH software development and testing began in June, and continued through the remainder of the year.

Along with reliability, one of the primary design considerations of CAMS is the ready access to data to allow the station staff to have active quality control of the measurements. This is accomplished in part by maintaining a file of the past 24 hourly average values, which can be printed at any time. At a specific time each day the file is recorded on tape. The observer can read and print the contents of any data file on tape when desired. The print-out of the file of hourly average values is formatted just as the computer resident file is. A single dot-matrix printer is provided for the three active CAMS. An RS-232 switch is used to select the active CAMS.

71

3.12.4 CAMS for CO_2

The design of the CO_2 CAMS incorporates two distinct modes of processing: (1) regular processing, during which ambient air is sampled for minutes 0-49, calibration gas W2 for minutes 50-54, and calibration gas W1 for minutes 55-59 of each hour; and (2) weekly calibration processing, during which six calibration gases are sampled repetitively for 5 minutes each. The CAMS automatically controls the flow of the various gases by switching solenoids.

The default mode of processing is regular processing. A weekly calibration may be started by pushing the F7 button on the front panel (fig. 40) and requesting the weekly calibration option. The F7 button has another option that allows manual setting of relays for a specified number of seconds to test the flow of gases from different tanks. When the relays are set in this manner no data are stored, since this function is for testing and is not part of normal data acquisition.

The weekly calibration consists of 5-7 hours or cycles of data. For each cycle, W1 and W2 concentrations are derived by finding the quadratic equation that best fits the four calibration points (low, mid, high, and Q gases), then solving for W1 and W2 along this parabola. The quadratic equation is fit by Gaussian elimination with row pivoting.

The operator may obtain printed reports that show minute voltages and the computed hourly concentration, hourly concentrations for the past 24 hours, or weekly calibration results. These data are also recorded on cassette.

3.12.5 CAMS for Meterology and Ozone

The specifications for the operation of the meterology-ozone CAMS called for detailed data display to facilitate quality control on the part of the observers at the station. Display takes the form of 1-min average values of all the active parameters being measured and a printout of a file of the previous 24 hourly values. The 1-min averages are displayed on the front panel of CAMS along with the date and time. Although these values are scaled, they are not recorded. Ten-minute and hourly averages are recorded along with a set of flags that indicate the proper operation of peripheral systems that can affect data quality. The printout of the hourly average values for the previous 24 hours will constitute part of a routine daily weather report.

The accurate reporting of weather conditions is important to the interpretation of all measurements at the observatories. The daily weather report, performed at a specific time (0000 GMT) daily, will serve as a definitive check on the continuous measurements. Included in these measurements is an estimate at the wind speed and direction, a direct comparison between the pressure transducer monitored by CAMS and the mercurial barometer, and a comparison between the air temperature at 2 m and the shelter temperature. Where conditions permit a meaningful comparison, a set of dewpoint temperatures will be measured as well. The precipitation amount will be recorded at the three northernmost stations. The comparison between independently observed values and those displayed on CAMS will serve as a daily check on data quality. The daily observations include determinations of the sky cover, cloud type, visibility, and weather conditions. These observations are reported on the printout of the hourly data, and are part of the official record.

3.13 Atmospheric Trajectories

Since 1981 GMCC has had a computer program that produces atmospheric trajectories. The development and use of this model is documented in the two previous Summary Reports (Bodhaine and Harris, 1982, pp. 71-74; Harris and Bodhaine, 1983, pp. 67-75) and by Harris (1982). Those publications detail the computational methods employed in the isobaric and the isentropic versions of the trajectory program.

This report updates the status of the program and gives examples of results obtained during 1983. A number of special projects in sec. 4 use trajectories in combination with other data to investigate airflow to various locations under study. See specifically secs. 4.1, 4.2, and 4.4. In addition, trajectories produced by this model were used to study origins of air arriving along a research cruise track and are presented in Parungo et al. (1984).

Table 26 gives a description of the input data obtained from NMC through NCAR for the trajectory program. Table 27 shows periods of missing data within this data set for which no trajectories can be computed. During 1983, the inventory of trajectories for BRW, MLO, and SMO (table 28) was expanded. To date, no trajectories have been computed for SPO.

Figure 42 shows a new feature of the trajectory plotting program, which allows four levels to be displayed on one map for comparison. Trajectories in this form are marked with letters A for 1000, B for 850, C for 700, and D for 500 mb and are plotted for one arrival time (0000 GMT or 1200 GMT).

The capability of computing forward trajectories was added to GAMBIT1, the Northern Hemisphere isobaric model. Forward trajectories departing Norilsk, U.S.S.R., on 16 February 1982 are shown in fig. 43. Five days later (the approximate travel time to Alaska) on 22 February, Shaw (1982) noted haze at Ester Dome, about 650 km southeast of BRW. He suggested Norilsk (69.4°N, 88.5°E), the largest copper-nickel smelting complex in the world, as a possible source for the haze. Backward trajectories arriving at BRW on this day (fig. 44) show transport from the area of Norilsk, which would be expected judging from the forward trajectories in fig. 43.

Table 26.--Description of NMC data purchased from NCAR

	Northern Hemisphere 65 × 65 grids	2.5° global grids
Dates	1975-1983	1977, 1979-1983
Parameters	u, v, z, T	u, v, z, T
Levels	1000-100 mb (mandatory levels)	1000-100 mb (mandatory levels)
Program	GAMBIT1, GAMBIT3	GAMBIT2

Table 27.--Breaks in NMC data for 1000, 850, 700, 500 mb

Year	Northern Hemisphere 65 × 65 grids	2.5° global grids
1975	14-15 Jan	N.A.
	16-31 Jan (1000 mb only)	
	16-18 May	
1976	None	N.A.
1977	None	None
1978	None	N.A.
1979	None	None
1980	07-08 Aug	26-28 Nov
	30-31 Dec	25-31 Dec
1981	01-07 Feb	01-07 Feb
	04-10 Oct	29 Aug-06 Sep
		03-11 Oct
		16-20 Dec
1982	12-19 Jan	22-25 Feb
	22-26 Feb	29 Jun-18 Jul
	03-11 Jul	28-30 Jul
	27-31 Jul	10-17 Aug
	09-16 Aug	
1983	09 Apr-01 May	08 Apr-01 May
	18-21 Jun	14-16 Oct
	03-05 Sep	(N.H. only)
		23-26 Nov
		(S.H. only)

In another example, forward trajectories (fig. 45) depart from Bennett Island on 18 February 1983, the date of a venting episode on this Russian island. At least 53 cases of venting have been documented by satellite photos during the past 11 years. At first this venting was thought to be volcanic, but scientists now believe it is a periodic methane hydrate release. Note that air arrived at BRW from Bennett Island after only 1-1.5 days.

Numerous questions were asked concerning the usefulness of trajectories in the Arctic, so the real data coverage north of 80°N was investigated by

Table 28.--Inventory of trajectories for GMCC observatories

Station	Dates	Levels (mb)
BRW	Feb, Mar, Apr 1979-1983	850, 700, 500
	Miscellaneous short periods	1000, 850, 700, 500
MLO	1975-1983	850, 700, 500
SMO	1977, 1979-1983	1000, 850
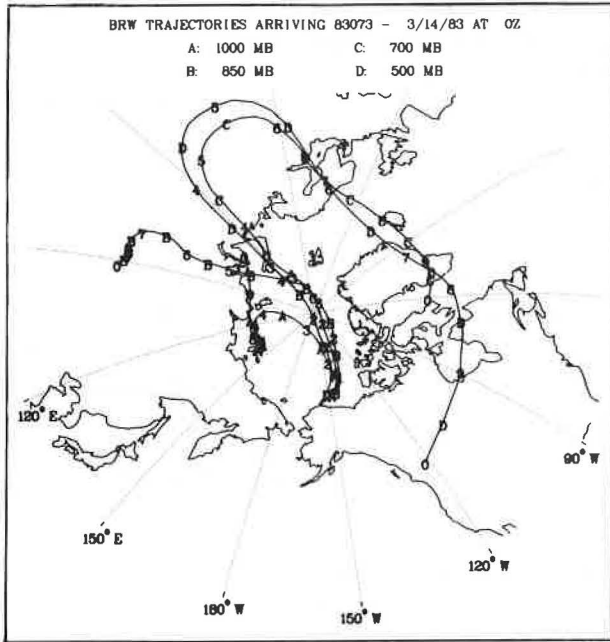
Figure 42.--BRW trajectories
arriving 14 March 1983 at 0000 GMT
on the (A) 1000-, (B) 850-, (C)
700-, and (D) 500-mb pressure sur-
faces. Numerals on the trajectories
indicate number of days to travel
from that point to the destination.
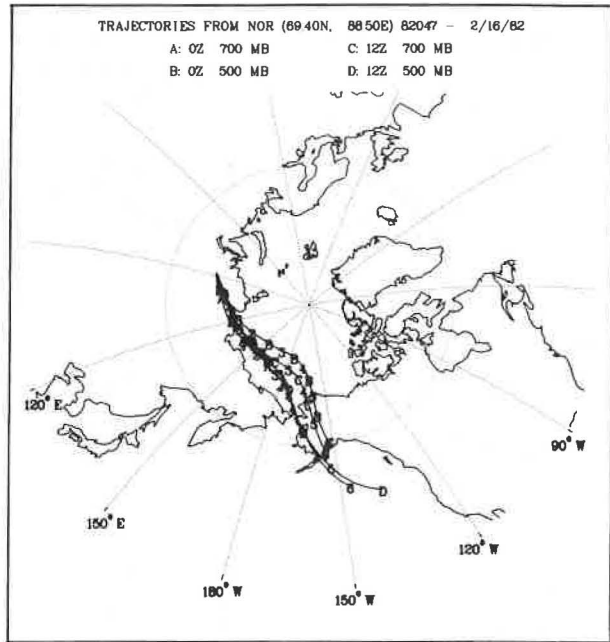
Figure 43.--Forward trajectories
departing from Norilsk on 16 Febru-
ary 1982 on the 700- and 500-mb
pressure surfaces.
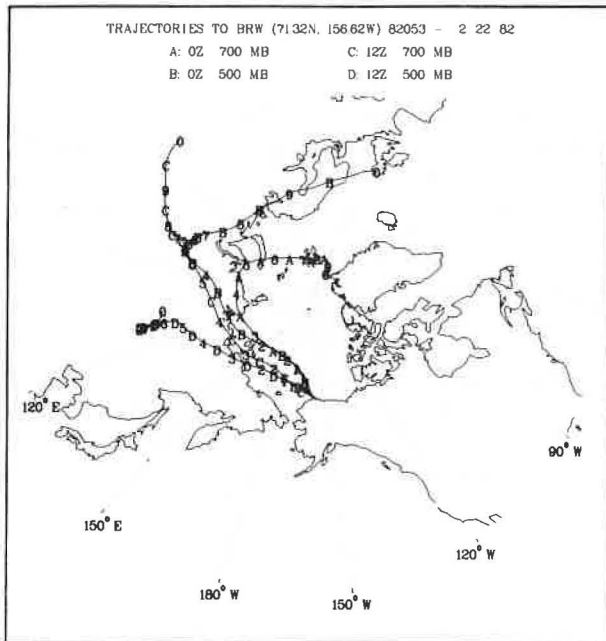
Figure 44.--BRW backward trajec-
tories arriving 22 February 1982 on
the 700- and 500-mb pressure sur-
faces.
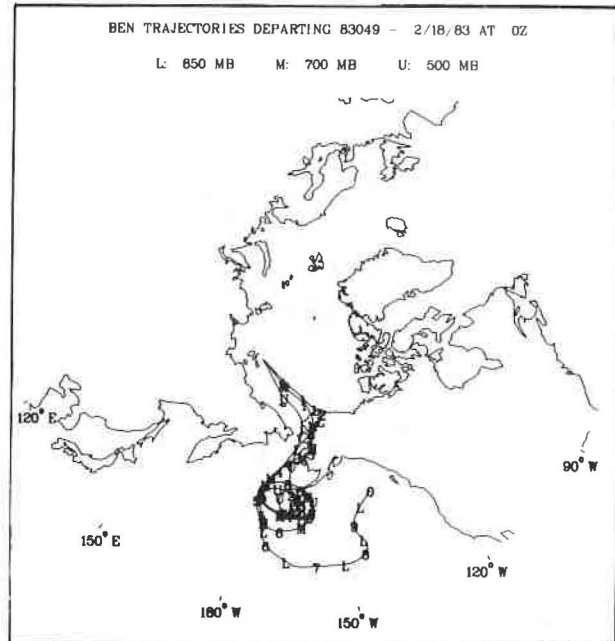
Figure 45.--Forward trajectories
departing from Bennett Island on
18 February 1983 at 0000 GMT on the
(L) 850-, (M) 700-, and (U) 500-mb
pressure surfaces.

75

obtaining from NMC lists of actual weather observations in that region. The
weather observations for 9 February 1984 1200 GMT were deemed representative,
though the numbers may vary somewhat from day to day:

TIROS (temperature soundings)--175
Upper-air reports (temperature, pressure, wind, moisture)--4
Drifting buoys (temperature, pressure)--13
Land stations (surface observations)--8
Aircraft reports (wind, pressure, altitude)--8.

For areas where no real data are available, the NMC global circulation
model obtains information using continuity and extrapolation from areas where
data are available; for example, continuity northward from lower latitudes,
continuity upward from the surface (when only a surface observation is
available), and continuity from the previous analysis. On the basis of the
numbers of real observatations and experience, it is felt that in most cases
valuable information can be gained from Arctic trajectories.

In contrast to trajectories that show possible transport paths for
industrial pollution into the Arctic (figs. 42 and 43), fig. 46 shows a fairly
common track that often results in cleaner conditions at BRW. Note the
trajectories show no travel over land. The cyclonic curvature is an
indication of possible cleansing by precipitation during transport to BRW.
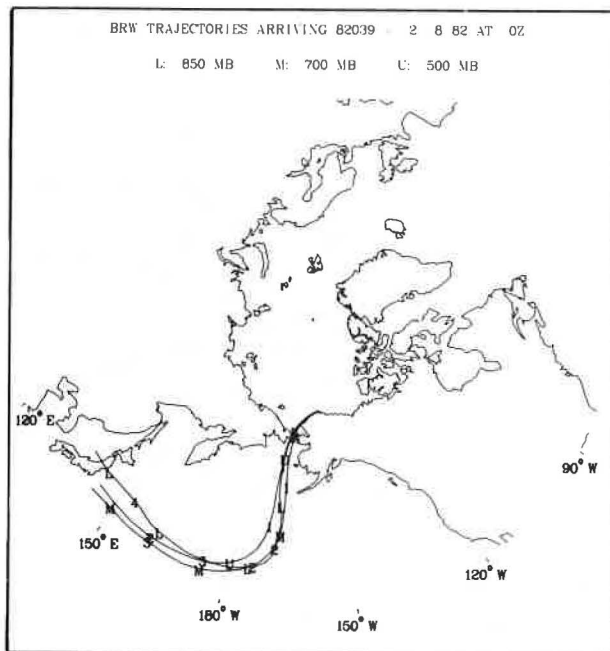
Figure 46.--BRW trajectories
arriving 8 February 1982 at 0000 GMT
on the (L) 850-, (M) 700-, and (U)
500-mb pressure surfaces.

4. SPECIAL PROJECTS

4.1 Trajectories During AGASP

Atmospheric trajectories were calculated for various Arctic locations for March and April 1983 during AGASP. The results of the trajectory study appear in Harris (1984); highlights are presented here. For information concerning the trajectory model, see sec. 3.13. The focus of this study was on trajectories arriving at BRW and along AGASP flight tracks 1-4 north of BRW. Trajectories along AGASP flight track 8 north of Bodø, Norway, were also analyzed. (See sec. 4.3 for flight tracks and background information on AGASP.)

Figure 47 shows trajectories arriving at BRW that are typical of those calculated for several days before the AGASP flights north of BRW. During this period (6-10 March 1983) trajectories circled the pole with cyclonic curvature, showing no contact with industrial areas. Also there is no evidence of direct steady flow from midlatitude oceans, as shown in fig. 46 (sec. 3.13), which could have the effect of bringing clean air into the Arctic Basin. At this time Bodhaine et al. (1984) found surface aerosols at BRW representative of background Arctic haze. During the week of the AGASP flights, which occurred close to 0000 GMT on 12, 14, 16, and 18 March, trajectories changed to over-the-pole flow from Eurasia at the 850-, 700-, and 500-mb levels. These levels were examined for long-range transport because Schnell and Raatz (1984) found the highest aerosol concentrations between 800-600 mb during the AGASP flights. The idea that long-range transport to BRW does not occur at the surface is consistent with the fact that air flowing adiabatically northward from midlatitude pollution sources must rise as it approaches the pole along an isentropic surface. A three-dimensional picture and discussion of airflow along these domed surfaces can be found in Harris and Bodhaine (1983, pp. 70-75).
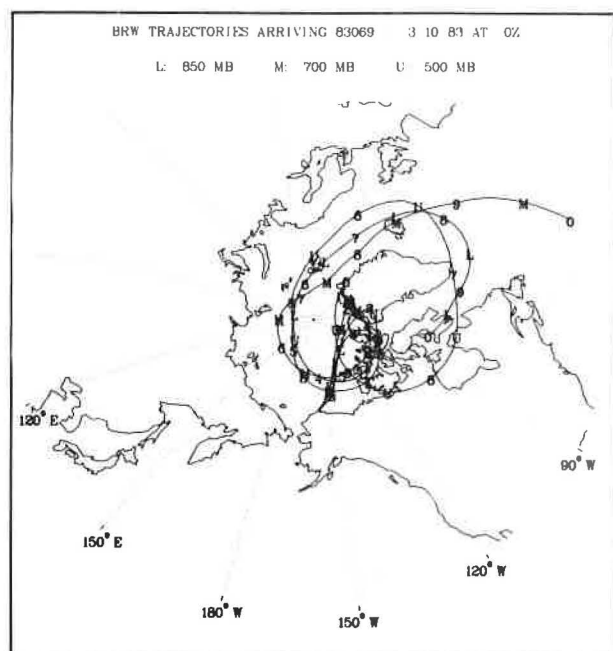
Figure 47.--BRW trajectories arriving 10 March 1983 at 0000 GMT on the (L) 850-, (M) 700-, and (U) 500-mb pressure surfaces. Numerals on the trajectories indicate number of days to travel from that point to the destination.

77

Figure 42 (sec 3.13) shows trajectories arriving at BRW on 14 March at 0000 GMT, the date when the strongest winds (about 15 m s^{-1}) and least vertical wind shear were seen in the 850-, 700-, and 500-mb trajectories (marked B, C, and D). Near this time the maximum optical depth measured during 10-20 March at BRW was recorded (Dutton et al., 1984), and surface aerosol concentrations at BRW were about 50% higher than the background haze levels found earlier (Bodhaine et al., 1984). The 1000-mb trajectory marked A in fig. 42 shows light meandering winds that, unlike at the higher levels, show no transport from known industrial sources to explain the haze events seen at the observatory and on the aircraft. This trajectory is typical of the 1000-mb trajectories studied for the AGASP period.

Trajectories arriving along AGASP flight tracks 1-4 north of BRW were computed and compared with the BRW trajectories. Trajectories arriving only several hundred kilometers north of the observatory showed significant differences from those arriving at BRW at the same time. The pattern that persisted in most of the trajectories from flight tracks 1-4 is demonstrated in fig. 48, which shows the relationship between the flight-track trajectories and the BRW trajectories for 0000 GMT on 12 March. In general, the influence of an Arctic anticyclone residing in the East Siberian Sea early in the period (Raatz, 1984) was stronger on the flight-track trajectories, whose destinations, being north of BRW, were closer to the center of the anticyclone. Hence more of these trajectories originated in northeastern Siberia compared with the BRW trajectories, which more often originated in western Asia or Europe. The fact that the origins of the air changed gradually as the aircraft flew north out of the transport zone and not uniformly throughout the three levels (Harris, 1984) might explain some of the haze-layering effects seen by Schnell and Raatz (1984) from the aircraft.

Forward trajectories from BRW were computed for the period of AGASP to track the air after it passed the observatory. Figure 49 shows air arriving at BRW (solid) and departing from BRW (dashed) on 12 March 1983 at 0000 GMT. These trajectories indicate that air reaching BRW on this date soon escaped the Arctic Basin and flowed into the North Pacific region. In contrast,
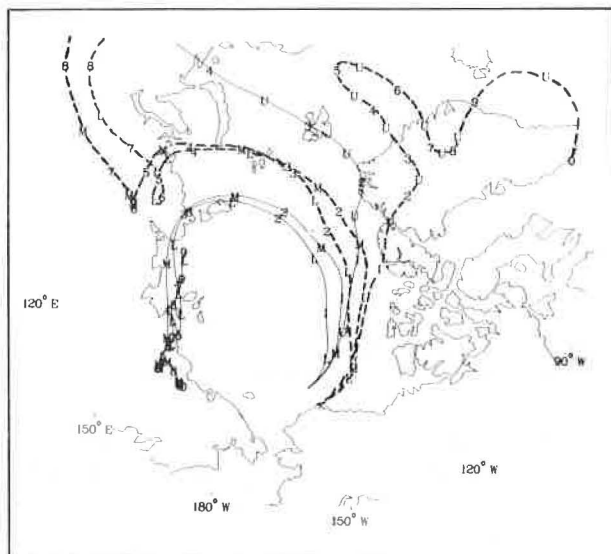
Figure 48.--Trajectories arriving at 73.07°N, 159.82°W (solid) along AGASP flight track 1, and trajectories arriving at BRW (dashed) for 12 March 1983 at 0000 GMT.
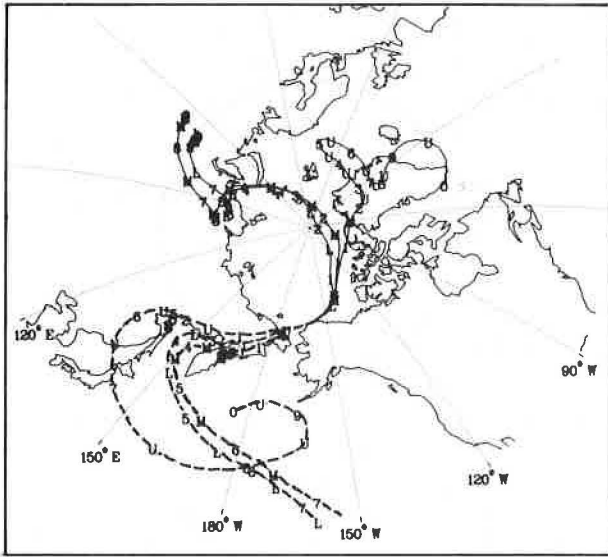
Figure 49.--Trajectories arriving (solid) and departing (dashed) from BRW on 12 March 1983 at 0000 GMT on the (L) 850-, (M) 700-, and (U) 500-mb pressure surfaces.
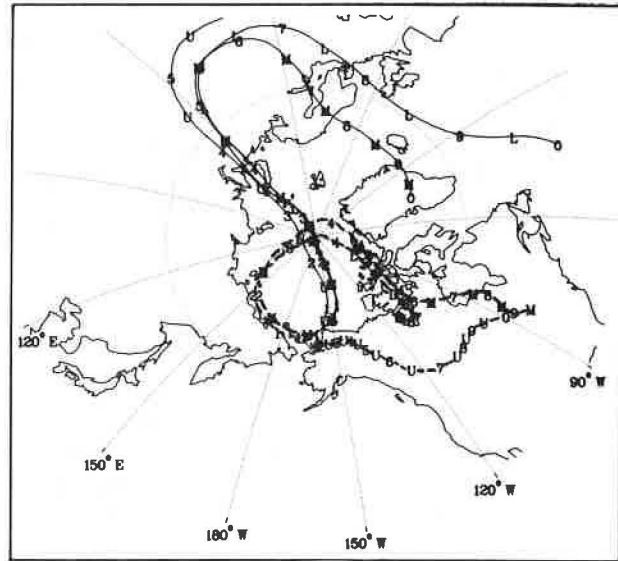
Figure 50.--Trajectories arriving (solid) and departing (dashed) from BRW on 14 March 1983 at 1200 GMT on the (L) 850-, (M) 700-, and (U) 500-mb pressure surfaces.

fig. 50 shows that the air arriving at BRW 2 days later on the 850- and 700-mb pressure surfaces remained in the Arctic, probably because of the influence of the anticyclone previously mentioned.

During AGASP flight 8 (31 March) from Bodø, Norway, north to Svalbard and beyond, haze was present during the southern portion of the flight. In the vicinity of 79.00°N, the aircraft flew through an aerosol front into clean air. This event was noted visually and shows up dramatically in measurements taken aboard the aircraft (Raatz and Schnell, 1984). Figure 51 shows trajec-
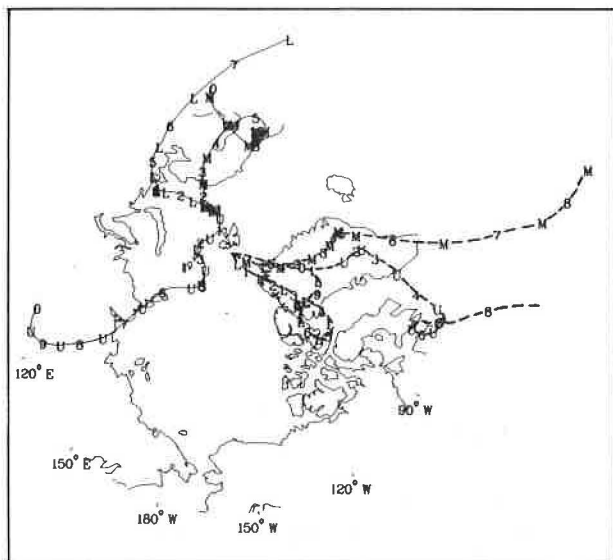
Figure 51.--Trajectories arriving at 73.76°N, 24.86°E (solid) and at 81.00°N, 17.00°E (dashed) along AGASP flight track 8 on 31 March 1983 at 1200 GMT.

tories arriving along flight track 8 at two locations about 800 km apart, for the time closest to the flight (1200 GMT). Those arriving at 73.76°N, 24.86°E during hazy conditions are south of the aerosol front. The source areas suggested by these trajectories are Europe at the lower levels and central Asia at 500 mb. The trajectories arriving at 81.00°N, 17.00°E, close to the northernmost point of AGASP flight 8, are north of the aerosol front. Source areas indicated by these trajectories are Greenland and northern Canada. At this point in the flight, the aircraft was in nonhazy air.

4.2 The Flow Climatology From Bermuda, and Its Implications on Long-Range Transport

The transport of pollutants off the North American Continent is one part of the overall chemical budget that is being studied under WATOX. As a contribution to the understanding of this transport, back trajectories were calculated from Bermuda and a flow climatology was developed for a 7-yr period. Highlights of this study are presented here; a more complete report can be found in Miller and Harris (1984). On a daily basis, 10-day back trajectories were produced for the 850- and 700-mb levels from January 1975 to December 1981. Details of the computer model that produced the trajectories are presented in Harris (1982). The 850-mb trajectories constitute the data base for determining the climatology; the 700-mb trajectories were used for comparison.

A classification system was adopted based on the hypothesis that the North American Continent is a source of pollutants and the fact that the precipitation that falls in Bermuda is strongly governed by the position and strength of the Bermuda high. The movement of this anticyclone north and south determines if the flow is strongly westerly (winter) or if it has a more southerly component (summer). Figure 52 shows the sectors used to categorize the trajectories: northwest (NW), west-southwest (WSW), south-southwest (SSW), southeast (SE), northeast (NE), and no direction (H). The NW and WSW categories were created because of the dual nature of North American pollution source configurations, and can be combined to cover all of North America. Category H in most cases was observed during periods when the Bermuda anticyclone was far north and flow was mainly of a weak circular nature. The distance back for the 10-day period was also measured, and was generally greater than 1000 km except during weak flow conditions (category H).
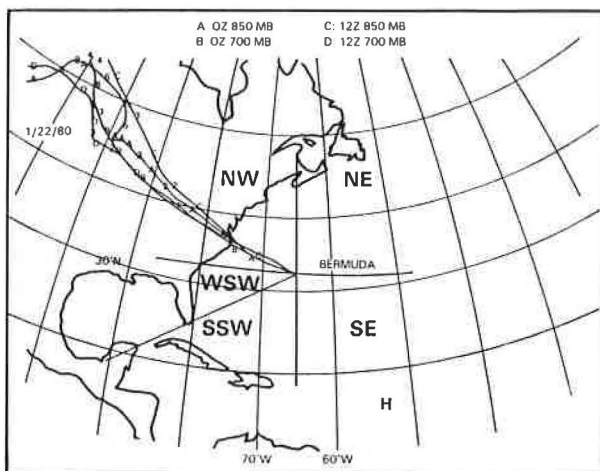
Figure 52.--The classification system used for the period of study (1975-1981).
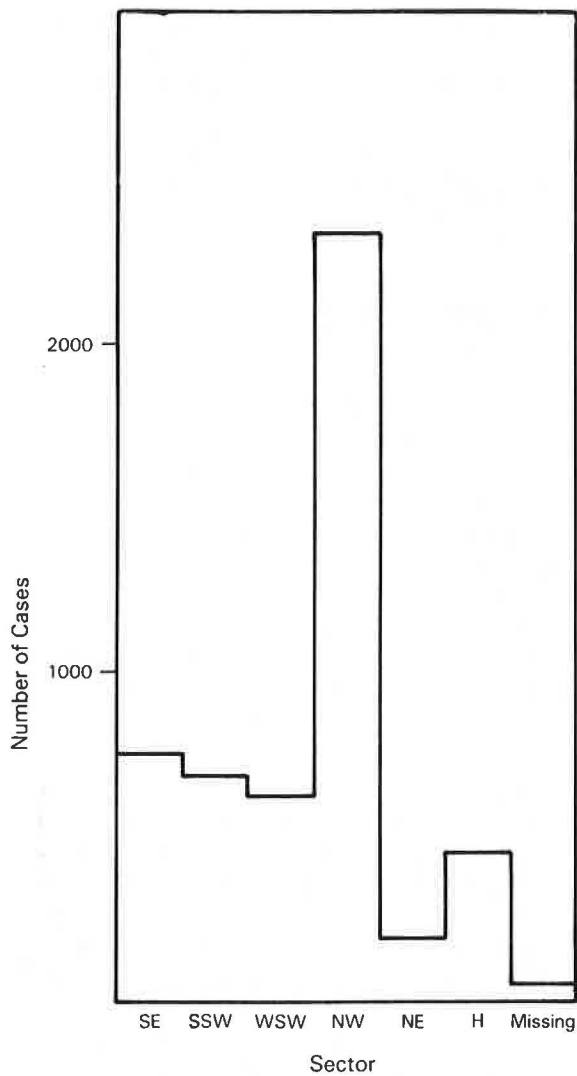
Figure 53.--A histogram of all
850-mb trajectories to Bermuda from
1975 to 1981.
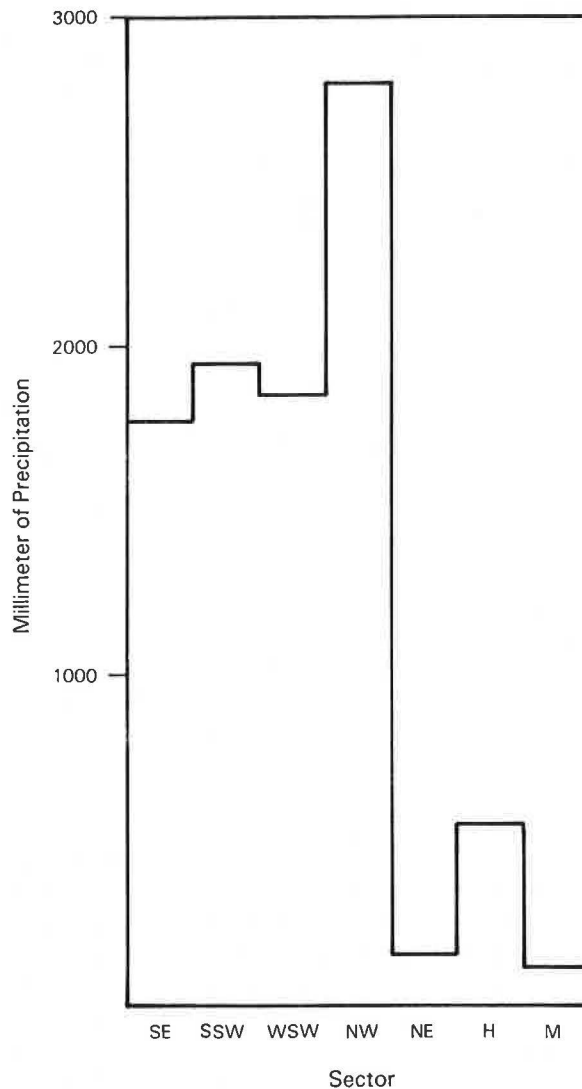
Figure 54.--A histogram of the
amount of rainfall for the associ-
ated trajectories to Bermuda.

Figure 53 presents the number of trajectories that fell in each category
for the entire 7-yr period. The obvious conclusion is the predominance of the
northwestern trajectory in the flow pattern to Bermuda. If WSW and NW are
combined, 58% of the trajectories are accounted for.

Because one of the objectives of the WATOX project is the determination
of the precipitation chemistry in Bermuda, a back trajectory was prepared for
each daily rain event in the 7-yr period. In fig. 54, the category of trajec-
tory is plotted vs. the total amount of rainfall for the associated trajectory
over the 7-yr period. It is important to note that precipitation is higher
for southerly flow than would be expected if the rainfall were distributed
evenly for all trajectories (compare figs. 53 and 54). As an initial compari-
son between the trajectories and the chemical data, the pH values published by
Jickells et al. (1982) are plotted against the number of trajectories from the

81
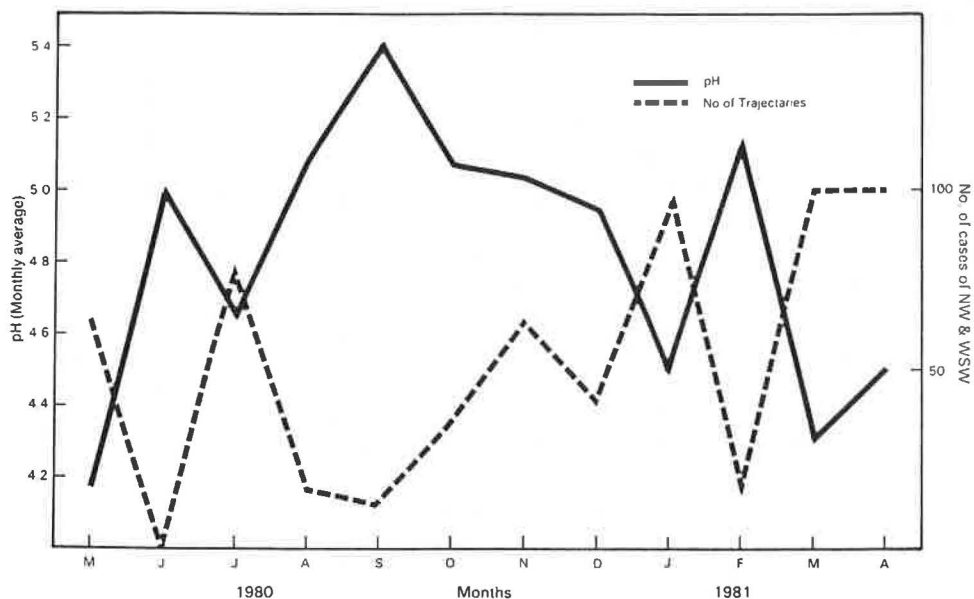
Figure 55.--A comparison of pH values at Bermuda for the first year of
WATOX vs. trajectories for that period from the WSW and NW categories
(rain only).

NW and WSW sectors (fig. 55). There is good agreement between high acidity
and flow from the North American sectors. This gives further credence to the
hypothesis of Jickells et al. that there is long-range transport of acidic
material to the Atlantic from the United States and Canada.

4.3 Arctic Gas and Aerosol Sampling Program (AGASP)

4.3.1 Introduction

Haze over the Arctic icecap was first extensively documented in contempo-
rary scientific literature by Mitchell (1957). He noted that the haze was
generally observed during periods of otherwise clean air, extended over
altitudes from near the ground to 500 mb, and extended over air routes up to
1000 km. On the basis of a range of optical and physical evidence, Mitchell
suggested that the haze was composed of non-ice particles less than 2 μm in
diameter. Beginning in the mid-1970's, research results of scientists such as
Holmgren et al. (1974), Radke et al. (1976), Bodhaine et al. (1981a), and Rahn
(1981a, 1981b) confirmed the presence of much higher concentrations of aerosols
in the Arctic atmosphere than one would expect in a remote and supposedly
pristine environment. The data further suggested that the haze had an anthro-
pogenic component.

Radiative-transfer modeling studies of Arctic haze have indicated that
average local atmospheric heating by solar absorption from a thick layer of
carbon aerosol in the Arctic haze may be comparable with that from doubling
atmospheric CO_2 concentrations (Porch and MacCracken, 1982; Vallero et al.,

1984). These effects are most pronounced in the high Arctic latitudes, partly because of the high surface albedo of large and persistent areas of snow and ice.

In the spring of 1983, Arctic haze was studied with six aircraft (three from the United States, two from the Federal Republic of Germany, and one from Norway) and from three surface-based networks operated by Norway and Sweden, Canada, and the United States. Each aircraft measurement program was coordinated with at least one surface station. In many cases the same make and model of instruments were used in the aircraft as on the ground. The most extensive aircraft program in the haze study was built around flights of the NOAA WP-3D Orion, the aircraft used for the airborne portion of NOAA AGASP.

NOAA AGASP was designed to extend into three dimensions the Arctic haze measurements conducted at surface stations such as those at BRW; Alert, Canada; and Ny Ålesund, Spitzbergen. In so doing, a much broader picture of haze over the Arctic icecap would be obtained and the representativeness of the ground-based measurements ascertained.

The WP-3D flew 144 flight hours on 12 separate research missions during AGASP; approximate flight tracks and mission numbers are shown in fig. 56. In support of aircraft operations, aerosol and radiation measurements were conducted at BRW (Bodhaine et al., 1984; Dutton et al., 1984) and the Alert background station (Hoff and Trivett, 1984), before, during, and after the flights.

Thirty-five scientists from 17 different institutions joined the WP-3D research program to conduct their specialty measurements and analyses. See Harris and Bodhaine (1983, p. 88) for a list of participants and programs.

AGASP provided funds for mounting instruments on the aircraft and for field expenses for the cooperating scientists. Support for data analyses was the responsibility of the respective scientists. CIRES and GMCC provided
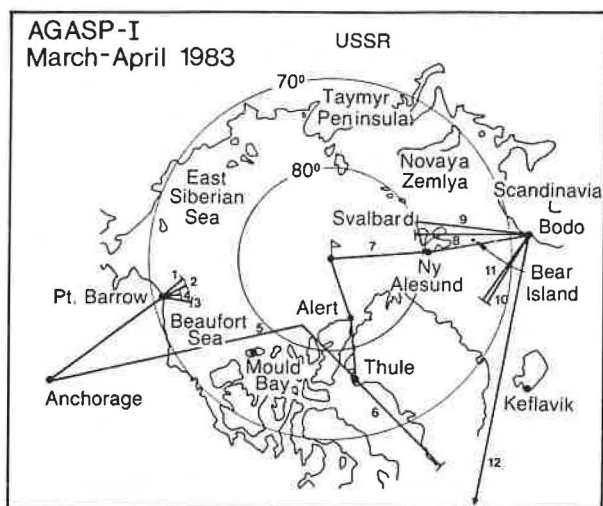
Figure 56.--Approximate flight tracks of the NOAA WP-3D during the AGASP project. Flight 6 went into the stratosphere during a tropopause fold event, and flight 12 was over the center of the Icelandic low, into which 11 dropwindsondes were released in a planned pattern.

83

personnel and support services for organizing and directing the program, and for data archiving and publishing. Support for AGASP was provided by NOAA, ONR, and NASA.

4.3.2 Haze in the Alaskan Arctic

Four NOAA WP-3D flights were conducted in the vicinity of BRW during 11-18 March 1983. These flights occurred during a period when there was strong organized transport of aerosol from midlatitudes across the pole into the Alaskan Arctic (Raatz, 1984; Harris, 1984). Aircraft instrumentation is discussed by Schnell (1984a).

In this report, CN concentrations reflect, for the most part, particles in the Aitken (<0.2-μm-diameter) size range. Particles of 0.370- to 0.495-μm diameter lie within the large-particle range (0.2- to 2.0-μm diameter). Giant particles (>2.0-μm diameter) are presented in spectral format. For a discussion of these terms see Junge (1963).

Large-particle data are an independent in situ measure of the aerosol involved in light scattering (σ_{sp}). The nephelometer, used to measure light scattering of aerosols, is most sensitive to particles in the size range 0.1- to 1.0-μm diameter, with maximum sensitivity for particles near 0.5-μm diameter. The range of 0.370- to 0.495-μm diameter (as measured by one channel of the 15-channel laser aerosol spectrometer) falls just below the maximum sensitivity of the nephelometer. Thus, light scattering would be expected to respond in the same manner as the large-particle concentrations. Also presented are aerosol spectra for 0.195- to 10-μm-diameter aerosols obtained from composites of the in situ PMS ASASP-100X and FSSP aerosol probe data.

A summary of data on the vertical structure of the Arctic haze observed in the vicinity of BRW is shown in fig. 57. On 11 March (fig. 57a), the haze was distributed in at least six well-defined layers. Two days later, on 13 March (fig. 57b) the haze was stronger but confined to a band from 600 to 800 mb. The haze became weaker on 15 March (fig. 57c) and 17 March (fig. 57d) as the Arctic anticyclone moved closer to BRW (Raatz, 1984).

Aerosol spectra for haze layer 4 (centered at 750 mb in fig. 57a) and for the clear air directly below this layer (centered at 820 mb) are shown in fig. 58. The haze band contains 4-8 times more aerosol particles (and mass) than the cleaner air. The aerosols in the haze layer and in the clear air both exhibit volume peaks in the 1- to 3-μm diameter range.

The positioning of the anticyclone after 17 March produced a change from a direct transport pathway for the aerosols (into the Alaskan Arctic from Eurasia) to a more complicated and less direct flow pattern (Harris, 1984). Except for 17 March, all profiles were taken within this aerosol transport zone, defined as a zone of strong pressure gradients (and therefore strong winds) between two synoptic pressure systems. Such relatively rapid transport of air pollutants into the Arctic was hypothesized by Carlson (1981), and transport zones were documented by Raatz (1984). The aerosol profiles (fig. 57) further suggest that the main level of transport of Arctic haze to BRW during this period was centered around 700 mb.
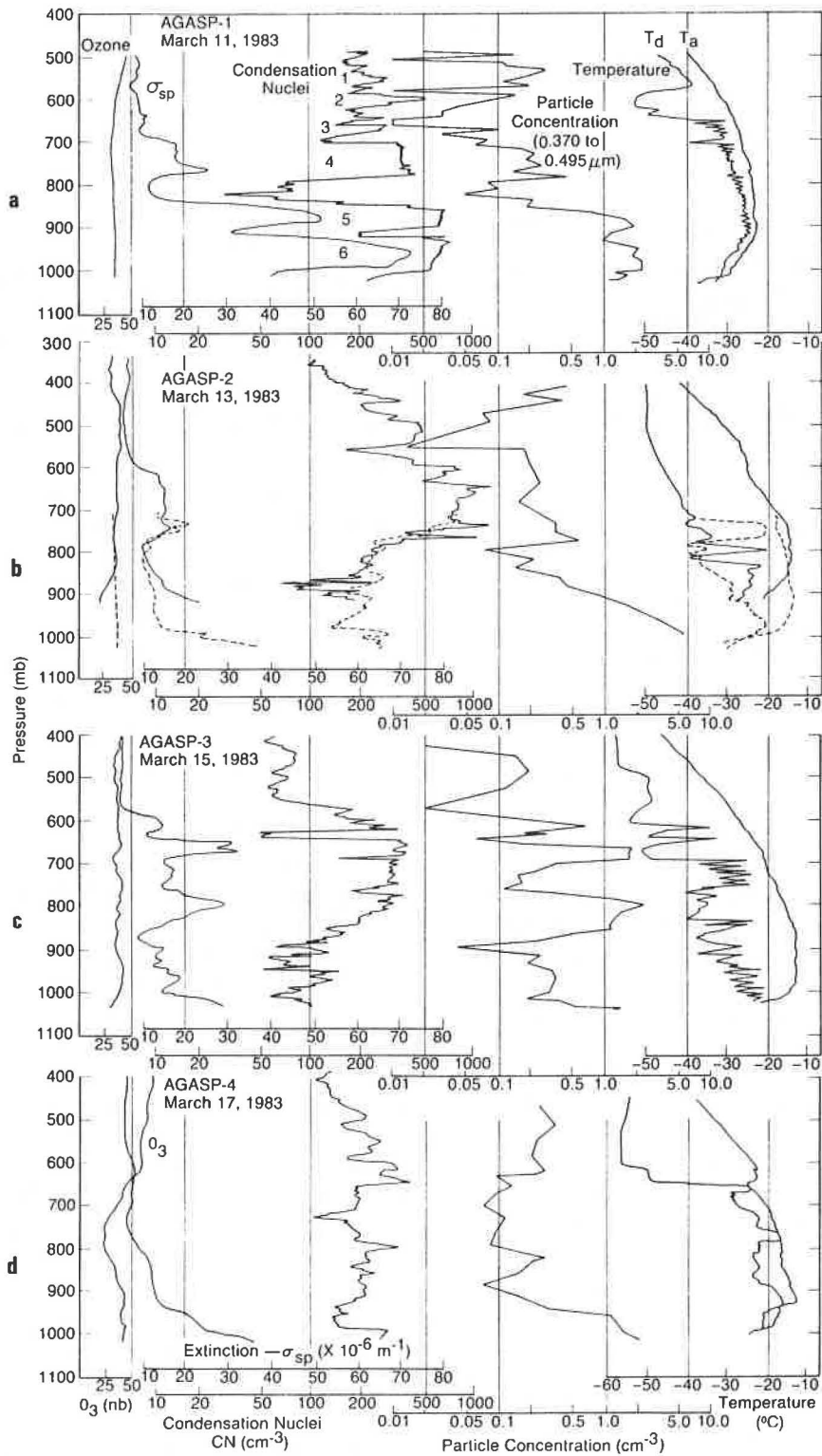
Figure 57.—Ozone, σ_{sp}, CN, large-particle concentrations (0.370- to 0.495-μm diameter) and temperature-dewpoint profiles upwind of BRW. (a) Descending, 2134-2226 GMT, 11 March. (b) Lower portion, descending (dashed line), 2204-2240 GMT, 13 March; upper portion, ascending (solid line), 0232-0258 GMT, 14 March. (c) Descending, 2224-2318 GMT, 15 March. (d) Descending, 2234-2325 GMT, 17 March.

85
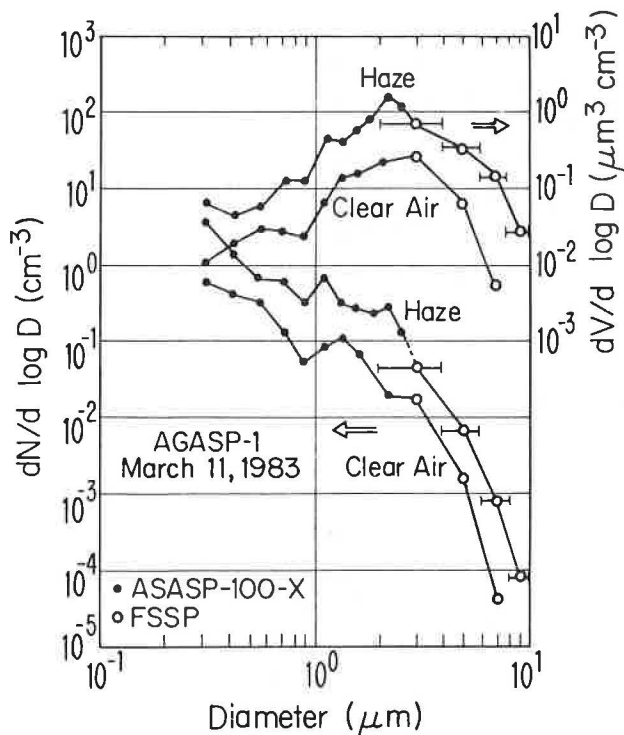
Figure 58.--Aerosol concentration and mass spectra for haze in layer 4 of fig. 57a (AGASP-1) centered at 750 mb, and for clear air below this layer, centered at 820 mb for 10-min sampling periods. The particle diameter range over which the FSSP data are measured is indicated by the range bars; the particle concentration (mass) is plotted at the center of the log interval.

4.3.3 Haze in the Norwegian Arctic

During the third period of the AGASP experiment, research flights were conducted out of Bodø, Norway, north into the Norwegian Arctic. Air masses entering this region have recently passed over various European and Asian industrial areas and are thus assumed to retain air mass and aerosol properties representative of their source regions.

The overall synoptic weather situation during this time period was characterized by a persistent return-flow pattern whereby a stationary, quasi-persistent cyclonic system transports aerosols from central Europe northeastward, and then returns the aerosols southwestward to Svalbard and Iceland on the back side of the cyclonic flow (Raatz, 1984).

Vertical profiles of Arctic haze from near Svalbard are shown in fig. 59. The haze pollution was of similar concentration to that observed in Alaska, but was persistent throughout the troposphere both on 31 March (fig. 59a) and on 4 April (fig. 59b). This haze was associated with both dry and moist layers in the atmosphere.

Figure 60 presents a time series of aerosol and meteorological parameters measured by the aircraft from 1200 to 1520 GMT immediately following the profiles shown in fig. 59a. During the major portion of the time series the aircraft was flying at the 622-mb level.

From 1220 to 1315 GMT, while the aircraft was northbound, CN concentrations averaged around 450 cm^{-3}. They abruptly decreased to a mean value of 80 cm^{-3} after 1320 GMT and remained at this low level until 1342 GMT. This
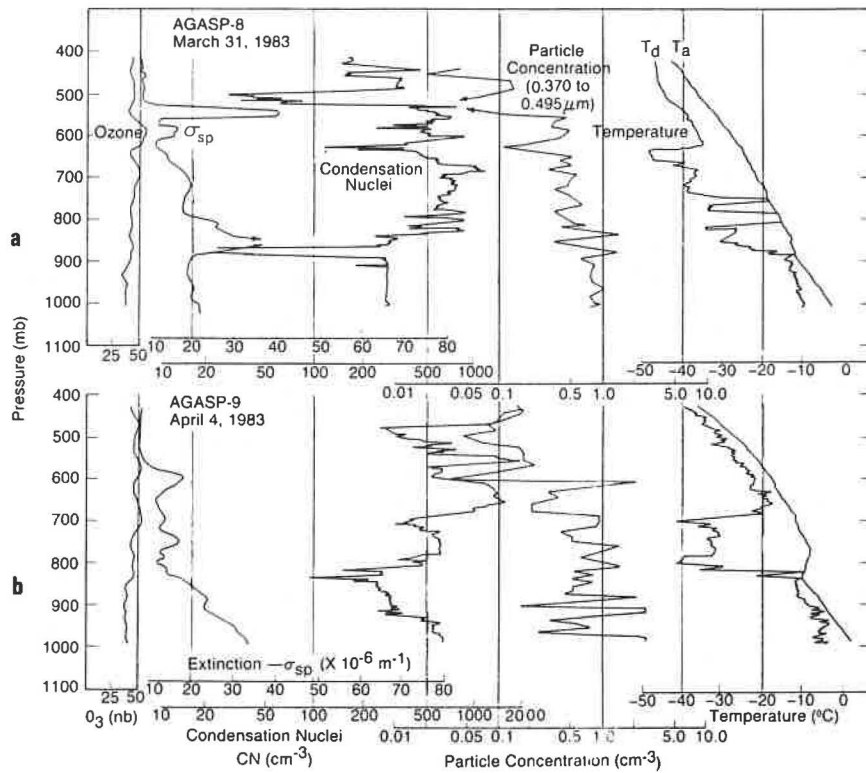
Figure 59.--Ozone, σ_{sp}, CN, large particle concentration, and temperature-dewpoint profiles near Svalbard: (a) descending, 1032-1145 GMT, 31 March 1983; (b) descending, 0806-0915 GMT, 4 April.
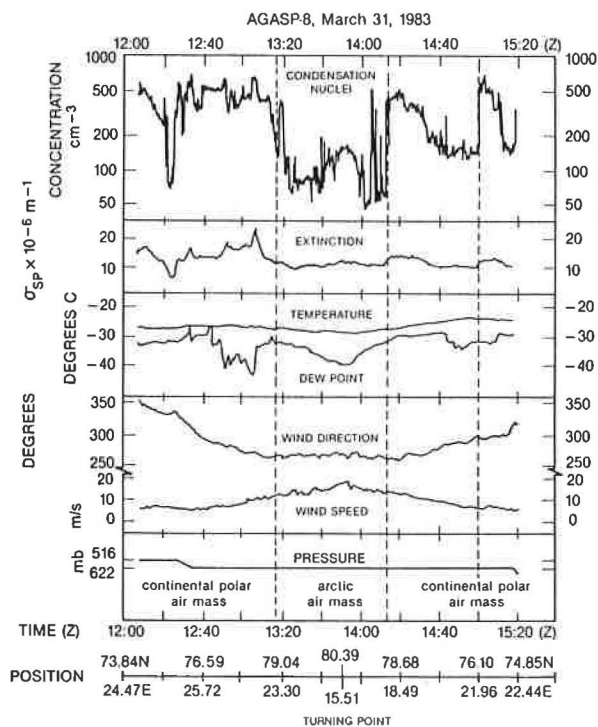
Figure 60.--Time series of meteorological and aerosol parameters for 31 March 1983 (immediately following the profiles in fig. 59a) as the aircraft passed through an Arctic aerosol front located in the region of 79°N, then turned and reentered it.

87

decrease in CN concentrations was accompanied by the disappearance of visual haze and extremely improved horizontal and vertical visibilities. At 80.39°N, 15.51°E (1350 GMT) the aircraft turned south and 20 minutes later reentered the haze-laden air mass at 1410 GMT, whereupon the CN concentrations rose again to 400-500 cm^{-3}. A similar but less dramatic variation is seen in the light-scattering data.

This aerosol front marks the boundary between polluted air from the Soviet Arctic being transported in a return-flow pattern and cleaner Arctic air originating over Greenland.

4.3.4 Summary and Conclusions

On the basis of these and a wide range of other measurements, the following conclusions may be drawn: (1) Arctic haze, associated light scattering, and increased aerosol concentrations occur in both dry and moist air layers throughout the Arctic winter troposphere. (2) Moist air depletes CN. (3) The haze may be in higher concentrations aloft than at the surface. (4) Aerosol concentrations (mass) can differ by an order of magnitude between haze and clean-air layers. (5) The boundaries of the haze in both the horizontal and vertical can be sharp and well defined (i.e., aerosol fronts).

4.3.5 Further Results from the AGASP Program

A special issue of Geophysical Research Letters, May 1984, contains 29 papers on the results of the 1983 Arctic haze studies. The AGASP data set is being maintained within the GMCC offices in Boulder. This includes all NOAA WP-3D sensor data tapes; relevant North American and European weather maps; Canadian, European, and U.S. radiosonde data for the Arctic; copies of all mission notes and reports; continuous 16-mm nose-camera movie film of all flights; and reports of the type, amount, and quality of data collected by cooperating scientists. Requests for access to these data should be forwarded to Director, GMCC, NOAA/ERL, U.S. Department of Commerce, 325 Broadway, Boulder, CO 80303.

4.4 CO_2 and Meteorology at SMO

Regimes of CO_2 concentration can be related to the different air masses being sampled at baseline stations to obtain a more accurate assessment of background levels from the complete record of CO_2 data. For example, during February 1979-January 1982, variations of up to 3 ppm in daily average CO_2 concentration at SMO (14.3°S, 170.6°W) over periods of a few days were related to the latitudinal gradient and changes in atmospheric circulation pattern. The amount of this variability had a seasonality that was related to seasonality in CO_2 latitudinal gradient and circulation regimes.

The atmospheric circulation patterns affecting SMO have been summarized by Bortniak (1981). The surface analysis of fig. 61 will allow a quick review of these patterns. This map presents the surface synoptic pattern for one particular day and was chosen only to show examples of the three main circulation features controlling the low-level atmospheric circulation at SMO. The

positions and strengths of these features varied, within limits, from day to
day over the course of the year. The most persistent feature, bringing the
easterly trade winds to SMO, consisted of one or two anticyclonic centers over
the central and eastern South Pacific Ocean. Next in importance is a southerly
current, produced by an anticyclonic center over the region from Australia to
New Zealand, at times in conjunction with travelling cyclones in the midlati-
tude westerlies. The third circulation feature was a cyclonic center or
trough to the northwest of SMO, producing a northwesterly air flow. This
feature, less frequent than the southerly current, but significant during
several months of the year, moved into or developed in a position whereby air
from north of the intertropical convergence zone was brought to SMO. This
conclusion is reinforced by the coincidence of peaks in CO_2 and methyl chloro-
form (CH_3CCl_3) associated with this circulation regime. Methyl chloroform is
released into the atmosphere by certain industries primarily in the Northern
Hemisphere and was measured at SMO as a part of ALE (Prinn et al., 1983). The
South Pacific easterly trade flow in fig. 61 was perturbed from the usual
situation in which there was a more continuous east-to-west flow across SMO.
The breakdown of the easterly trade flow into a weak trough or into one or
more weak closed circulations near the longitude of SMO was a second pattern
that sometimes resulted in the mixing of Northern Hemisphere air southward to
SMO. At SMO's latitude, the easterly trade-wind marine layer during all
seasons extends an average of about 2 km above the surface at 160°W, which is
about 10° east of SMO (Van Loon et al., 1971).

Shifts in position and changes in strength of the three main circulation
features resulted in a 3-yr-average seasonal variation in the lower tropo-
spheric circulation at SMO, which is consistent with long-term average patterns
discussed by Bortniak (1981). This seasonal variation is demonstrated in
fig. 62. It shows the average percentage frequency of occurrence by month of
the 10-day 1000-mb trajectory origins in four direction sectors from SMO
during the 3-yr study period. Throughout most of the year, airflow from the
ENE and ESE sectors around anticyclones in the central and eastern South
Pacific Ocean predominated. However, there were significant changes in the
frequency of occurrence of airflow from other sectors. During December-April
(austral summer and early austral autumn), the southerly current around
Australia-New Zealand anticyclones, and the northwest flow in cyclonic circula-
tions to the west and northwest of SMO also affected the circulation at SMO a
significant amount of time. By autumn, the frequency of periods of northwest
flow had decreased markedly, while the southerly current had begun to reach
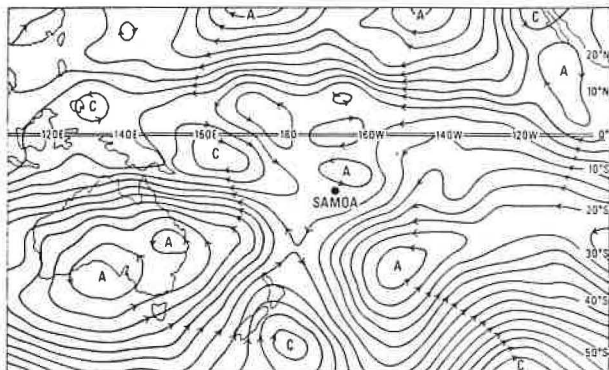
Figure 61.--NMC surface streamline
analysis for 29 April 1980 at
0600 GMT. A = anticyclone; C =
cyclone.

89
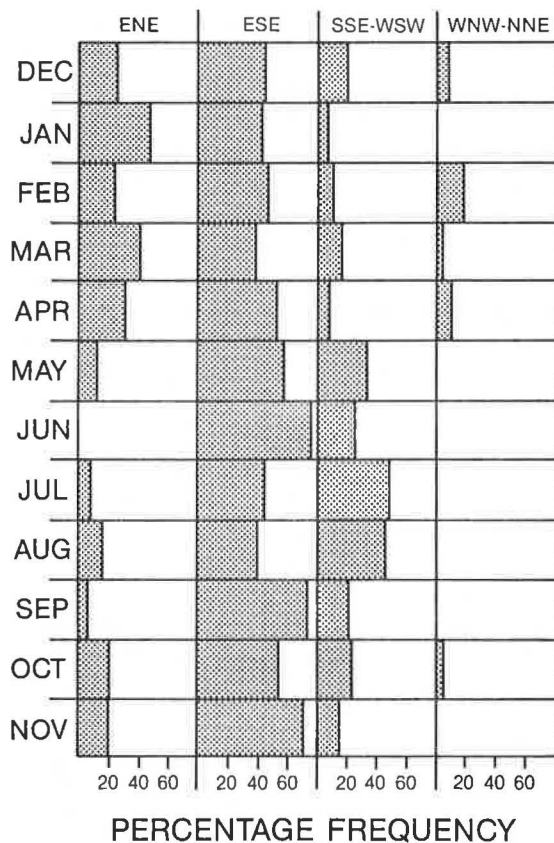
Figure 62.--Percentage frequency by month of 10-day, 1000-mb trajectory origins in four different direction sectors from SMO for 1979-1981.

SMO considerably more often. Thus, the austral winter circulation at SMO was characterized by an alternation between only two regimes--easterly flow around central and eastern South Pacific anticyclones and southerly flow around Australia-New Zealand anticyclones. The circulation during austral spring (September-November) was the steadiest of the year. Easterlies predominated; there was a reduced occurrence of southerlies; and northwest flow was still considerably less frequent than during the December-April period.

Komhyr et al. (1984a) have shown for the years 1979-1982 that the CO_2 gradient to the north and south of SMO was greatest from about February to May. The gradient to the north was increased by a bulge in CO_2 around $5°-15°N$, while CO_2 concentration decreased to the south with a weaker gradient. The latitudinal gradient was weakest between August and November. During this time, the CO_2 bulge was less pronounced, and the Southern Hemisphere gradient was nearly flat.

The seasonal changes in atmospheric circulation combined with this seasonally varying latitudinal gradient to produce the pattern of CO_2 variation observed at SMO averaged over the 3-yr study period. The period of maximum latitudinal gradient overlapped the period during which all three main circulation features contributed significantly to the low-level atmospheric circulation at SMO. Figure 63, showing CO_2 daily averages for 1980, demonstrates the tendency for the greatest day-to-day variation in CO_2 to occur
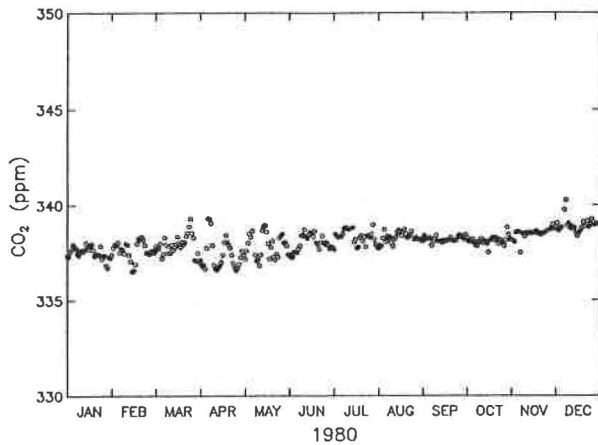
Figure 63.--CO_2 daily average concentrations at SMO for 1980. Values are in the X81 mole fraction scale.

during this February-May (day of year 32-152) period. Highest CO_2 concentrations were measured when cyclonic circulations to the west and northwest brought air to SMO from the CO_2 maximum at 5°-15°N, while lowest concentrations were observed when the Australia-New Zealand anticyclone controlled the circulation at SMO. Figure 64, a plot of average departure of CO_2 from spline value as a function of surface wind direction, demonstrates the effect of the maximum in latitudinal gradient at this time. Although during May there were no cyclonic circulations to the west or northwest of SMO strong and persistent enough to produce 10-day trajectory origins in the WNW-NNE sector, there were periods with northwest surface winds and 1- to 3-day trajectory origins to the northwest. These periods were associated with the type of perturbation in the easterlies mentioned earlier as sometimes being associated with the mixing of Northern Hemisphere air southward to SMO.

During the overlapping periods of least CO_2 latitudinal gradient and steadiest circulation pattern (day of year 214-335 and 245-335, respectively), fig. 63 demonstrates the tendency for the least day-to-day variation in CO_2 concentration. The plot of average CO_2 departure as a function of surface wind direction (fig. 65) for November shows the lack of dependence of CO_2 on wind direction at this time of year.

During the 3 years considered in this study, southern oscillation indices near the long-term average suggest that the atmospheric circulation over the tropical and South Pacific Ocean during this period was also about normal. Thus, the results of the study presented here probably apply to long-term average conditions. Although not completed yet, this study does suggest the following conclusions with regard to CO_2 at SMO: (1) Concentrations in unperturbed easterly trade flow are representative of the Southern Hemisphere tropics. (2) Concentrations associated with southerly flow around Australia-New Zealand anticyclones are influenced by Southern Hemisphere midlatitude levels, and thus are not representative of the tropics, except from about August through November when the Southern Hemisphere gradient is very small. (3) Concentrations in northwest flow are not representative of the Southern Hemisphere tropics, except during about September through November when the CO_2 bulge at 5°-15°N is slight.

91
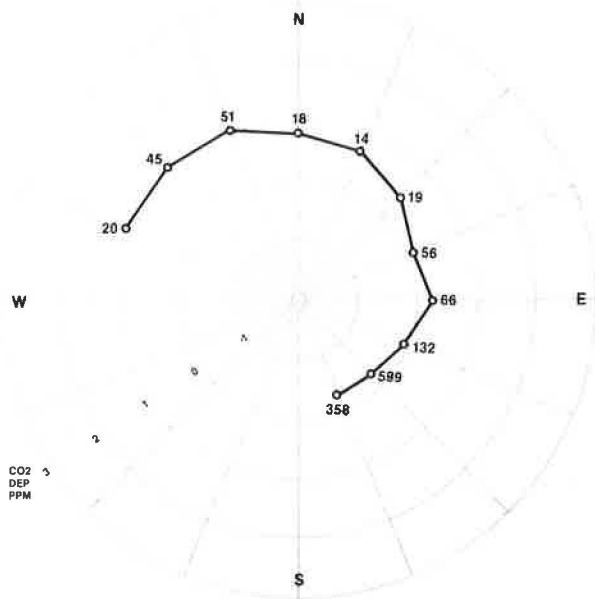
Figure 64.--Average departure of daily average CO_2 concentration as a function of surface wind direction for the month of May in 1979-1981. Data for south through west directions were eliminated because of local contamination. Numbers next to data points give the number of CO_2 hourly averages used in the average for the 3 months.
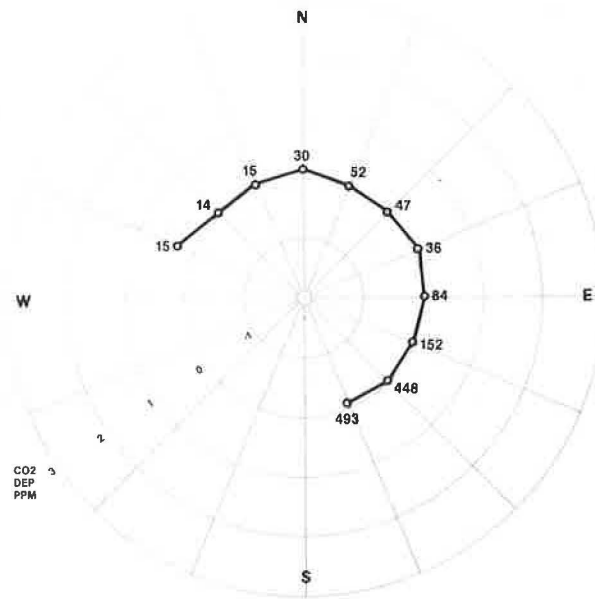
Figure 65.--Average departure of daily average CO_2 concentration as a function of surface wind direction, as in fig. 64, but for November.

4.5 The BRW Surface Aerosol During AGASP

4.5.1 Introduction

AGASP, an airborne and surface experiment, was conducted during March and April 1983 (Schnell, 1984a). During the first four flights, on 11, 13, 15, and 17 March, vertical aerosol profiles were made near BRW. Quantities measured aboard the aircraft included CN concentration, aerosol scattering extinction coefficient (σ_{sp}), and particle size distribution. Quantities measured routinely at BRW at the surface, and therefore during AGASP, included CN concentration and σ_{sp} (Bodhaine, 1983). For the duration of the AGASP experiment, an aerosol spectrometer and a special sunphotometer were operated at BRW (Bodhaine et al., 1984; Dutton et al., 1984).

4.5.2 Instrumentation

CN concentration was measured both on the aircraft and on the ground using G.E. automatic CN counters. Operation of these instruments was described

in GMCC Summary Report No. 5 (Hanson, 1977). On the aircraft, a single-wavelength (525 nm) nephelometer (model 1590, Meteorology Research, Inc.) measured σ_{sp}. A four-wavelength nephelometer at BRW operates continuously at 450-, 550-, 700-, and 850-nm wavelengths. A PMS ASASP-100X, which covers the aerosol size range of 0.09-3.0 μm (diameter) in 15 intervals, was operated on the aircraft, and an ASASP-X, which covers the same size range in 60 intervals, was operated at BRW. Surface-based measurement results are presented here.

4.5.3 Results

Ten days of surface-based hourly mean CN, σ_{sp}, and Angstrom exponent data from BRW are presented in fig. 66. Surface meteorological data are presented in fig. 67. The CN data in fig. 66 (bottom) vary between about 150 and 700 cm^{-3}, except for the large event on 14 March that is most likely of local origin. The σ_{sp} data in fig. 66 (middle) show a fairly constant background Arctic haze near 2×10^{-5} m^{-1} during 9-11 March, a series of events reaching 4×10^{-5} m^{-1} during 12-16 March, and a return to background Arctic haze for the remainder of the period. The Angstrom exponent data in fig. 66 (top) show three well-defined regimes: (1) relatively low values during 9-11 March; (2) higher values during 12-14 March; and (3) highest values during the remainder of the period. These Angstrom exponent data suggest a change in aerosol size distribution toward relatively more small particles on 12 March and again on 14 March.

The meteorological data in fig. 67 show that the surface winds were generally from north to north-northeast at about 4 m s^{-1} throughout the time period, suggesting that the known local sources identified by Bodhaine et al. (1981a) did not influence the 10-day period of surface measurements. The relatively constant RH data in fig. 67 suggest that the large events in σ_{sp} during 11-16 March were not caused by aerosol growth in response to increases
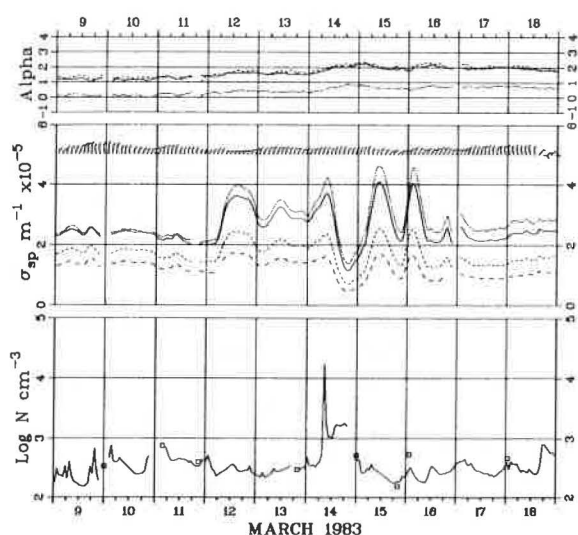
Figure 66.--Hourly means of (bottom) CN concentration, (middle) σ_{sp}, and (top) Angstrom exponent at BRW. The small squares are calibration points for CN concentration provided by the Pollak CN counter. The σ_{sp} data are given at 450 (dotted), 550 (solid), 700 (dashed), and 850 nm (long-dashed). Wind direction and speed are shown in the upper portion of the middle graph. Angstrom exponents were calculated from σ_{sp} data at 450 and 550 nm (dotted), 550 and 700 nm (solid), and 700 and 850 nm (dashed) using the formula $\alpha = -\Delta \log \sigma_{sp}/\Delta \log \lambda$. All times are GMT.

93
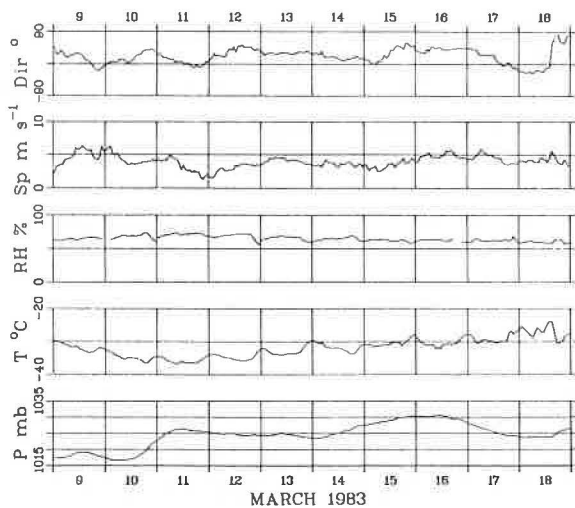
Figure 67.--Hourly means of wind direction (Dir), wind speed (Sp), relative humidity (RH), temperature (T), and pressure (P) at BRW. All times are GMT.

in relative humidity. The surface pressure data in fig. 67 are in agreement with the description by Raatz (1984) of a high-pressure system moving past the BRW site. The events in the σ_{sp} data were apparently caused by a change in trajectory origin as the high-pressure system moved. Harris (1984) shows that during 9-11 March, 5-day back trajectories from BRW originated over the Arctic Basin, whereas on 12 March a change occurred such that trajectories originated over Asia.

Figure 68 presents a time series of total particle numbers counted in each of three size ranges of the aerosol spectrometer. Ranges 1, 2, and 3 detect 0.24- to 0.84-μm, 0.15- to 0.30-μm, and 0.09- to 0.195-μm diameter particles respectively. Clearly, the data in fig. 68 qualitatively follow the σ_{sp} data in fig. 66. Furthermore, the events beginning on 12 March showed much larger increases in the small-particle ranges than in the large-particle ranges, in agreement with the Angstrom exponent data. Three events that occurred primarily in the small-particle range 3 are evident on 9, 13, and 18 March.
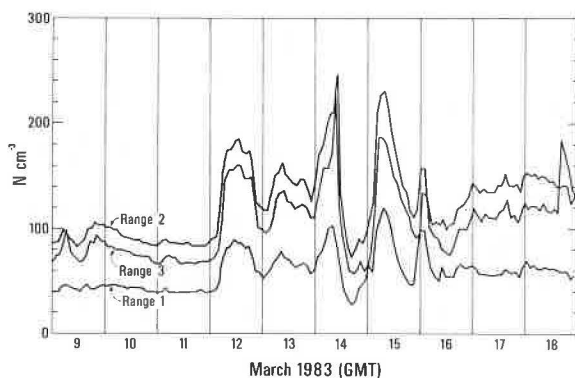
Figure 68.--Total number concentration for particle diameters in size ranges 1 (0.24-0.84 μm), 2 (0.15-0.30 μm), and 3 (0.09-0.195 μm) for aerosol spectrometer data at BRW. All times are GMT.

94
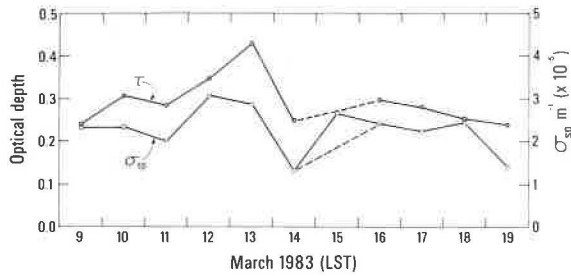
Figure 69.--BRW aerosol optical depth (τ) data (base e) at 550 nm, and σ_{sp} averages for the times during which optical depth data were taken. Data are plotted at 1200 LST. The dashed lines provide continuity for missing optical depth data on 15 March.

Figure 69 shows a comparison of daily mean aerosol optical depth data at 550 nm, and the σ_{sp} data averaged over the time intervals when the optical depth data were taken (about 0900-1600 LST). The two data sets show similar variations and a calculated correlation coefficient of 0.69. Therefore, surface aerosol measurements are qualitatively representative of the Arctic haze above the ground and account for approximately 48% of the variability.

4.6 Modeling ^{13}C

Some preliminary results of a model for ^{13}C/^{12}C variations are available for examination. The model differs from previous models in that biospheric-atmospheric carbon fluxes were specified by E. Box (University of Georgia, Athens; personal communication, November 1983). Box developed the fluxes as functions of climatic variables based on plant growth experiments. These carbon fluxes were used in a two-dimensional global diffusion model that simulated gas exchange with a two-layer noncirculating ocean. Fossil fuel burning as a function of latitude provided a major perturbation in the model. This model was more fully described in Harris and Bodhaine (1983, pp. 76-78).

The units used for ^{13}C in the model were not the same as for CO_2, because concentration units do not clearly show the variability between the ratio of ^{13}C to ^{12}C. Whereas extremes of $^{13}CO_2$ would differ by only a few tenths of a part per million, the normalized ratio, δ^{13}C, yields a convenient scale emphasizing differences in ^{13}C/^{12}C:

$$\delta^{13}C = \left[\frac{(^{13}C/^{12}C)}{R} - 1 \right] 1000$$

where R = 0.0112372.

The basis of the ^{13}C model is that the ratio ^{13}C/^{12}C changes slightly when carbon goes from one reservoir to another. For example, when CO_2 from burning of fossil fuel is added to the atmosphere, the lower ^{13}C/^{12}C of the new CO_2 dilutes the ratio of the total CO_2, and a new lower value of ^{13}C/^{12}C results. When CO_2 goes into the biosphere from the atmosphere (carbon goes from atmospheric CO_2 to organic plant material) ^{13}C is discriminated against, and only 98.2% of it enters the biosphere as compared with the amount of ^{12}C taken in by the biosphere. Consequently, the remaining ^{13}C/^{12}C is increased.

95

In vegetative rotting, the ^{12}C and ^{13}C are returned to the atmosphere, restoring the former $^{13}C/^{12}C$ ratio in the absence of any other influences.

In ocean-atmosphere exchange of CO_2 there is a preference (fractionation) for both the ocean-to-atmosphere flux and for the atmosphere-to-ocean flux. The amount of fractionation for those fluxes is smaller than for the atmosphere-biosphere flux, however, and a smaller effect is expected. Details of the ocean-atmosphere fractionation are given by Siegenthaler and Münnich (1981).
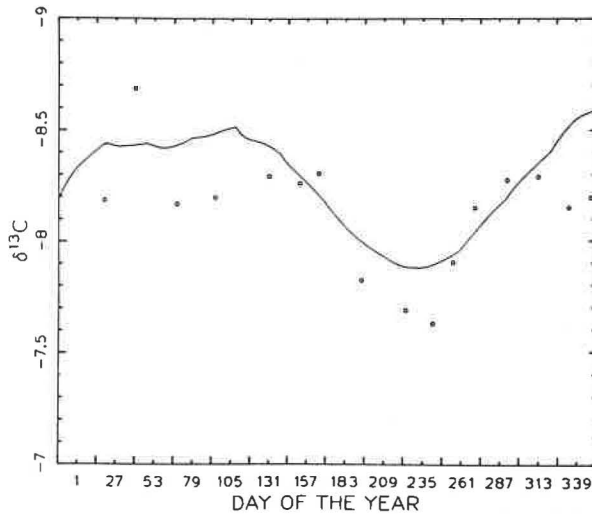
Figure 70.--Results from the $\delta^{13}C$ model (solid line) and from 1983 (unpublished) data from Friedman (dots) for BRW.
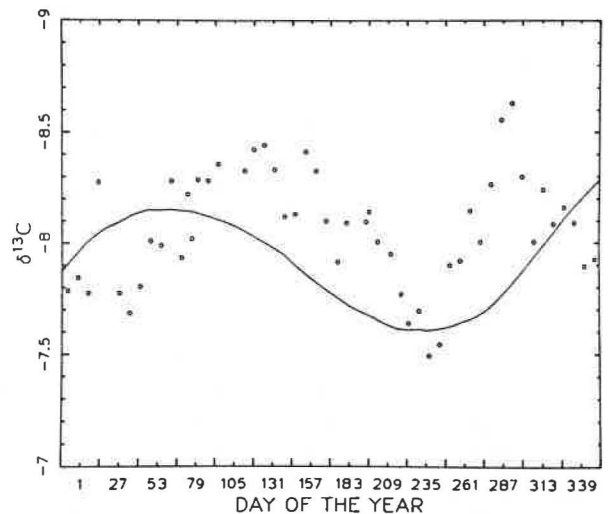
Figure 71.--Results from the $\delta^{13}C$ model (solid line) and from 1983 (unpublished) data from Friedman (dots) for MLO.

The carbon fluxes specified are given by Gillette and Box (NOAA/GMCC; unpublished manuscript, 1984). Model results for $\delta^{13}C$ are presented in figs. 70-73 along with experimental data for 1983 from I. Friedman (USGS, Denver, CO; personal communication, March 1984). Friedman's data are provisional and unselected. For the latitude and altitude of BRW, there is fairly good agreement between model results and Friedman's data. For the latitude of MLO, model results for sea level agree better with the observational data than do the model results for 3-5 km (the altitude interval in which MLO is situated). This fact has led to discussions on sampling times to avoid upslope air and how best to obtain air samples for $\delta^{13}C$ analysis. At SMO there is a much greater annual fluctuation of the model results for that altitude and latitude than is observed in the data. A preliminary explanation of this has to do with a large equatorial and tropical biosphere-atmosphere carbon exchange. We are presently looking into this problem. At SPO there is again a larger seasonal fluctuation in the model results than what has been observed by Friedman. We feel that this too is a reflection of the equatorial biosphere-atmosphere exchange rates that are used in the model.
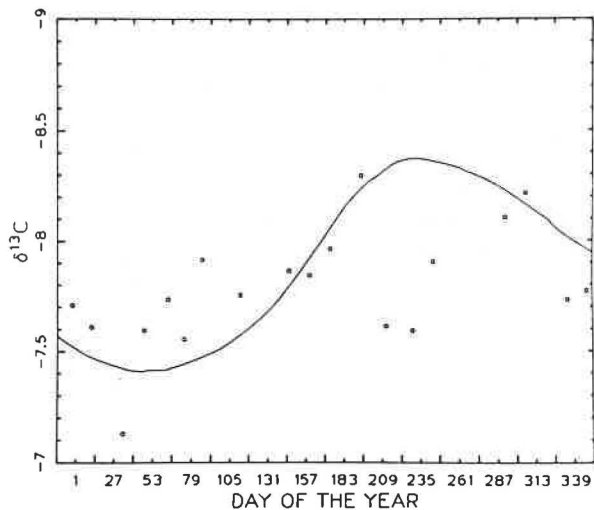
Figure 72.--Results from the $\delta^{13}C$ model (solid line) and from 1983 (unpublished) data from Friedman (dots) for SMO.
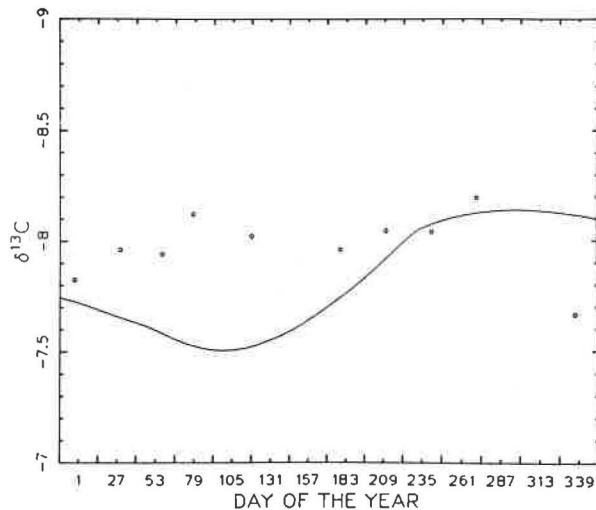
Figure 73.--Results from the $\delta^{13}C$ model (solid line) and from 1983 (unpublished) data from Friedman (dots) for SPO.

4.7 Analysis of SPO CO_2 Data for 1975-1982

GMCC CO_2 data for SPO were calibrated with SIO standard CO_2 gases, corrected for nonlinearities and pressure broadening, and corrected for discontinuities caused by instrument alterations. After removal of data representing known contamination episodes, spectral analysis showed negligible power in periods shorter than 5 days.

Comparison in fig. 74 of the GMCC CO_2 record with Australian CO_2 concentrations obtained in the midtroposphere by CSIRO (Pearman et al., 1983a) shows a similar growth rate of CO_2. There are differences in the annual cycles at the two locations, however. The Australian values are higher by 0.46 ppm on the average and the RMS difference is 2.35 ppm.

Comparison in fig. 75 of the GMCC continuous vs. SIO flask CO_2 record for SPO (Bacastow and Keeling, 1981) shows fairly good agreement except for 1975 where there appear to be systematic errors in the GMCC values. There are also noticeable differences at the end of 1978 after which the GMCC continuous CO_2 analysis was terminated for 1 year. The mean difference between GMCC and SIO CO_2 values is 0.15 ppm, and the RMS difference is 0.41 ppm.

In fig. 76 spectral analysis of the linearly detrended (1.51 ppm yr^{-1}) time series shows only one significant peak at 1 yr^{-1}. Little power is contained for periods shorter than 2 months. There is some unresolved power for periods of about 3.6 years, possibly associated with change of CO_2 input or with El Niño events.

Annual growth rates were computed by differentiating the spline-fitted function, which had knots at the beginning and end of each year. The spline was fit to monthly means with 2 years of ficticious data on either end of the record. If we disregard the suspect 1975 to mid-1976 data, fig. 77 shows a

97
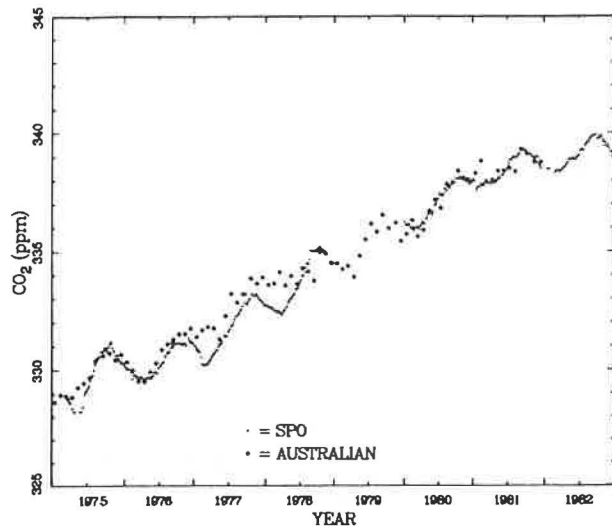
Figure 74.--Atmospheric CO_2 concentrations for the midtroposphere over Australia determined by CSIRO (Pearman et al., 1983a) compared with CO_2 concentrations derived from the GMCC continuous analyzer at SPO.
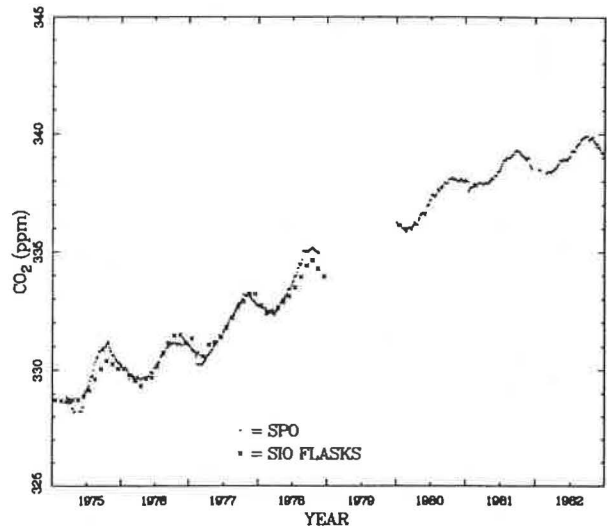
Figure 75.--Atmospheric CO_2 concentrations at SPO determined for flask samples analyzed by SIO (Bacastow and Keeling, 1981) compared with CO_2 concentrations derived from the GMCC continuous analyzer at SPO.
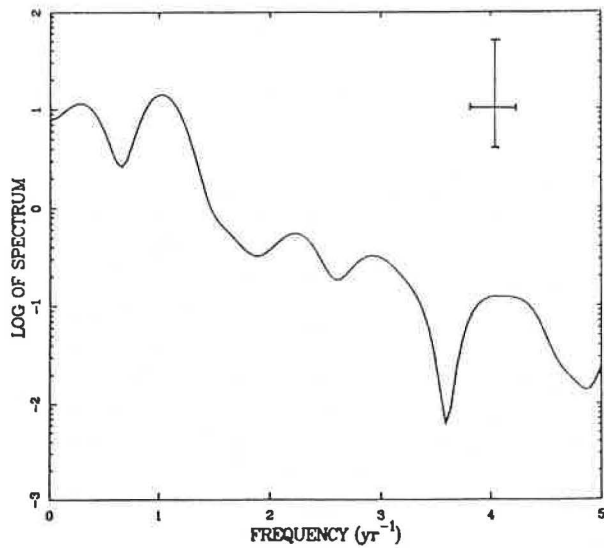
Figure 76.--Smoothed sample spectrum for 5-day means of atmospheric CO_2 concentrations from 1975 to 1982 at SPO. The CO_2 values were selected by a statistical method. Bandwidth of the Parzen lag window and 95% confidence intervals are shown on the figure. A linear trend was removed from the time series before the spectrum was computed.
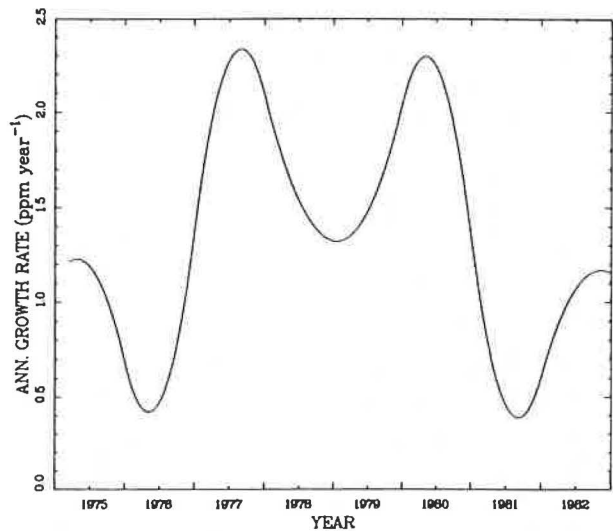
Figure 77.--Annual growth rate as a function of time for selected data.
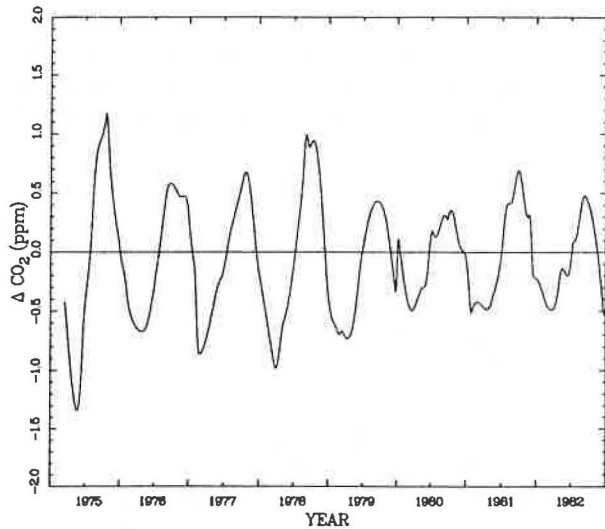
Figure 78.--Spline fit to 5-day means, reduced by the long-term function for selected data.

general lowering of the growth rate of CO_2 from about 1.7 ppm yr^{-1} (1977-1980) to about 1.0 ppm yr^{-1} (1981-1982).

Seasonal variations of the detrended data were obtained by fitting splines to the 5-day means after subtracting the long-term growth rate that was differentiated above. The knots were monthly and were movable. The results (fig. 78) show an apparent trend to smaller annual cycles.

4.8 Airborne Latitude Survey of El Chichon Optical Depth

The fourth, and apparently final, NASA-sponsored airborne survey of El Chichon volcanic optical properties was flown in May 1983. The flight series came about primarily as a result of the mechanical failure of the NASA SAGE satellite, which would have provided much of the needed information. The flights showed substantial latitudinal variation of the volcanic material more than a year after the eruption, and the distribution had changed differently with time than had been expected. GMCC participated in the four flight series by providing instruments and/or personnel for measuring aerosol optical depth in the 0.38- to 0.862-μm wavelength region. On two of the flight series, December 1982 and May 1982, GMCC also provided and operated additional instrumentation for measuring relative global diffuse, total, and reflected solar flux.

The latitudinal variation of El Chichon 500-nm optical depth at the times of the flights is shown in fig. 79. Flight series 1 and 3 display a broken trace because of lower flight altitudes and frequent night flights to facilitate lidar operations. The appearance of the relative minimum near 30°N was unexpected, but was recorded on several instruments on the last three of the four flight series and probably did not exist at the time of the first series.

The sunphotometers used on the flights were identical to the ones used at the GMCC baseline stations, but were independently calibrated. Additional details of the observational procedures, probable errors, and results are given by Dutton and DeLuisi (1983b) and DeLuisi et al. (1983).

99
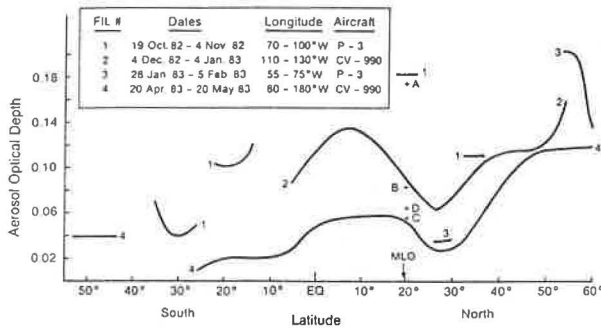
Figure 79.--Aerosol optical depth (500 nm) as a function of latitude from four NASA stratospheric survey flight missions as measured by GMCC. Numbers on curves correspond to flight numbers. Lettered points (A-D) indicate optical depth values obtained at MLO during times corresponding to the airborne latitude surveys (A → flight 1, B → 2, etc.).

The only GMCC site at which optical depth readings can be directly compared with the aircraft data is MLO, because of similar observing conditions and elevation. The 500-nm aerosol optical depths measured at MLO during the times of each flight series are indicated as lettered points A-D on fig. 79 (A corresponds to flight 1, B to 2, etc.). The MLO values were averaged over several days corresponding to when the aircraft crossed the MLO latitude, 19°N, even though the aircraft was at a much different longitude. The excellent agreement between aircraft and MLO data substantiates the areal representativeness of the MLO observations and the temporal representativeness of the aircraft results. Further discussion of these and other GMCC optical depth measurements of El Chichon spectral aerosol optical depth is given in Dutton and DeLuisi (1983a).

Climate sensitivity studies of Chou et al. (1984) have shown that the global climate response to stratospheric aerosols of volcanic origin is highly dependent on the latitude distribution of the optical depth. Inclusion of observed latitudinal distribution of aerosol in this and similar models should improve attempts to simulate El Chichon's actual climatic effects.

4.9   Concentrations of Trace Gases in the Atmosphere

A new program was begun to assemble and archive measurements of atmospheric trace gases for development of a worldwide data base that supplements the routine and special observing programs at the GMCC baseline stations. The intention is to identify deficiencies in the collection of data for specific constituents and to provide a focal point for data that have not been widely disseminated. Although the work has only just begun and the list of entries is relatively short, all available information is being put into the data base, which will be continually updated. A data base of this sort will be pertinent and useful to any individual presently working or considering starting to work on a specific trace constituent. The data base contains information on the measurement itself, the location, the time, and the source reference, thereby providing a basis for the determination of data-rich and/or data-void regions. Such a data base, which contains concentrations and fluctuations of a specific trace gas, may also aid in the location and identification of specific sources and sinks. In addition, as the data base becomes more complete, it will be capable of providing information to atmospheric air quality models of varying degrees of complexity.

Data have been collected for the following species: CH_4, CO, O_3, CO_2, H_2, and N_2O. These data were collected from many separate studies, and each

study may include one or more measurements. When the data from the separate studies are combined, one begins to obtain some measure of global coverage. Most of the readings were taken in the troposphere between 6 and 8 km. Current efforts also involve the collection of data for NO and for NO_2. However, it has been very difficult to find atmospheric concentration data involving SO_x, because of the short atmospheric lifetime of SO_x constituents; most of the work being done in this area involves the measurement of fluxes. The data base also includes names of individuals or organizations considered especially knowledgeable about a specific trace constituent, the work they are doing, and how long they have been doing it.

Although this project is still in its early stages, the data base will be expanded to include as many trace constituents as possible using concentration data throughout the troposphere and stratosphere.

4.10   The Photovoltaic Power System at SMO

In 1983, the solar power system at SMO was installed and tested. The system was purchased and installed with funds provided by the DOE Federal Photovoltaic Utilization Program, under interagency agreement DOE-A101-79CS-300-87. A request for proposal was released in September 1981 (NOAA 54-81). The source evaluation board selected the Solarex Corp. of Rockville, MD, as the system supplier (NOAA contract NA82RAC00041). To decrease costs, NOAA used the suppliers' specifications to purchase directly the batteries and the material for the photovoltaic array stand. Detailed specifications of the system were reported in Harris and Bodhaine (1983).

As stipulated in the contract, Solarex submitted a system acceptance test plan in March 1983. The plan called for testing the power from the PV panels when the Sun is unobstructed and within 10° of normal to the panels. The test involves isolating the individual strings, which consist of 10 modules each, and measuring the voltage and current output as the load is varied. The output is plotted as a function of voltage and current on an x-y plotter. Then the open circuit voltage, closed circuit current, and peak power output are determined from this plot. Each string contains one module with an imbedded thermometer that is intended to measure the cell temperature. The cell temperature determines the efficiency of the modules. Results of these tests are listed in table 29. The observed variation in cell temperature between strings is a function of systematic variations in the ventilation across the array and is not due to insolation differences. Smoke tests confirmed the observed lack of ventilation across the southern end of the array, and in particular string no. 9. The average output of the array is 5.5 kW at insolation levels of 1 kW m^{-2} and cell temperatures of 59°C. When adjusted to standard conditions (1000 W m^{-2}, 25°C) the calculated output is 6.2 kW. This is only slightly in excess of the specified power level of 6.0 kW.

The main problem discovered in these test results is the relatively low peak power voltage V_{pp} of 145 V for string no. 9. At this voltage the array will supply power, but it is too low to charge the batteries efficiently in the afternoon. The cause of this relatively low voltage is the excessive temperature of the modules in the absence of normal ventilation. The most logical first step, trimming the vegetation along this portion of the ridge to

Table 29.--Results of tests of the SMO photovoltaic system

| String no. | Time (LST) | Measured values | | Values derived from IV curves* | | | | |
		Insolation† (mW cm^{-2})	Cell temp.§ (°C)	V_{oc} (V)	I_{sc} (A)	V_{pp} (V)	I_{pp} (A)	P_p (W)
1	1220	104	62	196	3.98	149	3.48	520
2	1310	102	63	195	3.99	150	3.52	528
3	1225	103	58	201	3.96	155	3.44	532
4	1306	---	57	199	4.00	151	3.48	523
5	1230	---	55	202	4.11	154	3.66	563
6	1258	106	55	202	4.24	156	3.65	569
7	1235	104	52	204	4.03	158	3.50	553
8	1255	---	54	202	4.34	154	3.86	593
9	1240	104	65	193	4.00	145	3.53	510
10	1250	104	65	198	4.31	154	3.72	576

*IV is current voltage; V_{oc}, open-circuit voltage; I_{sc}, short-circuit current; V_{pp}, peak-power voltage; I_{pp}, peak-power current; P_p, peak power.

†Insolation is measured with the pyranometer at the same tilt as the panels. Scattered clouds were present.

§Throughout the test, the air temperature was approximately 29°C and the wind speed was less than 1 m s^{-1}.

allow better airflow, will be tried soon. A decrease in the cell temperature of 10°C is expected to result in an increase in the output of 10 V.

The Solarex engineers also recommended a means of varying the output of the array so that energy can be pumped into the batteries in conditions of slowly varying insolation. In the normal charging cycle, once the battery voltage reaches a level near its upper limit, its charging efficiency decreases in the presence of steady input. To increase the efficiency of charging, it is necessary to vary the input voltage. This was done by shorting two or three modules from each string, depending on conditions, and waiting for the voltage to recover. This method did not work as planned partly because of the reduced array voltage. Once the modules were "cutout," the system came into equilibrium at this new, reduced power level, charging at an even slower rate than before. Readjustment of the limit voltages only seems to help at specific charge levels. Further testing of the charging cycles will continue. Eventually it may be necessary to add a circuit to limit the time the arrays are in the clipped mode.

4.11 Shipboard Measurements of Atmospheric CO_2 in 1983

4.11.1 Introduction

The increase of atmospheric CO_2 concentration has been well documented through in situ measurements at the baseline observatories at MLO, BRW, SMO, and SPO (Harris and Bodhaine, 1983, pp. 24-26; Keeling et al., 1976a, 1976b).

Although high-quality data from a few stations may be sufficient to establish this global trend, higher spatial resolution is needed to locate regional sources and sinks of CO_2 and to provide boundary conditions and verification for carbon cycle models (Pearman et al., 1983b; Pearman and Beardsmore, 1984). For this reason the GMCC CO_2 flask sampling network was expanded in 1979 and now consists of 22 globally distributed stations collecting flask samples once or twice weekly (see sec. 3.1). This network is now producing data unique in coverage and quality, detailing the spatial and temporal variability of atmospheric CO_2 (Komhyr et al., 1984a, pp. 26-33).

To assess the suitability of the network sites for measuring regional or baseline atmospheric CO_2 concentration unperturbed by local sources or sinks, GMCC undertook a flask sampling program aboard the NOAA research vessel DISCOVERER during May and June of 1982. The results from this cruise demonstrated the feasibility of obtaining good samples collected by minimally trained but conscientious personnel, and the generally good agreement between the cruise data and the atmospheric CO_2 concentration determined from the flask network (Harris and Bodhaine, 1983, pp. 99-102). The shipboard data were also useful in pinpointing the locations of steep gradients in CO_2 concentration, which could only be inferred from the sparser network data.

The success of this limited project encouraged the CO_2 group to participate in several cruises in 1983 and 1984. The cruises and dates are listed in table 30, and the cruise tracks are shown in fig. 80. To date, the emphasis has been on the Pacific Ocean and the Southern Hemisphere. This is due to both specific interest in these regions and the availability of ships and cooperative investigators.

In general, the samples have been collected in pairs of 0.5-L glass flasks using a portable sampling unit (Komhyr et al., 1984a). On the AKADEMIC KOROLEV and the DISCOVERER 1984 cruises, samples were collected in 3-L evacuated flasks equipped with greaseless stopcocks. In all cases the samples were

Table 30.--GMCC shipboard flask sampling programs

| Cruise	Dates	Type of sampling	Species measured
DISCOVERER	May-Jun 1982	0.5-L flasks	CO_2
POLAR STAR	Dec 1982- Mar 1983	0.5-L flasks	CO_2, CH_4
KNORR (TTO/TAS)	Jan-Feb 1983	0.5-L flasks	CO_2
FUJI	Feb-Mar 1983	0.5-L flasks	CO_2
DISCOVERER	Mar-May 1983	0.5-L flasks	CO_2, CH_4
A. KOROLEV	Oct-Dec 1983	3-L flasks, gas chromatograph	CO_2, CH_4 CO_2, CH_4, pCO_2
KNORR (Long Lines)	Oct 1983, Jan 1984	0.5-L flasks	CO_2, CH_4
POLAR SEA	Dec 1983- Mar 1984	0.5-L flasks	CO_2, CH_4
DISCOVERER	Feb-May 1984	3-L flasks, gas chromatograph	CO_2, CH_4 CO_2, CH_4, pCO_2, pCH_4
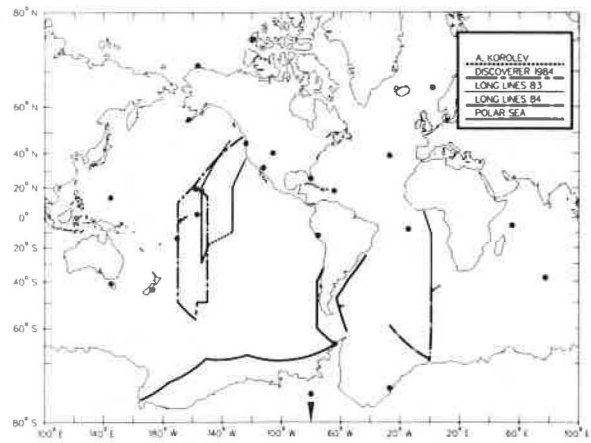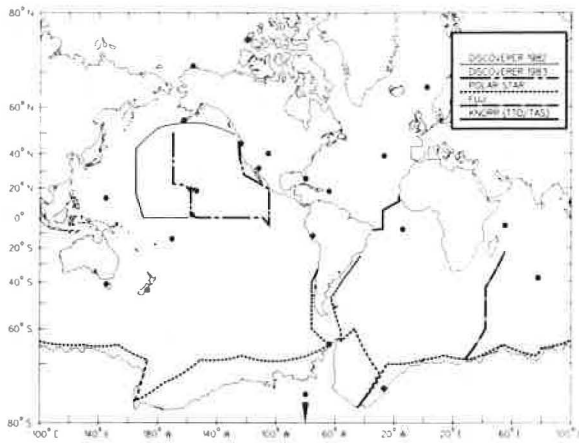
Figure 80.--Cruise tracks for the shipboard flask sampling programs carried out from 1982 to 1984. The closed circles indicate the locations of the GMCC CO_2 flask network sites (see sec. 3.1 for details of the network).

analyzed for CO_2 concentration on the semiautomatic NDIR CO_2 flask analysis apparatus at the GMCC laboratories in Boulder. As indicated in table 30, flasks from the more recent cruises have also been analyzed for CH_4. These data are discussed in sec. 5.15.

4.11.2 Results and Discussion

Selected CO_2 data for three of the 1983 cruises are presented in figs. 81, 82, and 83. The quality of the samples (as defined by the percentage of sample pairs agreeing to ≤ 0.5 ppm) varied among the three cruises: the POLAR STAR, 60%; the FUJI, 89%; and the DISCOVERER 1983, 75%. These values
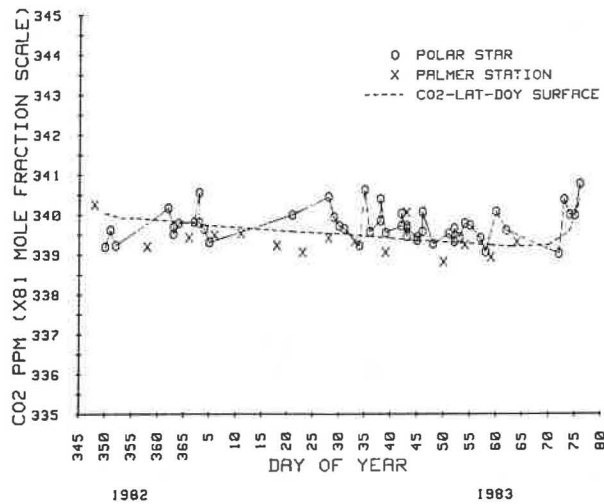
Figure 81.--CO_2 vs. DOY for the 1982-1983 POLAR STAR cruise flask samples. Palmer Station flask data are shown for comparison. The dashed line consists of data extracted from the CO_2-latitude-DOY surface of fig. 7, sec. 3.1.
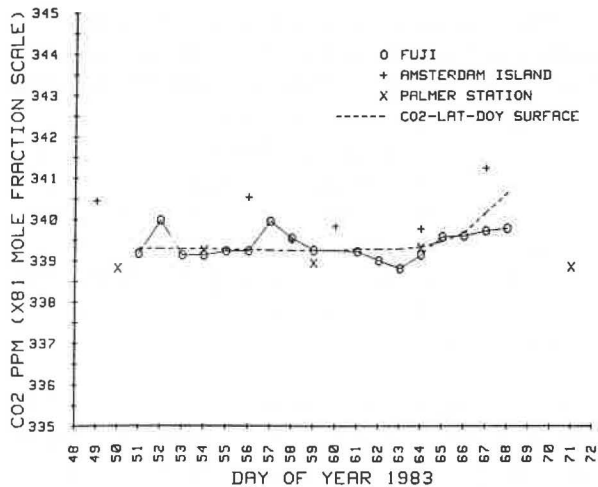
Figure 82.--CO_2 vs. DOY for the FUJI cruise flask samples. Amsterdam Island and Palmer Station flask data are shown for comparison. The dashed line is from fig. 7, sec. 3.1.
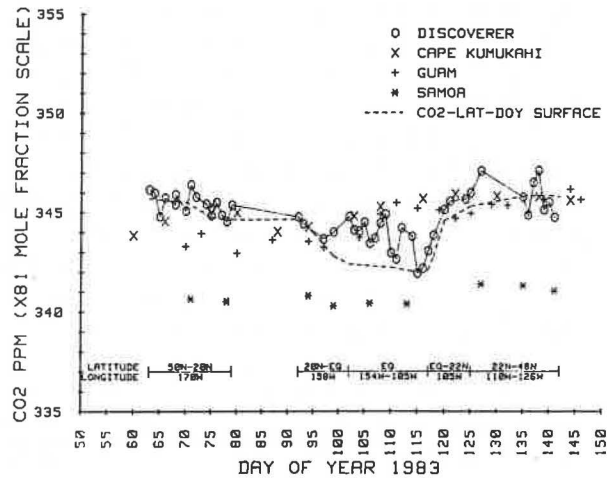
Figure 83.--CO_2 vs. DOY for the 1983 DISCOVERER cruise flask samples. Flask data from Cape Kumukahi, Guam, and Samoa are included for comparison. The dashed line is from fig. 7, sec. 3.1. The latitude-longitude scale indicates the five sections of the cruise as discussed in the text.

are comparable with the average (85%) for the flask network as a whole. The factors affecting sample quality include storage time (1-3 months for DISCOVERER 1983; 2 months for the FUJI; 3-6 months for the POLAR STAR), storage temperature, sample water vapor content, and technique of the sample taker. It is likely that storage time and temperature are responsible for the deterioration of some of the cruise samples. The data were selected by rejecting high members of bad pairs followed by a more subjective rejection of values lying far from the bulk of the data.

The cruise of the USCG vessel POLAR STAR sponsored by NSF's USARP during austral summer 1982-1983 was of particular interest in that it afforded an opportunity to assess directly the representativeness of Palmer Station for the latitude band centered at 65°S. In fig. 81 the weekly flask data from Palmer Station are plotted for comparison with the POLAR STAR data. From DOY 362, 1982, to DOY 63, 1983, the ship circumnavigated the Antarctic continent, remaining south of 60°S and going as far as 77°S. The mean CO_2 concentration for POLAR STAR flasks for this period is 339.9 ppm (N = 40, σ = 0.6), while for Palmer Station the mean is 339.4 ppm (N = 15, σ = 0.4).

Although the POLAR STAR data show a higher degree of variability, the agreement between the two data sets is quite good, indicating that atmospheric CO_2 in this part of the Southern Hemisphere is well mixed zonally, and that Palmer Station is indeed a regionally representative site. The variability in the POLAR STAR data is probably real and may be related to variation in sea ice cover, upwelling, and/or marine productivity causing short-term fluxes of

105

CO_2 between the ocean and the atmosphere. The dashed line in fig. 81 represents data extracted from a CO_2-latitude-DOY surface constructed from zonally averaged CO_2 data from the GMCC network (see sec. 3.1). The agreement between the surface and the circum-Antarctic cruise data supports the validity of zonally averaging CO_2 data, especially in the Southern Hemisphere. The slight downward trend until DOY 72 is due to the Southern Hemisphere seasonal cycle of ~1 ppm, while the increase from DOY 72 through 76 indicates a latitudinal gradient of ~1-2 ppm between 39°S and 26°S off the eastern coast of South America at this time of year. The latter feature is seen clearly in both the POLAR STAR data and the zonally averaged surface, while the scatter of the cruise data tends to obscure the small seasonal trend.

The GMCC flask sampling program aboard the Japanese research vessel FUJI was a cooperative venture with J. Kelley of the University of Alaska Geophysical Institute. The ship made a south-to-north transect across the Southern Indian Ocean from the Japanese station at Syowa, Antarctica, to the island of Mauritius. In fig. 82 the CO_2 data are plotted vs. DOY together with data from Amsterdam Island and Palmer Station for comparison.

The flask samples collected aboard the FUJI were quite good, with only 2 bad pairs out of 18, and 1 good pair rejected as being contaminated. The period from DOY 51 through 68 covers from 69°S to 23°S and shows little or no gradient, with a mean CO_2 concentration for the shipboard flask samples of 339.4 ppm (N = 17, σ = 0.3). For comparison, the mean concentration for this period is 340.2 ppm (N = 6, σ = 0.7) at Amsterdam Island and 339.0 ppm (N = 5, σ = 0.2) at Palmer Station. The agreement of the cruise data with station data is quite good, lending further support to the representativeness of the Southern Hemisphere flask sites. There is, however, a tendency for the Amsterdam Island flask data to be higher, as expected from the Southern Hemisphere latitude gradient, and more variable than the FUJI or Palmer Station data. The agreement of the cruise data with the CO_2-latitude-DOY surface is also quite good. The divergence occurring north of 30°S (DOY 66) is probably a result of the zonal averaging of the surface, and suggests the existence of a small longitudinal gradient in midlatitudes of the Southern Hemisphere.

The GMCC flask sampling program aboard the NOAA research vessel DISCOVERER during March through May of 1983 was a continuation of the GMCC CO_2 Group's collaboration with the NOAA PMEL's CO_2 Dynamics Study begun in 1982. The CO_2 data from the DISCOVERER are plotted vs. DOY in fig. 83 with station data and a projection from the CO_2-latitude-DOY surface for comparison. Since this cruise covered a large portion of the North and equatorial Pacific over a period of several months when latitudinal gradients are known to change (Komhyr et al., 1984a; Pearman et al., 1983b), it is useful to break it down into five sections. (1) From DOY 63 to 79 the ship steamed south along 170°W from 50°N to 20°N. A north-south gradient of ~1 ppm was observed, which is in good agreement with the zonally averaged surface. Near 20°N the agreement with Cape Kumukahi is good. The observed gradient is typical for the North Pacific at this time of year. (2) From DOY 92 to 102 the track is south along 158°W from 20°N to the Equator. Initially the CO_2 concentration gradient closely follows the CO_2-latitude-DOY surface, but after decreasing by ~1 ppm the concentration increases by ~1 ppm, between 2°N and the Equator. This feature is probably real and is an example of the type of variability that can be located by shipboard sampling but not by land-based sampling sites. (3) From DOY 102 to 117 the track is east along the Equator from 154°W to 105°W. The CO_2 concentrations measured here are variable and 1-2 ppm higher

than the projection from the surface, while agreeing well with Guam and Cape Kumukahi data. Although the variability is somewhat higher than expected, the difference between the cruise data and the surface can be explained by the fact that the surface is zonally averaged and the equatorial portion includes data from Ascension Island (8°S) in the Atlantic and the Seychelles (5°S) in the Indian Ocean, as well as Guam and Samoa. In this case it is clear that a large longitudinal gradient does exist, with the eastern equatorial Pacific some 2 ppm above the zonal mean. The magnitude of this difference probably varies from year to year and is large in 1983 following the strong ENSO event. The addition in 1984 of Christmas Island (2°N, 158°W) to the flask sampling network will greatly improve our equatorial coverage in the Pacific. (4) From DOY 117 to 125 the ship traveled from the Equator to 22°N along 105°W. On this segment a strong gradient of 4 ppm was observed in close agreement with the CO_2 surface, although the gradient from the cruise data occurs earlier than from the zonally averaged CO_2 surface, suggesting the influence of continental air as the ship approached the Mexican coast. (5) From DOY 125 to 142 the ship traveled along the west coast of the United States, stopping at San Diego, and terminating in Seattle. The CO_2 concentrations on this segment are in general agreement with the CO_2 surface while exhibiting significant variability probably caused by rapid exchange between the atmosphere and shallow coastal waters, and the proximity to the vegetated continent.

Overall, the DISCOVERER 1983 cruise supports the representative nature of the Pacific Ocean flask sampling sites and underscores the need for an equatorial Pacific site. Taken together, the results from the shipboard flask sampling programs have consistently shown that the GMCC CO_2 flask sampling network consists of regionally representative background sites from which a fairly detailed assessment of the global distribution of atmospheric CO_2 at the surface may be obtained. Further, it is shown that a zonally averaged CO_2-latitude-DOY surface represents this distribution quite well (typically within 0.5-1.0 ppm) although differences of 1-2 ppm between measurements and the surface may be found where longitudinal gradients become significant. Note that the 1983-1984 Long Lines cruise should provide some information on longitudinal gradients when compared with the KOROLEV and POLAR SEA cruises.

The acquisition of two custom built gas chromotographs from R. Weiss of SIO (Weiss, 1981) allows in situ, continuous measurements of CO_2 and CH_4 in the air and pCO_2 and pCH_4 in surface seawater. Such measurements were made on the SAGA expedition aboard the Soviet research vessel AKADEMIC KOROLEV and on the DISCOVERER 1984 cruise. These measurements will provide more detailed information on the air-sea exchange of CO_2 and CH_4 and on the distribution and variability of marine sources and sinks of these climatically important species, as well as allowing greater precision and higher resolution in determining gradients than can be obtained by flask sampling.

4.12 Results of the December 1983 NOAA-SIO CO_2 Intercomparison

4.12.1 Introduction

As part of a comparison of the 10-yr joint record of atmospheric CO_2 measurements at MLO by NOAA and SIO, a special set of field tests was cooperatively developed in 1983 to assess possible instrumental sources of disagreement in the present measurement programs. Seven tests were conducted, each lasting 8-33 hours. These tests, designated A to G, were carried out during the week of 5-12 December 1983. A summary is given in table 31.

Table 31.--Summary of NOAA-SIO CO_2 intercomparison at MLO, December 1983*

Test	Working air standard				Ambient air (high-tower line[s])			
	$No._s(No._t)$	N_s†	S_s†	$(N - S)_s$	$No._s(No._t)$	N_s†	S_s†	$(N - S)_s$
	Single-line air intake test; i.e., tests A, B, C, & F							
A	35(37)	336.95 (±0.025)	336.95 (±0.024)	0.00 (±0.029)	34(37)	341.95 (±0.060)	341.86 (±0.050)	0.09 (±0.039)
B	31(32)	343.39 (±0.029)	343.41 (±0.036)	-0.02 (±0.038)	---	---		---
C	14(15)	343.41 (±0.059)	343.36 (±0.051)	0.05 (±0.080)	13(15)	342.07 (±0.103)	341.95 (±0.092)	0.12 (±0.058)
F	16(18)	343.49 (±0.035)	343.42 (±0.025)	0.07 (±0.045)	17(18)	342.24 (±0.056)	342.09 (±0.044)	0.16 (±0.046)
	Dual-line air intake tests; i.e., tests D & E							
D	45(48)	343.41 (±0.021)	343.41 (±0.018)	0.00 (±0.028)	39(48)	341.99 (±0.056)	341.84 (±0.061)	0.15 (±0.024)
E	46(50)	343.41 (±0.022)	343.40 (±0.019)	0.01 (±0.022)	48(50)	341.86 (±0.072)	341.85 (±0.071)	0.01 (±0.025)
	Eavesdrop test; i.e., both systems under normal operation							
G	---	---	---	---	24(27)	342.25 (±0.121)	342.27 (±0.099)	-0.02 (±0.039)

*Concentrations are in parts per million. Entries in parentheses are standard deviations from the mean (σ_m).

†N_s refers to NOAA selected data, S_s refers to SIO selected data. Data omitted are individual 10-min averages that are greater than 2σ from the mean.

4.12.2 Experimental Procedures

During each test cycle, except in tests B and G, a control gas mixture of dried pressurized natural air, WA (for working air), was sampled for a 10-min period with another 10 minutes used to sample ambient air obtained 80 ft above the ground on a high tower, TW (for tower air). These were compared with two standard reference gases, designated W1 and W2. The gases W1, W2, and WA were specially prepared dried CO_2-in-air gas mixtures in pressurized steel cylinders with CO_2 concentrations determined in advance by GMCC. The analyzers used were an APC at SIO and a Hartmann and Braun URAS-2 at GMCC.

The timing and sequence of the gases used was 5 minutes of low reference gas W1, 5 minutes of high reference gas W2, 10 minutes of WA, and 10 minutes of TW. An array of four solenoid valves alternately selected one of the four gases. The WA and TW gases were treated as unknown, so that their CO_2 concentrations were calculated by interpolation of data from W1 and W2, assuming linear instrument response. For WA and TW, 10-min averages were computed each half-hour for each analyzer, taking into account short-term changes in sensitivity and drifts of the analyzer output.

The guiding principle in designing these tests was to take both systems offline and to begin by eliminating all differences between the systems except those from the two analyzers. Then the two systems were allowed to be brought to their respective normal configuration of sampling lines, plumbing, and water freeze traps.

In tests A, B, and C, beginning on 5 December, as many hardware differences as possible were eliminated between the analysis systems. Ambient air

was taken through a common line (SIO high tower) and through a common pumping system (SIO). The selected gas mixture passed through a common water vapor freeze trap, after which it flowed separately to each analyzer. In tests B and C, the times for reference gases W1 and W2 were increased to 10 minutes. Ambient air was not measured in test B.

Test D, begun on 8 December, was designed to determine whether certain identified hardware differences between the two systems would cause differences in the results. Specifically, each analyzer received ambient air from separate lines on the high tower through separate plumbing systems. Each system also included its separate water freeze-out trap. The timing sequence was the same as in test A. Test gases W1, W2, and WA were still common to both systems. Results from this test showed a consistent difference of about 0.15 ppm (URAS minus APC) between the NOAA and SIO tower air. Because the mean of the WA differences was ≤ 0.05 ppm, the bias in the TW data appears to have occurred in the tower air lines or the pumping systems, and not in the analyzers. In hopes of pinpointing the source of the difference, test E was run.

Test E, begun on 9 December, was designed to decide between the pumping system or the air lines as the source of the difference found in test D. The tower air lines were reversed so that one pump used the other's air line. The lines were also switched after the pumping system. The end result was that each analyzer sampled its own tower air, but the air was pumped by the other's pumping system. It was thought that if the difference found in test D changed sign, then the source was in one of the pumping systems. If there was no change in the offset from test D, the source might be a contaminated air intake line.

Test F, begun on 10 December, was similar to test E, following it continuously in time, except that a common air line (SIO high tower) was directed through the GMCC plumbing to both analyzers.

Test G, begun on 11 December, was an "eavesdropping" test on the normal operation of each analyzer, except that the SIO analyzer had previously been calibrated with CO_2-in-N_2 gas mixtures, and in this test it used CO_2-in-air mixtures. (Beginning on 18 December 1983, SIO changed its normal operation of the APC to CO_2-in-air reference gases.) Test G was based on averages every hour, rather than every half-hour, since this is the normal operation for the GMCC system.

4.12.3 Results

When the same CO_2-in-air test gas mixture (WA), sampling sequence, and plumbing (tests A, B, C, and F) were used, the analyzers were found to give nearly identical results. In test A, a gas mixture predetermined by GMCC to contain 336.95 ppm was assigned as WA. The difference in CO_2 concentration calculated for WA between the analyzers was 0.00 ppm with a standard deviation from the mean (σ_m) of 0.029 ppm. In tests B, C, and F, a gas mixture predetermined to contain 343.48 ppm was assigned as WA. The analyzers showed a difference (URAS minus APC) of -0.02 ppm with σ_m = 0.038 ppm in test B, a difference of 0.05 ppm with σ_m = 0.080 ppm for test C, and a difference of 0.07 ppm with σ_m = 0.045 ppm in test F. The average weighted difference for

109

all four tests (A, B, C, and F) was 0.011 ppm. With the possible exception of test F, WA gave no significant difference in recorded concentration for the two systems.

The agreement suggests that any difference in the nonlinearity of the two analyzers over the range 335-345 ppm was less than 0.1 ppm. The linear interpolation used to estimate WA was later determined to introduce a maximum error of 0.04-0.05 ppm from the true value of the nonlinear response of the URAS analyzer determined on 7 December 1983. To have achieved the best observed agreement, the nonlinearity of the APC must have been of similar magnitude and sign. Similar nonlinearities have been found in previous comparisons of APC and URAS analyzers undertaken at SIO.

A second significant result of tests A, B, C, and F was the similar RMS noise level (σ_s) for each instrument and test when measuring WA through common plumbing and water freeze-out trap. While the weighted σ_s for the APC over all four tests (0.16 ppm) represents typical performance, the weighted σ_s for the URAS (0.16 ppm) was greater than normal. This was not a serious hindrance to the testing, since a noise level for an individual measurement is an expression of a random error. In normal operation, as well as during these special tests, so many individual measurements are averaged that the noise-induced individual errors of about 0.20 ppm are unimportant compared with longer term, systematic errors.

The variance of the differences (URAS minus APC) of the 10-min average CO_2 concentrations determined by the two instruments measuring WA is approximately equal to the sum of the variances of the 10-min averages of each instrument. That is, $\sigma_\Delta \cong [(\sigma_{APC})^2 + (\sigma_{URAS})^2]^{\frac{1}{2}}$. This suggests that the variability was largely uncorrelated and not closely related to changes in a common environment such as vibration, temperature, or electrical interference.

Tests A, C, and F also included 10-min measurements during each cycle of ambient air from the SIO high-tower air intake line through common plumbing and cold trap. For this gas, TW, the analyzers gave a weighted average difference (URAS minus APC) of 0.12 ppm with a weighted average σ_m of 0.026 ppm. The mean ambient air values of TW had higher variability (σ_s = 0.10-0.37 ppm per test) compared with the mean values of WA (σ_s = 0.10-0.22 ppm per test). This increased variability of their values is attributable to the combined instrumental and real air variability. The difference between the analyzers (URAS minus APC) appears to be significant (over 4 times σ_m).

In test D the difference (URAS minus APC) for ambient air was 0.15 ppm, with σ_m = 0.024 ppm. Attempts in test E to cause this difference to reverse sign by interchanging plumbing but keeping the same air intake lines resulted in a URAS minus APC difference of 0.01 ppm with σ_m = 0.025 ppm.

It was observed during the first part of test E that a negative-pointing spike occurred on the URAS strip chart recorder trace, at the start of each 10-min sample of GMCC tower air. This spike was also found to have occurred on the APC chart recorder trace in test D, although it was much smaller, because of the larger sample cell of the APC analyzer compared with that of the URAS. The cause of this spike was found to be a faulty air pump in the

SIO plumbing system, used in test D to supply tower air to the APC and in test E to supply tower air to the URAS. During the last 3 hours of test E, after replacement of the pump, the difference in ambient air values between the two systems (URAS minus APC) rose to an average value of 0.15 ppm with σ_m = 0.042 ppm, similar to test D.

The short "eavesdropping" comparison of test G presents only a small sample of the ongoing comparison between the NOAA and SIO CO_2 analyzers at MLO. The results indicated a difference of -0.02 ppm with σ_m = 0.039 ppm. However, conclusions for this test will depend on final concentrations for the different reference gases employed as station standards in the normal operation of the SIO and NOAA CO_2 programs at MLO.

4.12.4 Summary

Tests A, C, D, E, and F showed that the GMCC and SIO CO_2 systems gave the same measured ambient atmospheric air value to within about 0.15 ppm. For tests through common plumbing the difference (URAS minus APC) on average was 0.12 ppm with σ_m = 0.026 ppm. For tests through different plumbing a similar difference of 0.15 ppm was observed, disregarding the period of faulty pump performance during test E. The weighted mean difference for all tests was 0.138 ppm with a weighted σ_m = 0.016 ppm. No single cause was discovered that accounted for these differences, which did not appear to correlate with permutations in plumbing except for the changes in pumps in test E. On average, no significant difference was observed when measuring CO_2 in air from a pressurized cylinder with common plumbing (URAS analyzer 0.01 ppm higher than the APC with σ_m = 0.014 ppm).

The observed differences are smaller but of the same sign as the mean difference (URAS minus APC) provisionally computed between the NOAA and SIO systems for calendar year 1983 (0.3 ppm). The overall level of agreement between the NOAA and SIO CO_2 records at MLO during the last decade has been provisonally determined at the 0.3- to 0.6-ppm level for monthly means, with a relative drift of about 0.08 ppm yr^{-1} (NOAA minus SIO) from an initial difference of about -0.5 ppm in 1974 to +0.6 ppm in 1982 (fig. 84). Except for the period from mid-1980 to mid-1982, the NOAA-SIO difference has remained at or below 0.1% ($\leq$0.3 ppm).
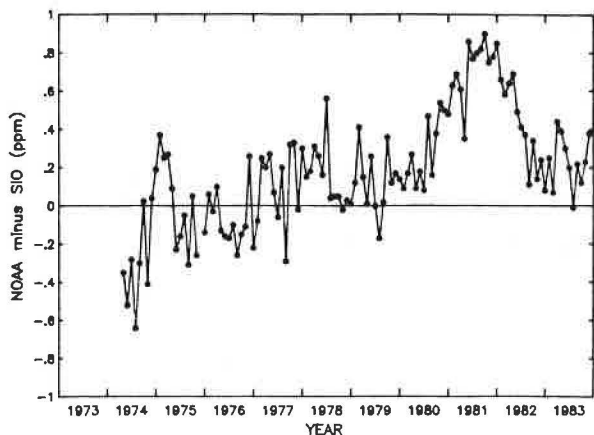
Figure 84.--Provisional selected monthly mean differences between NOAA and SIO for the common record of CO_2 sampling at MLO.

4.13 The 1982-1983 El Niño-Southern Oscillation Event as Recorded in the Global Atmospheric CO_2 Distribution

4.13.1 Introduction

After the seasonal variation and the secular increase due to fossil fuel combustion are removed, the dominant residual signal in time series of atmospheric CO_2 concentration from background monitoring stations is a fluctuation inversely correlated with the SOI. This was first shown by Bacastow (1976) in the CO_2 records for MLO and SPO. Bacastow found the best correlation between the SOI and inverted CO_2 derivatives of the de-seasonalized, detrended MLO and SPO time series. An increase in atmospheric CO_2 was found to lag the SOI minimum by two seasons at MLO and three seasons at SPO. Subsequent analyses by Bacastow and coworkers have extended this approach to stations in tropical latitudes (Fanning Is., MLO) and extratropical latitudes (Station P, SPO). These studies have confirmed the SOI signal in the CO_2 records corresponding to the ENSO events of 1965, 1969, 1972, and 1976 (Bacastow, 1977; Bacastow, 1979; Bacastow et al., 1980).

While Bacastow established the correlation of CO_2 anomalies with SOI, others studied SST, a parameter measurable in the CO_2 source and sink regions of the oceans. Various studies have shown relationships between atmospheric CO_2 variations and SST anomalies in the equatorial Pacific (Weare et al., 1976; Newell and Weare, 1977; Newell et al., 1978), the northwest Pacific (Hanson et al., 1981), and the Pacific, north of 20°N (Schnell et al., 1981). Plotted in fig. 85 (Gammon et al., 1984a), are the year-to-year change in atmospheric CO_2 at MLO, adjusted to remove the fossil fuel increase, and the year-to-year change in the mean air temperature in the northern subtropical zone (Angell and Korshover, 1983). The empirical relationship between the interannual temperature change and the observed CO_2 change is ~0.8 ppm $(°C)^{-1}$, similar to that reported by Schnell et al. (1981).

The relative importance of anomalies in atmospheric circulation, SST, and biospheric activity associated with ENSO events in perturbing atmospheric CO_2 levels remains an open question. For example, the reduced trade winds during El Niño imply reduced upwelling of CO_2 supersaturated deep water, hence a
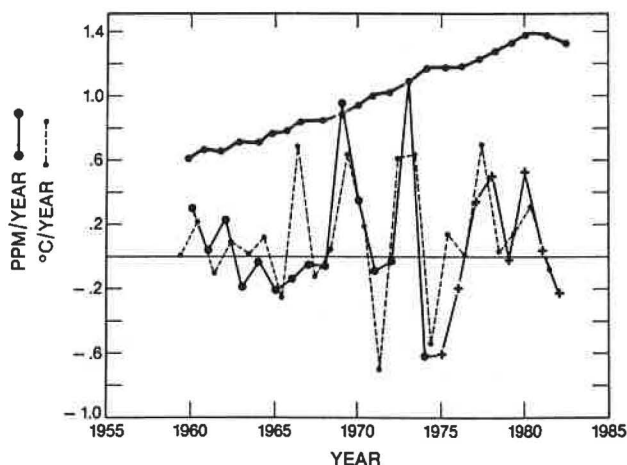

Figure 85.--A comparison of the MLO year-to-year change in atmospheric CO_2, adjusted for fossil fuels (•————•, SIO data; +————+, NOAA data) with the year-to-year temperature change in the northern subtropical zone, 10°-30°N (•-----•). The heavy line is the CO_2 growth rate, calculated from fossil fuel production data, which has been subtracted from the observed growth rate at MLO. (From Gammon et al., 1984a.)

weaker marine source of atmospheric CO_2, while the simultaneous failure of the marine productivity in the upwelling regions implies a less-effective marine sink for CO_2. Lower winds imply less-efficient air-sea CO_2 exchange, possibly affecting both source and sink regions, while warmer surface waters can accommodate less dissolved CO_2 in saturation equilibrium than can colder waters. The role of changing wind stress and SST anomalies in extratropical latitudes may be more important in controlling global atmospheric CO_2 than was previously considered (Komhyr et al., 1983a).

4.13.2 The 1982-1983 ENSO Event

From the established correlation of the SOI with anomalies in the CO_2 growth rate, it was expected that the extreme ENSO event that began in mid-1982 would measurably perturb the global atmospheric CO_2 distribution. This perturbation was observed in the GMCC global CO_2 data as an anomalously low rate of CO_2 increase in mid-1982 (Gammon and Komhyr, 1983; Gammon et al., 1984a, 1984b). The prediction of a post-ENSO maximum in the CO_2 growth rate for late 1983-early 1984 of 2-3 ppm yr^{-1} (Gammon and Komhyr, 1983) is confirmed by the latest results from the CO_2 flask network. The globally averaged year-to-year change in atmospheric CO_2, plotted by quarters in fig. 86, clearly shows the effect of the 1982-1983 ENSO event on the global atmospheric burden of CO_2 over the period from mid-1982 to mid-1984. Because the past 5 years have been a period of nearly constant global emission of ~5 Gt yr^{-1} of fossil fuel carbon to the atmosphere (Keeling, 1983), the zero growth rate from the third quarter of 1981 to the third quarter of 1982 implies that the equivalent of 5 Gt of fossil fuel carbon was removed from the atmosphere for temporary storage in the near-surface ocean and probably in the land biosphere as well. Now, more than a year after the SOI minimum was reached in January 1983, this 5 Gt of carbon appears to have returned to the atmosphere; the year-to-year global average CO_2 increase peaked in the first quarter of 1984 to 2.2 ± 0.3 ppm yr^{-1}, well above the mean growth rate of 1.4 ppm yr^{-1} for the past decade. Although previous investigators have focused on this high CO_2 growth phase that lags the SOI minimum, the precursor phase of low CO_2 growth is equally prominent in the 1982-1983 event and may offer predictive possibilities.
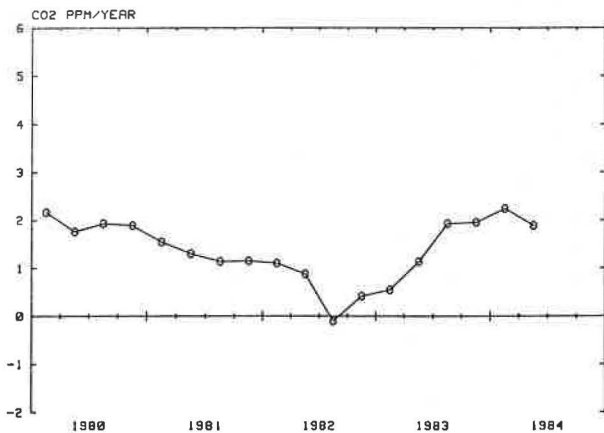

Figure 86.--The globally averaged CO_2 growth rate from the GMCC CO_2 flask network data. The points are differences between quarterly global means in consecutive years, plotted in the forward year.

113

A more detailed analysis of the latitude-dependent CO_2 response to the 1982-1983 ENSO event can be made using the zonally averaged CO_2 concentration surface constructed from the CO_2 flask network data (sec. 3.1.2 and Komhyr et al., 1984). The representativeness of the surface has been verified by atmospheric CO_2 sampling aboard several cruises in 1982 and 1983 (Harris and Bodhaine, 1983, pp. 99-102; this report, secs. 4.11 and 4.16). In fig. 87a, several CO_2 anomalies precede or accompany the 1982-1983 ENSO event. First, the normal seasonal migration of the steep interhemispheric gradient near the Equator is perturbed in 1982, with the southern boundary of the gradient appearing far south of its normal position in the fall. A similar southward dislocation of the ITCZ, which represents a boundary between Northern and Southern Hemisphere air, has been reported by Philander (1983).

Another anomaly seen in fig. 87a is the lack of a CO_2 increase from 1981 to 1982, which is most easily discerned in the Southern Hemisphere. The year-to-year CO_2 changes by latitude are shown clearly in fig. 87b, which consists of the difference between concentration surfaces for two consecutive years, plotted in the forward year. The most striking feature of fig. 87b is the strength and location of the anomalous low-to-negative CO_2 year-to-year change in 1982, which clearly suggests that extratropical sinks in both hemispheres intensified in concert during this period. In the high southern latitudes, neither changes in the response of the land biosphere in 1982 nor the direct effects of stratospheric dust from El Chichon could have been responsible for the observed CO_2 decrease. Thus, a more effective southern ocean sink and a decrease in meridional transport of fossil fuel CO_2 from the north are the most likely explanations for this decrease. The interpretation of the negative CO_2 growth rate anomaly in the Northern Hemisphere is complicated both by the presence of the El Chichon dust veil and the unusual land plant activity observed in 1982. The Northern Hemisphere ocean sinks for CO_2 were probably more effective during this period as a result of the extensive
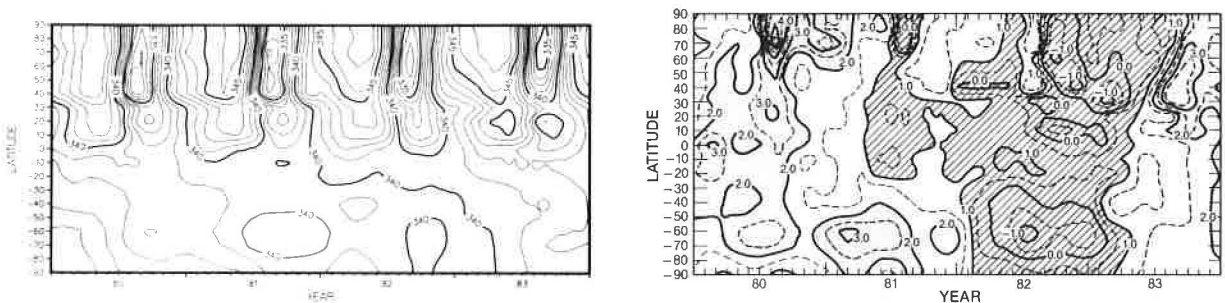

Figure 87.--(a) A contour plot of the distribution of atmospheric CO_2 in space and time, synthesized from the GMCC CO_2 flask network data. (This figure is the same as fig. 8, sec. 3.1, repeated here for convenience.) (b) The distribution of atmospheric CO_2 growth rates obtained by plotting in the forward year the differences between consecutive years in fig. 87a. Growth rates below 1.0 ppm yr^{-1} are shaded with lines; growth rates greater than 2 ppm yr^{-1} are shaded with dots; and values of 1-2 ppm yr^{-1}, typical growth rates for non-ENSO years, are not shaded.

and persistent negative SST anomalies (1-3°C) in the north Atlantic and northwest Pacific. As shown in fig. 88, the CO_2 growth rate anomalies appeared in phase at both northern subtropical and mid-to-high southern latitudes. This feature of the latitude dependence of the CO_2 response to the 1982-1983 ENSO perturbation suggests that the CO_2-ENSO signal is not generated at the Equator and propagated poleward, but rather appears nearly simultaneously in both hemispheres.

The recovery from low CO_2 growth rates was observed first at southern tropical latitudes in early 1983, followed by a recovery in the northern tropics a few months later. Higher-than-normal CO_2 growth rates (2.0-3.0 ppm yr^{-1}) peak in the fall of 1983 in the Northern Hemisphere and peak 2-3 months later in the Southern Hemisphere (fig. 87b). Although the data are incomplete, it appears that by mid-1984 the year-to-year CO_2 growth rates for the flask network are returning to normal values (1.5 ± 0.3 ppm yr^{-1}), signaling the end of the CO_2-ENSO response.

The effect of the 1982-1983 ENSO event on the latitude gradient of CO_2 concentration is clearly demonstrated by a comparison of gradients for the years 1979-1983 (fig. 89). A prominent feature in the 1979-1981 gradients is a 1-ppm equatorial enhancement in atmospheric CO_2 usually ascribed to an equatorial Pacific upwelling source (Keeling, 1983) and/or tropical deforesta-tion. The obvious suppression of the local maximum in 1982 and its weak recovery in 1983 well south of its normal location constitutes the first well-documented case of an ENSO modulation of this feature. This result, together with the isotopic record (Keeling et al., 1984), essentially rules out tropical deforestation as a source for this feature, leaving upwelling in the equatorial Pacific as the most likely explanation. The suppression of this feature during the 1982-1983 event may have been caused by enhanced meridional mixing out of the equatorial zone by more active Hadley cell
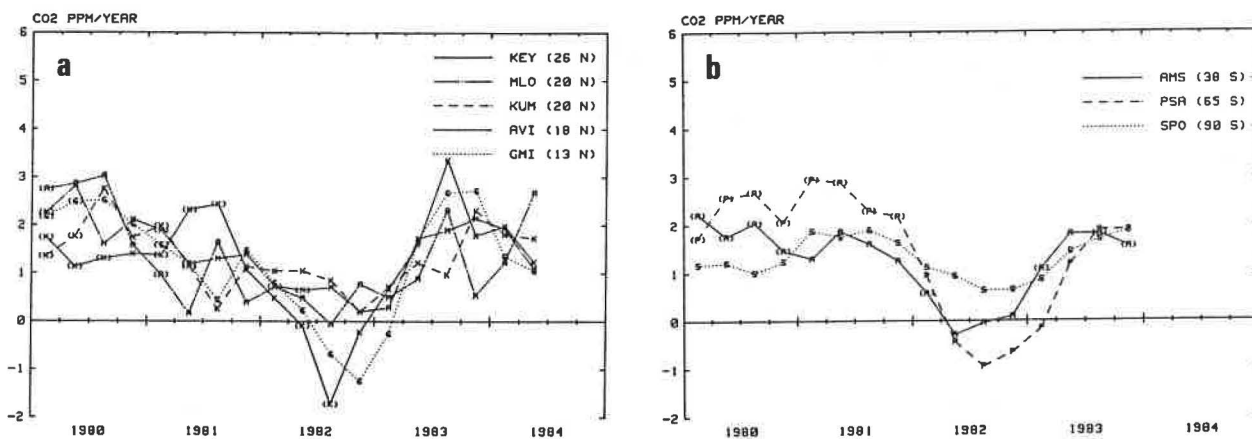

Figure 88.--CO_2 growth rates for flask network stations at (a) northern subtropical latitudes and (b) mid-to-high southern latitudes. The points are differences between quarterly means in successive years, plotted in the forward year. See table 7 for an explanation of network station codes.
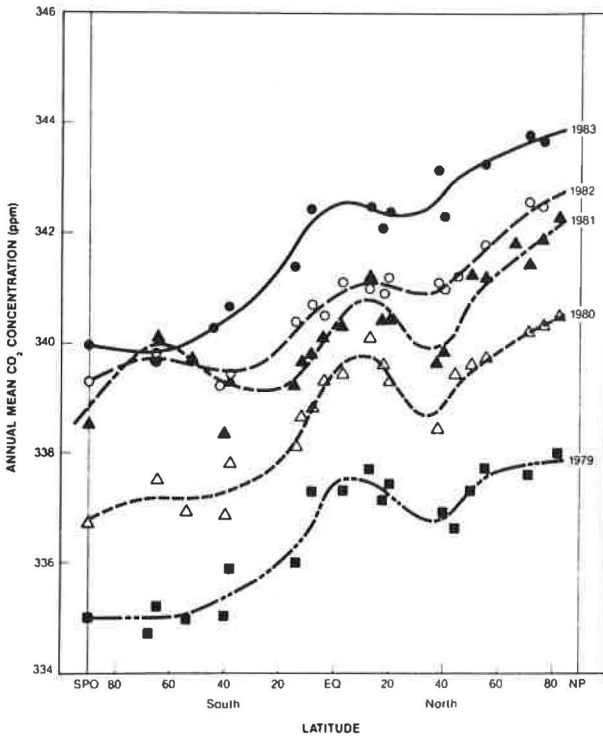
Figure 89.--The latitudinal variation of annual mean atmospheric CO_2 concentration using all available flask data, 1979-1983.

circulation (C. Ramage; U. of Hawaii, Hilo; personal communication, 1984), as well as by a weakening of the normal upwelling that brings cold, CO_2-saturated water to the surface in this region.

4.14 Total SO_2 Observations at MLO
Since the Eruption of El Chichon Volcano in 1982

Sulfur dioxide in the atmosphere interferes with Dobson spectrophotometer total ozone observations, because it absorbs ultraviolet radiation at the Dobson instrument wavelengths. Concern has been expressed about the accuracy of total ozone observations made at MLO following the eruption of El Chichon volcano in late March-early April 1982, since the volcano probably spewed 10 Mt of SO_2 into the stratosphere.

It is possible to measure both total ozone and SO_2 with a Dobson spectrophotometer (Komhyr, 1980) if observations are made simultaneously on AD and AB wavelengths. Following the eruption of El Chichon, specially calibrated Dobson instrument no. 65 was put into operation at MLO on 17 May 1982. Results of 2 years of measurements since that time are shown in fig. 90. It appears that conversion of SO_2 to H_2SO_4 occurred within several weeks after the eruption, because after about 1.5 months, the total SO_2 amount at MLO was slightly less than 2 milli-atm-cm. Since 17 May 1982, the SO_2 has continued to decrease slowly to a 30 May 1984 value of about 1.2 milli-atm-cm. The uncertainty in this value is probably ±1 milli-atm-cm, arising mostly from uncertainties in the absorption coefficients of SO_2 at the Dobson instrument wavelengths. This small amount of total atmospheric column SO_2 translates into total ozone measurement errors with a Dobson spectrophotometer of not more than about 1%.
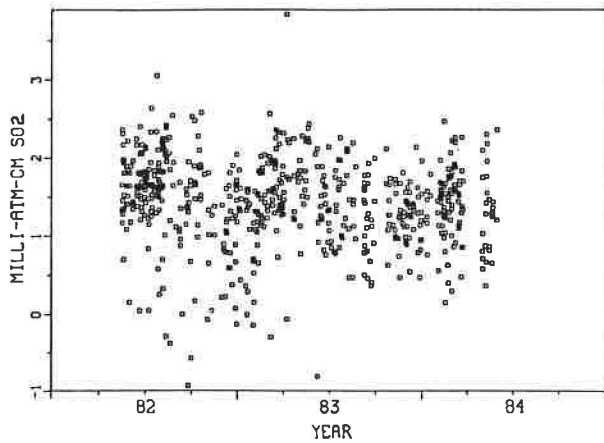
116

Figure 90.--Total atmospheric SO$_2$ measured at MLO with a Dobson spectrophotometer during 17 May 1982-30 May 1984.

4.15 Development of a Balloonborne SO$_2$-sonde

A balloonborne sonde for measuring the vertical distribution of SO$_2$ has been developed. The instrument, coupled to an NWS 1680-MHz radiosonde during flight, is a modification of the ECC ozonesonde developed by Komhyr (1969). When SO$_2$ is measured, ozone is prevented from entering the sensor with a rubber scrubber, while iodine is produced electrolytically within the cathode chamber of the cell. SO$_2$-in-air entering the cell reduces iodine according to

$$SO_2 + H_2O \rightarrow H_2SO_3$$

$$H_2SO_3 + H_2O \rightarrow SO_4^= + 4H^+ + 2e$$

$$I_2 + 2e \rightarrow 2I^- \quad .$$
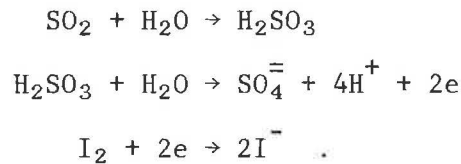
One molecule of SO$_2$, therefore, reduces one molecule of electrolytically-produced iodine to iodide. The fall in cell output current due to consumption of iodine by the sulfur dioxide is related coulometrically to the rate at which SO$_2$ enters the cell, and may be used to measure its concentration in air. SO$_2$ measurement sensitivities for the instrument are 0.7, 2.7, 15, and 34 ppbv at 750, 200, 50, and 10 mb, respectively.

The result of an SO$_2$ sounding made at State College, PA, on 25 February 1983 is shown in fig. 91. The source of the SO$_2$ was a local powerplant stack, located several hundred yards away from the site from which the balloon was launched.
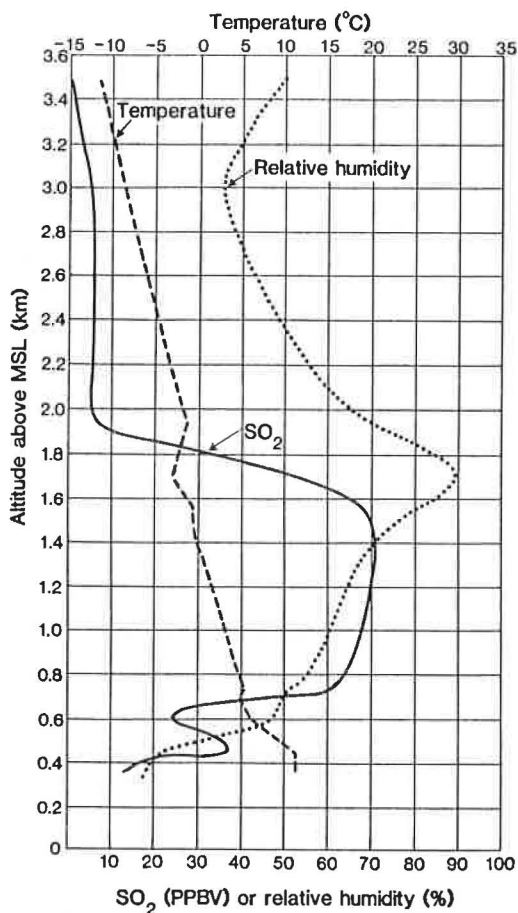
117

Figure 91.--SO$_2$, air temperature, and relative humidity vertical distribution data obtained with an SO$_2$-sonde on 25 February 1983 at State College, PA.

4.16 CO$_2$ Measurements in Surface Ocean Waters

Between 22 October and 5 December 1983, L. Waterman of the GMCC CO$_2$ Group participated in the SAGA Expedition aboard the U.S.S.R. research vessel AKADEMIK KOROLEV. The cruise track is shown in fig. 80b, sec. 4.11. The ship was at sea for 43.5 days with no ports of call. A modified Perkin-Elmer gas chromatograph (Weiss, 1981) was used for continuous monitoring of atmospheric carbon dioxide and methane. The condition of the surface ocean waters with respect to supersaturation or undersaturation of dissolved CO$_2$ and CH$_4$ were also continuously monitored using a Weiss-design equilibrator. The apparatus is fully automatic and is programmed to make three atmospheric and three ocean surface measurements per hour.

Atmospheric air was pumped continuously from intakes located on the bow of the ship and the top of the two forward cargo booms (starboard and port). The air lines were selected on the basis of wind speed, wind direction, and sea state. The airflow discharging into the laboratory was restricted to create a back-pressure in the line, which was needed for making periodic injections into the gas chromatograph (analyzer) column.

CO$_2$ in the surface waters was directly measured by circulating air in a closed loop between the analyzer and the equilibrator. This air was mixed in
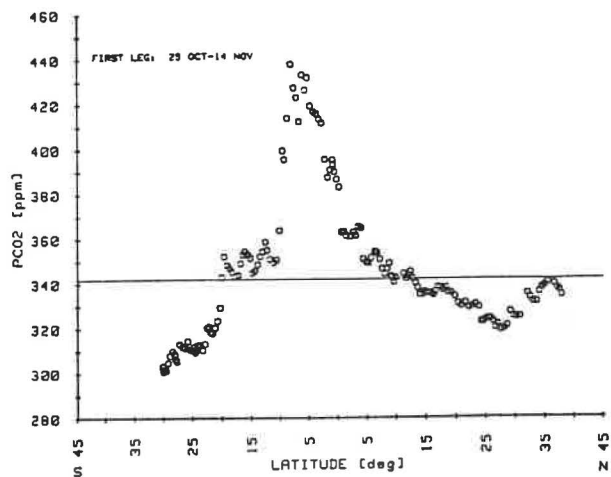
118

Figure 92.--The concentration of CO_2 in surface ocean water as a function of latitude for the SAGA Expedition, leg 1, north to south.
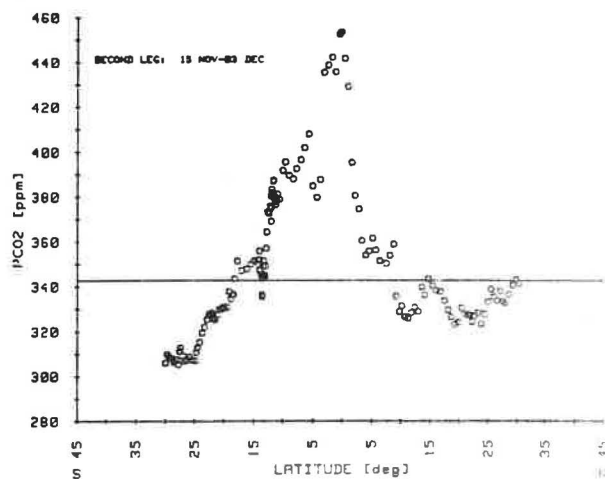
Figure 93.--The concentration of CO_2 in surface ocean water as a function of latitude for the SAGA Expedition, leg 2, south to north.

the equilibrator with a constantly renewed supply of ocean water pumped from a seachest located amidships and several meters below the water line of the vessel. This line was also equipped with a back-pressure regulator that served the same purpose as the one used in the atmospheric air line.

Figures 92 and 93 show the preliminary ocean surface results from the SAGA north to south, run (25 October-14 November) and the SAGA south to north, run (15 November-3 December) respectively. The mean atmospheric CO_2 concentration for the time interval is represented by a straight line in each case. This line is intended to be only a reference level for illustrating the CO_2 undersaturation and supersaturation in the ocean surface waters. The entire track, 25 October-3 December, represents 921 hours of observations that are depicted as 3-h means. The ocean water measurements have been corrected to remove the effects of warming the water by the seachest pump and of the residence time in the transmission line and equilibrator chamber.

The two SAGA equatorial crossings represent the eighth and ninth sections of a survey of the Pacific Ocean equatorial supersaturation feature. The survey began as part of the SIO Downwind Expedition during the International Geophysical Year (Keeling et al., 1965). A summary of all nine sections is given in table 32.

A detailed report for the five crossings made during the Eastropac and Nova expeditions has not been published, although the data were considered in the determination of the general features of the distribution of CO_2 in the surface waters of the world's oceans (Keeling, 1968).

119

Table 32.--Equatorial crossings of research vessels measuring pCO$_2$

Expedition	Date	Location & direction of crossing
Downwind	Oct-Dec 1957	130°W, N-S
Monsoon	Feb-Apr 1961	150°W, S-N
Eastropac	Jan-Mar 1967	~120°W, N-S; ~125°W, S-N
Nova	Apr-Sep 1967	~175°W, N-S; ~160°W, S-N; ~178°W, N-S
SAGA	Oct-Dec 1983	155°W, N-S; 133°W, S-N

The overall patterns of supersaturation and undersaturation in the SAGA record (figures 94 and 95) resemble those found on the Downwind and Monsoon expeditions (Keeling et al., 1965). SAGA I (north to south) is closest to the Monsoon track in the region of the Equator, although the crossings occur 4 months apart in time of year. The SAGA II (south to north) track closely parallels that of Downwind from 30°N to 30°S, and both expeditions occur in October-December. As was the case on all previous expeditions, the major features on the SAGA Expedition appear to be latitude dependent.

The tropical maximum on SAGA I occurs at about 6°S and on SAGA II at the Equator. The SAGA I and Monsoon tracks were approximately the same near the Equator, but the crossing occurred in different seasons, which might explain the southward shift of the SAGA I maximum. However, since the SAGA II track was close to the Downwind track geographically, and the Equator crossings were
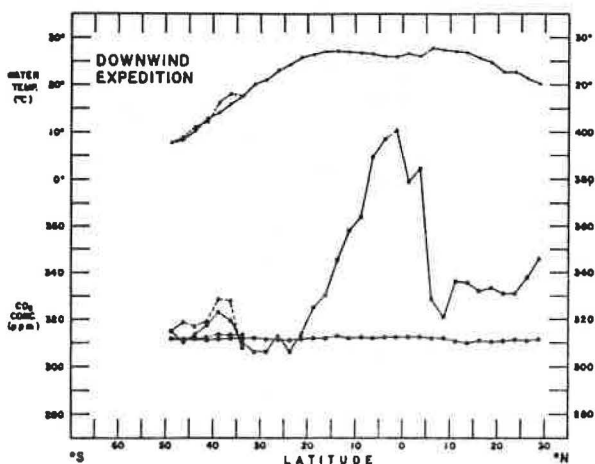
Figure 94.--Concentration of CO$_2$ near the ocean surface in the atmosphere (dots), and in sea water (squares), as a function of latitude for the Downwind Expedition, 21 October-23 December 1957. The dashed line pertains to the northward part of the voyage. (From Keeling et al., 1965.)
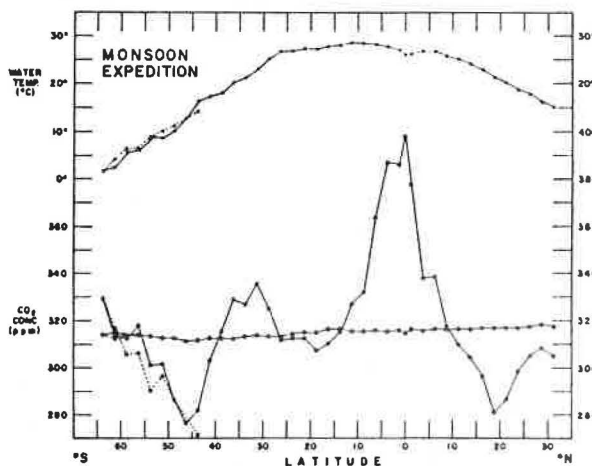
Figure 95.--Concentration of CO$_2$ near the ocean surface in the atmosphere (dots), and in sea water (squares), as a function of latitude for the Monsoon Expedition, 31 January-17 April 1961. The dashed line pertains to the southward part of the voyage. (From Keeling et al., 1965.)

made in the same month, one might expect to see more similarity than is actually present in these two data sets even if the tropical maximum had some longitudinal or seasonal dependency.

Keeling et al. (1965) attributed the tropical supersaturation to the presence of the subsurface Cromwell current. Similar areas of surface water supersaturation of CO_2, albeit less pronounced than in the Pacific, have been observed in both the equatorial Atlantic and Indian Oceans over areas where subsurface currents are also known to be present (Keeling and Waterman, 1968). In the Indian Ocean, a band of high CO_2 extended over two-thirds of the equatorial zone during the northeast monsoon at the same time that a steady undercurrent was observed at depths of 50-200 m. The supersaturation was not present during the southwest monsoon when the current was found to be weak and variable or absent. The variations in the location of the maximum observed on these three expeditions suggest the high CO_2 feature in the equatorial Pacific may be related to meandering of the subsurface current.

Outside the 10°N-10°S equatorial zone, the two SAGA data sets show much the same patterns of variability, and most of the areas are undersaturated. In the Northern Hemisphere, the same pattern seen at the beginning of SAGA I, a steady decline from equilibrium to about 20 ppm undersaturation followed by recovery to atmospheric level between 35° and 20°N, is repeated at the end of SAGA II between 15° and 30°N about a month later. This 5° displacement suggests some southward movement of a persistent undersaturated area. In the 10°-30°N band, the SAGA plots bear more resemblence to Monsoon than to Downwind even though they are separated by 4 months. In the Southern Hemisphere, the closest retracing of the SAGA I record by the SAGA II record occurs between 30°S and Tahiti (18°S) immediately following the ship's turning. All four plots show some degree of undersaturation in the 10°-30°S band.

5. COOPERATIVE PROGRAMS

5.1 Air Mass Characteristics at BRW During AGASP

W. E. Raatz
NRC-NOAA Research Associate
Geophysical Monitoring for Climatic Change, NOAA/ERL/ARL, Boulder, CO   80303

During AGASP (March 1983), a major Arctic haze episode was recorded in the Alaskan Arctic. This paper describes the occurrence of different air mass types at BRW during the period of 9-18 March, and characterizes air mass properties in terms of meteorological parameters, CN concentration, aerosol scattering extinction coefficient (σ_{sp}), ozone, and CO_2 concentrations as measured at the baseline station.

The overall synoptic condition over the Alaskan Arctic was determined by the gradual movement (both at the surface and at 500-mb) of the Arctic anticyclone out of the Laptev Sea, across the East Siberian Sea and into the Beaufort Sea area (Raatz, 1984). The associated change in air mass types present over BRW is reflected in the time-height cross sections of potential temperature and mixing ratio of water vapor (fig. 96). During the period 9-10 March, the air mass is characterized by moist air and by relatively warm temperatures that gradually decrease. This may indicate the diminishing influence of marine Pacific air at low levels and the diminishing influence of an upper-level cyclone. During the period 11-13 March, a very cold and very dry air mass is present, with temperatures gradually increasing following this
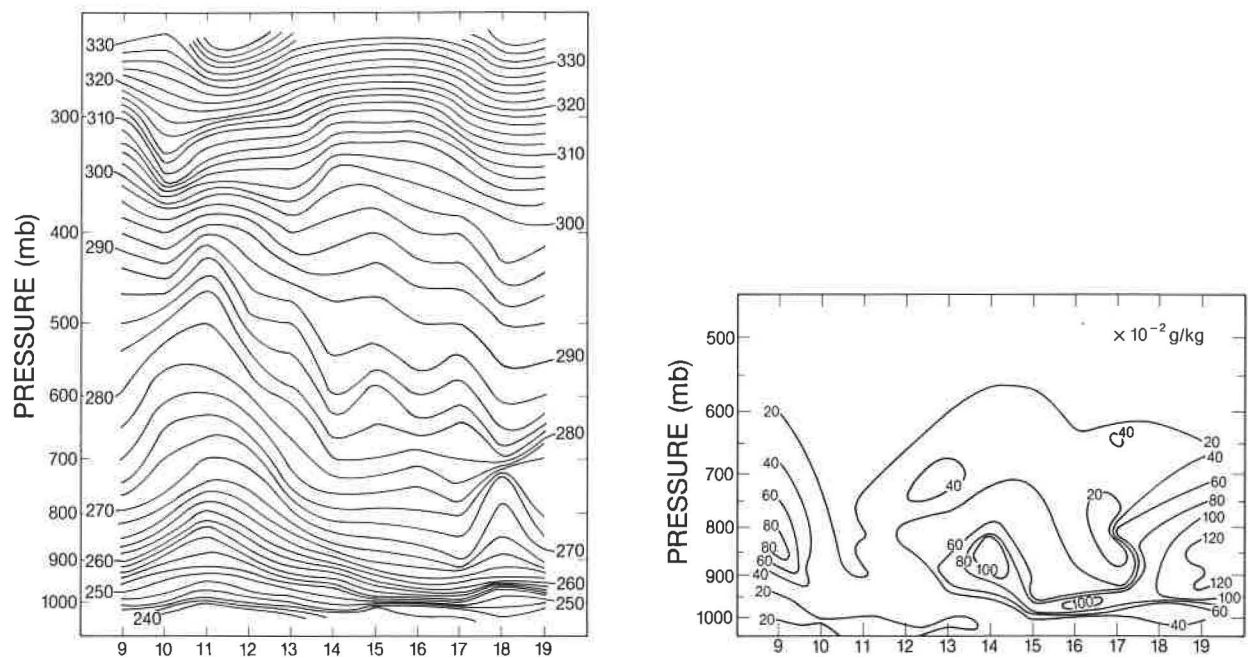

Figure 96.--Time-height cross sections of (left) potential temperature (K) and (right) water vapor mixing ratio ($\times 10^{-2}$ g kg^{-1}), at BRW during March 1983 at 0000 GMT.

period. The cold and dry air is advected along the Arctic anticyclone (at low and upper levels) originating from the inner Arctic Basin and Siberia. Beginning 12 March, the advection occurs along a transport zone connecting western Eurasia with the Alaskan Arctic (Raatz, 1984; Harris, 1984). During the period 14-17 March, temperatures continue to increase and the near-surface layer contains moister air, whereas the upper layers remain dry. This warm and dry air aloft is the result of anticyclonic subsidence; the moisture in the low levels may be of local origin. During the period 17-19 March, temperatures below 700 mb decrease and moisture content increases dramatically. The near-surface flow probably carries the influence of marine Pacific air, whereas the upper levels still remain under anticyclonic influence.

Surface-based CN and light-extinction data are shown in fig. 97 and have been discussed in detail by Bodhaine et al. (1984). The light-scattering data indicate background values of 2.3×10^{-5} m^{-1} during 9-11 and 17-18 March, with a maximum of 4.1×10^{-5} m^{-1} on 15-16 March. The variation in extinction is not caused by fluctuations in relative humidity, and the variations seen do not present a diurnal cycle due to temperature variations. Surface CO_2 concentrations also seem to fall into three regimes similar to the light-extinction data (fig. 98). Background concentrations of about 348 ppm are recorded during 9-11 March and 16-18 March. Highest concentrations are measured within the Arctic haze episode during 12-15 March. In contrast, surface-ozone concentrations (fig. 99) show a variation different from those described for σ_{sp} and CO_2. During the period 9-10 March, concentrations vary from 5 to 25 nb, followed by a period of low concentrations from 0 to 10 nb on 11-12 March. On 13 March, ozone concentrations significantly increase and then steadily increase through the end of 18 March.

In summary, the combination of time-height cross sections of potential temparture and mixing ratio is a powerful tool in identifying different types of air masses in terms of meteorological characteristics (Raatz, 1982). The
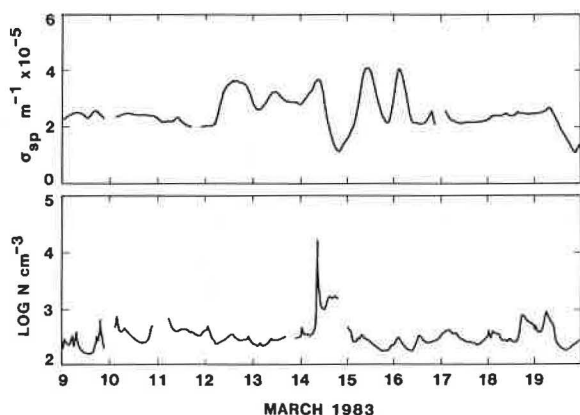

Figure 97.--(Top) Surface light extinction (σ_{sp}) ($\times 10^{-5}$ m^{-1}) and (bottom) surface CN concentration (cm^{-3}), at BRW during March 1983 (Bodhaine et al., 1984).

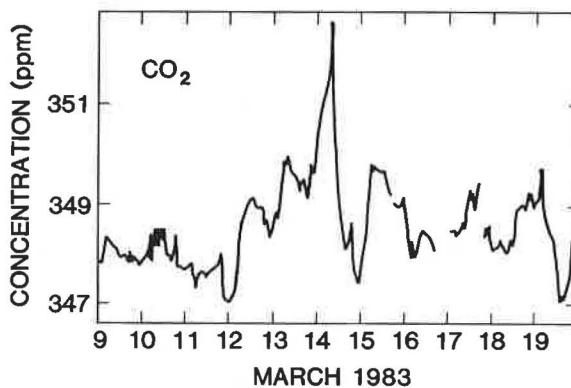

Figure 98.--Surface CO_2 concentration (ppm) at BRW during March 1983 (R. H. Gammon; NOAA/GMCC; personal communication, May 1984).
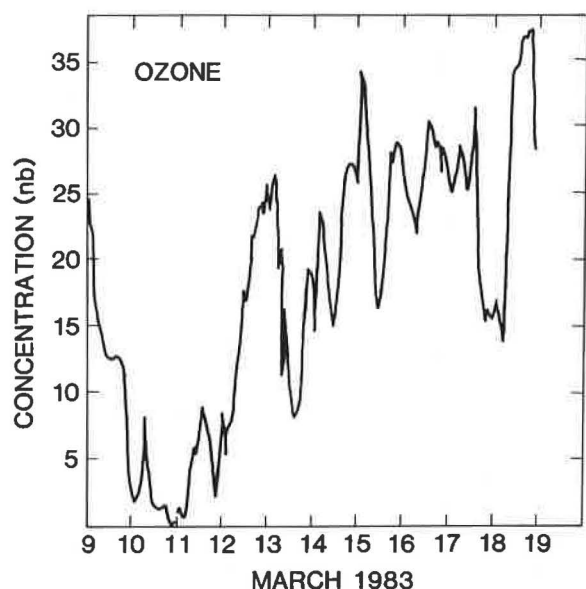
123

Figure 99.--Surface ozone concentration (nb) at BRW during March 1983 (S. J. Oltmans; NOAA/GMCC; personal communication, May 1984).

presence of Arctic haze is associated with an Arctic air mass characterized by enhanced σ_{sp} values and increased CO_2 concentrations. Ozone concentrations during Arctic haze are about normal. Prior to the Arctic haze episode, ozone concentrations are as low as 0 nb during the presence of a very cold and dry Arctic air mass. Such low ozone concentrations are unique to BRW (Oltmans, 1981), and seem to occur frequently during February-April, a time when BRW experiences its coldest temperatures.

5.2 Solar Radiation Measurements at BRW

G. Wendler
Geophysical Institute
University of Alaska, Fairbanks, AK 99701

The radiation measurements sponsored during 1982 by the University of Alaska were continued at BRW during 1983. Instrumentation for the following measurements is included in this program: (1) global radiation, (2) reflected short-wave radiation, (3) all-wave incoming radiation, (4) all-wave outgoing radiation, (5) sky radiation, (6) global radiation on the south slope inclined to latitude, and (7) global radiation on the south wall. The data are recorded on a Datel data logger. Some difficulties were experienced with the data logger as well as with the polyethylene covered domes of the all-wave radiation sensor.

The amount of global radiation received at BRW is relatively high, with a mean annual flux of 103 W m^{-2}. It is about the same value as that found for Kodiak (108 W m^{-2}), which is located 14° farther south. At first glance this is astonishing, because both stations have nearly identical amounts of cloudiness. However, the clouds are much thicker at Kodiak, where the annual precipitation is more than 10 times the amount found at BRW. This can be explained by examining the values of the clearness index K_T, which is the global radiation divided by the extraterrestrial radiation. The latter must

124

be corrected for Sun-Earth distance and reduced to the horizontal surface. This index yields much higher values for BRW than for Kodiak for overcast conditions. For clear days such a comparison was not possible, because not enough sunny days were observed. Besides the differences in cloud characteristics, the multiple reflection, which is of greater importance in BRW than in Kodiak, tends to increase the global radiation. This is discussed in Wendler (1983).

5.3 Elemental Carbon Measurements at Whiteface Mountain

R. Castillo
Atmospheric Sciences Research Center
State University of New York at Albany, Albany, NY   12222

5.3.1 Introduction

As part of a solar-chemical experiment at the ASRC field station, Whiteface Mountain, Wilmington, NY, a preliminary experiment was performed that attempted to measure the ambient total mass of organic and elemental carbon per unit volume in three different conditions: (1) clear air or haze, (2) the interstitial aerosol in a cloud (a mixture of cloud droplets and unactivated aerosol), and (3) the soluble and/or insoluble residue from cloud water.

Ogren (1982) found that the median concentration of EC in the ambient aerosol was 4.9 $\mu g\ m^{-3}$ and in rainwater was 60 $mg\ L^{-1}$. Generally accepted values of EC are 0.1-1 $\mu g\ m^{-3}$ and 10 $\mu g\ m^{-3}$ for rural sites and urban sites respectively. P. Chylek (ASRC, Albany, NY; personal communication, 1984) has obtained values of 6-23 $\mu g\ L^{-1}$ from snow samples. There is a decrease of EC with elevation greater than 1.1-3 km above sea level, by a factor of 3 to 4.

5.3.2 Procedures

Three different techniques were used to obtain samples for EC analysis. First, the clear air or haze aerosol was directly sampled in 1982 using a 20 $L\ min^{-1}$ flow rate through two Whatman GF/A (glass microfiber) filters in series. Second, in 1983 the ambient aerosol was drawn through a Pallflex Quartz filter mounted on a Hi-Vol sampler (1.6 $m^3\ min^{-1}$). Third, the interstitial aerosol was obtained by impacting the cloud water into a glass fiber mesh (>90% collection efficiency for $d \geq 10\ \mu m$) prior to the air stream flowing through a Pallflex Quartz filter. The latter system used a Hi-Vol sampler. The cloud water samples were prefiltered through a 0.4-μm Nuclepore filter to remove large insoluble material. The resulting liquid was either filtered (insoluble material), evaporated (insoluble and soluble), or freeze dried (insoluble and soluble), and all samples were then analyzed using a thermal-optical carbon technique. The results can be found in Huntzicker et al. (1982).

5.3.3 Results and Discussion

Under clear-air (visual range: 50 mi) to light-haze conditions (visual range: 20-30 mi), the total carbon varies from ~ 2 to ~ 37 $\mu g\ m^{-3}$ (table 33).

Table 33.--Clear air (C) and haze (H) carbon for summer 1982,
Whiteface Mountain, NY

Date	Visual range (mi)	RH (%)	Pollak CN count (cm^{-3})	Weather	Carbon (μg m^{-3})			Vol. sampled (m^3)
					Organic	Elemental	Total	
08 Jul	20-30 (H)	83	2500	After cloud, pH = 4.0; SW trajectory	23.1	14.1	37.5	1.2
12 Jul	20-25 (H)	81	3200	At end of warm frontal passage; pH = 3.7; SW trajectory	24.5	10.1	34.6	1.2
14 Jul	50 (C)	50	2100	Warm, dry air; calm all day	1.9	BDL*	1.9	6.5
20 Jul	50 (C)	64	---	Overcast; variable-light winds	2.2	BDL*	2.2	4.8

*Below detection limit.

The EC varies from below detection limits to 10-14 μg m^{-3}. These results are consistent with reported values.

The EC for 1982 and 1983 found in the interstitial aerosol (external mixture of cloud droplets and unactivated aerosol) was indicative of a source dependency (table 34). For air masses originating in the southwest and northwest, the air pollution loading is approximately the same (Galvin et al. 1983). Although the data set is not large, one is tempted to differentiate between the northwest and southwest, and the west EC loadings which differ by almost an order of magnitude. The haze aerosol EC from the southwest

Table 34.--Summer interstitial aerosol carbon, Whiteface Mountain, NY

Date	Trajectory	Cld. H$_2$O pH	EC (μg m^{-3})	Vol. sampled (m^3)
02-03 Aug 1982	NW	4.1	0.75	18.4
04-05 Aug 1982	NW	3.5	0.64	8.1
09-10 Aug 1982	SW	3.2	0.13	13.2
01-02 Jul 1983	SW	---	0.18	2×10^3
05 Jul 1983	SW	---	0.28	4.3×10^2
19 Jul 1982	W	3.7	BDL*	4.8
08-09 Jul 1983	W	---	0.049	8.3×10^2
04 Aug 1983	---	---	1.6	4.6×10^2
05 Aug 1983	---	---	1.3	1.7×10^3

*Below detection limit.

(table 33) is 1 order of magnitude larger than the northwest interstitial EC and 2 orders of magnitude larger than the corresponding southwest interstitial EC.

Table 35 presents the carbon results for cloud water. The soluble and insoluble EC ranges from 0.06 to 0.66 mg L^{-1} as compared with just the insoluble component, which ranges from 0.12 to 0.35 mg L^{-1}. These values are 2 orders of magnitude lower than these reported by Ogren (1982) for an urban area. When the values are converted to an equivalent clear-air value, assuming a liquid water content of 0.7 g m^{-3} for Whiteface Mountain stratiform, the values range from 0.1 to 0.46 μg m^{-3} EC.

Table 35.--Cloud water residue (soluble and/or insoluble) carbon for summers of 1982 and 1983, Whiteface Mountain, NY

Date	Sampling method	Carbon (μg) Organic	Elemental	Total	Vol. samp. (mL)	EC (mg L^{-1})
Summer 1982 Composite	Filtered	131	35	168	100	0.35
Summer 1983 Composite	Filtered	92	12	104	100	0.12
Summer 1982 Composite	Freeze-dried	405	33	436	50	0.66
04 Aug 1982 Composite	Filtered	43	14	59	100	0.14
28 Jul 1982 Composite	Evaporated	---	51	---	~768	0.06

5.3.4 Conclusion

These few comparisons suggest the following points. (1) It is possible for the interstitial and cloud water EC to be of the same magnitude and to exceed clear-air values. (2) There are instances of haze at this rural site with high EC (10-14 μg m^{-3}) similar to urban concentrations. (3) There is some indication of a source dependency of the amount of interstitial aerosol EC detected at this rural site.

Acknowledgments

5.4. Aircraft and Surface Observations of Arctic Haze Near BRW, April 1983

L. F. Radke, J. H. Lyons, D. A. Hegg, P. V. Hobbs, and I. H. Bailey*
Atmospheric Sciences Department
University of Washington, Seattle, WA 98195

5.4.1 Introduction

The polar regions are known to be sinks for many atmospheric trace constitutents. Recent studies (Rahn and Hiedam, 1981; Barrie et al., 1981; Rosen et al., 1981) have clearly established that episodes of anthropogenic pollution, which can cause hazes, are common at surface locations around the Arctic rim during winter. The hazes contain secondary aerosol (mainly acid sulfate), primary aerosol of industrial origins, and various soil and volcanic material. The goals of the more recent studies that are summarized here were to measure the vertical distributions of aerosol and trace gases in the Arctic atmosphere and to study their nature and origin.

5.4.2 Measurements

The University of Washington's B-23 research aircraft, which is instrumented for measurements of aerosol, trace gases, and cloud properties, was used to make 18 vertical soundings of the atmosphere to an elevation of ≤ 6 km within 400 km of BRW during 1-21 April 1983. The instrument package, described by Hobbs et al. (1976), Hegg and Hobbs (1980), Radke (1983), Radke and Whitby (1982), and Radke et al. (1984b), provides information on particle sizes of 0.01-4500 µm, particle characterization, and trace gas information. Three 47-mm filter packs, one 37-mm Teflon filter, and two seven-stage cascade impactors were exposed on each flight.

Several optically dense haze layers were penetrated on each sounding. As many as 10 distinct haze layers were found on a single sounding. The haze layers were often abruptly discontinuous and frequently bounded by extremely clean air, with visibility near the Rayleigh limit. Some layers were thin (a few hundred meters) and usually did not extend more than 100 km in the horizontal.

The particle spectra measured in haze and nonhaze conditions were quite similar (Radke et al., 1984a). Volume plots show peaks at particle diameters of ~0.25, 0.6, 4.5 µm and at an indeterminate size >10 µm. The greatest contrast in the size spectra between haze and nonhaze conditions was in the accumulation mode (0.1-2.0 µm), where substantially higher concentrations of particles were found in haze. Light-scattering properties are clearly linked to this mode. The coarse particle mode was most dominant in samples made near the surface and in light haze. Unexpectedly large concentrations of giant particles (>2 µm) were found in all of the samples (Radke et al., 1984a; Bailey et al., 1984).

---

*On leave from Western Australia Institute of Technology, Kent Street, Bentley, Western Australia 6102.

The nucleation mode (<0.1 µm) was difficult to size with confidence. The most successful technique for determining concentrations in the nucleation mode was a combination of a diffusion battery and a CN counter. Almost none of the nonhaze samples had measurable nucleation modes, whereas ~30% of the haze cases did have nucleation modes. The nucleation mode is most likely sustained by conversion of SO_2 to $SO_4^=$, since 80% of the nucleation modes that were detected during haze conditions were associated with SO_2 concentrations >1 ppb. None of the light haze or nonhaze cases were associated with such large SO_2 concentrations. Particulate sulfate data support this conclusion.

Filters and substrates were analyzed by ion chromatography for soluble sulfate, chloride, and nitrate using techniques similar to those described by Stevens et al. (1978). The results of this analysis for the cascade impactors is summarized in fig. 100. Most of the sulfate (81%) was in particles having diameters <1.0 µm. Chloride was uniformly distributed in size, except that little was found in particles with diameters <0.25 µm. Nitrate concentrations were quite low at all particle sizes. The fraction of total sulfate in the submicron range was largest (up to 100%) in samples from haze layers and smallest (up to 68%) in samples with little or no haze. Although the absence of small chloride particles is characteristic of the relatively unpolluted airmasses examined by Harrison and Pio (1983), the observed sulfate size distributions are similar to the polluted cases examined by them. Because the small chloride particles in the Harrison-Pio samples are most likely due to combustion of high-chloride coal, which is by no means the coal usually employed by industry, we judge the ionic mass distributions of our samples to be in general agreement with the polluted cases of Harrison and Pio.

The concentrations of the three ions and their relative abundances are summarized in table 36. Impactors were exposed predominantly in regions of haze. Filter packs (~1 m^3 sample) were distributed more uniformly with time and altitude and are therefore more representative of the average vertical column over which the aircraft flew. The increase in sulfate from nonhaze to haze conditions (0.5-1.8 µm m^{-3}) was virtually the same as the increase in the
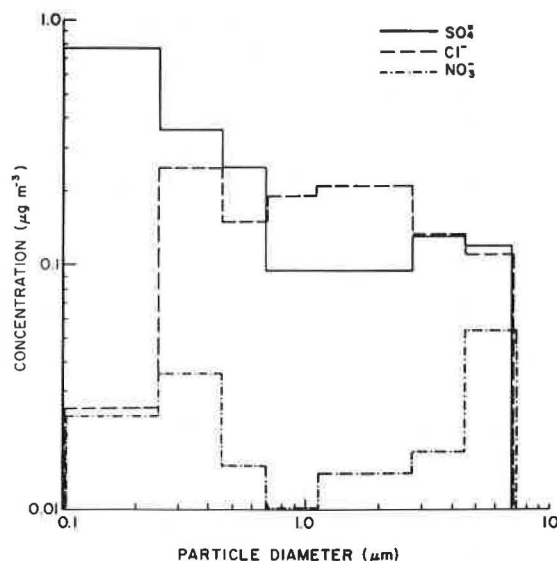

Figure 100.--Size-segregated average concentrations of the soluble fractions of sulfate, chloride, and nitrate in aerosol collected primarily in the Arctic hazes.

129

Table 36.--Average ion concentrations ($\mu g\ m^{-3}$) measured
in the Arctic, April 1983

Measurement technique	$SO_4^=$	Cl^-	NO_3^-	Total
Cascade impactor*	1.8	1.0	0.2	3.0
Teflon filters (all)†				
All	1.1	0.07	0.05	1.2
Haze ($\sigma_{sp} > 2 \times 10^{-1}$)	1.8	0.14	0.06	2.0
Little or no haze ($\sigma_{sp} < 2 \times 10^{-1}$)	0.47	0.02	0.02	0.5
Ground Teflon filters§	2.6	0.23	0.03	2.9

*Exposed from aircraft mainly in hazes.
†Exposed from aircraft in all haze conditions.
§Exposed at BRW nearly daily.

volume of the aerosol in the accumulation mode (Radke et al., 1984a). Similar
results were found by Barrie et al. (1981) for surface measurements in the
Canadian Arctic during winter.

The higher-than-expected fraction of chloride on the impactors (compared
with the filter packs and surface measurements) could indicate possible
deposition of acid sulfate causing chlorine loss on the surface and on pack
Teflon filters (Hitchcock et al., 1980). The particles on these filters were
subject to much greater ventilation and hence greater potential losses than
those on cascade impactor substrates.

The submicron and supermicron chloride fractions are highly correlated
with the supermicron sulfate ($r \cong 0.8$ and $r \cong 0.9$ respectively) whereas the
submicron chloride and sulfate fractions are essentially uncorrelated
($r \cong 0.08$), suggesting that supermicron sulfate and all of the chloride have a
common, probably oceanic, origin. A different origin for the submicron
sulfate is suggested by the relatively low correlation between either super-
micron chloride or sulfate, and submicron sulfate ($r \cong 0.3$ and 0.5 respec-
tively). Separate origins of submicron and supermicron sulfate are also
suggested in the more numerous filter-pack samples. Samples from the little
or nonhaze category show total sulfate and chloride modestly correlated
($r \cong 0.6$); in the haze category they were uncorrelated ($r \cong -0.07$). Total
sulfate, submicron sulfate, and total soluble ion concentrations all correlate
modestly with σ_{sp} ($r \cong 0.6$) whereas submicron chloride and nitrate are un-
correlated with σ_{sp} ($r \cong -0.2$ and $\cong 0.2$ respectively).

Sulfate measured at the ground is found predominantly in submicron
particles, while chloride spanned the submicron to supermicron particle size
range. The particle size spectra for these ions are shown in fig. 101 where
they can be compared with spectra measured at 0.3-1.2 km MSL 2 days later but
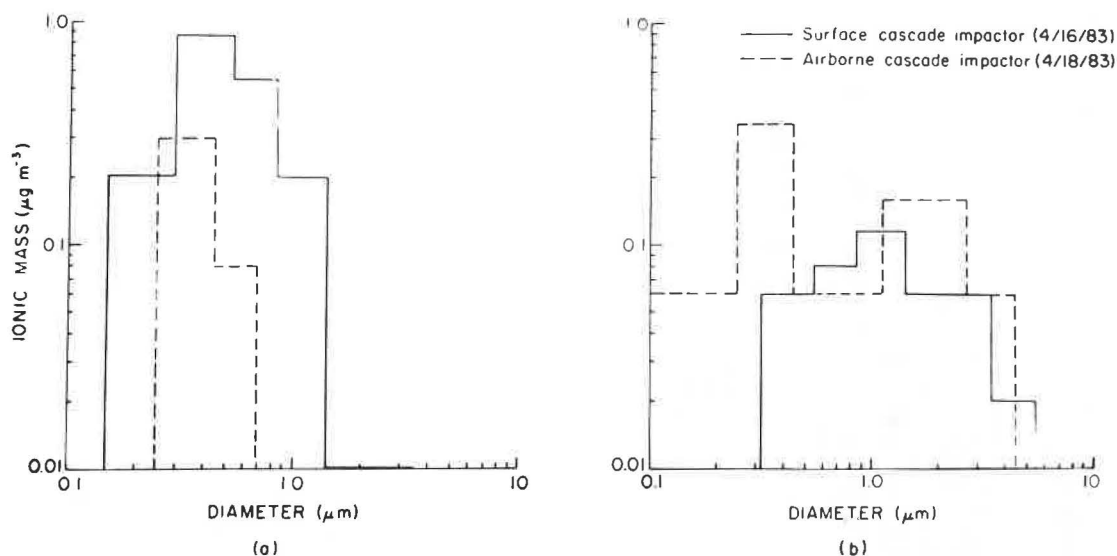under similar conditions. Sulfate was concentrated on submicron particles

Figure 101.--Comparison of particle spectra for (a) sulfate and
(b) chloride ions measured at the surface and at 0.3-1.2 km MSL.

both at the surface and aloft. Chloride was present in both submicron and
supermicron particles at the surface and at higher altitudes, although at
higher altitudes more of the chloride was found in submicron particles.

Concentrations of sulfate measured at the ground at BRW were, on average,
~2 times greater than those measured 1-5 km above the BRW area. However, this
difference was largely because the samples taken aloft were from both hazy and
clear air, while the surface samples were taken entirely in haze, albeit at
levels less intense than those aloft (visibility in one or more haze layers
aloft was generally worse than at the surface [Radke et al., 1984a]). This is
clear from the fact that the impactor samples and filter packs taken primarily
in haze differ from the ground samples by much less than a factor of 2
(table 36). Nevertheless, the generally higher sulfate levels and lower
light-scattering coefficients on the ground compared with the airborne measure-
ments strongly suggest that, in general, the sulfate concentrations measured
aloft are not representative of the haze as defined by light scattering, but
are rather systematically low. Support for this is provided by the one
sulfate measurement obtained entirely in an intense haze layer. The sulfate
concentration for this measurement was 13 μg m^{-3}, substantially higher than
either the airborne measurements in general, or the ground samples.

Further comparisons of the airborne and ground sulfate measurements
suggest that even though the thermal stability of the surface layer will tend
to isolate it from haze layers aloft, synoptic-scale variations can often
provide a sufficient link so that surface measurements of sulfate are indica-
tive of a change of air mass both at the surface and aloft, though not quanti-
tatively representative of the air found aloft. For example, although a
negative correlation coefficient of -0.65 was calculated for the 7 days when
both aircraft and surface observations of sulfate were available, the anti-
correlation is solely attributable to the data for 11 April when very high
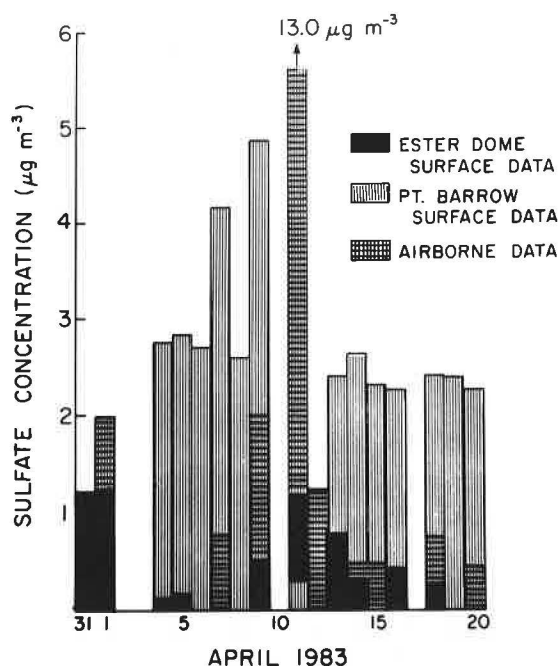sulfate concentrations were measured by aircraft at 4 km, while surface values

Figure 102.--Comparison of sulfate concentrations measured aloft near BRW and at Ester Dome near Fairbanks.

were low. Exclusion of this point from the correlation produces a positive correlation of 0.84. Concentrations of sulfate measured at the surface at Ester Dome, AK (~750 km south of BRW and on the other side of the Brooks Mountain Range) were less well correlated (r ≅ 0.55) with surface measurements at BRW (fig. 102).

5.4.3 Summary

Airborne studies of haze layers in the Arctic have shown that their light-scattering properties are due primarily to sulfate particles in the accumulation mode (0.1-2 μm). Evidence was also obtained for the formation of aerosol particles in the nucleation mode (<0.1 μm) by gas-to-particle conversion of SO_2.

In optically clear regions, chloride was a significant fraction of the total aerosol and was correlated with sulfate at all altitudes, possibly indicating oceanic origins. The nucleation mode was not detected in these regions. Ground-based impaction samples contained sulfate and chloride in submicron- and supermicron-sized particles in similar proportions to those measured aloft.

Acknowledgments

5.5 The ASRC Aerosol Impactor-Concentrator

A. W. Hogan
Atmospheric Sciences Research Center
State University of New York, Albany, NY 12222

5.5.1 Introduction

Aerosol concentrations in the polar regions are generally quite small, and advective events that transport midlatitude material to the polar regions are brief. Fenn and Weickmann (1959) found that the cascade impactor of May (1945) gave sufficient concentration of particulate material to facilitate analyses of Greenland aerosol with collection times of less than 30 minutes. For this study the Fenn-Weickmann-May techniques have been modified to permit aircraft sampling on substrates compatible with SEM analyses. The modified impactor was successfully used by Shapiro et al. (1984) during AGASP sampling.

The May (1945) cascade impactor and its commercial descendants cause particles in four size ranges to be serially impacted on four microscope slides or glass disks. Experiments with May's device at SPO showed that a detectable impaction line could be collected on the submicron particle stage (May IV) in about 1 hour, but it was extremely difficult to detect particles on the collection disks for supermicron particles (May I, II, III). The 25-mm glass disks used as impaction substrates were difficult to clean and transport, and were not compatible with SEM analysis.

The impaction jet of May's stage IV was fitted within a 10-cm diameter Delrin housing by W. Winters of ASRC, as shown in fig. 103. The features of

Figure 103.--Components of the Delrin housing for stage IV of the May (1945) impactor. This 10-cm-diameter housing seals the impactor to facilitate airborne use.

this apparatus are the following: (1) A large inlet diameter allows still air sampling. (2) An interchangeable 0.953-cm tube inlet that is isokinetic in typical polar surface winds of 4-5 m s^{-1} facilitates installation for aircraft sampling. (3) A conventional 25 × 75 × 1 mm microscope slide is used as a collecting substrate, but does not rely on slide dimensions to achieve the proper impaction distance. This allows gold foil or membrane substrates to be used, while maintaining the convenience of handling and storage of microscope slides. (4) The housing permits sealing of the entire impaction apparatus within a 10-cm Delrin cylinder and cover disk, thus facilitating both outdoor slide changes and aircraft use. (5) The single impaction stage causes the supermicron particles, which are few in number, to be collected along the same line as the submicron particles. This greatly enhances the probability of finding the larger particles during analysis. (6) Additional impactor-concentrator devices or filters can be connected in series with this impactor to allow selective removal of ice crystals or fog drops at the inlet, or to collect and concentrate the submicron particles passed by this impactor.

5.5.2 Results of Experiments

The ASRC impactor has been used with success in both polar regions. The results of a cooperative GMCC-ASRC aerosol experiment at SPO are shown in fig. 104. The upper panel shows particle area determined from nucleus counter
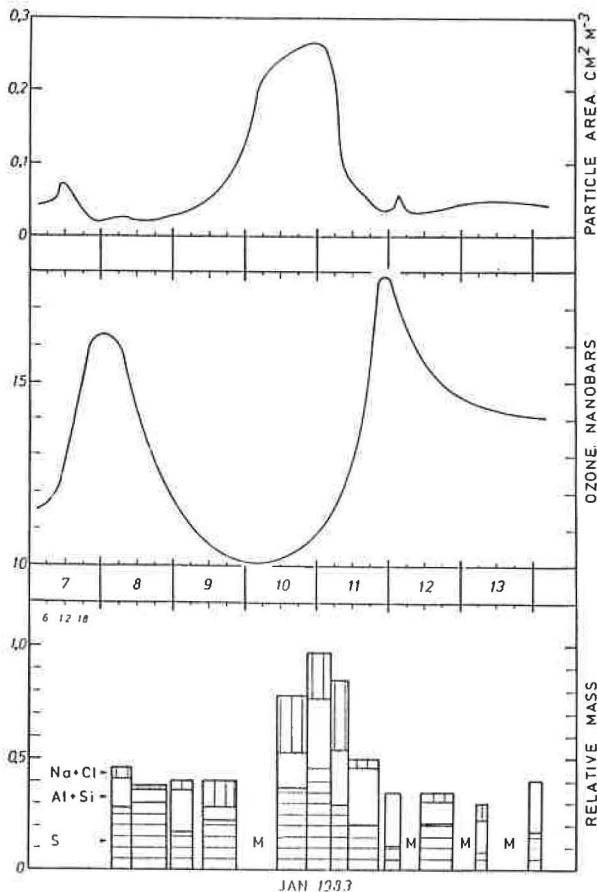

Figure 104.--Results of cooperative ASRC-GMCC aerosol sampling at SPO. (Top) Particle area determined by nucleus counter and diffusion battery data; (middle) Dasibi ozone data; and (bottom) impacted sulfur, crustal, and marine aerosol components normalized to scattering (nephelometer) mass.

134

(Pollak) and diffusion battery data; the center panel, GMCC ozone data; and the lower panel, elemental fractions of impacted aerosol particles relative to the total scattering mass recorded by the nephelometer. Comparison of the aerosol and ozone concentrations given in fig. 104 with meteorological data shows the marine (Na + Cl) and sulfur (S) components of the aerosol to be transported to the polar plateau in the warm advective phase of a storm, and the crustal (Al + Si) component to arrive during post-storm cold advection (Hogan et al., 1984).

The impactor used by Shapiro et al. (1984) during AGASP is the same unit that was used in Greenland (Hogan et al., 1983) and Antarctica (Hogan et al., 1984). Its first airborne use was by Shaw (G. Shaw; University of Alaska, Fairbanks; personal communication, 1980) in Antarctica in 1980. It has been operated at about 25-40 L min^{-1} during these polar programs, which causes a greater velocity to occur in the jet than the 17.5 L min^{-1} flow that was used in May's (1945) original calibration. Calculations using the data of May (1967) indicate that unit density spheres of 0.4-μm diameter should be impacted at the higher flow rates. SEM analysis of gold-coated membrane filter substrates impacted in the polar regions show that particles of 0.2-μm diameter were collected frequently. A series of experiments is currently in progress to calibrate the impaction efficiency of this impactor and accessory concentration devices.

Spherical pigment grains with a density of approximately 2 g cm^{-3} are diluted to a concentration of about 10 ppmm in distilled water. The pigment dispersion is aerosolized with a Collison atomizer (built at ASRC), and the atomizer output is diluted and dried with 30 L min^{-1} of dry air. This technique produces a few clusters of pigment particles as great as 5-μm diameter, and many individual pigment grains of 0.05- to 0.5-μm diameter. The output flows through a 0.5-m^3 plenum that houses the impactor, and exits through a pleated paper filter. Two atomizers are used with two types of pigment to produce more polydisperse aerosols.

SEM analysis of gold-coated membrane filter substrates exposed in this manner show the supermicron particles to be collected along the edges of the main impaction line. Particles of 0.2- to 0.5-μm geometric diameter are confined to a line less than 200 μm wide.

5.5.3 Conclusion

A modification of May's (1945) impactor has been found useful for polar aerosol collection, in agreement with Fenn and Weickmann (1959). Experiments are in progress to extend the concentration capabilities of this device to 0.01-μm particles for AGASP II.

5.6   Coarse Particle Soil Dust in Arctic Aerosols, Spring 1983

J. W. Winchester, S. Li, and S. Fan
Deptartment of Oceanography, Florida State University
Tallahassee, FL   32306

R. C. Schnell
Cooperative Institute for Research in Environmental Sciences
University of Colorado, Boulder, CO   80309

B. A. Bodhaine
Geophysical Monitoring for Climatic Change
NOAA/ERL/ARL, Boulder, CO   80303

In 6 out of 11 AGASP research flights, March-April 1983, particle size fractions collected by cascade impactors contained elemental constituents of soil dust--Al, Si, K, Ca, Ti, and Fe--primarily in the coarsest particles, >16-μm aerodynamic diameter (μmad), at concentrations much greater than in the samples of the remaining 5 flights. The relative concentrations of these elements were approximately those in average geochemical shale. They differed from concentrations of the average Earth by a several-fold depletion of Si in the aerosol samples, as well as from the composition of stratospheric samples of El Chichon volcanic dust, which had relatively higher K and Ti than did the Arctic haze aerosols. The results suggest two possible sources for these particles: (1) finely divided clay minerals generated at lower latitudes (e.g., in Asia during late winter), which are transported northward and, under suitable atmospheric conditions before sampling, may grow or coalesce as ice crystals or aqueous aerosols into much larger sizes; and (2) an eruption (probably not volcanic) of aerosol and water vapor into the Arctic troposphere. Some Cl of marine origin and some S from the oxidation of SO_2 may

Table 37.--Earth crust elements in coarse particles > 2 μmad,
summed over impactor stages 4-7

Sample no.	Concentration* (ng m^{-3}, STP)						Ratio Si/Al
	Al	Si	K	Ca	Ti	Fe	
1	627	257	80	644	160	95	0.41
2	40	65	17	17	<4	<14	1.62
3	54	64	<14	31	<4	<18	1.18
4	50	98	19	20	<12	<34	1.96
5	951	639	263	411	46	446	0.67
6	142	143	<48	~74	<24	<92	1.01
7	530	153	52	137	14	226	0.29
8	96	36	<6	~6	<4	<14	0.38
9	482	308	110	392	30	~206	0.64
10	208	111	28	~44	5	48	0.69
11	(160)	(92)	(36)	(45)	(5)	(125)	0.58

*Values in parentheses are approximate and include an estimate for missing stage 6.
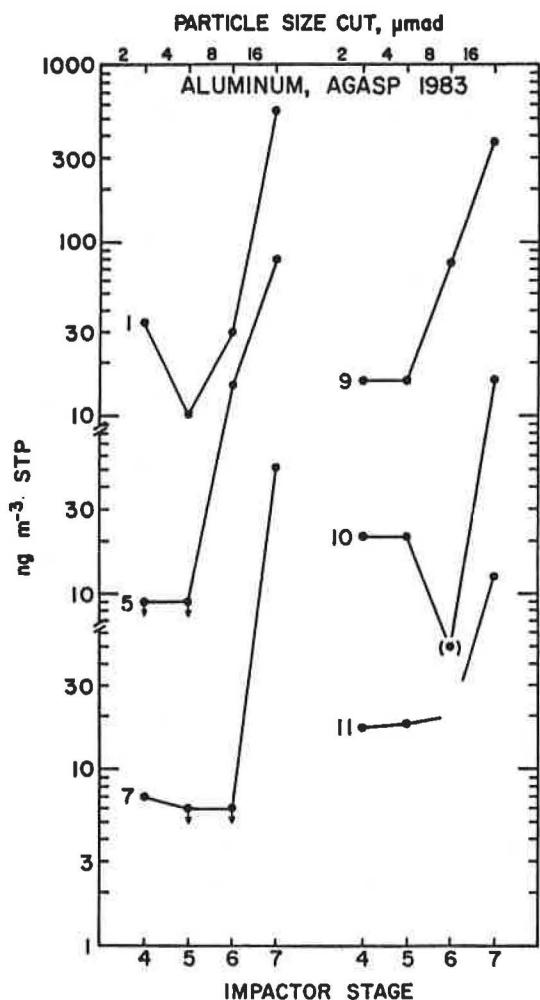
Figure 105.--Distribution of coarse aerosol Al concentration in >2-μmad particle size fractions for six AGASP samples having highest dust loadings. In smaller size ranges, Al was below detection limit (indicated by ↓). Blank Al on vaseline-coated Kimfol film (stages 4-7) has been subtracted. For stage 10, data point in parentheses is approximate. Estimated uncertainties in concentrations from PIXE analysis (<20%) are less than those for determining airflow rate during sampling (~30%).

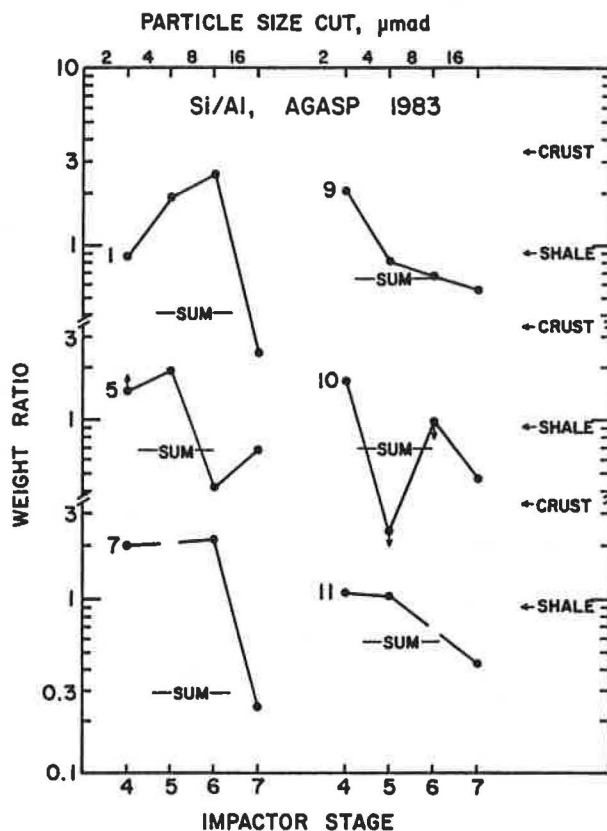Figure 106.--Distribution of Si/Al concentration ratio in >2-μmad particle size fractions for the six AGASP samples in fig. 105. For each, the ratio of the concentrations summed over stages 4-7 is indicated by horizontal lines. Ratios in average Earth crust and in average shale are indicated on the right. Aerosol Si/Al ratios are all much lower than in crust and also lower than in shales, but may approximate clay mineral composition. Upward arrow indicates point is at the lower limit of data; downward arrow, upper limit.

also be taken up by the coarse particles as they interact with the haze. Data on which these conclusions are based are presented in tables 37 and 38 and in figs. 105 and 106.

Table 38.--Ratios of Earth crust elements in coarse particle size fractions

| | Wt. ratio stages 7/6* | Weight ratios of sums of stages 4-7 (>2 μmad) | | | | | | |
		Si/Al	Si/Ca	Si/Fe	K/Al	K/Ca	K/Fe	Ti/Fe
Sample no.†								
1	2.6	0.41	0.40	2.71	0.128	0.124	0.84	1.68
5	5.4	0.67	1.55	1.43	0.277	0.64	0.59	0.103
7	11.9	0.29	1.12	0.68	0.098	0.38	0.23	0.062
9	3.2	0.64	0.79	~1.50	0.228	0.28	0.53	0.146
10	(>17.0)	0.69	2.52	2.31	0.135	0.64	0.58	0.104
11	---	0.58	2.04	0.74	0.225	0.80	0.29	0.040
Median	5.4	0.61	1.34	1.46	0.180	0.51	0.56	0.104
Shales§	---	0.91	3.30	1.55	0.333	1.204	0.564	0.097
Earth crust¶	---	3.41	7.64	5.54	0.318	0.714	0.518	0.088
Loess**	---	3.14	50.0	10.15	0.225	2.69	0.55	0.140
Volcanic ash††	---	---	---	---	0.541	1.463	2.548	0.323
Median, samples 2, 3, 4, 6, 8§§	---	1.18	3.82	>1.5	<3.4	~1.0	---	---

*Medians of six elements that are abundant in Earth crust minerals.
†In other samples the soil dust elements in coarse fractions were near or below detection limits.
§Averages of Turekian and Wedepohl (1961).
¶Averages of Mason and Moore (1982).
**From Nanking, China (Heller and Liu, 1982; Taylor et al., 1983).
††Stratospheric ash, May 1982, from El Chichon eruptions (Kotra et al., 1983).
§§From data in table 37.

5.7 Particulate Sulfur and Chlorine in Arctic Aerosols, Spring 1983

J. W. Winchester, S. Li, and S. Fan
Department of Oceanography, Florida State University
Tallahassee, FL 32306

R. C. Schnell
Cooperative Institute for Research in Environmental Sciences
University of Colorado, Boulder, CO 80309

B. A. Bodhaine
Geophysical Monitoring for Climatic Change
NOAA/ERL/ARL, Boulder, CO 80303

In each of 11 AGASP flights, particulate S and Cl were determined by PIXE analysis of eight cascade impactor fractions from <0.25- to >16-μm aerodynamic diameter (μmad). Sulfur occurred mainly in fine aerosol sizes of <2 μmad, whereas Cl was mainly in coarser sizes. Two fine S modes could be identified, one being ultrafine (nuclei) <0.25 μmad, and the other being fine (accumulation) centered around the 0.5- to 1.0-μmad range; the relative abundances of the two modes apparently depended on flight location. This suggests that both homogeneous gas phase and heterogeneous liquid phase reactions led to sulfuric
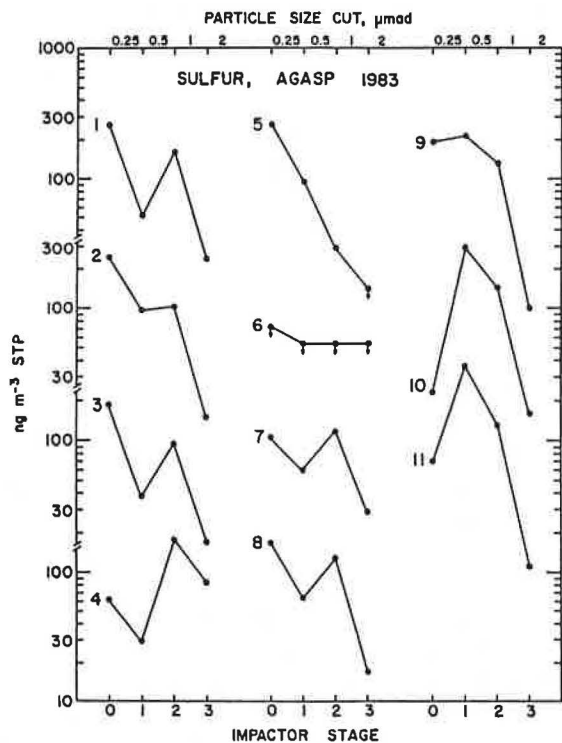
Figure 107.--Distribution of fine aerosol S concentrations in <2-µmad particle size fractions for AGASP samples 1-11. Blank S on Nuclepore filter (stage 0) and on paraffin-coated Kimfol film (stages 1-3) has been subtracted. Estimated uncertainties in concentrations from PIXE analysis (<10%) are less than those for determining airflow rate during sampling (~30%). Concentration below detection limit is indicated by ↓.

acid formation in the haze. Qualitative comparisons of aerosol S and Cl distributions with particle size suggest that Cl may be volatilized by processes that depend on the presence of acidic reactants in the atmosphere. Data on which these conclusions are based are presented in figs. 107 and 108 and tables 39, 40, and 41.
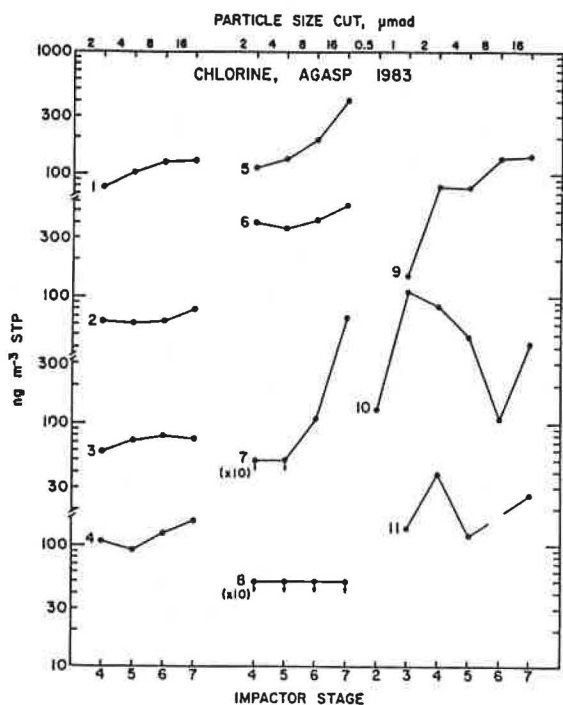

Figure 108.--Distribution of coarse aerosol Cl concentrations in >2-µmad particle size fractions (>0.5 µmad for sample 10 and >1 µmad for 9 and 11). In smaller size ranges Cl was below detection limit, indicated by ↓. Blank Cl on vaseline-coated (stages 4-7) and paraffin-coated (stages 1-3) Kimfol film has been subtracted. Estimated uncertainties in concentrations are the same as in fig. 107.

Table 39.--Conditions of aerosol sampling by cascade impactor,
March-April 1983*

Sample no.	Air volume (m³) Ambient	0°C, 1 atm	Starting time Date	GMT	Duration (min)	Haze in tropo- sphere
1	0.336	0.233	11 Mar	2140	420	Moderate
2	0.365	0.293	13 Mar	2023	457	Strong
3	0.364	0.251	15 Mar	2025	455	Moderate
4	0.228	0.125	17 Mar	2100	285	Light
5	0.228	0.174	21 Mar	1200	475	Moderate
6	0.095	0.047	23 Mar	1300	288	---
7	0.402	0.280	28 Mar	1340	503	Lt. to Mod.
8	0.460	0.303	31 Mar	0847	576	Strong
9	0.459	0.341	04 Apr	0710	574	Moderate
10	0.523	0.491	05 Apr	0848	513	Light
11	0.504	0.454	10 Apr	0750	495	Light

*AGASP sample nos. 1-4 from Anchorage over Alaska to BRW and north; no. 5 from Anchorage over Alaska and Arctic to Thule, Greenland; no. 6 (stratospheric) from Thule south in El Chichon dust; no. 7 from Thule via Alert and Svalbard to Bodø, Norway; nos. 8 and 9 from Bodø over Greenland Sea to Svalbard; nos. 10 and 11 from Bodø west over Greenland Sea at low altitude. All sampling was tropospheric except no. 6 and part of no. 4. All flights were round trips from Anchorage, Thule, or Bodø, except nos. 5 and 7.

Table 40.--Aerosol sulfur in fine and coarse particle size fractions*

Sample no.	Impactor stage concentrations (ng m⁻³, STP) 0	1	2	3	4	5	6	7	Sum of stages† Fine 0-3	Coarse 6-7	Coarse ratio 7/6
1	259	52	162	24	<12	<12	34	28	497	62	0.84
2	247	97	103	15	<9	<9	<9	<9	462	<13	---
3	187	38	95	17	<11	<11	<11	<11	337	<16	---
4	62	29	178	83	<22	<22	<22	<22	352	<31	---
5	263	95	29	<14	<16	<16	<16	102	387	102	<6.5
6	<73	<54	<54	<54	<58	<58	<58	<58	<120	<82	---
7	106	60	117	29	<10	<10	22	30	312	52	1.37
8	168	64	128	17	<9	<9	<9	<9	377	<13	---
9	193	213	130	10	~20	~8	21	45	551	66	2.11
10	23	294	143	16	~15	~6	9	23	476	32	2.65
11	70	362	131	11	~21	~91	---	19	574	(19)	---

*Aerodynamic diameter ranges: for impactor stage 0, <0.25; 1, 0.25-0.5; 2, 0.5-1; 3, 1-2; 4, 2-4; 5, 4-8; 6, 8-16; 7, >16 μmad; i.e., sizes of unit density spheres when sampled at 1 min⁻¹ airflow and 1 atm pressure.
†Means and standard deviations: 391 ± 73 for Alaska and Arctic samples 1-5 and 7; 494 ± 89 for Greenland Sea samples 8-11; and 432 ± 92 ng m⁻³ for all 10 tropospheric samples.

Table 41.--Aerosol chlorine in fine and coarse particle size fractions*

Sample no.	\multicolumn{8}{c}{Impactor stage concentrations (ng m^{-3} STP)}	Sum of stages	Coarse ratio 7/6
	0	1	2	3	4	5	6	7		
1	<60	<6	<6	<6	78	103	125	128	434	1.02
2	<48	<5	<5	<5	64	62	64	80	270	1.08
3	<56	<6	<6	<6	59	73	79	75	286	0.95
4	<112	<11	<11	<11	110	92	126	160	488	1.27
5	<81	<8	<8	<8	112	133	190	406	841	2.14
6	<300	<30	<30	<30	401	358	420	560	1639	1.33
7	<50	<5	<5	<5	<5	<5	11	68	79	6.18
8	<46	<5	<5	<5	<5	<5	<5	<5	<10	---
9	<41	<4	<4	15	80	78	134	142	449	1.06
10	>29	<3	13	111	85	48	11	43	311	3.91
11	<31	<3	<3	14	39	12	---	26	(91)	---

*See first footnote, table 40.

5.8 Trace Gases in the Arctic: Indexes of Air Pollution

M. A. K. Khalil and R. A. Rasmussen
Oregon Graduate Center
Beaverton, OR 97006

5.8.1 Introduction

Every spring for perhaps the last hundred years or more a haze consisting of fine particles has appeared over the Arctic (Schnell, 1984b). The origins and sources of the haze may have changed over the years, but at present the Arctic haze aerosol contains sulfate, soot, and organics and is believed to originate from the industrial regions of the world. Anthropogenic activities that produce the precursors of Arctic haze also produce dozens of trace gases that are more concentrated in the Arctic during the spring than at other times. The levels of the anthropogenic trace gases in the Arctic provide evidence for the origins of Arctic haze. Some gases--($C_2Cl_3F_2$, CF_3Br, CF_2BrCl) may identify the locations where Arctic pollution originates, whereas other tracers (CO_2, N_2O, nonmethane hydrocarbons, CO, CH_3Cl) are used to identify the types of sources such as powerplants that are common to all industrialized areas.

Results are discussed here of measurements of trace gases taken over the past 4 years at BRW and more recently on board aircraft during AGASP (Khalil and Rasmussen, 1983a; Rasmussen and Khalil, 1982; Rasmussen et al., 1983).

5.8.2 Seasonal, Vertical, and Spatial Variations of Tracers

In our first experiment it was established that significantly higher levels of $CHClF_2$ (CFC-22), CH_3CCl_3, C_2Cl_4, C_2HCl_3, CCl_2F_2 (CFC-12), and CCl_3F (CFC-11) exist in the Arctic during late winter and early spring (Khalil and

Rasmussen, 1983a). Statistical criteria were developed to detect the presence of higher springtime concentrations when the excess is not apparent. Many natural and anthropogenic trace gases are removed from the atmosphere by reacting with hydroxyl radicals (OH). In the Arctic, the concentration of OH must undergo large seasonal variations because of the variation of sunlight and water vapor that are needed to produce OH. In winter there may be no OH in the Arctic, and trace gases may thus accumulate; therefore, the high concentrations of some of the more reactive anthropogenic and natural trace gases may be explained entirely in terms of the natural variation of OH. This phenomenon of gases accumulating in the high northern latitudes during winter may itself contribute to the formation of Arctic haze as spring arrives and photochemical processes become active. The presence of higher concentrations of CFC-11 and CFC-12 suggests that more pollution is transported to the Arctic during winter than at other times, since these gases do not react with OH radicals. Moreover, calculations show that trace gases such as CH_3CCl_3, CFC-22, and some of the other chlorocarbons and hydrocarbons are much more abundant in the Arctic during winter than can be explained on the basis of their reactivity with OH (Khalil and Rasmussen, 1983a; Rasmussen et al., 1983).

After the occurrence of high concentrations of anthropogenic trace gases in the Arctic during winter and early spring was established, the vertical distribution of trace gases was investigated to detect the possible existence of layers within which the pollution could be transported. Our first experiments consisted of flying in small aircraft from Point Barrow and obtaining air samples up to about 4 km. Statistical evidence of bulges in the vertical distributions of the mixing ratios of C_2H_2, C_2H_6, C_3H_8, and C_2Cl_4 were found (Rasmussen et al., 1983; Rasmussen and Khalil, 1982, 1983). These hydrocarbons were also much more abundant in the Arctic during late winter and spring than at other times. No significant vertical variations in the concentrations of the long-lived trace gases such as the fluorocarbons were detected. The background concentrations of long-lived trace gases are so high that small perturbations are extremely difficult to detect either in a seasonal time series or in vertical concentration distributions. More recently, these experiments were repeated on board the flights for the AGASP experiment.

These early studies showed that anthropogenic trace gases are more abundant in the Arctic during winter and early spring and are probably transported in polluted layers. The tracers discussed here so far are emitted from all the major industrial regions of the world. To distinguish the various regions, several new tracers were chosen, namely, $C_2Cl_3F_2$ (CFC-113) and the fire-extinguishing compound CF_3Br, which are used primarily in the United States, and CF_2BrCl, which is used primarily in Europe. It is believed that none of these compounds is used in the U.S.S.R. The analytical procedures for measuring CF_3Br and CF_2BrCl at ambient concentrations of about 1 pptv have only just been refined, and some data have been obtained from BRW during the past year. Preliminary results suggest that CF_2BrCl is slightly more abundant during winter than at other times, suggesting some contribution to Arctic pollution from Europe (Rasmussen and Khalil, 1984).

A study of the spatial distribution of the gaseous tracers of Arctic haze was carried out to make certain that measurements taken at BRW represent the seasonal variations over the entire Arctic region where haze is observed, and to see if perhaps the locations of the source regions could be detected. During 1983 air samples were obtained from Spitzbergen, Norway (79°N). The
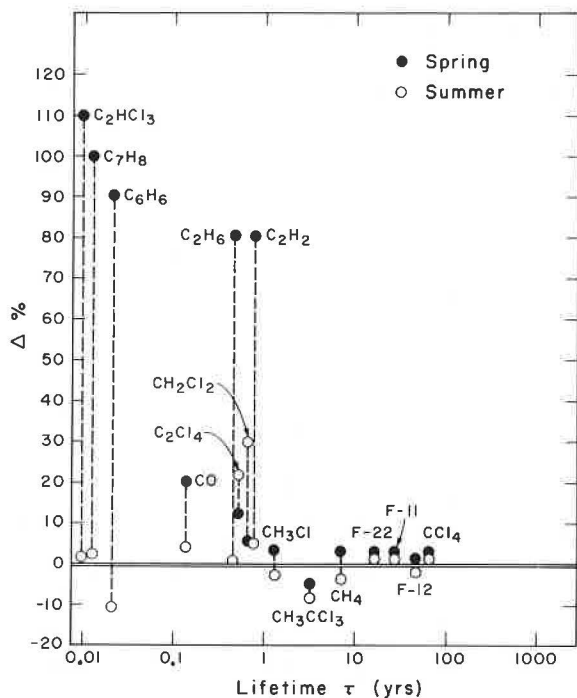
Figure 109.--Spatial variation of the gaseous tracers of Arctic haze. The relative difference Δ of concentrations C of trace gases observed at Sptizbergen, Norway, and at BRW are shown as a function of the average atmospheric lifetime of the trace gases. The open circles show Δ during summer (August-September); the dark circles represent Δ during spring (March-April). Δ% = 100 × [C(Spitzbergen) - C(BRW)]/C(BRW).

tracers followed similar seasonal cycles at both BRW and Spitzbergen sites with highest concentrations of trace gases during Spring (March-April) and lowest in summer (August-September). During spring, however, when Arctic haze is present, significantly higher concentrations of many hydrocarbons were observed at Spitzbergen compared with BRW (fig. 109). This could be either due to local pollution or because Spitzbergen is closer to the U.S.S.R. and Europe, which may be sources of Arctic pollution and haze.

5.8.3 Tracers in Haze Layers

During the flights for AGASP a large number of samples of air were obtained in both the polluted layers and the clean Arctic air on the same days. The results, summarized in table 42, showed that a large number of chlorofluorocarbons, chlorocarbons, hydrocarbons, and other trace gases were more abundant in the haze layers then outside the haze. As expected, the percent difference of concentrations in and out of the haze layers was much greater for short-lived species (Khalil and Rasmussen, 1984). The background concentrations of short-lived trace gases are extremely small; thus, polluted layers contain a relatively large excess. For long-lived trace gases the background concentration consists of accumulated amounts from many years, and thus the relative excess in the polluted layers is small.

In the data analyzed (AGASP 8 and 9, flown 31 March and 4 April 1983, respectively) no clean air was encountered near the surface. It is possible that the concentrations of some short-lived gases decline with height, which would have led to underestimation of the background concentrations and therefore overestimation of the relative excess in the haze layers. The effect of such a possibility was investigated by reanalyzing the data after discarding measurements taken below 2 km. The remaining data, between 2 and 8 km,

143

Table 42. The estimated differences (Δ) of concentrations* and the
associated 90% confidence limits (lower, upper) of trace
gases in and out of Arctic haze

	Δ		Δ%		Δ > 0?	Δ'†		Δ'%	
Chlorofluorocarbons									
CCl_2F_2 (CFC-12)	10	(5, 18)	2.7	(1.4, 5)	yes	---		---	
CCl_3F (CFC-11)	5	(3, 9)	2	(1.4, 4)	yes	---		---	
$CHCF_2$ (CFC-22)	3	(0, 10)	3.8	(0, 13)	no	---		---	
$C_2Cl_3F_3$ (CFC-113)	1.4	(0.5, 2.8)	6	(2, 12)	yes	---		---	
$C_2Cl_2F_4$ (CFC-114)	0.3	(-0.2, 0.7)	3	(-2, 7)	no	---		---	
Chlorocarbons									
CH_3CCl_3	15	(5, 25)	12	(4, 20)	yes	---		---	
C_2Cl_4	45	(21, 65)	67	(±39)	yes	39	(19, 61)	58	(±38)
CCl_4	9	(6, 12)	6	(±2)	yes	---		---	
CH_3Cl	18	(-13, 38)	3	(-2, 6)	no	---		---	
CH_2Cl_2	8	(6, 13)	33	(25, 54)	yes	7	(4, 11)	31	(15, 48)
$CHCl_3$	8	(6, 14)	35	(26, 61)	yes	7	(4, 12)	31	(15, 49)
C_2HCl_3	10	(4, 16)	167	(40, 800)	yes	8	(0.7, 14)	138	(6, 242)
Hydrocarbons									
CH_4 (ppbv)	41	(28, 49)	2.5	(1.7, 2)	yes	---		---	
C_2H_2	305	(208, 442)	66	(±28)	yes	257	(53, 400)	56	(10, 90)
C_2H_4	41	(10, 80)	100	(25, 200)	yes	39	(7, 54)	100	(18, 138)
C_2H_6	930	(560, 1400)	40	(22, 70)	yes	740	(300, 1200)	32	(13, 50)
C_3H_6	5	(0, 44)	63	(0, 500)	no	0	(-1, 21)	0	(---)
C_3H_8	854	(302, 1267)	120	(±70)	yes	469	(122, 1140)	66	(17, 160)
$I-C_4H_{10}$	253	(92, 330)	243	(±145)	yes	154	(30, 308)	148	(>20)
$N-C_4H_{10}$	415	(150, 590)	256	(±170)	yes	235	(48, 540)	145	(>20)
$I-C_5H_{12}$	107	(47, 167)	630	(>100)§	yes	86	(21, 143)	540	(>60)
$N-C_5H_{12}$	125	(72, 188)	1000	(>500)§	yes	83	(30, 148)	630	(>100)
C_6H_6	164	(68, 214)	5000	(>500)§	yes	127	(12, 192)	4200	(>15)
C_7H_8	26	(0, 58)	200	(---)	no	---		---	
CO, CO_2, & N_2O									
CO (ppbv)	47	(27, 66)	36	(±15)	yes	42	(10, 55)	32	(8, 42)
CO_2 (ppmv)	3.5	(2, 5)	1	(±0.4)	yes	---		---	
N_2O (ppbv)	1	(0, 2)	0.3	(±0.3)	no	---		---	
Other trace gases									
OCS	97	(47, 157)	26	(11, 50)	yes	---		---	
CH_3I	0.1	(0, 0.3)	142	(0, 430)	no	0.1	(0, 0.3)	142	(0, --)
CH_2BrCl	0	(-0.1, 0.2)	0	(-10, 20)	no	---		---	
CH_2Br_2	1.7	(0.5, 2.3)	68	(±40)	yes	---		---	
$C_2H_4Br_2$	0.8	(0.2, 1.2)	200	(22, 1200)	yes	0.8	(0, 1.2)	200	(0, --)
CF_3Br	0	(-0.1, 0.2)	0	(-10, 20)	no	---		---	
CH_3Br	-0.3	(-1, 0.6)	-3	(-10, 6)	no	---		---	

*Units are pptv unless otherwise noted.
†Data reanalyzed after discarding measurements taken below 2 km.
§Lower confidence limit only; upper limit not determined.

consisted of both clean and polluted air samples at each height. The results
of the calculations show that while in some cases the estimated relative
excess is slightly smaller, the conclusions remain the same. Most of the
trace gases studied are much more concentrated in the haze layers than outside
(see table 42).

The results of these flights showed that many trace gases that originate
from high-temperature combustion, such as in coal-fired powerplants and
automobiles, were more abundant in the haze than outside the haze, including
N_2O and CO_2. Excess CH_3Cl, the tracer of low-temperature biomass combustion,
was not present. Moreover, excess concentrations of exotic manmade compounds
such as CFC-113 and CF_3Br, which would represent pollution from the United

144

States, and CF_2BrCl, representing pollution from Europe, were also not observed. These findings suggested that the haze encountered on these two flights originated in the U.S.S.R. This conclusion was also obtained independently by trajectory analyses of air masses encountered during these flights.

Measurements from the AGASP studies showed for the first time that the gaseous tracers are directly associated with the Arctic haze layers, whereas from ground-based measurements one could only infer such a relationship.

5.8.4 Conclusions

Studies of the gaseous tracers of Arctic haze have yielded valuable information. It has been demonstrated that many anthropogenic trace gases are more abundant in the Arctic during the time of haze and that these tracers are transported to the Arctic in polluted air that contains the Arctic haze aerosol. The tracers can be used to detect both the regions where Arctic pollution originates and the types of sources that might contribute to its formation. An extremely large array of gaseous tracers is available and can provide an exquisite characterization of sources and regions to advance further the usefulness of gaseous tracers in large-scale receptor models for a quantitative assessment of the sources, sinks, and effects of Arctic haze.

5.9 Atmospheric Particulates at MLO and SPO

C. M. Thompson, J. R. Parrington, G. Tuncel, and W. H. Zoller
Department of Chemistry, University of Maryland
College Park, MD 20742

5.9.1 Introduction

Particles have been collected on a weekly basis almost continuously at MLO since February 1979 and have been analyzed for about 40 elements at the University of Maryland. Results from the overall project are summarized below from Parrington (1983, abstract); data presented in the paper are summarized in fig. 110 and table 43.

Mauna Loa Observatory, Hawaii, was selected as a remote northern hemisphere site from which to collect atmospheric particles for chemical analyses of background aerosols in the free troposphere of the northern hemisphere. An automatic digital sampling controller was designed and installed at this site to aid in the isolation of uncontaminated particles of the free troposphere, based on wind direction and speed, time-of-day and particle characteristics at the observatory.

The three primary components measured on these background particles between 1979 and 1982 were sulfates, continentally derived crustal material and marine particles with average geometric mean concentrations of 240 ng/m^3, 50 ng/m^3, and 15 ng/m^3, respectively, during the months of July to mid-February. Other months showed a ten-fold increase in continental crustal material, geometric avg = 730 ng/m^3, (which has been traced to Asian deserts) and doubling of sulfate mass to 480 ng/m^3 while the marine mass showed no significant changes. The average geometric mean concentration of local basalt was determined to be 15 ng/m^3 in downslope winds and, thus, does not represent a major interference to most studies

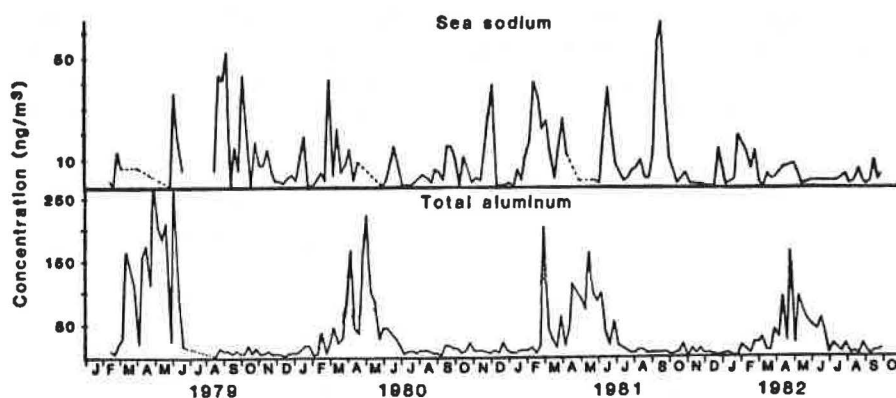Figure 110.--Weekly downslope marine sodium (as excess sodium) and aluminum concentrations (ng m^{-3}) for high-volume aerosol collections at MLO. (From Parrington et al., 1983.)

at MLO as a majority of the crustal dust in the atmosphere, even in relatively clean periods, is transported over thousands of kilometers to the island from continents surrounding the Pacific Ocean.

Several components, $SO_4^=$, V, Co, Cu, Zn, As, Se, Ag, Sb, W and Au, show variations that suggest anthropogenic or volcanic sources during episodes throughout the year. Several of these major episodes have been traced to populated areas of Asia and North America and in one case emissions from copper smelters in the southwestern United States may have been transported to MLO. About 40% of the total yearly mass of sulfate (the major component by mass which reaches MLO in these episodes) is transported in these relatively short episodes. The major source of sulfate is apparently natural and may be due to biomethylation in the marine environment.

Table 43.--Downslope concentrations of crustal and marine components, and calculated crustal and marine mass concentrations observed in dust and nondust periods of each year

Material	Concentration (ng m^{-3})				
	Total aluminum	Total sodium	Marine sodium	Mass marine	Mass crustal
Dust 1979	115.0 ± 68.0	31.0 ± 22.0	8.6 ± 7.7	27 ± 24	1400 ± 830
Dust 1980	57.0 ± 40.0	21.0 ± 11.0	7.7 ± 6.3	24 ± 19	690 ± 490
Dust 1981	61.0 ± 33.0	29.0 ± 3.0	15.3 ± 8.7	46 ± 27	740 ± 400
Dust 1982	46.0 ± 34.0	19.0 ± 6.0	6.5 ± 5.4	20 ± 17	560 ± 410
Average dust	71.0 ± 51.0	25.0 ± 13.0	9.7 ± 7.5	30 ± 23	860 ± 620
Nondust 1979	6.4 ± 2.0	17.0 ± 9.8	16.5 ± 9.7	51 ± 30	78 ± 24
Nondust 1980	8.2 ± 2.2	9.0 ± 4.7	7.3 ± 5.4	23 ± 17	100 ± 27
Nondust 1981	6.2 ± 2.5	9.6 ± 11.0	8.4 ± 11.3	26 ± 35	75 ± 30
Nondust 1982	5.3 ± 4.0	6.9 ± 6.1	5.6 ± 5.5	17 ± 17	64 ± 49
Average nondust	6.7 ± 2.3	11.0 ± 9.2	9.5 ± 9.2	29 ± 28	81 ± 28

Parrington et al. (1983, abstract) describe general features of the annual incursions of Asian dust to the Hawaiian Islands:

> Analyses of atmospheric particles collected at Mauna Loa Observatory in Hawaii from February 1979 through September 1982 reveal strong influxes of Asian dust in the spring of each year. Concentrations of a typical crustal element, aluminum, are more than an order of magnitude greater between February and June than during the remainder of the year (71±51 versus 6.7±2.3 nanograms per cubic meter). The mass of crustal material transported during the relatively short dust episodes accounts for an average of 80 percent of the total yearly mass of atmospheric particles at 3400 meters on Mauna Loa.

5.9.2 The Atmospheric Aerosol at MLO

During the spring of 1982 and of 1983, size-fractioned atmospheric particulates were collected at MLO. The samples were collected during the clean downslope phase of the diurnal wind cycle at MLO, and are therefore typical of the midtroposphere at 3.4 km (Parrington and Zoller, 1984). These experiments were done to characterize the continentally derived material that is transported into the Pacific Basin during the spring (Parrington et al., 1983; Bodhaine et al., 1981b). Many investigators (Parrington et al., 1983; Shaw, 1980; Duce et al., 1980; Darzi and Winchester, 1982) have concluded that this material has its origins on the Asian continent and is transported eastward by tropospheric flow during periods of high dust storm activity in central Asia.

Five impactor sets from each sampling season were analyzed by instrumental neutron activation analysis to determine their elemental composition. Figure 111 shows the mass distributions determined for the suite of impactor data collected during each year. The mass is approximately log-normally distributed about 2-μm particle diameter with some mass on stage 1 and some on the backup filter (BU). The mass discontinuity at stage 2 suggests that the
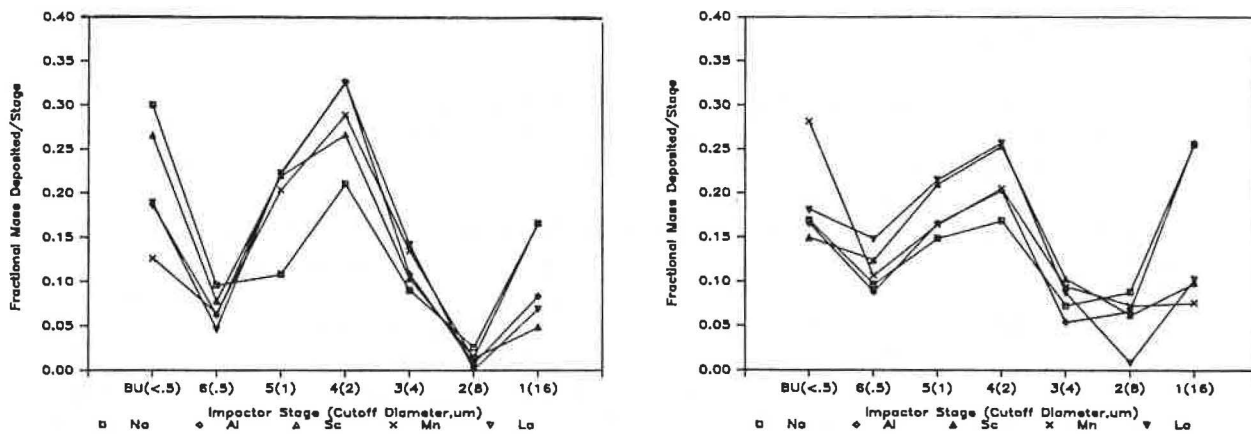

Figure 111.--Size distributions of particles bearing several elements at MLO under downslope conditions: (left) spring 1982; (right) spring 1983. BU is backup filter.
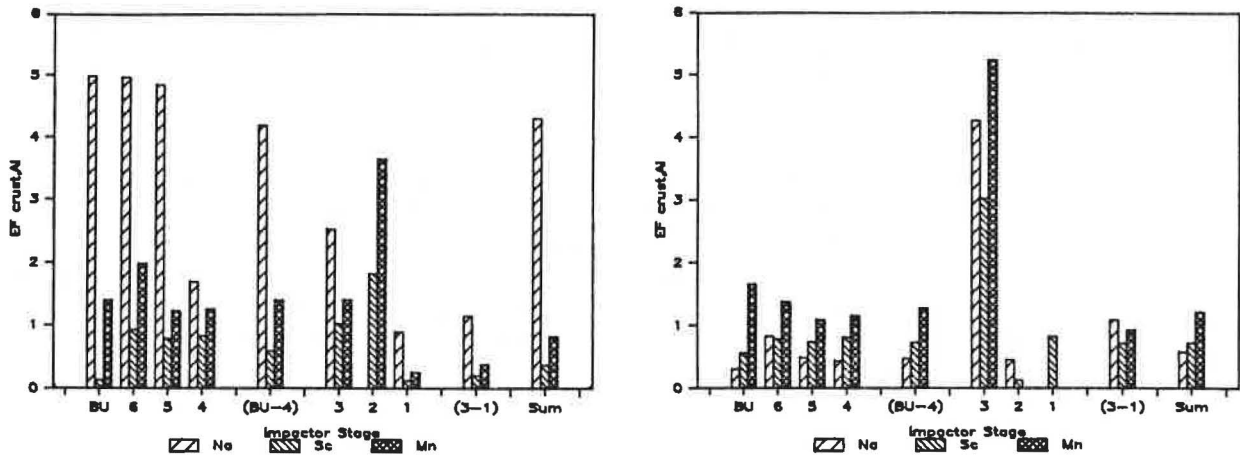
Figure 112.--Crustal enrichment factors for two MLO downslope impactor samples collected during Spring 1983: (left) aerosol DS1; (right) aerosol DS6. BU-4 is the small-particle stage; 3-1, the large-particle; Sum, the total mass on the impactor. The crustal enrichment factor of an element x with respect to Al is defined as the following: [atm. conc. (x)/atm. conc. (Al)]/[crust. conc. (x)/crust. conc. (Al)].

larger particles (stages 1, 2, and 3) may be of a different origin than the smaller particles (stages 4, 5, 6, and BU). This possibility was examined by using crustal enrichment factors (EF's) to compare the various size fractions. Figure 112 shows results from two typical impactor sets collected during the spring of 1983. The values of EF$_{crust}$ for Na, Sc, and Mn are plotted vs. impactor stage, including the small-particle (BU-4) and large-particle (3-1) fractions and the total mass on the impactor (Sum). There are distinct differences between the two main size fractions (BU-4) and (3-1). Further-more, the BU-4 fraction closely resembles the Sum, indicating that the small-particle fraction is dominant.

5.9.3 Atmospheric Aerosols at SPO

Trace-element concentrations have been obtained from atmospheric parti-culates collected at SPO. Use of instrumental neutron activation analysis allows for collection of up to 40 elements on filter samples. Elements collected at SPO can be separated into three categories: those of crustal origin, those of marine origin, and those that are unusually enriched with respect to crustal and marine sources. Crustal and enriched elements can be easily distinguished from marine elements by their summer-winter behavior. The crustal and enriched elements usually have higher concentrations in the summer period. The high winter averages observed for most elements in 1978 resulted from a large spike observed in the winter season. This is shown in fig. 113, where the Al concentrations observed over the period are plotted. Other crustal elements also show this regular cycle. They start to increase around September and drop back to low values around March. Enriched elements follow about the same cycle. Marine elements, on the other hand, follow a completely different pattern. They start to increase around May or June and
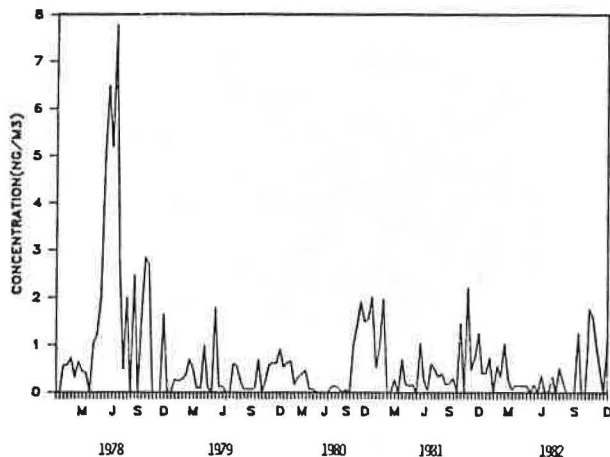
Figure 113.--Aluminum concentrations (ng m^{-3}) measured at SPO.

drop quite rapidly in November and December. The period of high marine input overlaps with crustal input, so it is not possible to separate summer and winter distinctly by looking at fluctuations in the marine and crustal elements.

Enriched elements follow a pattern similar to that of crustal elements. The easiest way to distinguish these enriched elements is by crustal enrichment factors. Arsenic, Se, Br, and Cl are enriched significantly (as are S, Cu, Zn, Ag, Sb, I, and Au). Most of these are believed to have natural sources.

5.10 The Search for Particles of Cosmic Origin at SPO

R. E. Witkowski and W. A. Cassidy
University of Pittsburgh
Pittsburgh, PA 15260

G. W. Penney
Carnegie-Mellon University
Pittsburgh, PA 15213

As part of the University of Pittsburgh Antarctic Search for Meteorites project, an atmospheric particle collector was designed, constructed, and installed at SPO during December 1983. Its operation is based on the electrostatic precipitation concept, whereby individual particles are electrically charged in an ionization chamber and subsequently collected on specimen plates maintained at an oppositely charged potential. The collector design parameters were so selected as to optimize particle collection in the size range of 0.01-1.0 μm with a maximum at 0.3 μm.

The overall view of the particle collector is shown in fig. 114. Outside air enters the unit at the left inlet port and is drawn through the ionizer and collector regions at a flow rate of 300 ft min^{-1}. The combined ionizer and collector region is 10 in long and has a cross section of 6 × 3 in; the entire assembly is fabricated from Plexiglas. The ionizer is simply an
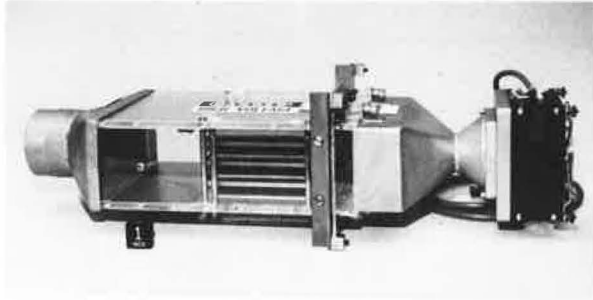
149

Figure 114.--Electrostatic particle collector. The specimen plates are clearly visible in the center section of the device.
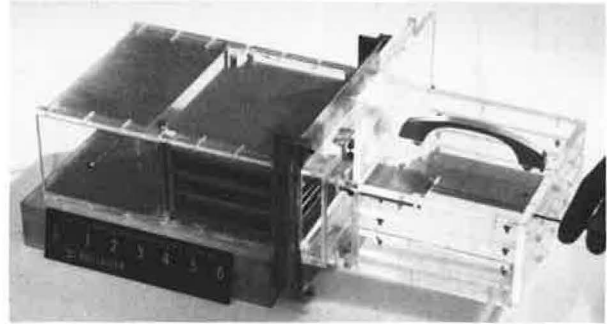

Figure 115.--Specimen plate transfer to the storage and transport container.

electrically charged 0.006-in-diameter tungsten wire stretched perpendicular (axially) to the air sample. For this work at SPO, it was found that a potential of -12,000 V DC (35 μA) could be maintained; an even glow along the length of the tungsten wire was visible when the room was darkened. The collector region is made up of a series of stacked stainless steel specimen plates arranged in a 3 × 3 matrix configuration. Each 1.5- × 5-in plate is gold plated and has a 200-mesh copper grid coated with carbon attached to the active collector area. A +7,300-V DC potential is maintained.

A special arrangement of shutters between the collector and the storage and transport container, shown in fig. 115, permits exposed specimen plates to be transferred directly to the laboratory for study using scanning transmission electron microscopy. No sample preparation or handling is required prior to analysis, thus minimizing contamination.

The particle collector will operate throughout the 1984 year, and sample plates will be withdrawn at specific time intervals. The preliminary results obtained to date were from plates exposed for 168 hours. The data indicate that the collector has collected particles in the anticipated size range; preliminary energy-dispersive spectrometry analysis shows that, in addition to sulfur-rich material, particles composed of varying amounts of Mg, Si, K, Ca, and Fe have been isolated. Analysis will continue on samples obtained from plates exposed during December 1983 and January 1984 for periods up to 1000 hours. The last set of plates, which is being exposed for various periods throughout the 1984 winter season (February-November), will be retrieved subsequently for study.

Acknowledgments

5.11 CO_2 and Other Air Chemistry Studies at Palmer Station

E. Robinson and W. L. Bamesberger
Laboratory for Atmospheric Research, College of Engineering
Washington State University, Pullman, WA 99164

The second year of operation of the air chemistry facility at Palmer Station, Anvers Island, Antarctica, was completed in February 1984, and sampling results for CO_2 and other trace atmospheric constituents can be reported. A description of the station and its operation can be found in Robinson and Bamesberger (1982).

The air chemistry facility is used as a base for gathering CO_2 flask samples for analysis in the GMCC laboratories. Also, gas-chromatographic instrumentation is operated to measure CO_2 and other trace constituents continuously. A Carle Model 211 automatic GC is used for CO_2 monitoring. The instrument is calibrated against standard CO_2-in-air mixtures that in turn have been given a preliminary standardization check by the GMCC CO_2 laboratory.

Table 44 shows the results of regression calculations on the concentration time trends. These data continue the general trends reported on the basis of the 1982 results.

The values of N_2O concentrations at Palmer have shown an increase of about 3 ppb yr^{-1}, or about 1%, compared with an average concentration of about 300 ppb. This rate is higher than the 0.3%-0.4% observed at other stations and higher than the 0.4% long-term increase reported for SPO by Rasmussen et al. (1981) for the period 1977-1981. The Palmer N_2O data showed apparent seasonal fluctuations over the 1982-1983 2-yr period; thus the higher rate of

Table 44.--Trace atmospheric constituent mixing ratio results*,
Palmer Station, Antarctica

Constituent	Observed average mixing ratio week of 9 Jan 1983	Annual trend†	Corre-lation coef.	Data period
CCl_3F (CFC-11)	189.8 ppt	8.9 ± 0.2 ppt yr^{-1} (4.7%)	0.97	04 Apr 1982-11 Dec 1983
CCl_2F_2 (CFC-12)	314.4 ppt	12.4 ± 0.2 ppt yr^{-1} (3.9%)	0.99	04 Apr 1982-11 Dec 1983
CH_3CCl_3	118.6 ppt	7.8 ± 0.3 ppt yr^{-1} (6.6%)	0.91	04 Apr 1982-11 Dec 1983
CCl_4	148.9 ppt	2.4 ± 0.2 ppt yr^{-1} (1.6%)	0.81	04 Apr 1982-11 Dec 1983
N_2O	301.6 ppb	3.0 ± 0.2 ppb yr^{-1} (1.0%)	0.84	04 Apr 1982-11 Dec 1983
CO_2	337.4 ppm	---§		31 Jan 1982-11 Dec 1983¶
CH_4	1.51 ppm	---§		31 Jan 1982-11 Dec 1983
CO	57.0 ppb	---§		31 Jan 1982-11 Dec 1983
O_3	10-30 ppb (approx. annual range)			24 Jan 1982-11 Dec 1983
CN	200-1000 cm^{-3} (approx. annual range)**			24 Jan 1982-11 Dec 1983

*Expressed on a dry-air basis.
†Based on weekly average data; % calculated from observed data for week of 09 Jan 1983.
§Pronounced seasonal cycle precludes estimation of useful annual trend.
¶No samples for period 18 Jul 1982-18 Jan 1983.
**CN expressed as concentration rather than mixing ratio.

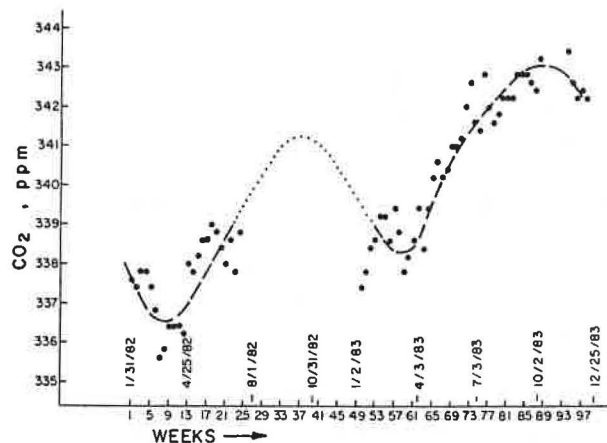Figure 116.--Average weekly CO_2 concentrations (ppm), 6 February 1982-11 December 1983, Palmer Station, Antarctica. The curve is a subjective approximation of the apparent data trend.

increase observed here may be due to the short sampling period and a lack of adequate compensation for the cyclical nature of the data.

The CO_2 record described in table 44 covers the period from 31 January 1982 to 11 December 1983, but with a break from 18 July 1982 to 18 January 1983 due to instrumentation problems during the Antarctic winter. Figure 116 shows a plot of the CO_2 record based on weekly average data. The data are expressed on a dry-gas basis (Pearman, 1975). The concentration trend and apparent seasonal cycle over this 2-yr period have been approximated by the subjectively drawn curve shown in the figure. The annual trend indicated by these data approximates the 1.2 ppm yr^{-1} trend found for SPO data; however, the seasonal cycle as indicated by this curve is larger than what would be expected from the previous Southern Hemisphere data. The CO_2 data collection at Palmer is continuing, and more details on this apparent seasonal cycle should be provided in future analyses. The analyses of the seasonal data for CO and CH_4 also show seasonal cycles similar in phase to the CO_2 pattern shown in fig. 116.

5.12 Vertical Profiles of Carbon Particles in the Arctic

H. Rosen and A. D. A. Hansen
Lawrence Berkeley Laboratory
University of California, Berkeley, CA 94720

One of the major uncertainties in modeling the effects of the Arctic haze on the solar radiation balance has been the limited knowledge of the vertical distribution of the haze and, in particular, the vertical distribution of graphitic carbon particles and their associated absorption coefficients. The first measurements of such distributions in the Arctic atmosphere and, to the best of our knowledge, in the atmosphere in general are reported here.

During March and April 1983 a series of flights (AGASP) organized by NOAA explored the vertical and horizontal distributions of the Arctic haze. One of the instruments used in this program was the aethalometer (Hansen et al., 1982), which was developed at LBL and has the capability of determining graphitic carbon concentrations (Rosen and Novakov, 1983) on a real-time basis using the calibration of Gundel et al. (1984).

Vertical profiles were obtained by dividing the atmosphere into altitude
bins and determining the average aethalometer response in each of these bins
over the particular time periods of interest. The bin size was chosen so that
the errors due to the minimum detection limit of the aethalometer were small
compared with the average aethalometer response in the altitude bin. Error
bars shown in the profiles are based on 3 times the minimum detectable limit
of the aethalometer and correspond to a change in the transmission of the
filter deposit of 0,075%. The error bars are different at different altitudes
because they are inversely proportional to the volume of air sampled in a
given altitude bin.

In figs. 117 and 118 vertical profiles of graphitic carbon concentrations
vs. altitude are shown for AGASP flights 8 and 10 respectively in the Norwegian
Arctic. Flight 8 was essentially in a northerly direction over Bear Island to
northern Spitzbergen at 80°N, 15°E; it then returned to Bodø. The flight
profile included a slow descent from 7 km to 0.1 km at 74°N, 25°E near Bear
Island. The graphitic carbon concentrations as a function of altitude are
shown for this descent in fig. 117. Also shown for comparison are the average
ground-level concentrations found at BRW for April 1982, and the annual
average ground-level concentrations found in various urban areas in the United
States. It is clear from this figure that the vertical profile has consider-
able structure, with at least three layers located at approximately 1.0 km,
2.5 km, and 4.5 km, and what appears to be a very narrow layer at 1.7 km. The
haze layers can have sharp boundaries with dramatic changes in concentration
over distances less than 100 m. The concentrations within these layers are
large; the peak concentrations at 1 km are as large as typical ground-level
concentrations in the United States (Berkeley, Denver, Gaithersburg) and only
about a factor of 2.5 lower than those in New York City. The concentrations
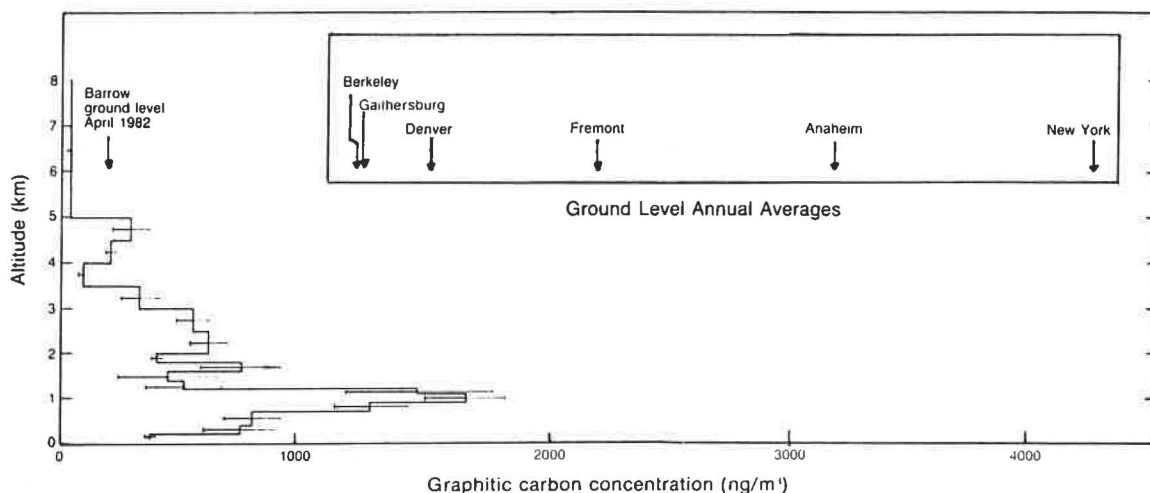in this band are about a factor of 10 higher than the April 1982 ground-level

Figure 117.--Vertical profile of graphitic carbon concentrations, ex-
pressed as ng m^{-3}, on AGASP flight 8, 31 March 1983 at ~74°N, 25°E.
Shown for comparison are the annual average ground-level graphitic
carbon concentrations at various urban locations in the United States
and the average April 1982 ground-level values at BRW. See text for a
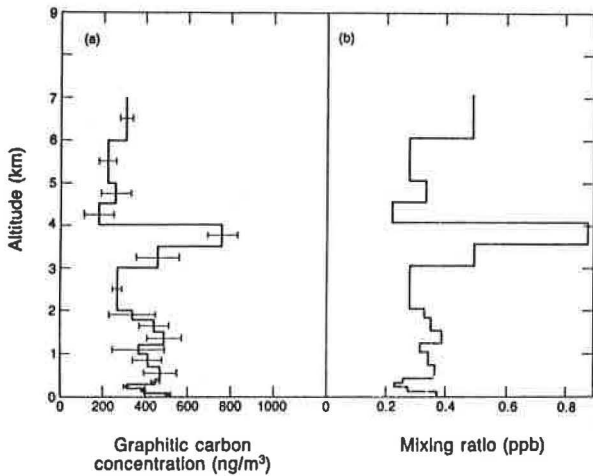discussion of the error bars.

Figure 118.--Vertical profile of graphitic carbon concentrations on AGASP flight 10, 5 April 1983 at ~70°N, 0°E, expressed (a) in ng m^{-3} and (b) as a mixing ratio (ppb).

concentrations at BRW (0.15 μg m^{-3}). The flight profile also indicates a relatively clean region at low altitudes, which is consistent with the BRW results (Hansen and Rosen, 1984) and the limited ground-level measurements made in the Norwegian Arctic.

Flight 10 also originated in Bodø, Norway, but flew west across the Norwegian Sea on 5 April 1983 to an area near 70°N, 0°E over the open ocean and then returned to Bodø. The plane remained within 70° ± 2° latitude and ranged from 5°E to 5°W in longitude between 0914 and 1604 GMT. The average vertical profile of graphitic carbon concentrations for this period is shown in fig. 118a. This profile is quite distinct from the one shown in fig. 117; it has much less structure with only one sharp band at 3.75 km superimposed over an almost uniform haze layer, decreasing only slightly with altitude even close to the top of the troposphere. If this profile is plotted as a mixing ratio, as in fig. 118b, it is essentially flat to the top of the troposphere, with a very intense band located at about 3.75 km. This profile could indicate significant transport at high altitudes above the planetary boundary layer. However, it may also be indicative of changes in the vertical distribution that have occurred after the air mass has reached the Arctic.

Acknowledgment

5.13 SO_2, Ozone, and Aerosol Over MLO Since El Chichon

W. F. J. Evans, G. M. Shah, and J. B. Kerr
Atmospheric Environment Service
Downsview, Ontario, M3H 5T4, Canada

5.13.1 Introduction

The El Chichon volcano in southern Mexico, which erupted between 28 March and 4 April 1982, injected enormous amounts of SO_2, H_2O, fine ash, and other debris into the troposphere and stratosphere, and provided a unique measure-

ment opportunity for the characterization of the distribution of the volcanic cloud and the assessment of its optical and radiative properties.

In April 1982, after the eruption of El Chichon, the Experimental Studies Division at AES began a study of SO_2, ozone, and aerosol optical depth in the atmosphere at several sites including MLO. During the same period, arrangements were made to make similar measurements on the NASA CV 990 flying laboratory on a latitude survey mission. The first flight was carried out in early May 1982. Subsequent flights were carried out in July and December 1982 and May 1983.

This report presents the measurements of SO_2, ozone, and aerosol optical thickness made at MLO between April 1982 and December 1983.

5.13.2   Instrumentation

The Brewer spectrophotometer (Brewer, 1973), calibrated against the standard Dobson spectrophotometer, was used to measure SO_2 and ozone. It is a remote sensing instrument that measures SO_2 and ozone by the absorption of the solar ultraviolet spectrum as it traverses the stratospheric layers. On the ground, the instrument is pointed at the Sun, and the intensity of light in the ultraviolet absorption spectrum of ozone at five wavelengths (306.3, 310.1, 313.5, 316.8 and 320.1 nm) with a resolution of 0.6 nm is measured. Sulfur dioxide also has strong variable absorption in this spectral region.

The optical depth measurements were made with a sunphotometer (Shah, 1979), a small hand-held instrument that is manually pointed at the Sun. The spectral selection is obtained by manually switching through a sequence of narrowband (HBW 10 nm) interference filters centered at 380-, 500-, 862-, and 935-nm wavelengths. The sunphotometer was calibrated by the Langley method in Boulder, CO, in December 1981 and at MLO in September 1982.

5.13.3   Observations

Figure 119 presents the monthly means of the apparent SO_2 column overburden measured at MLO from April 1982 to November 1983. Just after the
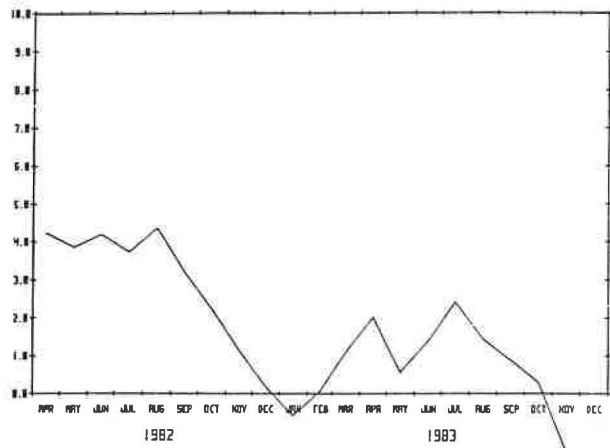

Figure 119.--Monthly means of sulfur dioxide (milli-atm-cm) in the atmosphere measured with the Brewer spectrophotometer at MLO.

155

eruption in May 1982, the SO_2 amount was over 4.0 milli-atm-cm and reached its maximum of 4.5 milli-atm-cm in August 1982. It decayed slowly with time, and by the end of the year, it had decreased to less than 0.5 milli-atm-cm (estimated threshold of detection). In 1983, the maximum SO_2 amount of about 2.5 milli-atm-cm was found in July, and then it decreased to less than 0.5 milli-atm-cm in October.

On the basis of the latitudinal distribution of SO_2 from aircraft measurements and SO_2 column overburden measurements with time at Hawaii, Evans and Kerr (1983) have estimated the total amount of SO_2 injected by El Chichon to be over 13 Mt. This is consistent with total sulfate aerosol mass of 14 Mt estimated by Shah and Evans (1984) from aircraft measurements of optical depths.

Figure 120 presents the monthly means of total ozone measured at MLO from April 1982 to December 1983. A maximum of 276 milli-atm-cm was found in April 1982, and a minimum of 220 milli-atm-cm was found in January 1983. Total ozone again increased with a seasonal maximum of about 266 milli-atm-cm in June 1983.

The total ozone values for the months of August 1982 to January 1983 are about 8% on an average lower than those found for the same period in 1983. This reduction in ozone is attributed to the El Chichon eruption cloud. Comparison of ozone data for August to January of 1980, 1981, and 1983, published by AES in cooperation with WMO (Ozone Data for the World, World Ozone Data Center, Atmospheric Environment Service, 4905 Dufferin Street, Downsview, Ontario M3H5T4), has indicated that the values were very similar for those periods.

Figure 121 presents the monthly means of the aerosol optical thickness at 500-nm wavelength calculated from the measurements of the extinction of solar radiation made at MLO from April 1982 to December 1983. Large increases in
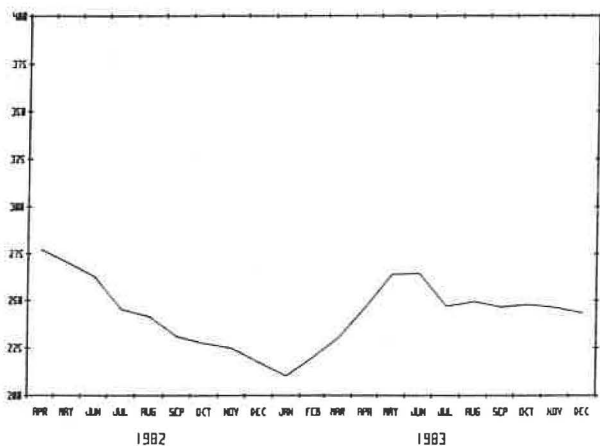

Figure 120.--Monthly means of total ozone (milli-atm-cm) in the atmosphere measured with the Brewer spectrophotometer at MLO.
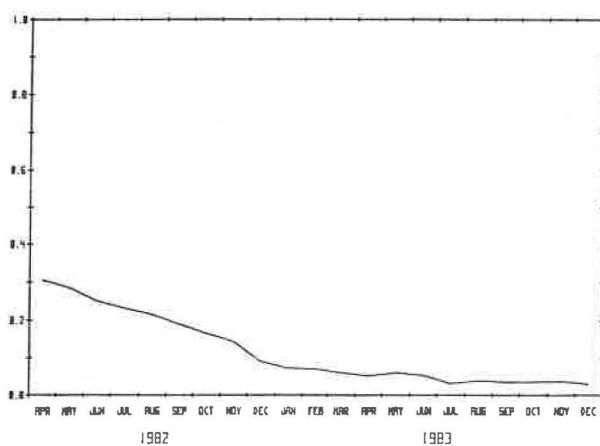
Figure 121.--Monthly means of aerosol optical thickness in the atmosphere at 500-nm wavelength measured with the sunphotometer at MLO.
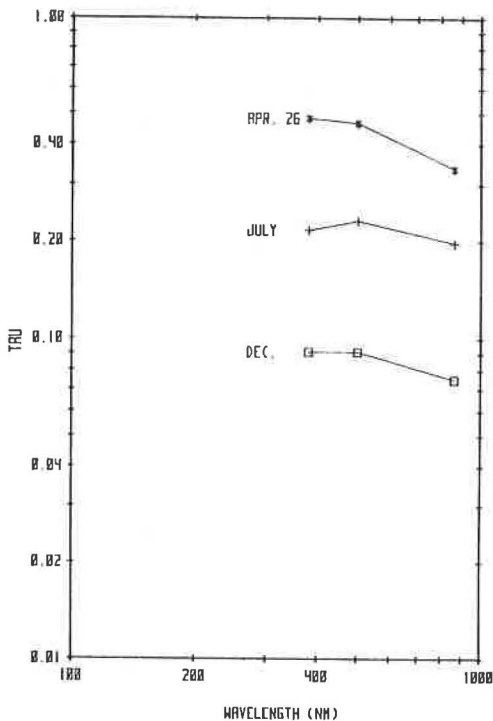
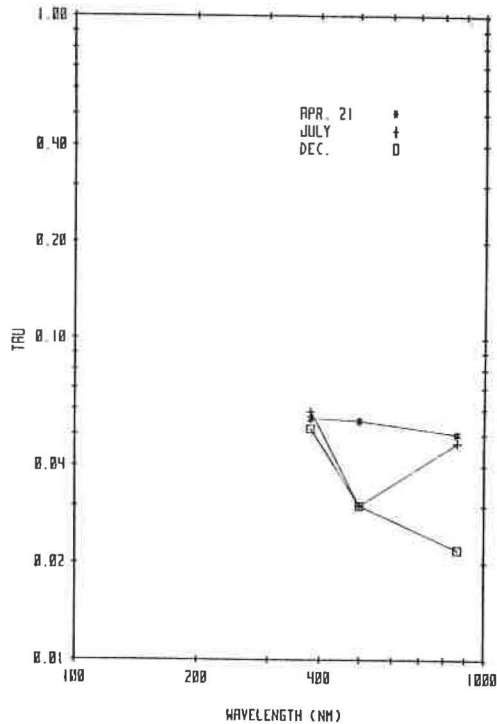Figure 122.--Spectral dependence of monthly means of aerosol optical thickness τ in 1982.

Figure 123.--Spectral dependence of monthly means of aerosol optical thickness τ in 1983.

optical thickness were observed at all wavelengths just after the El Chichon eruption. The cloud had stabilized by the end of May 1982, and it decayed slowly to less than 0.1 in December 1982. The optical thickness continued to decrease, and by May 1983 it was below 0.05, nearly the background level. It remained at that level for the rest of the year.

Figures 122 and 123 are plots of mean monthly aerosol optical thickness, $\tau(\lambda)$ vs. wavelength λ on a log-log scale graph. From April 1982 to April 1983, the spectral variation of optical thickness was essentially flat. In July 1983, a strong inflection was found at 500-nm wavelength, and in December 1983 log $\tau(\lambda)$ decreased monotonically with an increase in wavelength.

5.13.4 Discussion

The SO_2 measurement at MLO indicates the slow decrease of SO_2 over several months as the sulfate aerosol occurred by the conversion of SO_2 into H_2SO_2, and was removed by sedimentation and vertical transport.

The time variation of optical depth at MLO demonstrates the morphology of the growth and decay of the resulting volcanic sulfate layer. The optical depth measurements show that the El Chichon eruption cloud produced the largest optical depth increase in the Northern Hemisphere since Krakatoa in 1883. A perturbation of this size in the incident solar flux should be of interest to climatologists in future years.

The ground-based measurements at MLO together with the aircraft measurements of SO_2 have provided an estimate of the amount of SO_2 injected by El Chichon into the stratosphere. It is hoped that these measurements will provide a significant contribution to the data base for the most measured volcanic climate event in history.

Acknowledgments

5.14 Optical and Chemical Features of Aerosol Present in the Arctic Snowpack

A. D. Clarke and K. J. Noone
Civil Engineering Department
University of Washington, Seattle, WA 98195

Since the early reports of banded-haze structures in the Arctic atmosphere (Mitchell, 1957), several investigators have identified relatively high concentrations of light-absorbing particles associated with these haze events at ground level (Barrie et al., 1981; Heintzenberg, 1982). Some of these measurements have identified elemental carbon (soot) as the primary absorber and suggest anthropogenic emissions as the primary source (Rosen et al., 1981). The presence of aerosols with high specific absorption, such as soot, have raised questions about perturbations to the radiative fluxes in this region that are due to Arctic haze. Assessment of such perturbations can be gained through determination of the aerosol light-scattering coefficient and the aerosol light-absorption coefficient. Taken together, these coefficients define the single-scattering albedo, which determines their net effects in the equations that govern radiative transfer in the atmosphere. During the past 2 years we have actively participated in NOAA-AGASP and University of Washington flight programs in the Arctic and measured these radiatively important parameters. Our results, recently reported elsewhere (Clarke et al., 1984), support evidence of combustion sources for the Arctic haze aerosol and indicate concentrations of light-absorbing aerosol of 1-2 orders of magnitude above tropospheric background values. These measurements also indicate possible aerosol heating rates on the order of $0.1^{\circ}C$ day^{-1}, values that are well above background but less than some other terms affecting atmospheric heating rates (Porch and MacCraken, 1982).

In addition to the atmospheric aerosol measurements made under our Arctic haze program, we have initiated a wide-ranging study of the aerosol present in the Arctic snowpack. Because of the high surface albedo of uncontaminated fresh snow, trace concentrations of light-absorbing material (e.g., soot) in the snowpack can markedly effect its albedo and alter the amount of solar radiation absorbed at the surface (Warren and Wiscombe, 1980; Chylek et al., 1983). In sufficient quantity, such soot could affect snowmelt rates and result in both primary and secondary effects on radiative climate parameters. Furthermore, once deposited on the snowpack, inert soot is likely to remain and accumulate on the surface during snowmelt and become exposed to the increased Arctic solar insolation even after elevated levels of springtime Arctic haze have dissipated. Consequently, our program attempts to collect snow from representative locations throughout the Arctic, and to determine the
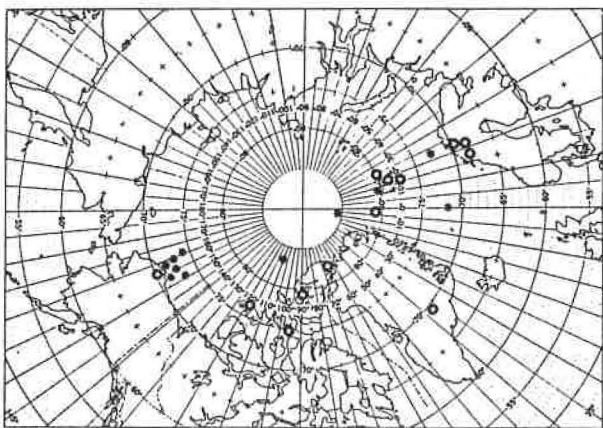
Figure 124.--Map of Arctic sampling locations for the University of Washington atmospheric (black stars) aircraft samples and snowpack (white stars) samples for 1983-1984.

amount of light-absorbing material in the snowpack and the fraction of absorption that can be attributed to soot.

The network of stations providing snow samples for 1983-1985 are indicated in fig. 124, and the samples collected to date are indicated in table 45. Most samples were collected during winter months and kept frozen until analysis. This procedure minimizes possible losses of particulate material to the container walls (600-cm^3 glass jar) and spurious effects due to algae growth or chemical reaction after sampling. Analysis began in March 1984 on some randomly selected representative samples from each location. Initial extraction of particulates was accomplished by dual sequential filtration of meltwater obtained from rapid microwave melting of the sample. The filters were analyzed for visible light absorption at four wavelengths

Table 45.--Arctic snow samples collected under the current University of Washington field program

	1983	1984
BRW	11	6
Spitzbergen (Norway)	9	6
Resolute (Canada)	5	5
Eureka (Canada)	4	4
Alert (Canada)	4	4
Mould Bay (Canada)	4	4
Dye 3 (Greenland)	24	0
Ice Floe 80°N (Greenland)	12	0
Abisko (Sweden)	0	20
Karesuando (Sweden)	0	3
Kautokeno (Norway)	0	3
Alta (Norway)	0	4
Total	73	59

(475, 525, 660, 800 nm) using either the integrating plate method (Lin et al., 1973) and/or integrating sandwich method (Clarke, 1982). The filtrate was then measured for pH and conductivity before being refrozen or refrigerated for later measurement of major ions using ion chromatography.

Results of the optical analysis for several random snow samples are indicated in fig. 125. To compare the behavior of samples with different concentrations, the absorption measured at each wavelength is divided by the 550-nm value, and the normalized absorption wavelength dependence indicated is obtained. Four wavelengths are used to help discriminate absorption due to crustal aerosol compared with absorption due to soot. Figure 125 illustrates
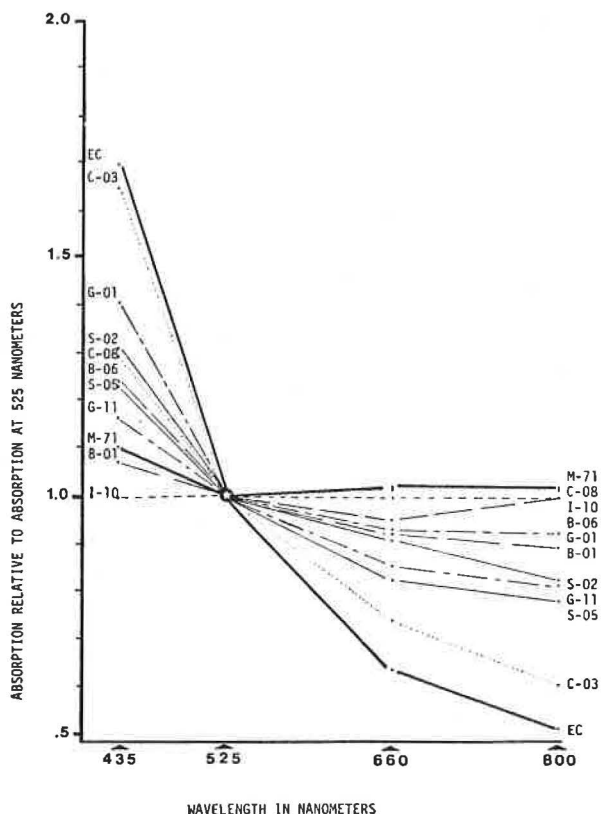
Figure 125.--Normalized wavelength dependence of particulate light absorption for Arctic snow samples in table 45. Heavy lines are for El Chichon volcanic ash (EC) and a prepared calibration soot, Monarch 71 (M-71); the remaining samples are identified in table 46 and discussed in the text.

the wavelength dependence of several samples compared with those characteristic of prepared submicron calibration soot (Monarch 71, Cabot Corp.) and crustal material (El Chichon volcanic ash), both emphasized by heavy lines in the same figure. The majority of these samples indicates that the light absorption due to particulates is dominated by soot in most locations, and that crustal material is present but generally of secondary importance. It should be noted that the greatest crustal influence appears in the sample from Resolute, Canada (C-03). This sample was collected close to the local airport where low precipitation and substantial exposed soil was noted. In contrast, the clearest soot signatures are present in the most remote samples collected

on ice floes at 80°N (I-10) and for the samples from BRW (B-01, B-06). The wavelength dependence of absorption is similar for the Greenland (G-01, G-07) and Spitzbergen (S-02, S-05) samples and suggests absorption due to both soot and crustal components, with the former slightly dominant. It is of interest to note that the mixing ratios measured in the snow samples (average 2×10^{-8}) are consistent with those expected from applying scavenging ratios (Barrie and Neustadter, 1983) to the typical atmospheric concentrations of elemental carbon ($\sim 2 \times 10^{-7}$ g m^{-3}) obtained during our 1983 aircraft measurements (Clarke et al., 1984).

The slope of the wavelength dependence in fig. 125 can be used to provide an approximate estimate of the relative contribution of soot to particulate light absorption. This estimate has been used in conjunction with the measured light absorption values at 550 nm to obtain the apparent soot mass per mass of liquid water in each sample. Recent model calculations (S. Warren; University of Washington, Seattle; personal communication, April 1984) indicate that a 1% change in snow albedo (a minimum detectable effect relative

Table 46.--Arctic haze snow sample data

| I.D. | Date | Location | Type (depth) | Concentration in snow melt (ppm) | | | | | [C (g)/ H$_2$O (g)] $\times 10^9$ | pH | Cond. (μmho) |
				NA$^+$ (12%)*	NH$_4^+$ (50%)*	K$^+$ (50%)*	NO$_3^-$ (14%)*	SO$_4^=$ (8%)*			
B-01	830413	BRW	Old (1-15 cm)	?	--	--	--	8.96	12	6.10	2500
B-02	830413	BRW	Old (2-4 cm)	?	--	--	--	6.06	13	6.15	?
B-04	830413	BRW	Old (3-15 cm)	33.8	--	2.0	0.39	8.20	32	5.50	366
B-05	830413	BRW	Old (15-30 cm)	60.5	--	5.3	0.28	4.82	16	5.60	764
B-06	830420	BRW	Fresh (surface)	19.2	--	--	0.40	2.75	52	5.50	221
C-03	830311	Resolute	Fresh (surface)	?	--	--	--	0.14	?	6.30	?
C-08	831117	Mould Bay	Fresh (surface)	0.35	--	0.38	0.11	0.20	35	6.12	11.3
IF-01	830715	Ice Floe	Fresh (surface)	0.54	--	0.75	0.06	0.15	3	6.55	9.5
IF-10	830717	Ice Floe	Old (5-20 cm)	?	--	--	--	0.95	9	5.6	?
G-01	830516	Greenland	Recent (0-12 cm)	0.24	0.14	0.12	0.18	0.09	21	5.92	3.1
G-03	830216	Greenland	Old (12-22 cm)	0.57	0.14	0.12	?	?	10	5.7	3.3
G-11	830423	Greenland	Fresh (surface)	0.46	0.01	0.20	--	0.05	11	6.0	?
S-02	830516	Spitzbergen	Old (10-20 cm)	1.29	--	0.56	0.09	0.88	55	6.05	14.8
S-05	840108	Spitzbergen	Fresh (0-10 cm)	0.56	0.03	0.12	0.08	0.43	25	6.0	4.5
SS-02	840308	Spitzbergen	Fresh (surface)	0.53	--	0.05	0.15	0.64	6	5.10	22.8

Note: ? means not measured;-- means below detection limit.
* % uncertainty in analytic measurement.

to pure snow) could be expected for $\sim 1 \times 10^{-8}$ mass fraction of soot in fresh snow and 0.3×10^{-8} in coarse-grained, aged snow. Estimated soot mass fractions obtained from the slopes for fig. 125 samples are included in the data summary found in table 46. The range of values is $\sim(0.3-5.5) \times 10^{-8}$ for this limited data set. If these values are typical of the samples that remain to be analyzed (~ 100), then soot appears to be common in concentrations capable of reducing fresh snow albedo by 1%-3% (a measureable effect). This reduction for a given initial soot mass fraction in fresh snow may increase during a season to as much as 10% for some of these samples because of snow ablation, melting, and morphological changes in grain size (S. Warren; University of Washington, Seattle; personal communication, April 1984). The lowest mass fraction is seen in a fresh summer snowfall (IF-01) and is approximately an

order of magnitude lower than average winter values. This is consistent with an order of magnitude winter-summer variability seen in other atmospheric aerosol measurements (Heintzenberg, 1982).

Chemical data reported in table 46 were obtained from the meltwater filtrate subsequent to the extraction of insoluble components. The random selection of these samples makes any interpretation of chemical signatures premature. This is particularly true of older snow where soluble ions may have migrated during periods of partial melting. However, the BRW samples (including fresh snow) clearly have major ion concentrations and conductivity up to 2 orders of magnitude higher than other samples. Because the mass mixing ratio of carbon is not greatly elevated for the BRW samples, it is likely that a natural aerosol such as seasalt may be primarily responsible. The lowest concentrations of major ions and light-absorbing aerosol is found for the Ice Floe ($80°N$, $4°W$) and at Dye 3 in Greenland. If one observes the relationship of pH to conductivity (Winkler, 1980), the deduced free acidity of these samples appears to be less than 5%. We intend to improve on the above data through the more complete analysis of the entire sample set that is currently under way.

In summary, climatic impacts may arise from the scavenging and accumulation of absorbing material into the Arctic snowpack to result in a reduced surface snow albedo. Measurements are reported here on the aerosol deposited to the snowpack at diverse Arctic sites including visible light absorption at four wavelengths. Preliminary data on the wavelength dependence of absorption (430-800 nm) indicate that soot is primarily responsible for aerosol light absorption in snow at most locations under investigation and is present at concentrations that may appreciably affect snow albedo. Crustally derived material in the snow pack appears as a minor contributor to visible light absorption at most locations but may play a secondary role at several others. More extensive measurements are presently being assessed throughout the Arctic under the snow sampling program currently under way. After the remaining samples are analyzed, it is hoped that information can be obtained about the areal distribution of soot in the snowpack and its relationship to other measured chemical features. Spatial and temporal effects of these concentrations on snow albedo will be modeled to determine the possible impact on Arctic radiative transfer and climate.

Acknowledgments

5.15   Global Atmospheric Measurements of CH_4 and CO_2 by Gas Chromatography

L. P. Steele
NRC-NOAA Research Associate
Geophysical Monitoring for Climatic Change, NOAA/ERL/ARL, Boulder, CO   80303

P. J. Fraser[*]
Research Assoc., Cooperative Institute for Research in Environmental Sciences
University of Colorado, Boulder, CO   80309

R. A. Rasmussen, M. A. K. Khalil, and A. J. Crawford
Oregon Graduate Center
Beaverton, OR   97006

T. J. Conway and R. H. Gammon
Geophysical Monitoring for Climatic Change
NOAA/ERL/ARL, Boulder, CO   80303

During 1983 a cooperative program between CSIRO, NOAA/GMCC, and OGC was initiated by P. Fraser of CSIRO while visiting GMCC for 1 year as a CIRES Research Associate. The major purpose of the program is to investigate any possible relationship between the observed seasonal cycles of both methane (CH_4) and CO_2 in the atmosphere.

This program uses the existing NOAA/GMCC global network of flask sampling sites to provide samples of air for analysis by gas chromatography for its CH_4 and CO_2 content. The gas chromatographic procedures adopted are similar to those described by Rasmussen and Khalil (1981) using Carle model 211-M gas chromatographs fitted with flame ionization detectors. One of the gas chromatographic systems used in this work has been loaned to NOAA/GMCC by R. Rasmussen of OGC. About 500 flask samples taken at approximately weekly intervals at 20 sites were analyzed during 1983. The gas chromatographic analysis is carried out on only one of the pair of flasks normally filled using the P^3 sampler, and is performed prior to the analysis of both members of each pair for the CO_2 concentration by the method of infrared absorption. This procedure is possible because of the slight pressure above ambient that is achieved in the flasks at the time of sampling. The excess pressure is used to purge the low-volume sampling system of the chromatograph, including the sample loop itself, which has a volume of about 2 mL. This purging and filling procedure consumes only small quantities (~20 mL) of air sample. The analysis of every flask air sample is bracketed by the analysis of a sample of calibration gas.

The calibration gases used in the program are those supplied by R. Rasmussen, and are regularly intercalibrated with a suite of CH_4 standards maintained by him at OGC. In addition, routine intercalibrations with an NBS CH_4-in-air standard gas with a nominal concentration of 1 ppm are performed. To date, no significant drift in the CH_4 concentration of the calibration

---

[*]On leave from Division of Atmospheric Research, CSIRO, Mordialloc, Victoria, 3195 Australia.

gases has been detected. The CO_2 concentration of these calibration gases is checked routinely against standards maintained at NOAA/GMCC using the method of infrared absorption.

To check the reliability of CH_4 concentrations in air samples collected in the 500 cm^3 glass flasks with greased (Apiezon N) stopcocks, a number of storage tests have been performed. In one test, air samples were analyzed as soon as the flasks arrived in Boulder, and a selection of those flasks with sufficient remaining pressure was set aside for periods of time ranging from a few days to several weeks, and then analyzed again. In another test, flasks were filled to a pressure a little above ambient with a known CH_4-in-air calibration gas from a cylinder. Some of these flasks were analyzed immediately, while others were set aside for periods up to 6 months, and then analyzed. The results of all these tests indicate that CH_4 is remarkably stable in these glass flasks, with no evidence of either a loss or a gain in concentration. This appears to be so whether the air sample in the flask is dry or not.

The routine precision of these gas chromatographic measurements can be estimated readily since, whenever possible, at least two aliquots are taken from each flask for analysis. Histograms of differences between the concentration in the first and second aliquot show no significant bias for either CH_4 or CO_2. These histograms also show the distribution of these differences to be approximately normal, yielding an estimate of the standard deviation (based on several hundred samples) of 4 ppbv for CH_4 and 0.8 ppm for CO_2. This level of precision for CH_4 is very good, but for CO_2 is significantly worse than that routinely achieved at NOAA/GMCC with the method of infrared absorption.

Since the CO_2 concentration is determined in these flasks by two different methods of analysis, the results have been compared by means of a histogram of differences in concentration obtained from both methods. The histogram obtained from several hundred samples is approximately normal, but with a mean value of 0.6 ppm and a standard deviation of 0.9 ppm. The gas chromatographic estimate is almost always larger than that found by the infrared method. This surprising result cannot be explained by calibration errors, since both types of measurements are referenced to the same calibration standards.

Although the NOAA/GMCC flask sampling network gives relatively good global coverage, it was decided to supplement these samples with data from oceanographic cruises. The results so far from this type of comparison indicate that in general the network gives a very reliable guide to the background concentration of both CH_4 and CO_2. This is illustrated in fig. 126 which shows the monthly mean CH_4 concentrations for November 1983 at a number of the network sampling sites, together with flask samples taken by L. Waterman on the cruise of the AKADEMIK KOROLEV during 25 October-14 November 1983 in the mid-Pacific. It should be noted, however, that the location of the very abrupt change in concentration near the Equator is not detected in data from the network alone because of the scarcity of sites in this latitude band.

Given the early stage in the development of this program, it is too soon to evaluate the data fully. However, several features are already apparent. The latitudinal gradients of CH_4 (see fig. 126) confirm the results of previous measurements (e.g., Khalil and Rasmussen, 1983b) and are the most
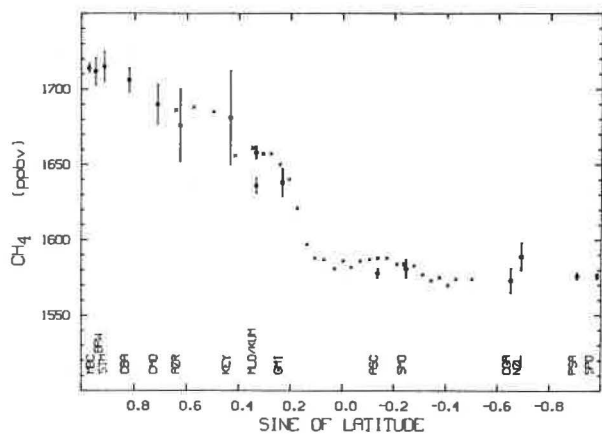
Figure 126.--Monthly mean CH$_4$ concentrations for November 1983 determined from NOAA flask sampling sites (dots). Error bars indicated are 1 standard deviation from the mean value. Data indicated by × are individual flask values taken on the cruise of the AKADEMIK KOROLEV during 25 October-14 November 1983 in the mid-Pacific.

detailed of any available at this time. Measurements of CH$_4$ in the Southern Hemisphere are in excellent agreement with previously published data (Fraser et al., 1984), but for the first time the remarkable uniformity of background CH$_4$ concentrations over most of this hemisphere has been demonstrated. The time series of CH$_4$ at most sites in the Northern Hemisphere also show good agreement with the type of seasonal behavior described by Khalil and Rasmussen (1983b), that is, a strong minimum during the northern summer.

6. INTERNATIONAL ACTIVITIES

In June 1983, GMCC hosted a WMO meeting of experts on CO_2 concentrations from pre-industrial time to the IGY. Fourteen international experts participated in the discussion. A summary of the meeting, presented by W. Elliott in EOS (26 June 1984), was entitled "The Pre-1958 Atmospheric Concentration of Carbon Dioxide."

J. Peterson participated in the WMO Technical Conference on Observation and Measurement of Atmospheric Contaminants held in Vienna, Austria, during October 1983. He presented papers with W. Komhyr on CO_2 measurements at BRW, with R. Schnell on AGASP, and with J. DeLuisi, E. Dutton, and E. Flowers on NOAA turbidity measurements. He also gave a summary report to conclude the conference. All of these reports will be presented in a WMO document on the conference proceedings.

W. Komhyr and R. Evans visited Haute Provence Observatory, France, during late August-early September 1983 to install automated Dobson instrument no. 85 at the observatory and implement a program of total ozone and Umkehr observations. Haute Provence Observatory is one of seven global sites where Umkehr observations will be made on a long-term basis using automated Dobson instruments to monitor possible atmospheric ozone depletion by halocarbons near 40-km altitude.

W. Komhyr visited Aire Sur L'Adour, France, 2-17 September 1983 to participate in MAP/GLOBUS balloon ozone instrument comparisons. Successful experiments were conducted on two occasions.

CIRES Research Assistant, A. Chopra of the Indian Meteorological Service, New Delhi, India, completed his assignment with GMCC and returned to India in December 1983. While in Boulder, Chopra assisted with ECC ozonesonde evaluations, the 1983 MLO ECC ozonesonde observations program, and special ozone and SO_2 observations made at MLO following the eruption of El Chichon in late March-early April 1982.

Huancayo, Peru, Dobson instrument no. 87 was modernized, optically aligned, and recalibrated in August 1983, in preparation for automation of the instrument and its reestablishment in Huancayo for long-term Umkehr observations.

R. Gammon traveled to Leningrad, U.S.S.R., in July 1983 to participate in a meeting of experts on anthropogenic climatic change. The travel was under the auspices of the U.S.-U.S.S.R. bilateral scientific exchange agreement, Working Group VIII. He gave a talk entitled "Global Atmospheric CO_2, 1968-1983: Summary of the United States/NOAA Monitoring Program."

R. Gammon also attended the IAMAP/IUGG Symposium in Hamburg, F.R.G., in August 1983. He gave two papers: the first, by Gammon and Komhyr, was entitled "Response of the Global Atmospheric CO_2 Distribution to the Atmospheric/Oceanic Circulation Perturbations in 1982"; the second, by Komhyr, Gammon, and Gillette was "The Southern Ocean Sink for Atmospheric CO_2."

R. Gammon also participated in the oceanographic cruise of the ship KNORR based out of Woods Hole Oceanographic Institution. The ship sailed from Dakar, Senegal, to Recife, Brazil. This cruise was part of the tropical

Atlantic study of the Transient Tracers in the Ocean Program. One of the objectives was to measure chlorofluorocarbons in the ocean, which are very useful as an index of ocean circulation.

Flask sampling for CO_2 analysis at Halley Bay, Antarctica (75°S, 27°W), began in 1983 in cooperation with the British Antarctic Survey. In June a second year's supply of flasks was shipped to England for transshipment to Halley Bay for sampling in 1984. The 1983 samples will return to Boulder for analysis during the summer of 1984. Initial inquiries were made to D. Walton of BAS concerning the possibility of obtaining flask samples at South Georgia Island, as a replacement for the discontinued Falkland Islands site.

Agreements were reached with C. Keeling of SIO to begin flask sampling at Christmas Island (2°N, 175°W) and with P. Fraser of CSIRO to begin sampling at Cape Grim, Tasmania (41°S, 145°E). Both programs, scheduled to start in 1984, will fill existing gaps in the GMCC CO_2 flask network coverage and will provide interlaboratory comparison data.

From 22 October to 5 December, L. Waterman participated in the Soviet-American Gases and Aerosols Expedition aboard the Soviet research vessel AKADEMIK KOROLEV. Measurements of CO_2 and CH_4 in the atmosphere, and pCO_2 and pCH_4 in surface waters were made by the method of gas chromatography, between 40°N and 30°S in the mid-Pacific Ocean. The joint cruise was organized through the U.S.-U.S.S.R. Working Group VIII Committee on the Environment and included measurements of several gases, aerosols, and oceanographic parameters by Soviet and American scientists using a variety of techniques.

A noncontaminating gas transfer pump used for analyzing flask air samples for CO_2 concentration (Komhyr et al., 1983b) was built for C.S. Wong of the Institute for Ocean Sciences, British Columbia. In conjunction with this transfer of technology, G. Smith of IOS visited GMCC for a week in August for discussions of CO_2 measurement systems and testing of the new transfer pump.

N. Trivett of Environment Canada, AES, Downsview, Ontario, visited GMCC for 2 days in October to discuss AES plans to begin in situ continuous monitoring of atmospheric CO_2 by NDIR analysis at Alert, Northwest Territory. AES is planning a comprehensive measurement program at Alert similar to those at the GMCC baseline observatories.

J. DeLuisi issued a call to lidar research scientists having sites in the United States, Japan, Europe, South America, and Australia for a collaborative global stratospheric aerosol monitoring program to support Umkehr observations of stratospheric ozone profiles. The lidar data will be used to improve the quality of the Umkehr measurements because of their susceptibility to errors caused by stratospheric aerosols. All responses to the call were positive. Arrangements are being made to archive data in the Canadian-issued book, Ozone Data for the World. DeLuisi submitted to the WMO a preliminary lidar data archiving format. He arranged a meeting of lidar scientists at the Twelfth International Radar Conference to formulate activities of the group and discuss the preliminary data format. He also prepared a paper (given by P. McCormick of NASA/Langley at that conference) on the application of lidar measurements for correction of Umkehr measurements.

R. Schnell, director of AGASP, traveled to Alaska, Canadian Arctic, Greenland, and Norway with 40 people in the field operation. He also helped

organize and conduct the Ringberg Castle Arctic Haze Symposium, Kreuth, F.R.G., 5-9 September 1983. AGASP supported nine scientists attending this meeting.

B. Bodhaine also traveled to Kreuth, F.R.G., to participate in the Ringberg Castle Arctic Haze Meeting. This meeting provided the participants a first opportunity to discuss and compare Arctic haze data obtained during the AGASP flight program in March-April 1983. In addition to giving presentations of preliminary data, the attendees discussed plans for comprehensive publication of the AGASP data.

P. Steele, visiting scientist from Australia, continued his appointment at GMCC as an NRC-NOAA Research Associate during 1983. His work continued on the modeling of the global carbon cycle. He also became heavily involved in the cooperative program between CSIRO, NOAA/GMCC, and OGC to use gas chromatographic methods to measure CH_4 and CO_2 concentrations in the flask air samples routinely received from the GMCC global flask sampling network.

P. Fraser of CSIRO, Division of Atmospheric Research, finished a 1-yr position as a CIRES Research Associate sponsored by GMCC, departing in November 1983. His appointment continued an informal, reciprocal arrangement for cooperative research by the staffs of NOAA and CSIRO. During his visit, he undertook a detailed comparison of gas chromatographic and infrared absorption techniques for the measurement of CO_2 concentrations in the atmosphere. His major contribution was an investigation into the feasibility of measuring methane and CO_2 by gas chromatographic techniques from the 0.5-L glass flasks routinely collected for the CO_2 program. By conducting an extensive series of laboratory tests, he determined that a small volume of air could be taken from the flasks prior to CO_2 analysis without influencing the gas concentrations within the flask. Largely through his efforts, a pilot program was begun for routine global-scale CH_4 measurements based on flask analyses. Some preliminary results are presented in sec. 5.15.

W. Raatz from the F.R.G. began a 1-yr term as an NRC-NOAA Research Associate on 15 September 1983. He had participated in the AGASP project during spring 1983, and his objective is to continue work on the meteorological aspects of long-range transport leading to the presence of Arctic haze.

R. Boonprakai, a meteorologist in the Meteorological Department in Bangkok, Thailand, was a guest worker with the GMCC Division in Boulder, CO, from 14 April 1983 to 14 October 1983. Boonprakai was on a WMO training fellowship to receive technical training and experience in making atmospheric ozone and turbidity measurements. While here, she was trained on the Dobson spectrophotometer and the GMCC turbidity instruments. She participated in an international sunphotometer comparison and calibration workshop.

7. PUBLICATIONS AND PRESENTATIONS BY GMCC STAFF, 1983

Bodhaine, B. A.   Aerosol measurements at four background sites.   J. Geophys. Res.   88(C15):10753-10768.

Bodhaine, B. A.   Surface aerosol measurements at Barrow.   Paper presented at the Ringberg Castle Arctic Haze Workshop, Kreuth, F.R.G., 5-9 September 1983.

Bodhaine, B. A., J. J. DeLuisi, J. M. Harris, and R. C. Castillo.   Aerosol light scattering, condensation nuclei, and air mass trajectories at Whiteface Mountain.   Paper A12-05 presented at the AGU Spring Meeting, Baltimore, MD, 30 May-3 June 1983.

Bodhaine, B. A., J. J. DeLuisi, J. M. Harris, and R. C. Castillo.   Light scattering, condensation nuclei, and air mass trajectories at Whiteface Mountain: Summer 1982.   NOAA Data Rep. ERL ARL-3, NOAA Environmental Research Laboratories, Boulder, CO, 69 pp.

Bullister, J., R. Weiss, and R. Gammon.   Freon transient tracer distributions in the tropical Atlantic Ocean.   Paper presented at the AGU Fall Meeting, San Francisco, CA, December 1983.

DeLuisi, J. J., and J. M. Harris.   A determination of the absolute radiant energy of a Robertson-Berger meter sunburn unit.   Atmos. Environ. 17(4):751-758.

DeLuisi, J. J., E. G. Dutton, K. L. Coulson, T. E. DeFoor, and B. G. Mendonca.   On some radiative features of the El Chichon volcanic stratospheric dust cloud and a cloud of unknown origin observed at Mauna Loa.   J. Geophys. Res.   88(C11):6769-6772.

DeLuisi, J., E. Dutton, E. Flowers, and J. Peterson.   Recent developments in atmospheric turbidity measurements in the NOAA Geophysical Monitoring for Climatic Change Program.   Paper presented at the WMO TECOMAC Conference, Vienna, Austria, October 1983.

DeLuisi, J. J., B. G. Mendonca, E. G. Dutton, M. A. Box, and B. M. Herman.   Radiative properties of the stratospheric dust cloud from the May 18, 1980, eruption of Mount St. Helens.   J. Geophys. Res.   88(C9):5290-5298.

Dutton, E. G., and J. J. DeLuisi.   Optical thickness features of the El Chichon stratospheric debris cloud.   Paper presented at the Fifth Conference on Atmospheric Radiation, Baltimore, MD, 31 October-4 November 1983.

Dutton, E. G., and J. J. DeLuisi.   Spectral extinction of direct solar radiation by the El Chichon cloud during December 1982.   Geophys. Res. Lett.   10:1013-1016.

Gammon, R.   Global atmospheric CO_2, 1968-83: Summary of the United States/ NOAA monitoring program.   Paper presented at the Meeting of Experts on Anthropogenic Climatic Change, Leningrad, U.S.S.R., 3-9 July 1983.

Gammon, R. Global carbon dioxide distributions from the NOAA monitoring program: Implications for the global carbon cycle. Paper presented in the Climate Seminar Series, National Center for Atmospheric Research, Boulder, CO, December 1983.

Gammon, R., and W. Komhyr. Response of the global atmospheric CO_2 distribution to the atmospheric/oceanic circulation perturbations in 1982 (El Chichon-El Niño). Paper presented at the IAMAP/IUGG Symposium, Hamburg, F.R.G., August 1983.

Gammon, R., W. Komhyr, and J. Peterson. The global atmospheric CO_2 distribution 1968-83: Interpretation of the results of the NOAA/GMCC measurement program. Paper presented at the Sixth Oak Ridge National Laboratory Life Sciences Symposium on the Global Carbon Cycle: Analysis of the National Cycle and Implications of Anthropogenic Alterations for the Next Century, Knoxville, TN, 31 October-3 November 1983, Dept. of Energy.

Gillette, D. A. Future research in resuspension. Proceedings, Fourth International Conference on Precipitation Scavenging, Dry Deposition, and Resuspension, Santa Monica, CA, 29 November-3 December 1982, H. R. Pruppacher, R. G. Semonin, and W. G. N. Slinn (eds.), Vol. 2, Elsevier, NY, 1443-1445.

Gillette, D. A. The concept of resuspension rates applied to problems of fugitive dust emissions and wind erosions. Proceedings, Fourth International Conference on Precipitation Scavenging, Dry Deposition, and Resuspension, Santa Monica, CA, 29 November-3 December 1982, H. R. Pruppacher, R. G. Semonin, and W. G. N. Slinn (eds.), Vol. 2, Elsevier, NY, 1059-1072.

Gillette, D. A. Threshold velocities for wind erosion on natural terrestrial arid surfaces (A summary). Proceedings, Fourth International Conference on Precipitation Scavenging, Dry Deposition, and Resuspension, Santa Monica, CA, 29 November-3 December 1982, H. R. Pruppacher, R. G. Semonin, and W. G. N. Slinn (eds.), Vol. 2, Elsevier, NY, 1047-1057.

Gillette, D. A., and K. J. Hanson. Sampling strategy to obtain data used in models of global annual CO_2 increase and global carbon cycle. J. Geophys. Res. 88(C2):1345-1348.

Gillette, D. A., and A. T. Steele. Selection of CO_2 concentration data from whole-air sampling at three locations between 1968 and 1974. J. Geophys. Res. 88(C2):1349-1359.

Halter, B., and J. M. Harris. On the variability of atmospheric carbon dioxide concentration at Barrow, Alaska, during winter. J. Geophys. Res. 88(C11):6858-6864.

Harris, J. M., and B. A. Bodhaine. Air mass trajectories in the Arctic. Paper presented (by Bodhaine) at the Ringberg Castle Arctic Haze Workshop, Kreuth, F.R.G., 5-9 September 1983.

Harris, J. M., and B. A. Bodhaine (eds.). Geophysical Monitoring for Climatic Change, No. 11: Summary Report 1982. NOAA Environmental Research Laboratories, Boulder, CO, 160 pp.

Komhyr, W. D. An aerosol and gas sampling apparatus for remote observatory use. J. Geophys. Res. 88(C6):3913-3918.

Komhyr, W., R. Gammon, and D. Gillette. The southern ocean sink for atmospheric CO_2: A two-dimensional model interpretation of the GMCC global atmospheric CO_2 distribution, 1979-82. Paper presented at the IAMAP/IUGG Symposium, Hamburg, F.R.G., August 1983.

Komhyr, W. D., L. S. Waterman, and W. R. Taylor. Semiautomatic nondispersive infrared analyzer apparatus for CO_2 air sample analyses. J. Geophys. Res. 88(C2):1315-1322.

Mastenbrook, H. J., and S. J. Oltmans. Stratospheric water vapor variability for Washington, DC/Boulder, CO: 1964-82. J. Atmos. Sci. 40(9):2157-2165.

Peterson, J. T., and K. J. Hanson. Report of Mount Kenya feasibility study. WMO/Environmental Pollution Monitoring Programme No. 12, World Meteorological Organization, Geneva, Chapter 6, 107-113.

Peterson, J. T., and W. D. Komhyr. Atmospheric CO_2 measurements at Barrow, Alaska. Paper presented at the WMO TECOMAC Conference, Vienna, Austria, October 1983.

Rasmussen, R. A., M. A. K. Khalil, and R. J. Fox. Altitudinal and temporal variation of hydrocarbons and other gaseous tracers of Arctic haze. Geophys. Res. Lett. 10(2):144-147.

Schnell, R. C. Aerosol measurements during AGASP. Paper presented at the Ringberg Castle Arctic Haze Workshop, Kreuth, F.R.G., 5-9 September 1983.

Schnell, R. C. Arctic haze and the Arctic Gas and Aerosol Sampling Program (AGASP). Proceedings of the 21st Aerospace Science Meeting, Reno, NV, January 1983.

Schnell, R. C., J. T. Peterson, and W. E. Raatz. Arctic Gas and Aerosol Sampling Program (AGASP). Paper presented at the WMO TECOMAC Confenerce, Vienna, Austria, October 1983.

Weiss, R., J. Bullister, and R. Gammon. Anthropogenic chlorofluoromethanes in the tropical Atlantic. Paper presented at the IAMAP/IUGG Symposium, Hamburg, F.R.G., August 1983.

8. REFERENCES

Angell, J. K., and J. Korshover, 1983. Global temperature variations in the troposphere and stratosphere, 1950-1982. Mon. Weather Rev. 111:901-921.

Bacastow, R. B., 1976. Modulation of atmospheric carbon dioxide by the Southern Oscillation. Nature 261:116-118.

Bacastow, R., 1977. Influence of the Southern Oscillation on atmospheric carbon dioxide. In The Fate of Fossil Fuel CO_2 in the Oceans, N. Anderson and A. Malahoff (eds.), Plenum Press, NY, 33-43.

Bacastow, R., 1979. Dip in the atmospheric CO_2 level during the mid-1960's. J. Geophys. Res. 84:3108-3114.

Bacastow, R. B., J. A. Adams, C. D. Keeling, D. J. Moss, J. P. Whorf, and C. S. Wong, 1980. Atmospheric carbon dioxide, the Southern Oscillation, and the weak 1975 El Niño. Science 210:66-68.

Bacastow, R. B., and C. D. Keeling, 1981. Atmospheric carbon dioxide concentration and the observed airborne fraction. In Carbon Cycle Modelling, SCOPE 16, B. Bolin (ed.), John Wiley and Sons, NY, 103-112.

Bailey, I. H., L. F. Radke, J. H. Lyons, and P. V. Hobbs, 1984. Airborne observations of Arctic aerosols: II, Giant particles. Geophys. Res. Lett. 11(5):397-400.

Barrie, L. A., and J. Neustadter, 1983. The dependence of sulfate scavenging ratios on meteorological variables. Proceedings, Fourth International Conference on Precipitation Scavenging, Dry Deposition, and Resuspension, Santa Monica, CA, 29 November-3 December 1982, H. R. Pruppacher, R. G. Semonin, and W. G. N. Slinn (eds.), Elsevier, 203-215.

Barrie, L. A., R. M. Hoff, and S. M. Daggupaty, 1981. The influence of mid-latitudinal pollution sources on haze in the Canadian Arctic. Atmos. Environ. 15:1407-1419.

Bodhaine, B. A., 1983. Aerosol measurements at four background sites. J. Geophys. Res. 88(C15):10753-10768.

Bodhaine, B. A., J. M. Harris, and G. A. Herbert, 1981a. Aerosol light scattering and condensation nuclei measurements at Barrow, Alaska. Atmos. Environ. 15(8):1375-1389.

Bodhaine, B. A., B. G. Mendonca, J. M. Harris, and J. M. Miller, 1981b. Seasonal variations in aerosols and atmospheric transmission at Mauna Loa Observatory. J. Geophys. Res. 86(C8):7395-7398.

Bodhaine, B. A., and J. M. Harris (eds.), 1982. Geophysical Monitoring for Climatic Change, No. 10: Summary Report 1981. NOAA Environmental Research Laboratories, Boulder, CO, 158 pp.

Bodhaine, B. A., E. G. Dutton, and J. J. DeLuisi, 1984. Surface aerosol measurements at Barrow during AGASP. Geophys. Res. Lett. 11(5):377-380.

Bortniak, J. C., 1981. The wind climatology of American Samoa. NOAA Tech. Memo. ERL ARL-98, NOAA Environmental Research Laboratories, Boulder, CO, 67 pp.

Brewer, A. W., 1973. A replacement for the Dobson spectrophotometer. Pure Appl. Geophys. 106-108:919-927.

Carlson, T. N., 1981. Speculations on the movement of polluted air to the Arctic. Atmos. Environ. 15:1473-1477.

Clarke, A. D. 1982. Integrating sandwich: A new method of measurement of the light absorption coefficient for atmospheric particles. Appl. Opt. 21:3011-3020.

Clarke, A. D., R. J. Charlson, and L. F. Radke, 1984. Airborne observations of Arctic aerosol: IV, Properties of Arctic haze. Geophys. Res. Lett. 11(5):405-408.

Chou, M. D., L. Peng, and A. Arking, 1984. Climate studies with a multilayer energy balance model: Part II, Climate impact of stratospheric volcanic aerosols. J. Atmos. Sci. 41:759-767.

Chylek, P., V. Ramaswamy, and V. Srivastava, 1983. Albedo of soot contaminated snow. J. Geophys. Res. 88:10837-10843.

Darzi, M., and J. W. Winchester, 1982. Aerosol characteristics at Mauna Loa Observatory, Hawaii, after east Asian dust storm episodes. J. Geophys. Res. 87:1251-1258.

DeLuisi, J. J., E. G. Dutton, K. L. Coulson, T. E. DeFoor, and B. G. Mendonca, 1983. On some radiative features of the El Chichon volcanic stratospheric dust cloud and a cloud of unknown origin observed at Mauna Loa. J. Geophys. Res. 88(C11):6769-6772.

DeLuisi, J. J., C. L. Mateer, and W. D. Komhyr, 1984. Effects of the El Chichon stratospheric aerosol cloud on Umkehr measurements at Mauna Loa, Hawaii. Proceedings, Quadrennial International Ozone Symposium, Thessaloniki, Greece, 3-7 September 1984 (to be published).

Duce, R. A., C. K. Unni, B. J. Ray, J. M. Prospero, and J. T. Merrill, 1980. Long-range atmospheric transport of soil dust from Asia to the tropical North Pacific: Temporal variability. Science 209:1522-1524.

Dutton, E. G., and J. J. DeLuisi, 1983a. Optical thickness features of the El Chichon stratospheric debris cloud. Preprints, Fifth Conference on Atmospheric Radiation, Baltimore, MD, 31 October-4 November 1983, American Meteorological Society, Boston, MA, 361-363.

Dutton, E. G., and J. J. DeLuisi, 1983b. Spectral extinction of direct solar radiation by the El Chichon cloud during December 1982. Geophys. Res. Lett. 10(11):1013-1016.

Dutton, E. G., J. J. DeLuisi, and B. A. Bodhaine, 1984. Features of aerosol optical depth observed at Barrow, 10-20 March 1983. Geophys. Res. Lett. 11(5):385-388.

Evans, W. F. J., and J. B. Kerr, 1983. Estimates of sulphur dioxide from volcanoes: Mt. St. Helens, Mystery and El Chichon. Geophys. Res. Lett. 10(11):1049-1051.

Fenn, R. W., and H. K. Weickmann, 1959. Some results of aerosol measurements. Geofis. Pura Appl. 42:53-61.

Fraser, P. J., M. A. K. Khalil, R. A. Rasmussen, and L. P. Steele, 1984. Tropospheric methane in the mid-latitudes of the Southern Hemisphere. J. Atmos. Chem. 1:125-135.

Galvin, P., V. Mohnen, J. Kadlecek, J. Wilson, and T. Kelly, 1983. Cloud chemistry studies at the Whiteface Mountain field station. ASRC Publ. 973, State University of New York at Albany, Albany, NY, 136 pp.

Gammon, R. H., and W. D. Komhyr, 1983. Response of the global atmospheric CO_2 distribution to the atmospheric/oceanic circulation perturbation in 1982. IAMAP/IUGG Symposium, Hamburg, F.R.G., August 1983 (to be published).

Gammon, R. H., Komhyr, W. D., and J. T. Peterson, 1984a. The global atmospheric CO_2 distribution 1968-83: Interpretation of the results of the NOAA/GMCC measurement program. Proceedings, Sixth Oak Ridge National Laboratory Life Sciences Symposium on The Global Carbon Cycle: Analysis of the Natural Cycle and Implications of Anthropogenic Alterations for the Next Century, Knoxville, TN, 31 October-3 November 1983, Dept. of Energy (to be published).

Gammon, R. H., W. D. Komhyr, L. S. Waterman, T. J. Conway, and K. W. Thoning, 1984b. Estimating the natural variation in atmospheric CO_2 since 1860 from interannual changes in tropospheric temperature and the history of major El Niño events. Proceedings, Chapman Conference on Natural Variations in Carbon Dioxide and the Carbon Cycle. Tarpon Springs, FL, 9-13 January 1984, American Geophysical Union Monograph (to be published).

Grass, R. D., and W. D. Komhyr, 1984. Traveling standard lamp calibration checks on Dobson ozone spectrophotometers during 1981-1983. Proceedings, Quadrennial International Ozone Symposium, Thessaloniki, Greece, 3-7 September 1984 (to be published).

Gundel, L. A., R. L. Dod, H. Rosen, and T. Novakov, 1984. The relationship between optical attenuation and black carbon concentration for ambient and source particles. Sci. Total Environ. (accepted).

Hansen, A. D. A., and H. Rosen, 1984. Vertical distributions of particulate carbon, sulfur, and bromine in the Arctic Haze and comparison with ground-level measurements at Barrow, Alaska. Geophys. Res. Lett. 11:381-384.

Hansen, A. D. A., H. Rosen, and T. Novakov, 1982. Real-time measurement of the absorption coefficient of aerosol particles. Appl. Opt. 21:3060-3062.

Hanson, K. J. (ed.), 1977. Geophysical Monitoring for Climatic Change, No. 5: Summary Report 1976. NOAA Environmental Research Laboratories, Boulder, CO, 110 pp.

Hanson, K. J., J. T. Peterson, J. Namais, R. Born, and C. S. Wong, 1981. On the influence of Pacific Ocean temperatures on atmospheric carbon dioxide concentrations at Ocean Weather Station P. J. Phys. Oceanogr. 11:905-912.

Harris, J. M., 1982. The GMCC atmospheric trajectory program. NOAA Tech. Memo. ERL ARL-116, NOAA Environmental Research Laboratories, Boulder, CO, 30 pp.

Harris, J. M., 1984. Trajectories during AGASP. Geophys. Res. Lett. 11(5): 453-456.

Harris, J. M., and B. A. Bodhaine (eds.), 1983. Geophysical Monitoring for Climatic Change, No. 11: Summary Report 1982. NOAA Environmental Research Laboratories, Boulder, CO, 160 pp.

Harrison, R. M., and C. A. Pio, 1983. Size-differentiated composition of inorganic atmospheric aerosols of both marine and polluted continental origin. Atmos. Environ. 17:1733-1738.

Hegg, D. A., and P. V. Hobbs, 1980. Measurements of gas-to-particle conversion in the plumes from five coal-fired electric power plants. Atmos. Environ. 14:99-116.

Heintzenberg, J., 1982. Size-segregated measurements of particle elemental carbon and light absorption at remote Arctic locations. Atmos. Environ. 16:2461-2469.

Heller, F., and T. S. Liu, 1982. Magnetostratigraphical dating of loess deposits in China. Nature 300:431-433.

Hitchcock, D. R., L. L. Spiller, and W. E. Wilson, 1980. Sulfuric acid aerosols and HCl release in coastal atmospheres: Evidence of rapid formation of sulfuric acid particulates. Atmos. Environ. 14:165-182.

Hobbs, P. V., L. F Radke, and E. E. Hindman, 1976. An integrated airborne particle measuring facility and its preliminary use in atmospheric aerosol studies. J. Aerosol Sci. 7:195-211.

Hoff, R. M., and N. B. A. Trivett, 1984. Ground-based measurements of Arctic haze made at Alert, N.W.T., during the Arctic Gas and Aerosol Sampling Program (AGASP). Geophys. Res. Lett. 11(5):389-392.

Hogan, A. W., S. C. Barnard, K. Kebschull, R. Townsend, and J. A. Samson, 1983. Aerosol variation in the Western Hemisphere Arctic. J. Aerosol Sci. 15:13-33.

Hogan, A., J. Samson, K. Kebschull, R. Townsend, S. Barnard, and B. Murphy, 1984. On the interaction of aerosol with meteorology. J. Rech. Atmos. (in press).

Holmgren, B., G. Shaw, and G. Weller, 1974. Turbidity in the Arctic atmosphere. AIDJEX Bull. 27:135-148.

Huntzicker, J., R. L. Johnson, J. J. Shah, and R. A. Cary, 1982. Analysis of organic and elemental carbon in ambient aerosols by a thermal-optical method. In Particulate Carbon: Atmospheric Life Cycle, G. T. Wolff and R. L. Klimisch (eds.), Plenum, NY, 79-88.

Jickells, J., A. Knap, T. Church, J. Galloway, and J. Miller, 1982. Acid rain on Bermuda. Nature 297(5861):55-57.

Junge, C. E., 1963. Air Chemistry and Radioactivity. Academic Press, NY, 382 pp.

Keeling, C. D., 1968. Carbon dioxide in surface ocean waters: 4, Global distribution. J. Geophys. Res. 73:4543-4553.

Keeling, C. D., 1983. The global carbon cycle: What we know and could know from atmospheric, biospheric, and oceanic observations. Proceedings, Carbon Dioxide Research Conference: Carbon Dioxide, Science and Consensus, Berkeley Springs, WV, 19-23 September 1982, prepared for DOE by Inst. for Energy Analysis, Oak Ridge Associated Universities, Washington, DC, II.3-II.62 (available NTIS, Rep. No. CONF-820970).

Keeling, C. D., and L. S. Waterman, 1968. Carbon dioxide in surface ocean waters: 3, Measurements on Lusiad Expedition, 1962-1963. J. Geophys. Res. 73:4529-4541.

Keeling, C. D., N. W. Rakestraw, and L. S. Waterman, 1965. Carbon dioxide in surface waters of the Pacific Ocean: 1, Measurements of the distribution. J. Geophys. Res. 70:6087-6097.

Keeling, C. D., J. A. Adams, Jr., C. A. Ekdahl, Jr., and P. R. Guenther, 1976a. Atmospheric carbon dioxide variations at the South Pole. Tellus 28:552-564.

Keeling, C. D., R. B. Bacastow, A. E. Bainbridge, C. A. Ekdahl, P. R. Guenther, L. S. Waterman, and J. F. S. Chin, 1976b. Atmospheric carbon dioxide variations at Mauna Loa Observatory, Hawaii. Tellus 28:538-551.

Keeling, C. D., A. F. Carter, and W. G. Mook, 1984. Seasonal, latitudinal, and secular variations in the abundance and isotopic ratios of atmospheric CO_2: 2, Results from oceanographic cruises in the tropical Pacific Ocean. J. Geophys. Res. 89:4615-4628.

Keene, W. C., J. N. Galloway, and J. D. Holden, 1983. Measurement of weak organic acidity in precipitation from remote areas of the world. J. Geophys. Res. 88(C9):5122-5130.

Khalil, M. A. K., and R. A. Rasmussen, 1983a. Gaseous tracers of Arctic haze. Environ. Sci. Technol. 17:157-164.

Khalil, M. A. K., and R. A. Rasmussen, 1983b. Sources, sinks, and seasonal cycles of atmospheric methane. J. Geophys. Res. 88:5131-5144.

Khalil, M. A. K., and R. A. Rasmussen, 1984. Statistical analysis of trace gases in Arctic haze. Geophys. Res. Lett. 11(5):437-440.

Komhyr, W. D., 1969. Electrochemical concentration cells for gas analysis.
    Ann. Geophys. 25(1):203-210.

Komhyr, W. D., 1980. Dobson spectrophotometer total ozone measurement errors
    caused by interfering absorbing species in polluted air such as SO_2, NO_2,
    and photochemically produced O_3. Geophys. Res. Lett. 1(2):157-160.

Komhyr, W. D., R. H. Gammon, and D. A. Gillette, 1983a. The southern ocean
    sink for atmospheric CO_2: A two-dimensional model interpretation of the
    GMCC global atmospheric CO_2 distribution 1979-82. IAMAP/IUGG Symposium,
    Hamburg, F.R.G., August 1983 (to be published).

Komhyr, W. D., L. S. Waterman, and W. R. Taylor, 1983b. Semiautomatic non-
    dispersive infrared analyzer apparatus for CO_2 air sample analysis. J.
    Geophys. Res. 88(C2):1315-1322.

Komhyr, W. D., R. H. Gammon, T. B. Harris, L. S. Waterman, T. J. Conway,
    W. R. Taylor, and K. W. Thoning, 1984a. Global atmospheric CO_2 distribu-
    tion and variations from 1968-1982 NOAA/GMCC CO_2 flask sample data. J.
    Geophys. Res. (submitted).

Komhyr, W. D., S. J. Oltmans, A. N. Chopra, and P. R. Franchois, 1984b. Per-
    formance characteristics of high-altitude ECC ozonesondes. Proceedings,
    Quadrennial International Symposium, Thessaloniki, Greece, 3-7 September
    1984 (to be published).

Komhyr, W. D., S. J. Oltmans, A. N. Chopra, R. K. Leonard, T. E. Garcia, and
    C. McFee, 1984c. Results of Umkehr, ozonesonde, total ozone, and sulfur
    dioxide observations in Hawaii following the eruption of El Chichon vol-
    cano in 1982. Proceedings, Quadrennial International Ozone Symposium,
    Thessaloniki, Greece, 3-7 September 1984 (to be published).

Kotra, J. P., D. L. Finnegan, W. H. Zoller, M. A. Hart., and J. L. Moyers,
    1983. El Chichon: Composition of plume gases and particles. Science
    222:1018-1021.

Lin, C. L., M. G. Baker, and R. J. Charlson, 1973. Absorption coefficient for
    atmospheric aerosols: A method for measurement. Appl. Opt. 12:1356-1363.

Mason, B., and C. B. Moore, 1982. Principles of Geochemistry. 4th ed., John
    Wiley and Sons, NY, 46-47.

Mastenbrook, H. J., and S. J. Oltmans, 1983. Stratospheric water variability
    for Washington, DC/Boulder, CO: 1964-82. J. Atmos. Sci. 40:2157-2165.

Mateer, C. L., and J. J. DeLuisi, 1981. The estimation of the vertical distri-
    bution of ozone by the short Umkehr method. Proceedings, Quadrennial
    International Ozone Symposium, J. London (ed.), Boulder, CO, 4-9 August
    1980, International Association of Meteorology and Atmospheric Physics,
    Boulder, CO, 64-73.

Mateer, C. L., and H. U. Dütsch, 1964. Uniform evaluation of Umkehr observa-
    tions from the World Ozone Network: Part 1, Proposed standard evaluation
    technique. NCAR Rep., Boulder, CO, 105 pp.

May, K. R., 1945. The cascade impactor, an instrument for sampling coarse aerosols. J. Sci. Instrum. 22:187-195.

May, K. R., 1967. Physical aspects of sampling airborne microbes. Symp. Gen. Microbiol. 17:60-81.

Mendonca, B. G. (ed.), 1979. Geophysical Monitoring for Climatic Change, No. 7: Summary Report 1978. NOAA Environmental Research Laboratories, Boulder, CO, 131 pp.

Miller, J. M., and J. M. Harris, 1984. The flow climatology from Bermuda and its implications on long-range transport. Atmos. Environ. (in press).

Mitchell, J. M., Jr., 1957. Visual range in the polar regions with particular reference to the Alaskan Arctic. J. Atmos. Terr. Phys., Spec. Suppl. Pt. 1:195-211.

Newell, R. E., A. R. Navato, and J. Hsiung, 1978. Long term global sea surface temperature fluctuations and their possible influence on atmospheric CO_2 concentrations. Pure Appl. Geophys. 116:351-371.

Newell, R. E., and B. C. Weare, 1977. A relationship between atmospheric carbon dioxide and Pacific sea surface temperature. Geophys. Res. Lett. 4(1):1-2.

NRC (National Research Council), 1984. Causes and effects of changes in stratospheric ozone: Update 1983. The National Academy Press, Washington, DC (Library of Congress Catalog No. 84-60100), 254 pp.

Ogren, J., 1982. Elemental carbon in the atmosphere. Ph.D. Dissertation, University of Washington, Seattle, 134 pp.

Oltmans, S. J., 1981. Surface ozone measurements in clean air. J. Geophys. Res. 86(C2):1174-1180.

Parrington, J. R., 1983. The chemistry of background atmospheric particles collected at Mauna Loa Observatory, Hawaii. Ph.D. Thesis, Dept. of Chemistry, Univ. of Maryland, College Park, 180 pp.

Parrington, J. R., W. H. Zoller, and N. K. Aras, 1983. Asian dust: Seasonal transport to the Hawaiian Islands. Science 220:195-197.

Parrington, J. R., and W. H. Zoller, 1984. The chemistry of Asian dust. J. Geophys. Res. (submitted).

Parungo, F., C. Nagamoto, J. Harris, B. Rosenwasser, and L. Ruhnke, 1984. Analysis of aerosol and precipitation samples collected during a transatlantic research cruise. NOAA Tech. Memo. ERL ESG-5, NOAA Environmental Research Laboratories, Boulder, CO, 63 pp.

Pearman, G. I., 1975. A correction for the effect of drying of air samples and its significance to the interpretation of atmospheric CO_2 measurements. Tellus 27:311-317.

Pearman, G. I., and D. J. Beardsmore, 1984. Atmospheric carbon dioxide measurements in the Australian region: Ten years of aircraft data. Tellus 36B:1-24.

Pearman, G. I., D. J. Beardsmore, and R. C. O'Brien, 1983a. The CSIRO (Australia) atmospheric carbon dioxide monitoring program: Ten years of aircraft data. Division of Atmospheric Physics Tech. Paper No. 45, Commonwealth Scientific and Industrial Research Organization, Australia.

Pearman, G. I., P. Myson, and P. J. Fraser, 1983b. The global distribution of atmospheric carbon dioxide: 1, Aspects of observations and modeling. J. Geophys. Res. 88(C6):3581-3590.

Peterson, J. T. (ed.), 1978. Geophysical Monitoring for Climatic Change, No.6: Summary Report 1977. NOAA Environmental Research Laboratories, Boulder, CO, 145 pp.

Philander, S. G. H., 1983. El Niño Southern Oscillation phenomena. Nature 302:295-301.

Porch, W. M., and M. C. MacCracken, 1982. Parametric study of the effects of Arctic soot on solar radiation. Atmos. Environ. 16:1365-1371.

Prin, R. G., R. A. Rasmussen, P. G. Simmonds, F. N. Alyea, D. M. Cunnold, B. C. Lane, C. A. Cardelino, and A. J. Crawford, 1983. The Atmospheric Lifetime Experiment: 5, Results for CH_3CCl_3 based on three years of data. J. Geophys. Res. 88:8415-8426.

Raatz, W. E., 1982. On the meteorological characteristics of polluted air masses at Barrow, Alaska. Pageoph 120:662-672.

Raatz, W. E., 1984. Tropospheric circulation patterns during the Arctic Gas and Aerosol Sampling Program (AGASP), March/April 1983. Geophys. Res. Lett. 11(5):449-452.

Raatz, W. E., and R. C. Schnell, 1984. Aerosol distribution and an Arctic aerosol front during AGASP: Norwegian Arctic. Geophys. Res. Lett. 11(5):373-376.

Radke, L. F., 1983. Preliminary measurements of the size distribution of cloud interstitial aerosol. Proceedings, Fourth International Conference on Precipitation Scavenging, Dry Deposition, and Resuspension, Santa Monica, CA, 29 November-3 December 1982, H. R. Pruppacher, R. G. Semonin, and W. G. N. Slinn (eds.), Vol. 1, Elsevier, NY, 71-78.

Radke, L. F., and K. T. Whitby, 1982. Field comparisions of aerosol size distributions measured from the air and on the ground. Proceedings, In-Situ Air Quality Monitoring From Moving Platforms, San Diego, CA, 18-21 January 1982, APCA SP-44, Air Pollution Control Assoc., Pittsburgh, PA, 287-298.

Radke, L. F., P. V. Hobbs, and J. E. Pinnons, 1976. Observations of cloud condensation nuclei, sodium-containing particles, ice nuclei and the light-scattering coefficient near Barrow, Alaska. J. Appl. Meteorol. 15:982-995.

Radke, L. F., J. H. Lyons, D. A. Hegg, and P. V. Hobbs, 1984a. Airborne observations of Arctic aerosols: I, Characteristics of Arctic haze. Geophys. Res. Lett. 11(5):393-396.

Radke, L. F., P. V. Hobbs, and I. H. Bailey, 1984b. Airborne observations of Arctic aerosols: III, Origins and effects of airmasses. Geophys. Res. Lett. 11(5):401-404.

Rahn, K. A., 1981. The Mn/V ratio as a tracer of large-scale sources of pollution aerosol for the Arctic. Atmos. Environ. 15:1457-1464.

Rahn, K. A., 1981b. Relative importances of North America and Eurasia as sources of Arctic aerosols. Atmos. Environ. 15:1447-1455.

Rahn, K. A., an N. A. Heidam, 1981. Progress in Arctic air chemistry 1977-1980: A comparison of the first and second symposia. Atmos. Environ. 15:1345-1348.

Rasmussen, R. A., and M. A. K. Khalil, 1981. Atmospheric methane (CH_4): Trends and seasonal cycles. J. Geophys. Res. 86:9826-9832.

Rasmussen, R. A., and M. A. K. Khalil, 1982. Atmospheric trace gases and Arctic haze at BRW. Geophysical Monitoring for Climatic Change, No. 10: Summary Report 1981, B. A. Bodhaine and J. M. Harris (eds.), NOAA Environmental Research Laboratories, Boulder, CO, 114-120.

Rasmussen, R. A., and M. A. K. Khalil, 1983. Natural and anthropogenic trace gases in the lower troposphere of the Arctic. Chemosphere 12:371-375.

Rasmussen, R. A., and M. A. K. Khalil, 1984. Gaseous bromine in the Arctic and Arctic haze. Geophys. Res. Lett. 11(5):433-436.

Rasmussen, R. A., M. A. K. Khalil, and R. W. Dalluge, 1981. Atmospheric trace gases in Antarctica. Science 211:285-287.

Rasmussen, R. A., M. A. K. Khalil, and R. J. Fox, 1983. Altitudinal and temporal variations of hydrocarbons and other gaseous tracers of Arctic haze. Geophys. Res. Lett. 10:144-147.

Reinsel, G. C., G. C. Tiao, J. J. Deluisi, C. L. Mateer, A. J. Miller, and J. E. Frederick, 1984. Analysis of upper stratospheric Umkehr ozone profile data for trends and effects of stratospheric aerosols. J. Geophys. Res. 89(D3):4833-4840.

Robinson, E., and W. L. Bamesberger, 1982. Air chemistry monitoring at Palmer Station. Geophysical Monitoring for Climatic Change, No. 10: Summary Report 1981, B. A. Bodhaine and J. M. Harris (eds.), NOAA Environmental Research Laboratories, Boulder, CO, 108-109.

Rosen, H., and T. Novakov, 1983. Combustion-generated carbon particles in the Arctic atmosphere. Nature 306:768-770.

Rosen, H., T. Novakov, and B. A. Bodhaine, 1981. Soot in the Arctic. Atmos. Environ. 15:1371-1374.

Rotty, R. M., and G. Marland, 1984. Fossil fuel combustion: Recent amounts, patterns, and trends of CO_2. Proceedings, Sixth Oak Ridge National Laboratory Life Sciences Symposium on the Global Carbon Cycle: Analysis of the Natural Cycle and Implications of Anthropogenic Alterations for the Next Century, Knoxville, TN, 31 October-3 November 1983, Dept. of Energy (to be published).

Schnell, R. C., 1984a. Arctic haze and the Arctic Gas and Aerosol Sampling Program (AGASP). Geophys. Res. Lett. 11(5):361-364.

Schnell, R. C. 1984b. Arctic haze: Editorial. Geophys. Res. Lett. 11(5):359.

Schnell, R. C., and W. Raatz, 1984. Vertical and horizontal characteristics of Arctic haze during AGASP: Alaskan Arctic. Geophys. Res. Lett. 11(5):369-372.

Schnell, R. C., J. M. Harris, and J. A. Schroeder, 1981. A relationship between Pacific Ocean temperatures and atmospheric carbon dioxide concentration at Barrow and Mauna Loa. Papers presented at the WMO/ICSU/UNEP Scientific Conference on Analysis and Interpretation of Atmospheric CO_2 Data, Bern, Switzerland, 14-18 September 1981, World Meteorological Organization, Geneva, Switzerland, 155-162.

Shapiro, M. A., R. C. Schnell, F. P. Parungo, S. J. Oltmans, and B. A. Bodhaine, 1984. El Chichon volcanic debris in an Arctic tropopause fold. Geophys. Res. Lett. 11(5):421-425.

Shaw, G. E., 1980. Transport of Asian desert aerosol to the Hawaiian Islands. J. Appl. Meteorol. 19:1254-1259.

Shaw, G. E., 1982. Evidence for Central Eurasian source area of Arctic haze in Alaska. Nature 299:815-818.

Shah, G. M., 1979. Multiwavelength sunphotometer. Internal AES Rep. No. ARQA-70-79, Atmospheric Environment Service, Downsview, Ont., Canada, 22 pp.

Shah, G. M., and W. F. J. Evans, 1984. Aircraft latitude survey measurements of El Chichon eruption cloud. Geophys. Res. Lett. (submitted).

Siegenthaler, V., and K. O. Münnich, 1981. $^{13}C/^{12}C$ fractionation during CO_2 transfer from air to sea. In Carbon Cycle Modelling, SCOPE 16, B. Bolin (ed.), John Wiley and Sons, NY, 249-257.

Stevens, R. K., T. G. Dzubay, G. Russwurm, and D. Rickel, 1978. Sampling and analysis of atmospheric sulfates and related species. Atmos. Environ. 12:55-68.

Taylor. S. R., S. M. McLennan, and M. T. McCulloch, 1983. Geochemistry of loess, continental crustal composition and crustal model ages. Geochim. Cosmochim. Acta 47:1897-1905.

Turekian, K. K., and K. H. Wedepohl, 1961. Distribution of the elements in some major units of the Earth's crust. Bull. Geol. Soc. Am. 72:175-192.

Vallero, F. P. J., T. P. Ackerman, and W. J. Y. Gore, 1984. Radiative effects of the Arctic haze. Geophys. Res. Lett. 11(5):1184-1187.

VanLoon, H., J. J. Taljaard, R. L. Jenne, and H. L. Crutcher, 1971. Climate of the upper air--The Southern Hemisphere: Vol. II, Zonal geostrophic winds. NCAR TN/STR-57, National Center for Atmospheric Research, Boulder, CO, 43 pp.

Warren, S. G., and W. J. Wiscombe, 1980. A model for the spectral albedo of snow: II, Snow containing atmospheric aerosols. J. Atmos. Sci. 37:2734-2745.

Weare, B. C., A. R. Navato, and R. E. Newell, 1976. Empirical orthogonal analysis of Pacific sea surface temperatures. J. Phys. Oceanogr. 6:671-678.

Weiss, R. F., 1981. Determinations of carbon dioxide and methane by dual catalyst flame ionization chromatography and nitrous oxide by electron capture chromatography. J. Chromatogr. Sci. 19:611-616.

Wendler, G., 1983. Solar radiation assessment for BRW. Geophysical Monitoring for Climatic Change, No. 11: Summary Report 1982, J. M. Harris and B. A. Bodhaine (eds.), NOAA Environmental Research Laboratories, Boulder, CO, 114 pp.

Winkler, P., 1980. Observations on acidity in continental and in marine atmospheric aerosols and in precipitation. J. Geophys. Res. 85:4481-4486.

9. GMCC STAFF, 1983

Director's Office

James Peterson, Director
Bernard Mendonca, Deputy Director
Jeanne Kelsey, Secretary
Joanne Edwards, CIRES
Carol Fee, Computer Programmer
Paul Fraser, Guest Scientist, CSIRO
Dale Gillette, Physical Scientist
Everett Nickerson, Meteorologist
Rita Rosson, Clerk-Typist
Russell Schnell, CIRES
Chandra Shastri, CIRES
Gregory Siedelberg, Electronic Technician
Paul Steele, Guest Scientist

Acquisition and Data Management Group

Gary Herbert, Chief
Bonnie Hill, Secretary
Richard Clark, Computer Programmer
Edward Green, CIRES
Joyce Harris, Computer Specialist
Troy Higgins, Jr. Fellow
Gloria Koenig, Computer Programmer
Kenneth Thaut, Electronic Technician

Monitoring Trace Gases Group

Walter Komhyr, Chief
Susan Dozier, Secretary
Amar Chopra, CIRES
Robert Evans, CIRES
Robert Grass, Physicist
Kent Leonard, CIRES
Samuel Oltmans, Physicist
Frank Polacek, III, Meteorological Technician
Thayne Thompson, Physicist

Aerosols and Radiation Monitoring Group

John DeLuisi, Chief
Bonnie Hill, Secretary
Barry Bodhaine, Meteorologist
Forrest Cook, Electronic Technician
Ellsworth Dutton, Meteorologist
Stuart Naegele, CIRES
Kenneth Thorne, CIRES
Wolfgang Raatz, NRC Postdoctoral Research Associate

Carbon Dioxide Group

Richard Gammon, Chief
Susan Dozier, Secretary
Thomas Conway, CIRES
Bradley Halter, Meteorologist
Kenneth Masarie, CIRES
Steven Rush, CIRES
Kirk Thoning, CIRES
Lee Waterman, Chemist

Mauna Loa Observatory
Kinsell Coulson, Director
Judith Pereira, Secretary
Arnold Austring, Physical Scientist
John Chin, Physicist
Thomas DeFoor, Electrical Engineer
Thomas Garcia, Physical Science Aid
Darryl Kuniyuki, Jr. Fellow
Cynthia McFee, NOAA Corps
Mamoru Shibata, Electonic Technician
Alan Yoshinaga, Chemist

Barrow Observatory
Randy Fox, Station Chief
Daniel Beard, Station Chief
Timothy Wolfe, Electronic Technician

Samoa Observatory
Donald Nelson, Station Chief
Roger Williams, Electronic Technician
Efaraima Peau, W. G. Laborer

South Pole Observatory
Rusty Brainard, NOAA Corps, Station Chief
Steven Fahnenstiel, Physicist
Frank Migaiolo, NOAA Corps, Station Chief
Robert Platzer, Engineer